JAERI-M
83-026

EVALUATION REPORT ON CCTF CORE-I REFLOOD TESTS C1-5 (RUN 14), C1-7 (RUN 16) AND C1-14 (RUN 23) —EFFECTS OF INITICAL CLAD TEMPERATURE—

February 1983

Jun SUGIMOTO and Yoshio MURAO

日本原子力研究所
Japan Atomic Energy Research Institute

JAERI-M レポートは，日本原子力研究所が不定期に公刊している研究報告書です。

入手の問合わせは，日本原子力研究所技術情報部情報資料課（〒319—11 茨城県那珂郡東海村）あて，お申しこしください。なお，このほかに財団法人原子力弘済会資料センター（〒319—11 茨城県那珂郡東海村日本原子力研究所内）で複写による実費領布をおこなっております。

JAERI-M reports are issued irregularly.

Inquiries about availability of the reports should be addressed to Information Section, Division of Technical Information, Japan Atomic Energy Research Institute, Tokai-mura, Naka-gun, Ibaraki-ken 319—11, Japan.

編集兼発行　日本原子力研究所
印　　刷　日立高速印刷株式会社

JAERI-M 83-026

Evaluation Report on CCTF Core-I Reflood Tests C1-5 (Run 14), C1-7 (Run 16) and C1-14 (Run 23) —— Effects of Initical Clad Temperature ——

Jun SUGIMOTO and Yoshio MURAO

Division of Nuclear Safety Research,
Tokai Research Establishment, JAERI

(Received January 29, 1983)

The present report describes the effects of the initial clad temperature on the reflood phenomena observed in the Cylindrical Core Test Facility (CCTF) at Japan Atomic Energy Research Insitute. The evaluation is based on the data of tests C1-5, C1-7 and C1-14 of the CCTF-Core I test series. Nominal initial peak clad temperatures in these tests are 600°C, 700°C and 800°C, respectively.

With the higher initial clad temperature, the higher loop mass flow rate and the lower water accumulation in the core and the upper plenum were obtained in an early reflood transient. However, the core inlet flow conditions, which is sensitive to the core cooling, were not much affected by the higher initial clad temperature. The slower quench front propagation was observed with the higher initial clad temperature. However, the heat transfer coefficient was almost identical with each other before the turnaround time, which resulted in the lower temperature rise with the highest initial clad temperature. This qualitatively agreed with the results of the forced feed FLECHT experiment.

Keywords: Reflooding, LOCA-ECCS, Initial Clad Temperature, Heat Transfer, Two-phase Flow

---

The work was performed under contract with the Atomic Energy Bureau of Science and Technology Agency of Japan

大型再冠水円筒第1次炉心試験C1－5（Run 14），C1－7(Run 16)及びC1－14（Run 23）評価報告書
－被覆管初期温度の影響－

日本原子力研究所東海研究所安全工学部
杉本　純・村尾　良夫

（1983年1月29日受理）

本報告書は，日本原子力研究所における大型再冠水円筒炉心試験装置（CCTF）で観測された再冠水現象に及ぼす被覆管初期温度の影響について述べている。本評価報告は，CCTF第一次炉心試験C1－5，C1－7及びC1－14の結果に基づいている。これらの試験における被覆管の初期温度はそれぞれ600℃，700℃及び800℃であった。

再冠水後初期においては被覆管初期温度が高い程ループ流量は増加し，炉心と上部プレナムでの蓄水は減少した。炉心冷却にとって重要な炉心入口条件は被覆管初期温度の増加に対して大きな影響は受けなかった。炉心内では被覆管初期温度が高い程クエンチ点の進行は遅れたが，ターンアラウンド点までの熱伝達率はほとんど影響を受けなかった。このため被覆管初期温度が高い程最高到達温度までの温度上昇は減少した。この傾向はFLECHTにおける強制注入実験の結果と定性的に一致した。

本報告書は，電源開発促進対策特別会計法に基づき，科学技術庁からの受託によって行った研究の成果である。

Contents

目　　次

List of Tables

List of Figures

[Nomenclature]

C_p : Specific heat (J/kg·K)

H_{fg} : Latent heat of evapolation (J/kg)

h : Heat transfer coefficient (W/m^2K)

L_q : Distance from quench front (m)

P : Pressure (Pa)

T_q : Wall temperature just before quench (K)

T_s : Saturation temperature (K)

T_w : Wall temperature (K)

u_q : Quench front velocity (m/s)

α : Void fraction (-)

ΔT_{sat} : Wall super heat (K)

ΔT_{sub} : Subcooling of coolant (K)

ε : Emissivity (-)

λ : Thermal conductivity (W/m·K)

μ_g : Dynamic viscocity (Pa·s)

ρ : Density (kg/m^3)

σ : Stefan Boltzman constant ($W/m^2 \cdot K^4$)

(Subscripts)

g : Gas phase, ℓ : Liquid phase

1. Introduction

The present report describes the effects of the initial clad temperature on the reflood phenomena observed in the Cylindrical Core Test Facility (CCTF) at Japan Atomic Energy Research Institute (JAERI).

The large scale reflood test program has been conducted at JAERI in order to demonstrate the effectiveness of the emergency core cooling (ECC) system, to verify the best-estimate analysis codes and to supply information for the improved thermo-hydrodynamic models during the reflood phase of a hypothetical loss-of-coolant accident (LOCA) of a PWR. For that purpose the CCTF and the Slab Core Test Facility (SCTF) have been constructed. The CCTF is a 1/20 scale integral test facility with a cylindrical core, 4-loop primary systems, and active steam generators. Whereas the SCTF is designed to simulate the two-dimensional flows in the core with an eight fuel bundles arranged in a slab geometry.

The clad temperature at reflood initiation much depends on the heat transfer in the preceeding blowdown and refill phases in LOCA. In a safety analysis, for example, the initial clad temperature is conservatively evaluated at about 1140 K assuming the adiabatic heat-up during the refil phase. However, the initial clad temperature was set at a fairly low temperature (about 873 K) in most CCTF-Core I tests to minimize the core damage during the test. Therefore, the parametric tests were conducted with CCTF to investigate the effect of the initial clad temperature.

The FLECHT[1] experiment has shown that the higher initial clad temperature induces the higher peak clad temperature, the later quench time and the lower temperature rise under the constant forced-feed reflood condition. However it is important to clarify the effect of the initial clad temperature under the system feed-back condition as in an actual PWR. This is because the core inlet flow rate is controlled by the capability of the system to exhaust the steam generated in the core.

The present data evaluation is based on CCTF Test C1-5, C1-7 and C1-14. Test C1-5 is a base case of CCTF Core I test series.[2] The nominal peak clad temperatures of Tests C1-5, C1-17 and C1-14 are 600°C, 700°C and 800°C, respectively at the reflood initiation. Detailed analysis and the data evaluation of the base case Test C1-5 is reported in reference (2). The main results of Tests C1-5, C1-7 and C1-14 are compiled in Appendixes for the better understanding of the test results.

2. Test description

2.1 Test facility

The CCTF is an experimental test facility designed to simulate the flow conditions in the primary system of a PWR during the refill and reflood phases of a LOCA. The vertical dimensions and locations of the system components are kept as close to those of a reference 1000 MW-PWR with four primary loops. The flow area of the system components are based on the core flow area scaling ratio of 1:21.4. The schematic diagram of the facility is shown in Fig. 2.1. The scaled diameters and the elevations of the components are given in Tables 2.1 and 2.2.

The pressure vessel is a cylindrical type with the downcomer, the upper and lower plenums, and the core as shown in Fig. 2.2. The core consists of thirty-two 8×8 electrically heated rod bundles arranged in a cylindrical array. Each bundle simulates 15×15 array fuel assemblies including non-heated rods. The cross section of the pressure vessel and the arrangement of the rods in the core are shown in Figs. 2.3 and 2.4, respectively.

The heated length and the outer diameter of the heater rods are 3.66 m and 10.7 mm, respectively. The heating element is a herical nichrome coil with a 17 step chopped cosine axial power profile as shown in Fig. 2.5. The locations of the temperature and the differential pressure measurement in the core are also indicated in the figure.

The primary loop consists of three intact loops and a broken loop. Each loop consists of hot leg and cold leg pipings, a steam generator with active secondary side and a pump simulator. A 200% cold leg break is simulated for the broken cold leg. The broken cold leg is connected to containment tanks. The inner diameter of the piping is scaled down in proportion to the core flow area scaling. The length of each piping section is almost the same as the corresponding section of the reference PWR. ECCS consists of an accumulator (Acc) and a low pressure coolant injection (LPCI) system. The injection points are at each cold leg and at the lower plenum. The primary loop arrangement is shown in Figs. 2.6 and 2.7.

Approximately 1500 channels of data are recorded on a magnetic disk and tape, which include temperatures, pressures, differential pressures, liquid levels, mass flow rates and void fractions. Measurement locations

in the pressure vessel and the primary system are shown in Figs. 2.8 through 2.11.

2.2 Test procedure

The test procedures were as follows: After establishing the initial conditions of the test, the electric power for the preheating was turned off and the lower plenum was filled to a specified level directly from the saturated water tank. When the water level in the lower plenum reached 0.90m and other initial conditions of the test stabilized, the electric power was applied to the heater rods in the core and the data recording was started. When a specified initial temperature was reached, direct injection of the Acc water into the lower plenum was initiated. Decay of the power input to the rods was scheduled to begin when the water reached the bottom of the heated length of the heater rods. The specified initial clad temperature of the heater rods for the initiation of the coolant injection was predetermined by interpolation between the initial clad temperature and the clad temperature assumed for the time of the bottom of the core recovery. The specified power decay is based on the decay curve of the ANS standard$\times$1.2+^{238}U capture decay at 30 s after shutdown.

When the assumed water level reached the specified height from the bottom of heated length, the injection port was changed from the lower plenum to the three intact cold leg ECC ports. At about 17 s after the initiation of Acc injection, the valves in Acc line and LPCI circulation line were closed and the valve in LPCI injection line was opened. These actions transferred the ECC injection from Acc injection mode to LPCI mode.

The generated steam and the entrained water flowed via broken and intact loops to the containment tanks. The steam was then vented to the atmosphere to maintain the pressure in the containment tanks constant.

When all thermocouples on the surface of heater rods indicated temperature close to the saturated temperature, the power supply to the heater rods and the ECC injection were turned off terminating the test.

2.3 Test conditions

Table 2.3 gives the comparison of the major initial and boundary conditions for Tests C1-5, C1-7 and C1-14. These test conditions are basically identical for the three tests except for the initial peak clad temperature.

Table 2.4 gives the comparison of the chronology of events for three tests. As the clad temperatures at the power supply were set to almost the same saturation temperatures, the required heat-up time until the reflood initiation is longer with the higher initial clad temperature test. According to the integrated power supply, the initial stored energies of Tests C1-7 and C1-14 were evaluated as about 26% and 53% larger, respectively, than that of the base case Test C1-5.

Table 2.1 Component Scaled Dimensions of Cylindrical Core Test Facility

COMPONENT		PWR	CCTF	RATIO
PRESSURE VESSEL				
VESSEL INSIDE DIAMETER	(mm)	4394 (173")	1084	1/4.05
VESSEL THICKNESS	(mm)	216 (8 1/2")	90	1/2.4
CORE BARREL OUTSIDE DIAMETER	(mm)	3974	961	1/4.14
CORE BARREL INSIDE DIAMETER	(mm)	3760	929	1/4.05
THERMAL SHIELD OUTSIDE DIAMETER	(mm)	4170	——	——
THERMAL SHIELD INSIDE DIAMETER	(mm)	4030	——	——
DOWNCOMER LENGTH	(mm)	4849	4849	1/1
DOWNCOMER GAP	(mm)		61.5	
DOWNCOMER + CORE BUFFLE FLOW AREA	(m^2)	4.23	0.197	1/21.44
LOWER PLENUM VOLUME	(m^3)	29.6	1.38	1/21.44
UPPER PLENUM VOLUME	(m^3)	43.6	2.04	1/21.44
FUEL (HEATER ROD) ASSEMBLY				
NUMBER OF BUNDLES	(——)	193	32	——
ROD ARRAY	(——)	15 × 15	8 × 8	——
ROD HEATED LENGTH	(mm)	3660	3660	1/1
ROD PITCH	(mm)	14.3	14.3	1/1
FUEL ROD OUTSIDE DIAMETER	(mm)	10.72	10.7	1/1
THIMBLE TUBE DIAMETER	(mm)	13.87	13.8	1/1
INSTRUMENT TUBE DIAMETER	(mm)	13.87	13.8	1/1
NUMBER OF HEATER RODS	(——)	39372	1824	1/21.58
NUMBER OF NON-HEATED RODS	(——)	4053	224	1/18.09
CORE FLOW AREA	(m^2)	5.29	0.25	1/21.2
CORE FLUID VOLUME	(m^3)	17.95	0.915	1/19.6
PRIMARY LOOP				
HOT LEG INSIDE DIAMETER	(mm)	736.6 (29")	155.2	1/4.75
HOT LEG FLOW AREA	(m^2)	0.426	0.019	1/22.54
HOT LEG LENGTH	(mm)	3940	3940	1/1

Table 2.1 (continued)

COMPONENT		PWR	CCTF	RATIO
PUMP SUCTION INSIDE DIAMETER	(mm)	787.4 (31")	155.2	1/5.07
PUMP SUCTION FLOW AREA	(m^2)	0.487	0.019	1/25.77
PUMP SUCTION LENGTH	(mm)	7950	7950	1/1
COLD LEG INSIDE DIAMETER	(mm)	698.5 (27.5")	155.2	1/4.50
COLD LEG FLOW AREA	(m^2)	0.383	0.019	1/20.26
COLD LEG LENGTH	(mm)	5600	5600	1/1
STEAM GENERATOR SIMULATOR				
NUMBER OF TUBES	(—)	3388	158	1/21.44
TUBE LENGTH (AVERAGE)	(m)	20.5	15.2	1/1.35
TUBE OUTSIDE DIAMETER	(mm)	22.225 (0.875")	25.4	1/0.875
TUBE INSIDE DIAMETER	(mm)	19.7 (0.05")	19.6	1/1
TUBE WALL THICKNESS	(mm)	1.27	2.9	
HEAT TRANSFER AREA	(m^2)	4784 (51500 ft^2)	192	1/24.92
TUBE FLOW AREA	(m^2)	1.03	0.048	1/21.44
INLET PLENUM VOLUME	(m^3)	4.25	0.198	1/21.44
OUTLET PLENUM VOLUME	(m^3)	4.25	0.198	1/21.44
PRIMARY SIDE VOLUME	(m^3)	30.50 (1077 ft^3)	2.4	1/15.25
SECONDARY SIDE VOLUME	(m^3)	157.33 (5556 ft^3)	4.9	1/26.22
CONTAINMENT TANK I	(m^3)		30	
CONTAINMENT TANK II	(m^3)		50	
STORAGE TANK	(m^3)		25	
ACC. TANK	(m^3)		5	
SATURATED WATER TANK	(m^3)		3.5	

Table 2.2 Component elevations of Cylindrical Core Core Test Facility

COMPONENT		PWR	CCTF	DISCREPANCY
BOTTOM OF HEATED REGION IN CORE	(mm)	0	0	0
TOP OF HEATED REGION IN CORE	(mm)	3660	3660	0
TOP OF DOWNCOMER	(mm)	4849	4849	0
BOTTOM OF DOWNCOMER	(mm)	0	0	0
CENTERLINE OF COLD LEG	(mm)	5198	4927	-271
BOTTOM OF COLD LEG (INSIDE)	(mm)	4849	4849	0
CENTERLINE OF LOOP SEAL LOWER END	(mm)	2056	2047	- 9
BOTTOM OF LOOP SEAL LOWER END	(mm)	1662	1959	+297
CENTER OF HOT LEG	(mm)	5198	4927	-271
BOTTOM OF HOT LEG (INSIDE)	(mm)	4830	4849	+ 19
BOTTOM OF UPPER CORE PLATE	(mm)	3957	3957	0
TOP OF LOWER CORE PLATE	(mm)	- 108	- 50	+ 58
BOTTOM OF TUBE SHEET OF STEAM GENERATOR	(mm)	7308	7307	- 1
LOWER END OF STEAM GENERATOR PLENUM	(mm)	5713	5712	- 1
TOP OF TUBES OF STEAM GENERATOR (avg)	(mm)	17952.7	14820	-3132.7

Table 2.3 Comparison of initial and boundary condition

Condition	Test C1-5	Test C1-7	Test C1-14
Total power (MW)	9.36	9.38	9.40
Averaged linear power (kW/m)	1.40	1.41	1.41
Radial power distribution	1.16:1.08:0.88	1.16:1.08:0.88	1.15:1.08:0.89
Containment pressure (MPa)	0.20	0.20	0.20
SG secondary side pressure (MPa)	4.9	5.0	5.1
Downcomer wall temperature (K)	455	453	449
Primary piping wall temperature (K)	393	393	391
SG secondary side temperature (K)	535	537	537
Peak clad temperature (K)			
at ECC initiation	775	899	984
at reflood initiation	868	966	1045
Lower plenum filled water temperature (K)	387	385	394
ECC water temperature (K)	312	312	313
Lower plenum water level (m)	0.87	0.86	0.86
SG secondary side water level (m)	7.3	7.4	7.5
Accumulator injection rate (m^3/s)	7.72×10^{-2}	7.75×10^{-2}	7.69×10^{-2}
LPCI injection rate (m^3/s)	8.39×10^{-3}	8.44×10^{-3}	8.44×10^{-3}

Table 2.4 Comparison of chronology of events

(unit: s)

Event	C1-5	C1-7	C1-14
Test initiated (Heater rod power on) (Data recording initiated)	0	0	0
Accumulator injection initiated	52.5	68.0	85.5
Power decay initiated (Bottom of core recovery)	63.0	79.5	96.5
Accumulator injection switched from lower plenum to cold legs	67.0	85.0	102.5
Accumulator injection ended and LPCI initiated	76.0	91.5	109.5
All heater rods quenched	598.0	611.0	660.0
Power off	648.0	678.0	738.0
LPCI ended	738.0	888.0	948.0
Test ended	1068.0	1086.0	1104.0

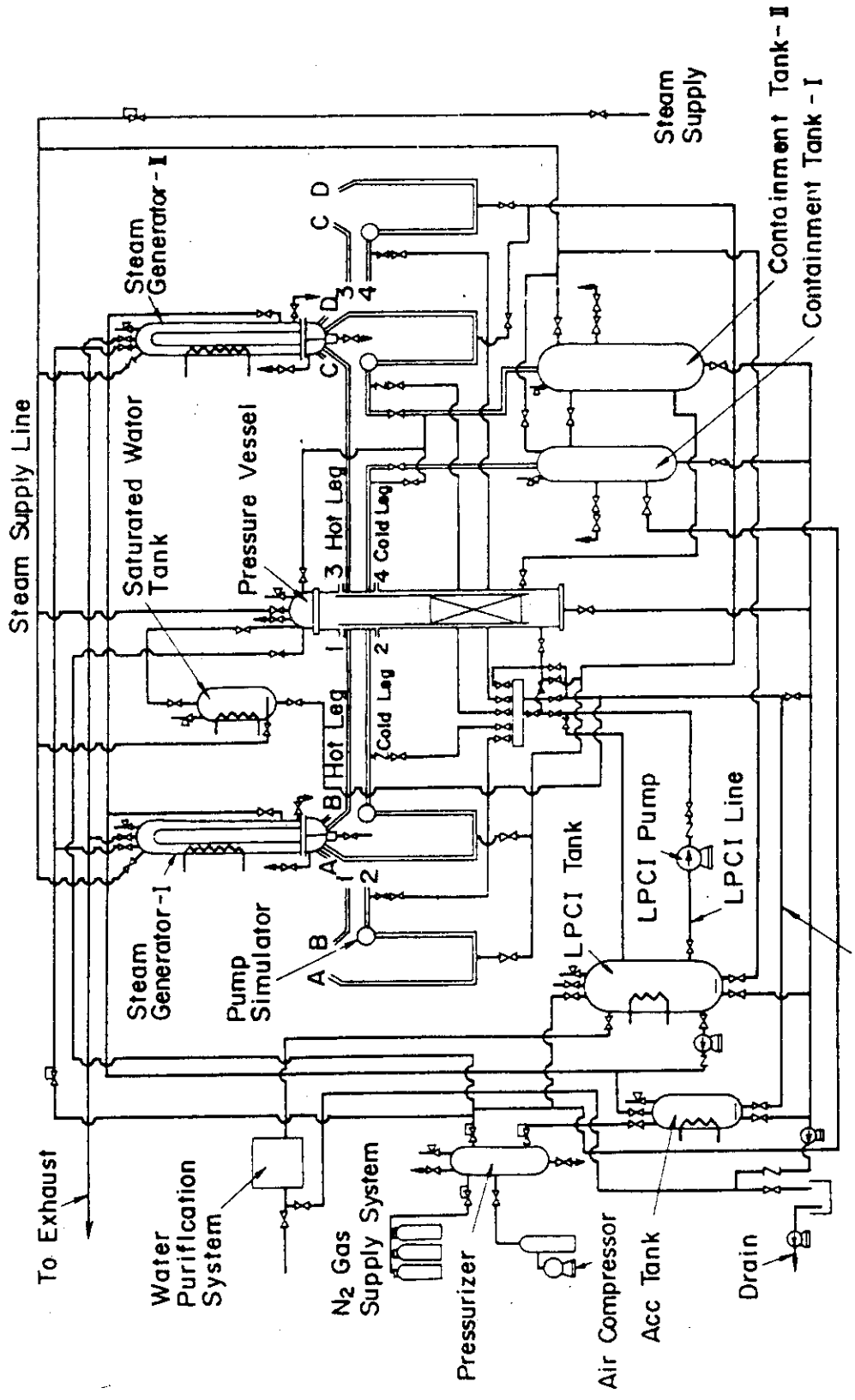

Fig.2.1 Schematic Diagram of Cylindrical Core Test Facility

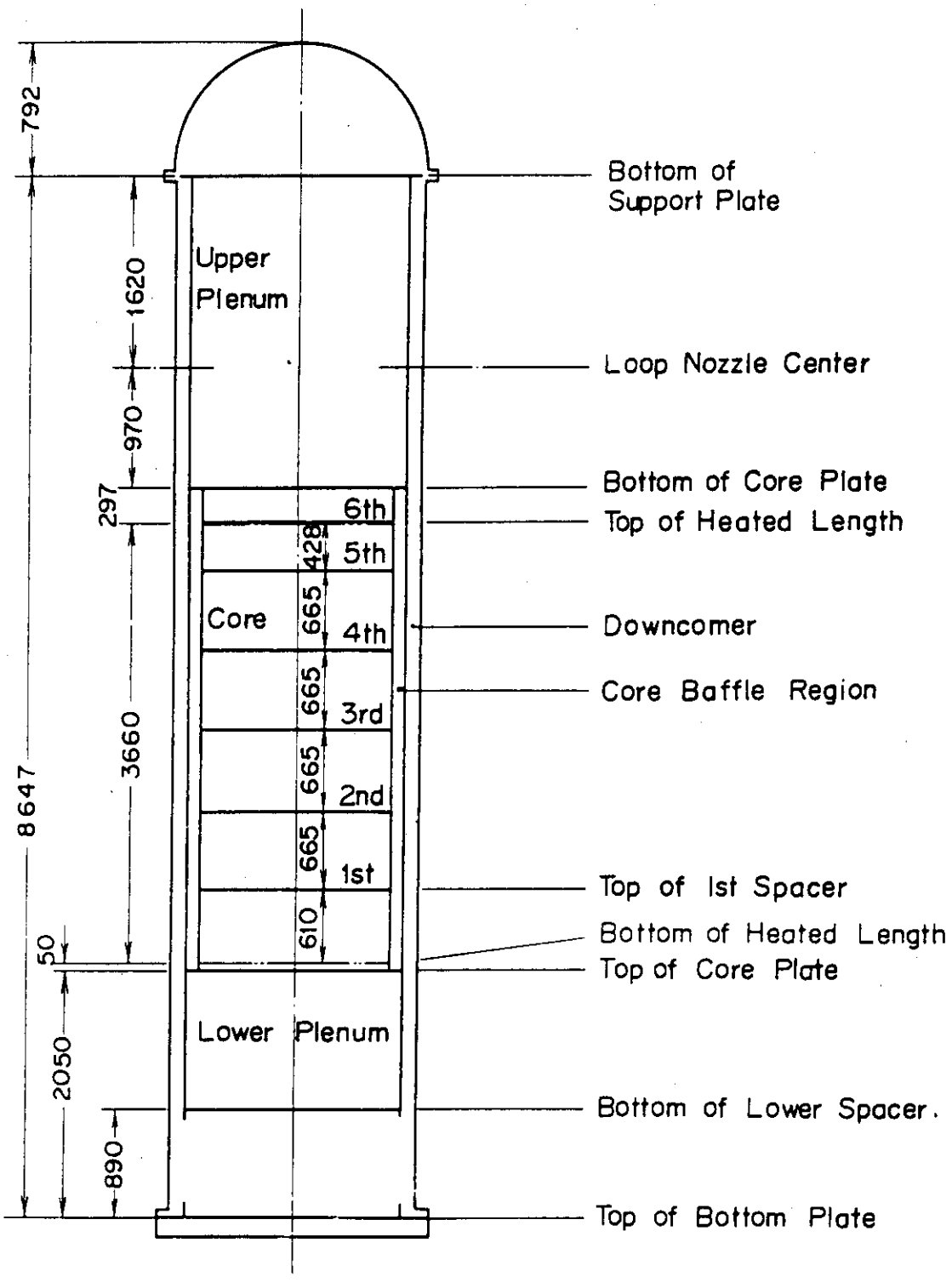

Fig.2.2 Dimensions of Pressure Vessel

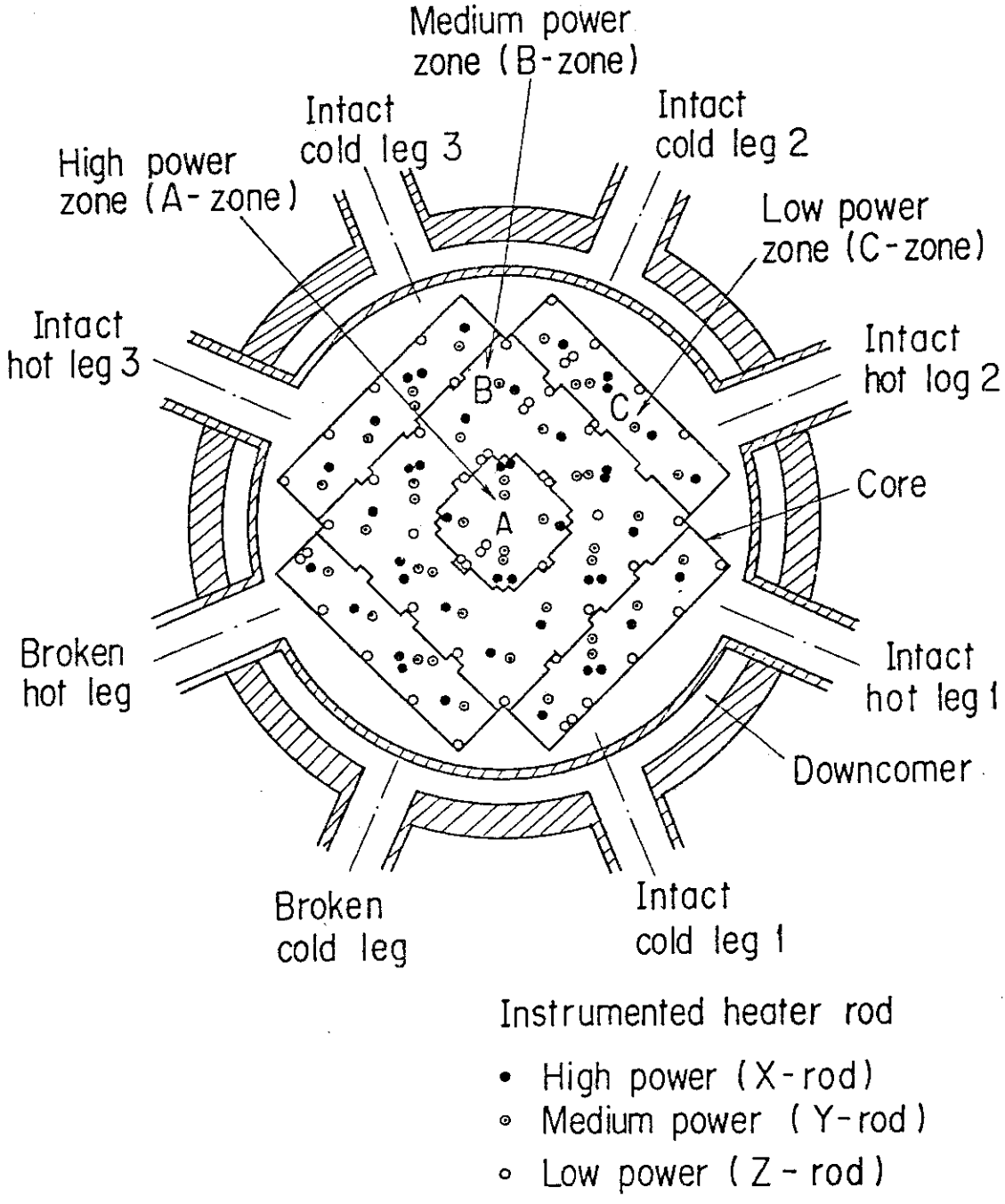

Fig.2.3 Cross Section of Pressure Vessel

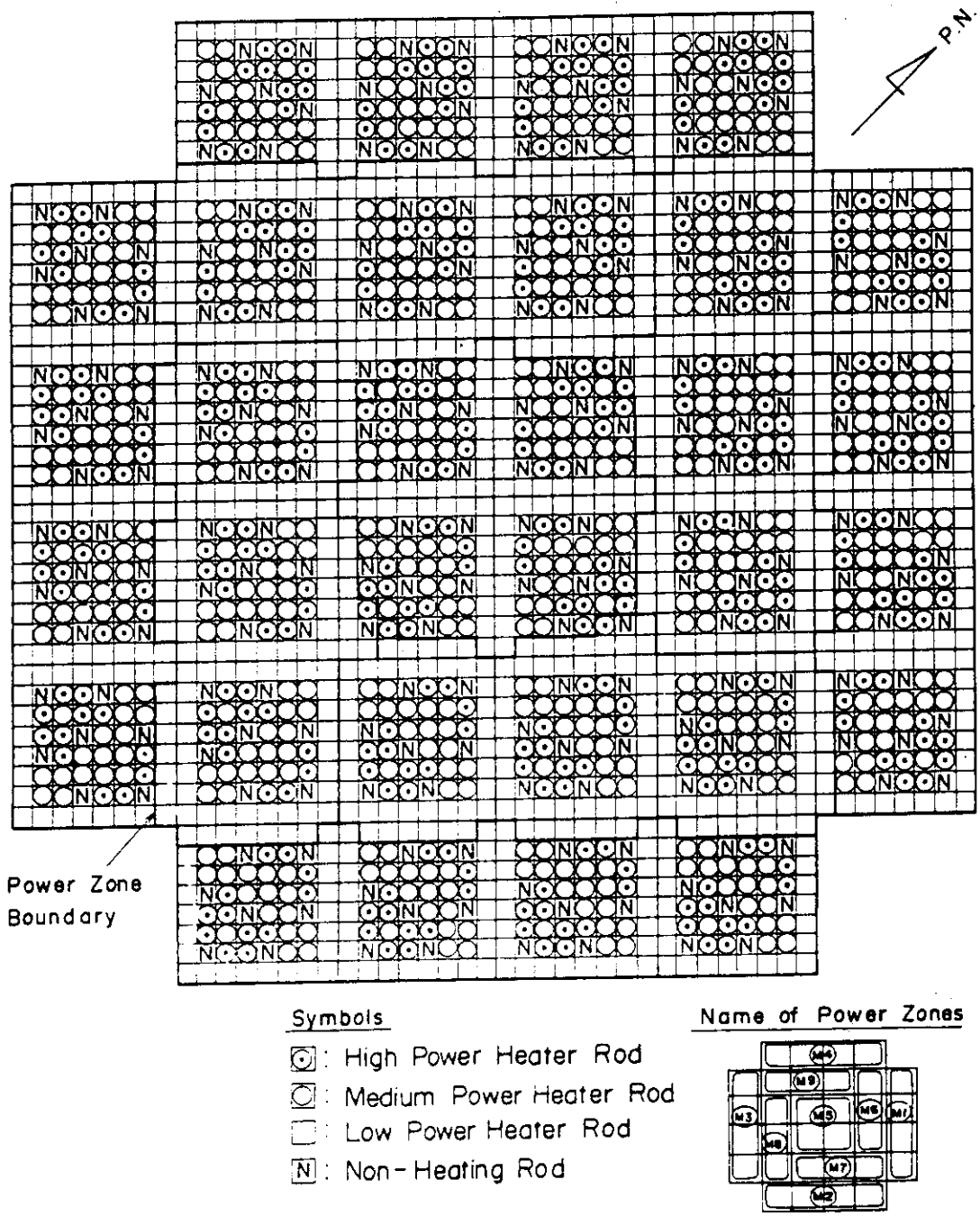

Fig. 2.4 Configuration of Rods in Core

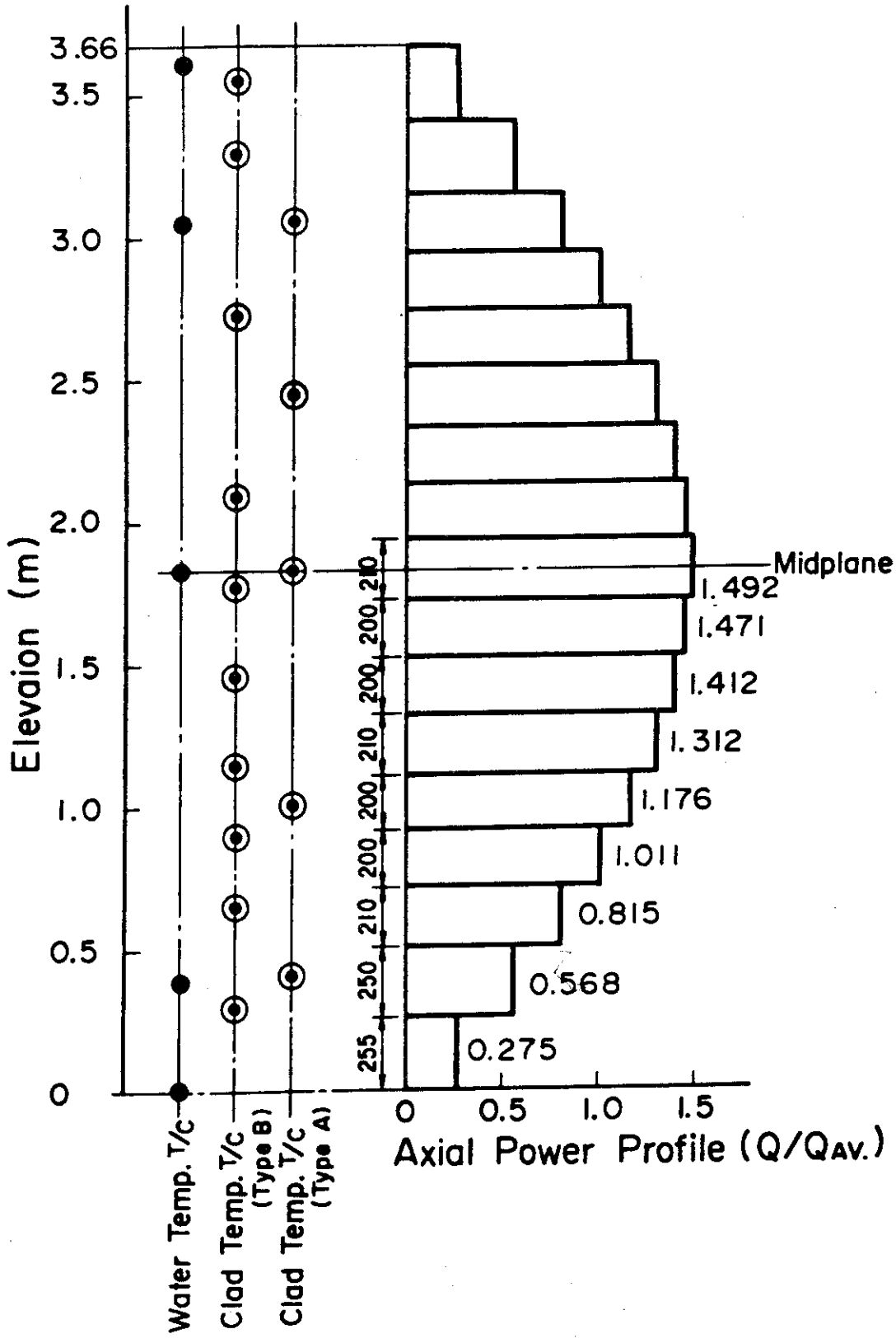

Fig.2.5 Power Profile and Thermocouple Elevations of Heater Rods

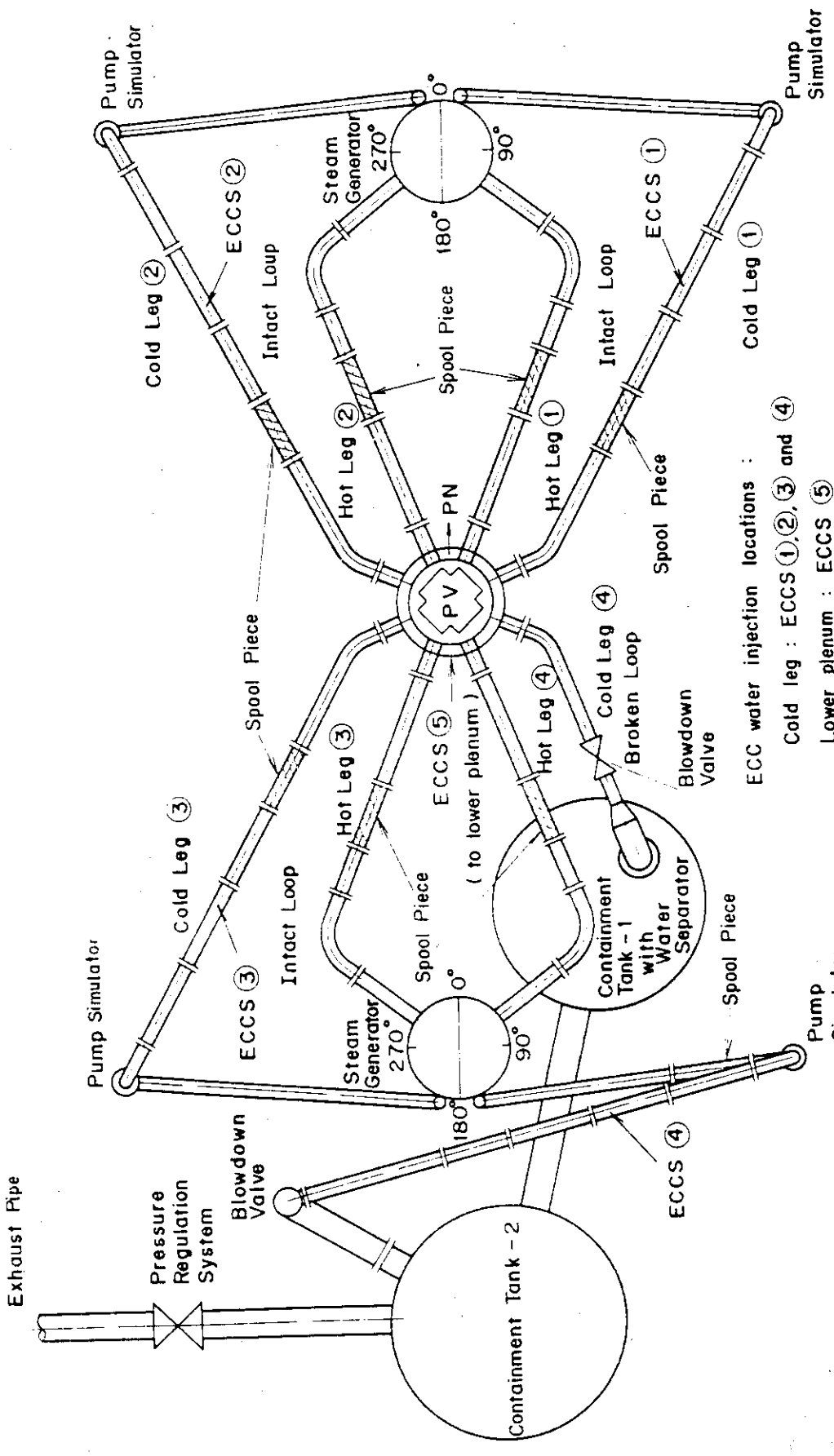

Fig.2.6 Primary Loop Piping

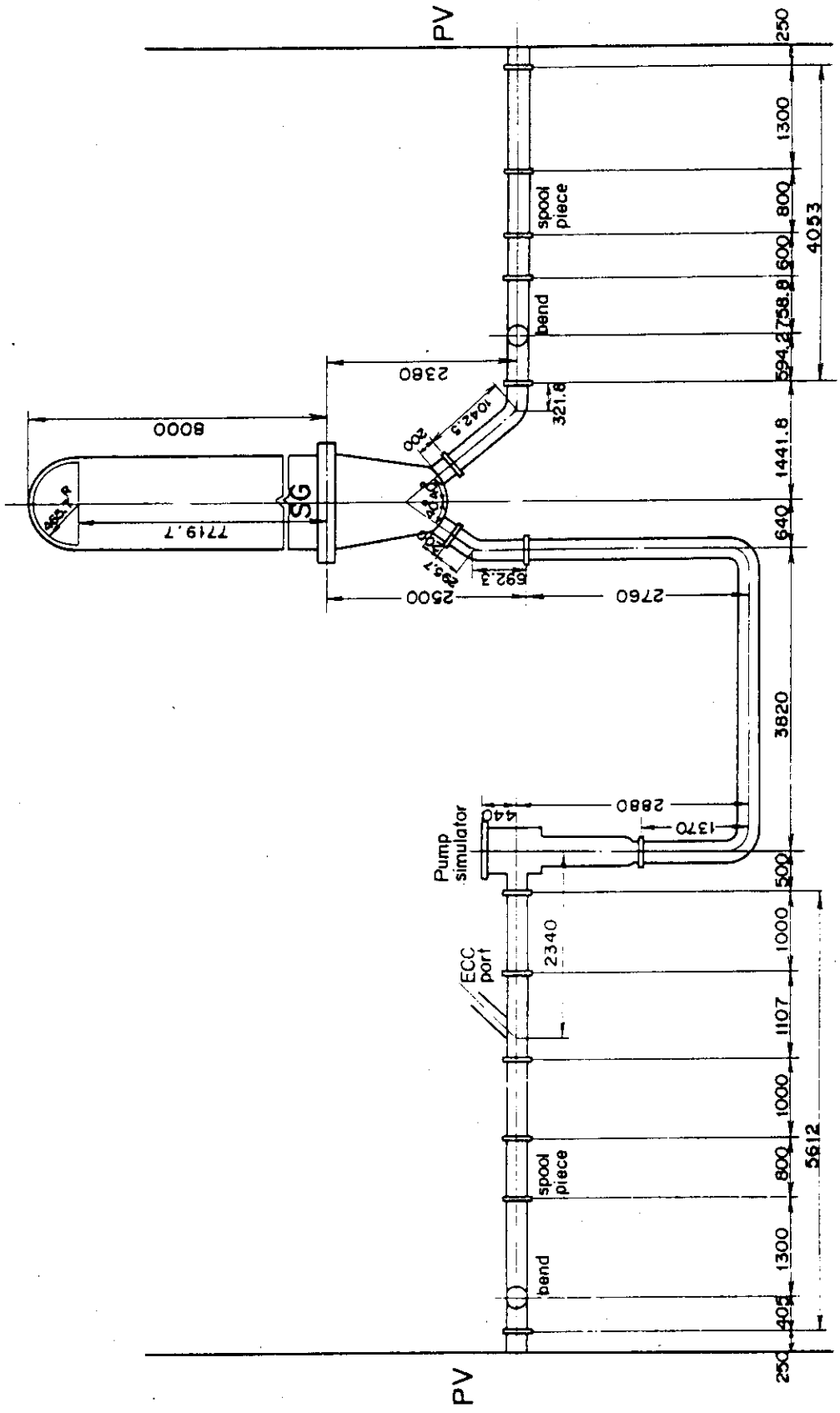

Fig.2.7 Primary Loop

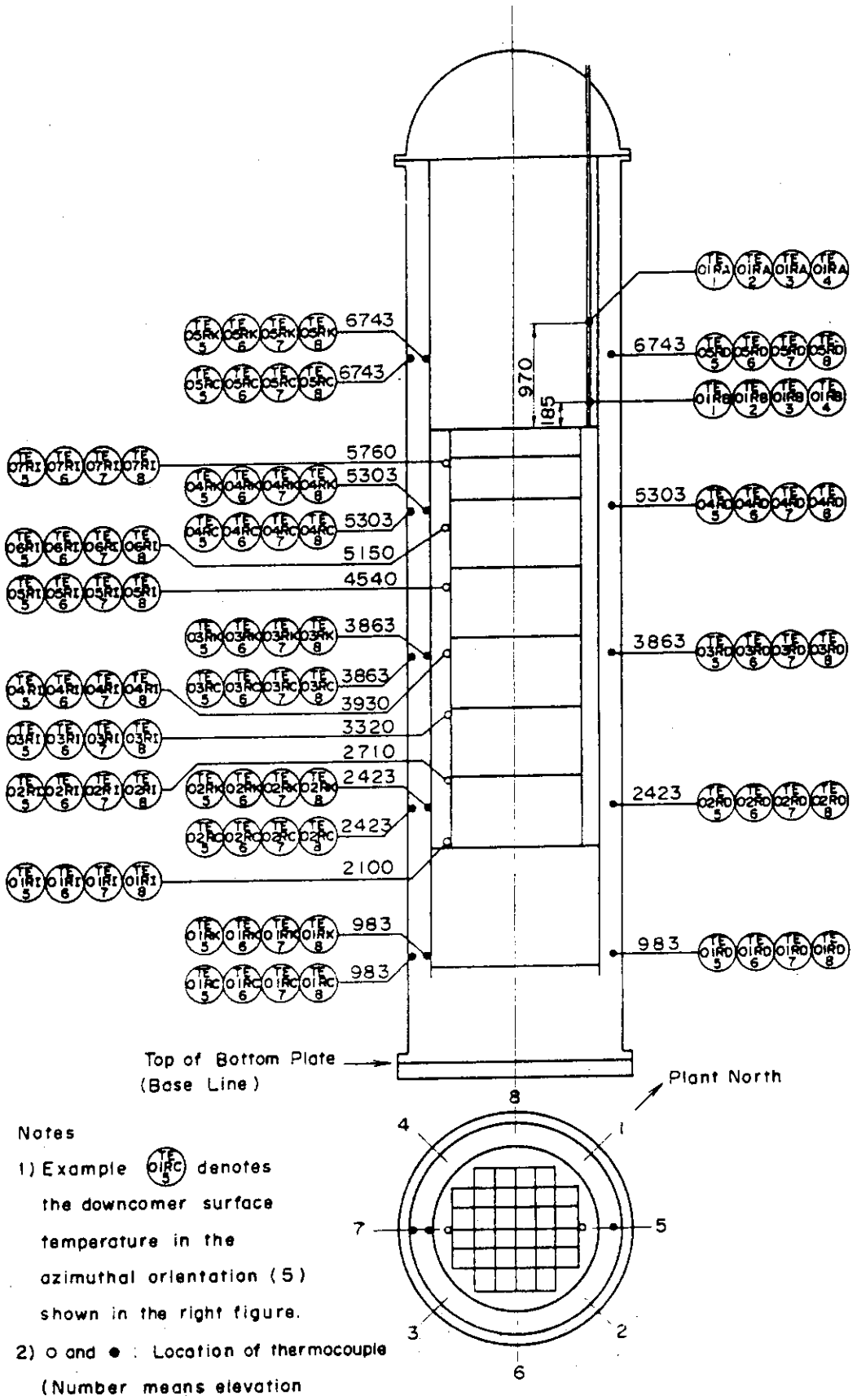

Notes

1) Example (TE 01RC 5) denotes the downcomer surface temperature in the azimuthal orientation (5) shown in the right figure.

2) ○ and ● : Location of thermocouple (Number means elevation from base line in mm.)

Fig.2.8 Thermocouple Locations in Pressure Vessel

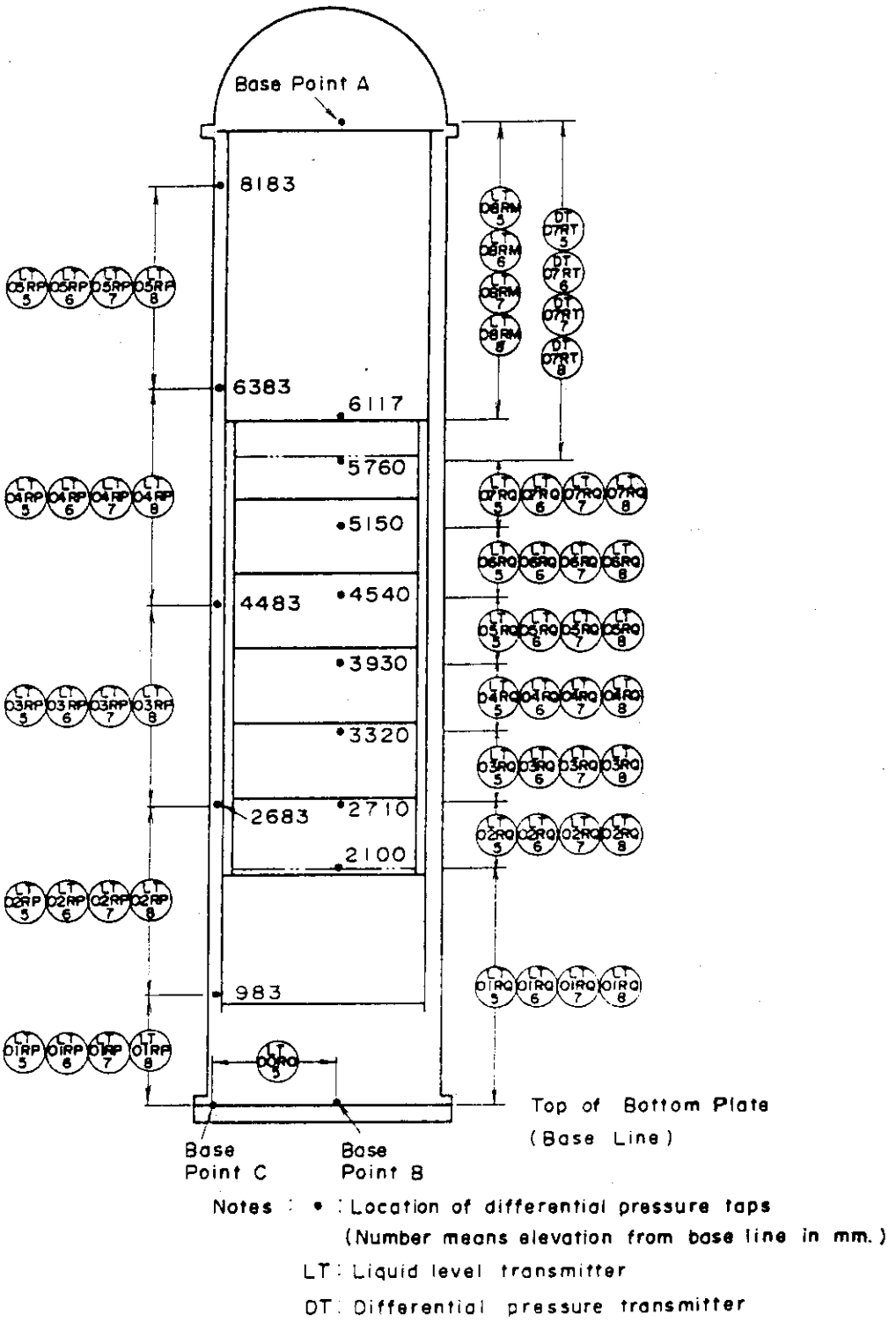

Fig.2.9 Pressure, Differential Pressure and Liquid Level Instrumentation Locations in Pressure Vessel

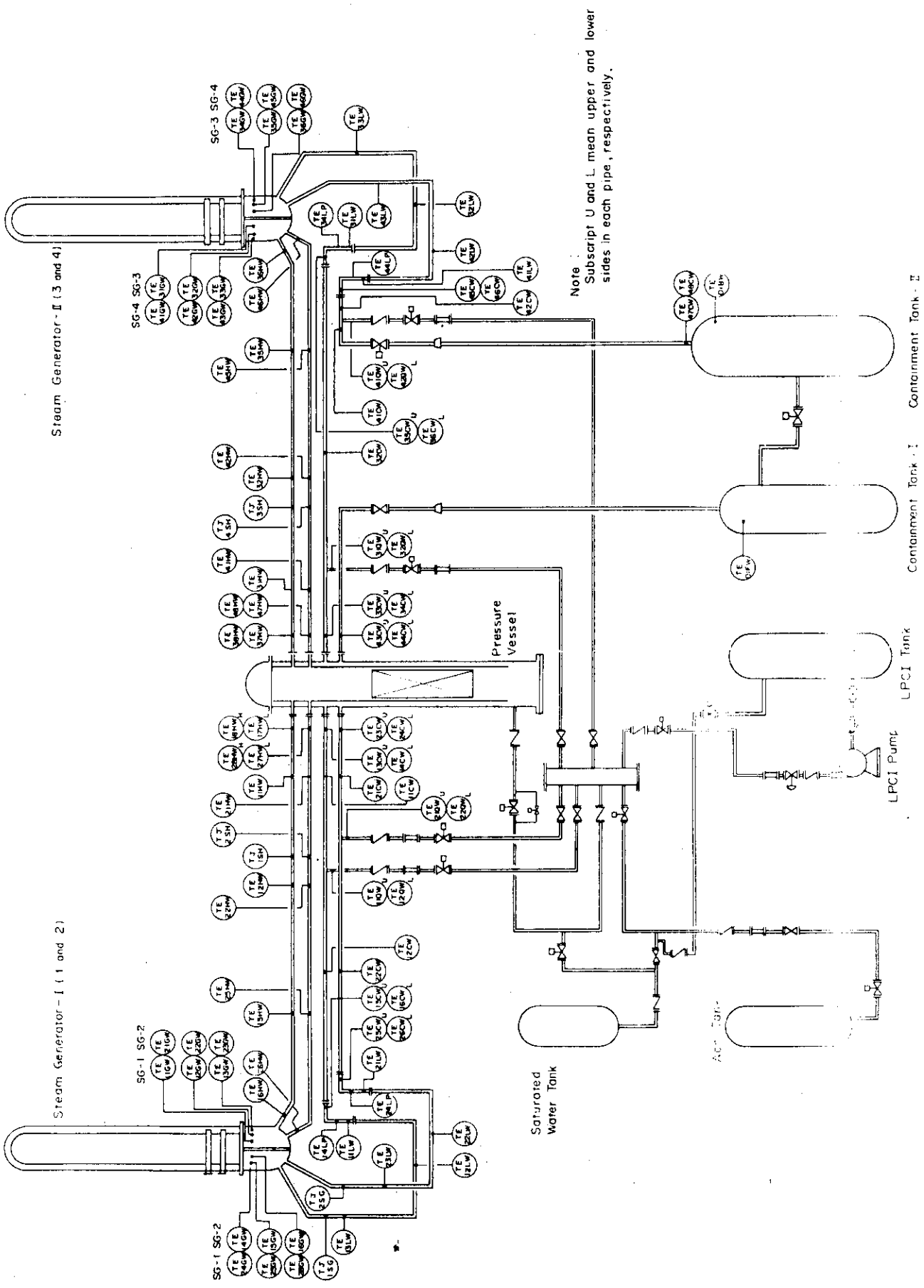

Fig.2.10 Thermocouple Locations in Primary Loop

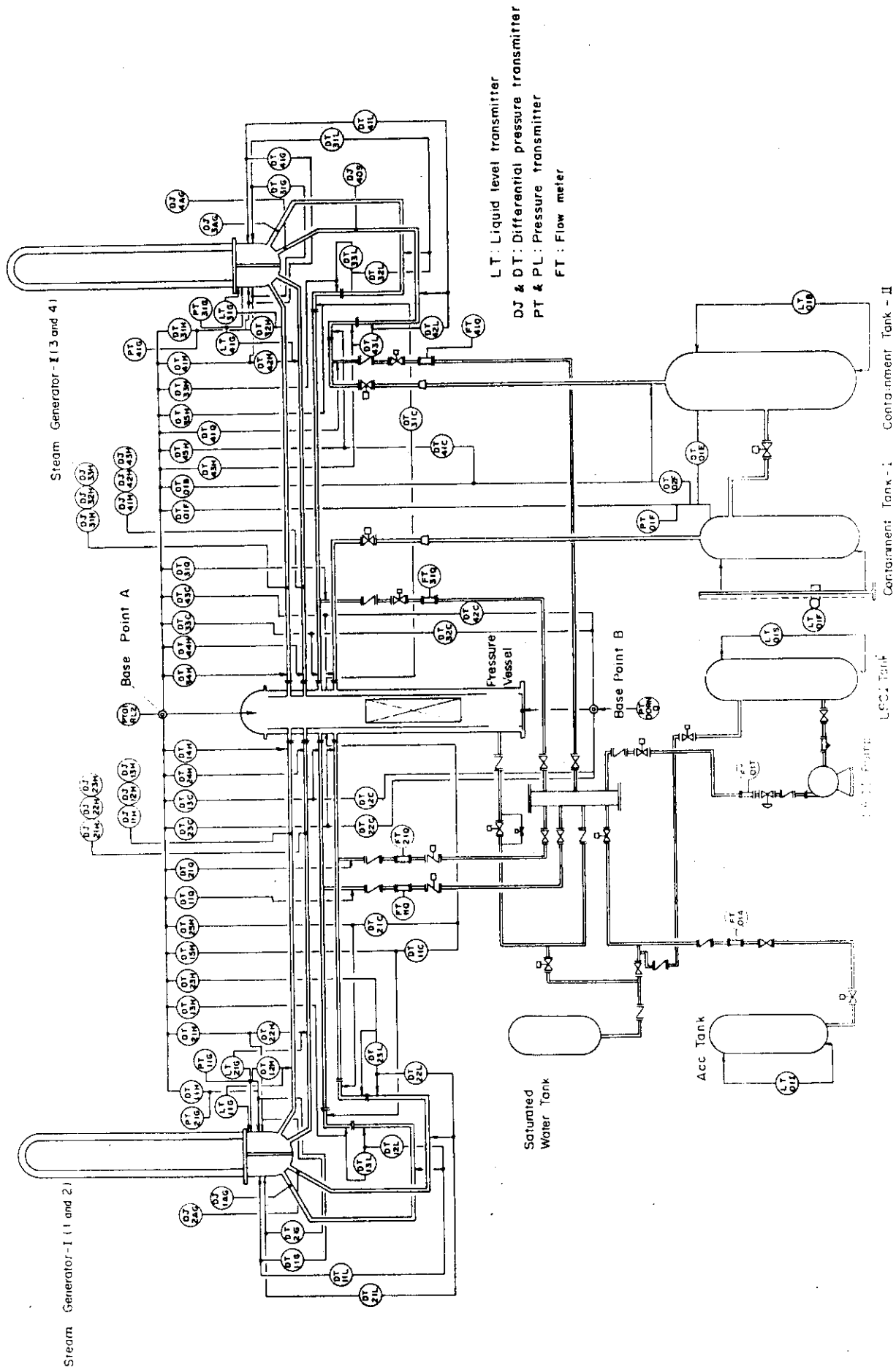

Fig.2.11 Pressure, Differential Pressure and Liquid Level Instrumentation Locations in Primary Loop

3. Results and discussion

3.1 System behavior

Figure 3.1 shows the observed differential pressures in the core and the downcomer for the three different initial clad temperature tests. With the higher initial clad temperature, the differential pressure in the downcomer is higher until about 100 s. While the core pressure drop is slightly lower with the higher initial clad temperature in the early reflood transient. Those trends are decreasing with time, and the differential pressures in the downcomer become nearly same with each other after about 200 s. The smaller core differential pressure is still observed after 200 s, which shows a long lasting effect of the initial clad temperature on the core water accumulation behavior.

The loop pressure drops are shown in Fig. 3.2. Broken and intact loop pressure drops are higher with the higher initial clad temperature in the early reflood transient. The same tendencies are observed for the mass flow rates through the loops as shown in Fig. 3.3. The mass flow rate is converted from the differential pressure across the orifice in the pump simulator downstream the steam generator assuming the single phase vapor flow. The mass flow rate through the loops are higher with the higher initial clad temperature until about 200 s. This is due to the higher steam generation rate in the core, which is caused by the larger initial stored energy. The effect of the initial clad temperature is also negligible after about 200 s. The averaged mass flow rate of the broken loop is about 40% higher than that of the intact loop.

The pressure drop across the broken cold leg nozzle is shown in Fig. 3.4. Large difference between the broken and the intact loop pressure drops shown in Fig. 3.2 is attributed to the pressure drop between the broken cold leg nozzle at the pressure vessel and the Containment 1. The pressure drop across the broken cold leg nozzle is higher with the higher initial clad temperature, due to the higher mass flow rate in the intact loops as shown in Fig. 3.3. Figure 3.5 shows the water mass flow rates through the broken cold leg nozzle measured by the water accumulation rate in the Containment 1. The water mass flow through the broken cold leg is higher with the higher initial clad temperature up to about 200 s. Since the water head in

the downcomer is higher with the higher initial clad temperature as shown in Fig. 3.1, it is considered that this is due to the higher vapor mass flow rates through the intact loops, causing the more entrained water in the upper part of the downcomer.

Figure 3.6 shows the superficial steam velocity at the core outlet evalulated by the heat balance in the core region. The superficial steam velocity was evaluated by the heat balance of the decay power input, the heat release of the stored energy, and the energy required to heat up the core inlet water to a saturation temperature. The superficial steam velocity is higher in the early transient, probably due to the higher heat release of the initial stored energy with the higher initial clad temperature.

Figure 3.7 shows the differential pressure between the top of the pressure vessel and the upper surface of the upper core support plate (UCSP) in the upper plenum. Although the the magnitude of the difference between the tests is relatively small, the higher initial clad temperature tends to cause a smaller amount of water accumulation in the upper plenum in the early reflood transient. This can be attributed to the higher steam mass flow rate at the core outlet as already shown in Fig. 3.6. Since the vaporization or the condensation can be negligible in the upper plenum, this means that the deentrainment efficiency is lower with the higher vapor mass flow rate in the upper plenum. The effect of the initial clad temperature on the water accumulation in the upper plenum appears to last longer than those on the loop behaviors. This is because the water accumulation in the upper plenum is closely related to the thermo-hydraulic behavior in the core, which is shown in the following sections.

3.2 Core inlet flow conditions

Figure 3.8(a) shows the effect of the initial clad temperature on the mass flow rate into the core. The mass flow rate is based on the mass balance calculation using the differential pressure measurements in the core and the upper plenum, and the flow measurement at the pump simulator orifice. The core inlet mass flow rate tends to be smaller with the higher initial clad temperature just after the reflood initiation. This is due to the larger pressurization in the upper plenum, which was caused by the larger steam generation rate

in the core. However, the integrated core inlet mass flow rate shown in Fig. 3.8(b) is almost identical with each other after about 20 s. It was found that about 5 kg/s (2 cm/s) of the core inlet mass flow rate (liquid velocity) was preserved for the rest of the transient.

Figure 3.9 shows the effect of the initial clad temperature on the dynamic behavior of the differential pressure in the lower plenum. The oscillatory behavior with the period of several seconds was observed at the beginning of the reflood initiation. The measured location of the differential pressure is just below the lowest portion of the core, therefore, the observed oscillation is closely related to the flow oscillation of the core inlet mass flow rate. The larger amplitude of the oscillation with the higher initial clad temperature, can be attributed to the larger fluctuation of the generated steam in the core during the Acc injection period. This is because the high ECC injection rate tends to force the water into the core, whereas the pressurization in the upper plenum due to the steam generation retards the core inlet flow. The oscillation lasted 20 s at most, and no regular oscillation is observed after 20 s. Therefore, the effect of the oscillation is only significant just after the reflood initiation, and it is almost negligible for the rest of the transient.

The fluid temperature at the core inlet is shown in Fig. 3.10. The initial clad temperature gives little effect on the core inlet water temperature after about 100 s. However, the slightly higher fluid temperature is observed for 800°C (1073 K) test before 100 s. The fluid temperature of 800°C test shows the coincident oscillatory behavior with the differential pressure oscillation shown in Fig. 3.9. Therefore, the higher fluid temperature appears to be the result of the better mixing of the hot water in the lower part of the core and the water in the lower plenum due to the flow oscillation.

3.3 Core thermo-hydraulic behavior

The temperature histories of the maximum powered rod at the mid-plane (1.83 m elevation) is shown in Fig. 3.11. The clad temperature gradually increases after the reflood initiation and it reaches its maximum at the turnaround point. The clad temperature is then decreasing to the quench point where the temperature rapidly decreases to a

saturation temperature. The temperature rise is defined as the difference between the turnaround and the initial clad temperatures. The higher initial clad temperature results in the higher turnaround temperature and the later quench time as expected. The quench temperature does not appear to be affected by the initial clad temperature.

Figure 3.12 shows the axial distribution of the turnaround and the quench times of the medium powered rod in the middle power region. The mean values of the 16 data are indicated in the figure with a standard deviation (σ_{n-1}). Turnaround times are nearly the same at a given elevation for the three cases. While the quench times are later with the higher initial clad temperature due to the slower quench front propagation especially in the lower part of the core. The quench front tends to advance at nearly the same rate after about 100 s.

Figure 3.13 shows the axial distribution of the turnaround and the quench temperatures, and a temperature rise of the same average powered rods as in Fig. 3.12. The quench temperature is slightly higher with the higher initial clad temperature, especially in the lower part of the core. The maximum clad temperature was experienced at either 1.83 m or 2.44 m elevation in the upper part of the core. The higher turnaround temperature is to be expected with the higher initial clad temperature, however, the temperature rise generally decreases with the higher initial clad temperature.

The safety margin of the fuel rod temperature can be expressed as the difference between the allowable peak clad temperature and the turnaround temperature. Figure 3.14 shows two extrapolation methods of the clad temperature obtained with a lower initial clad temperature to a higher temperature case. One simple method is shown by a shifted temperature history upward in order to evaluate the turnaround temperature for a higher initial clad temperature. Another method is the application of the heat transfer coefficient to the higher temperature case. As shown in the figure, the experimental results with the lower initial clad temperature can be conservatively extrapolated to the higher temperature case, by shifting the temperature history upward. It is also shown that the use of the heat transfer coefficient gives a more reasonable estimation of the calculated peak clad temperature.

Analysis of the quench front velocity by Murao[3] has shown that the quench front velocity, u_q, is expressed as

$$u_q^{-1} = \frac{C_p \rho\{T_q - (594.2 + 2.32 \times 10^4 P)\}}{254.5\ (1 + 2.778 \times 10^{-5}\ \Delta T_{sub}^3)} \quad . \qquad (1)$$

The comparision of the measured and the calculated quench front velocities against the measured quench temperature are shown in Fig. 3.15. Although a good agreement with the data was not obtained for the lower quench temperature, the calculation shows a fairly good agreement for the higher quench temperature.

The heat transfer coefficient and the heat flux of the maximum powered rod at the midplane are shown in Fig. 3.16. With the higher initial clad temperature, the heat transfer coefficient is slightly higher just after the reflood initiation. It then becomes slightly lower near the turnaround through the quench times. The difference of the heat transfer coefficient among three tests is quite small before the turnaround time. This indicates that the heat transfer coefficient obtained with the lower initial clad temperature can be applicable to a higher temperature case to better estimate the maximum temperature than the use of the shifted temperature history. The heat flux is higher with the higher initial clad temperature until the turnaround due to the higher temperature difference as shown in Fig. 3.16.

The comparison of the measured and the calculated heat transfer coefficients are shown in Fig. 3.17. The calculation is performed based on the correlation developed by Murao and Sugimoto[4] for the saturated film boiling flow. The correlation is written as

$$h = 0.94(1-\alpha)^{1/4} \left(\frac{\lambda_g^3 \rho_g \rho_\ell H_{fg}}{L_q \mu_g \Delta T_{sat}} \right)^{1/4} + \varepsilon\sigma(1-\alpha)^{1/2} \frac{T_w^4 - T_s^4}{\Delta T_{sat}} \quad . \qquad (2)$$

Although the correlation tends to slightly underestimate the heat transfer coefficient near the quench point, a reasonable agreement with the data was obtained. This implies that the flow regime above the quench front is more like a film boiling flow or a slug flow with fairly low void fractions, rather than a dispersed flow with extremely high void fractions.

Figure 3.18 shows the void fraction at several elevations in the core. The void fraction was evaluated from the differential pressure measurement neglecting the frictional presssure loss. The measured locations and the time when the quench front reached the upper pressure tap are indicated in the figure. The void fraction decrease is rapid

during the accumulator injection period due to the high flooding rate into the core. The void fraction then decreases slowly untill the quench front reaches the upper pressure tap. The higher initial clad temperature tends to give the higher void fraction before the quench time. It is considered that this is due to the higher vapor flow rate and the slower quench front propagation until the quenching occures at a given elevation. As the quench front moves at nearly the same rate in the upper part of the core as shown in Fig 3.12, the effect of the initial clad temperature on the core thermal and hydraulic behaviors last longer than that on the system behavior.

3.4 Comparison with FLECHT data

Figure 3.19 shows the temperature rise and the quench time versus initial clad temperature in CCTF and FLECHT[1] tests. The FLECHT data are based on the forced-feed flooding test and the system pressure is higher (0.28 MPa) than the CCTF tests described here (0.2 MPa). The averaged core flooding rate in the CCTF tests is nearly same as that of FLECHT tests (2 cm/s) during LPCI injection period as shown in Fig. 3.8, however, the temperature rise of CCTF tests is generally smaller than FLECH data. It is considered that this is due to tne large effect of the peaking factor of the heater rods and also of the accumulator injection period in the CCTF tests. The peaking factor of CCTF and FLCHT are 1.49 and 1.66, respectively, and the flooding rate of the CCTF tests is several times higher than that of FLECHT tests for the first crucial 13 s. The similar trends, that is the decreasing temperature rises and the increasing quench times with the higher initial clad temperature, are obtained for both CCTF and FLECHT tests as shown in Fig. 3.19.

Also shown in the figure are the results of the Evaluation Model (EM) test[5] in CCTF. The nominal initial clad temperathre of the EM test is 1143 K (870 °C), and the ECC flow rates are about 30 % higher than those of the present parametric tests. As shown in Fig. 3.19 the quench time of the EM test can be extrapolated from the data of the present parametric tests. However, the temperature rise is rather lower than the extrapolated value. This again shows that the ECC flow rate much affects the core heat transfer, especially the temperature rise in the early reflood transient.

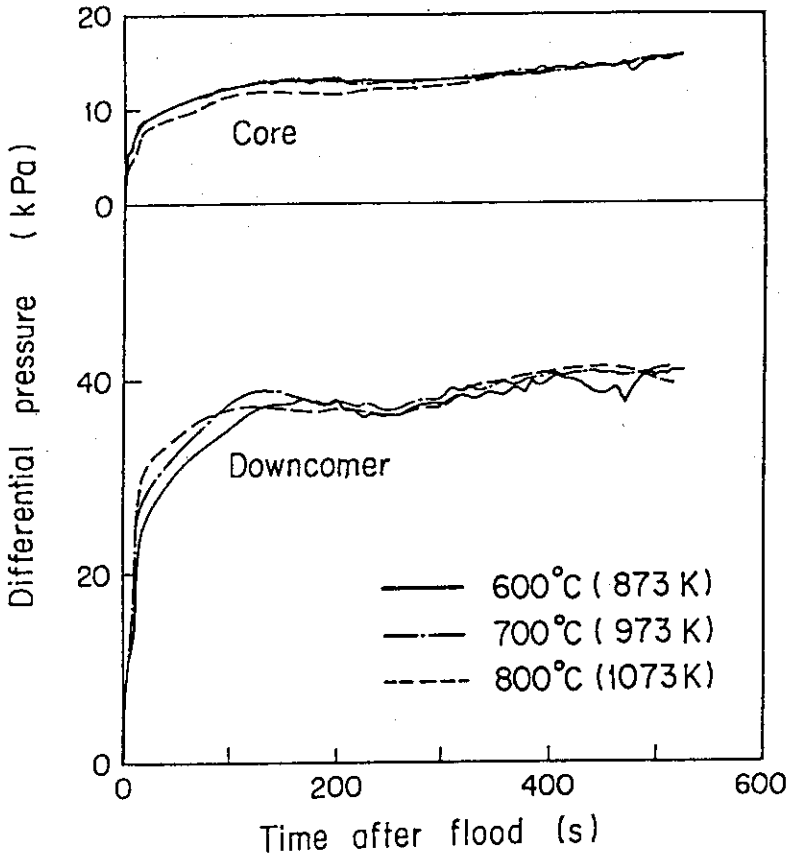

Fig. 3.1 Effect of initial clad temperature on differential pressure in core and downcomer

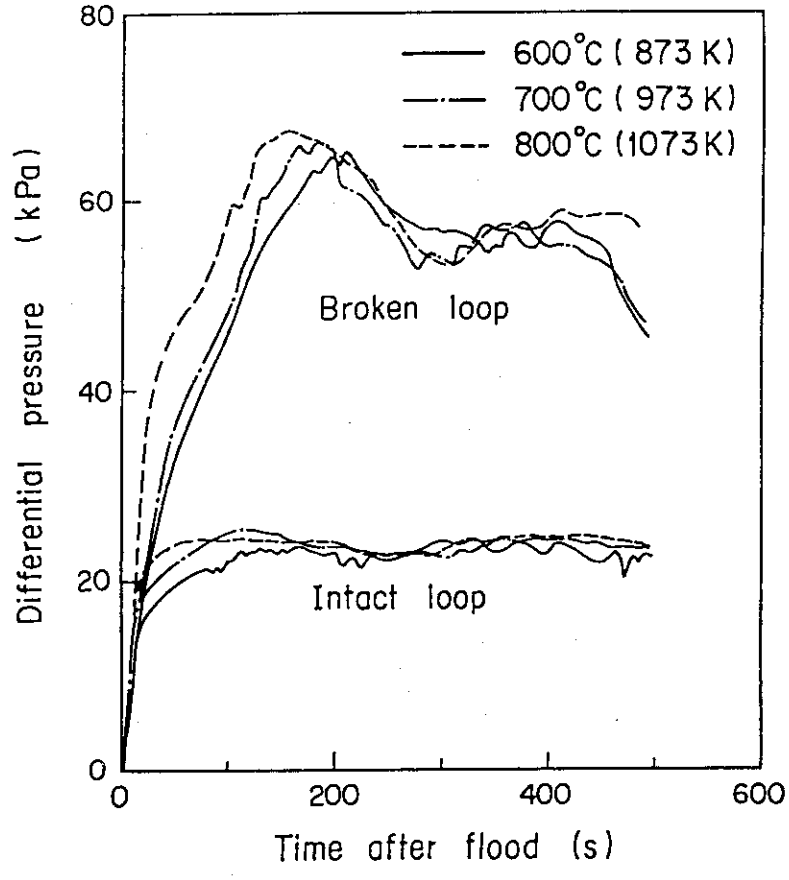

Fig. 3.2 Effect of initial clad temperature on loop pressure drop

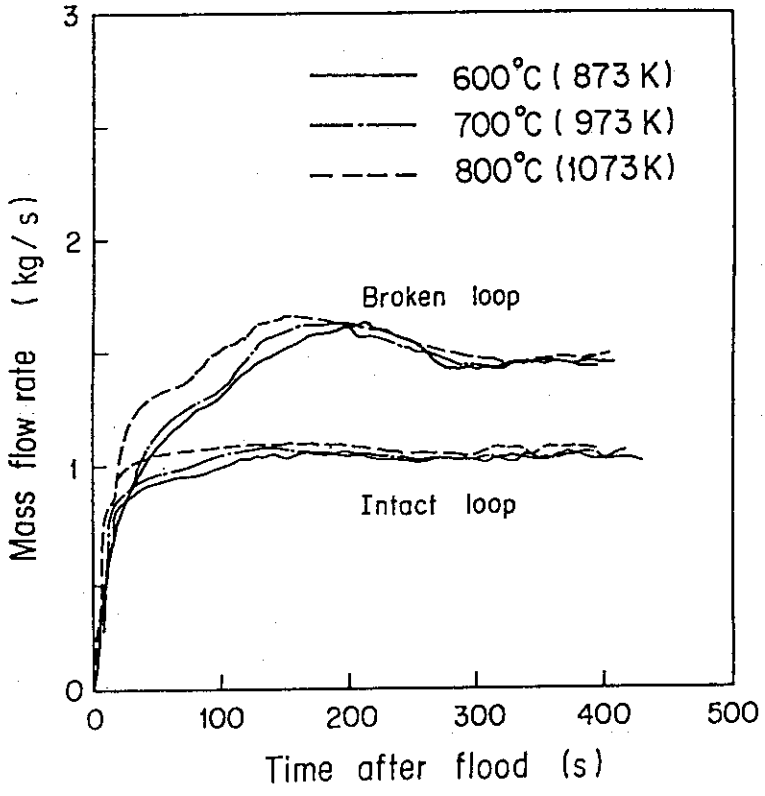

Fig. 3.3 Effect of initial clad temperature on mass flow rate through loops

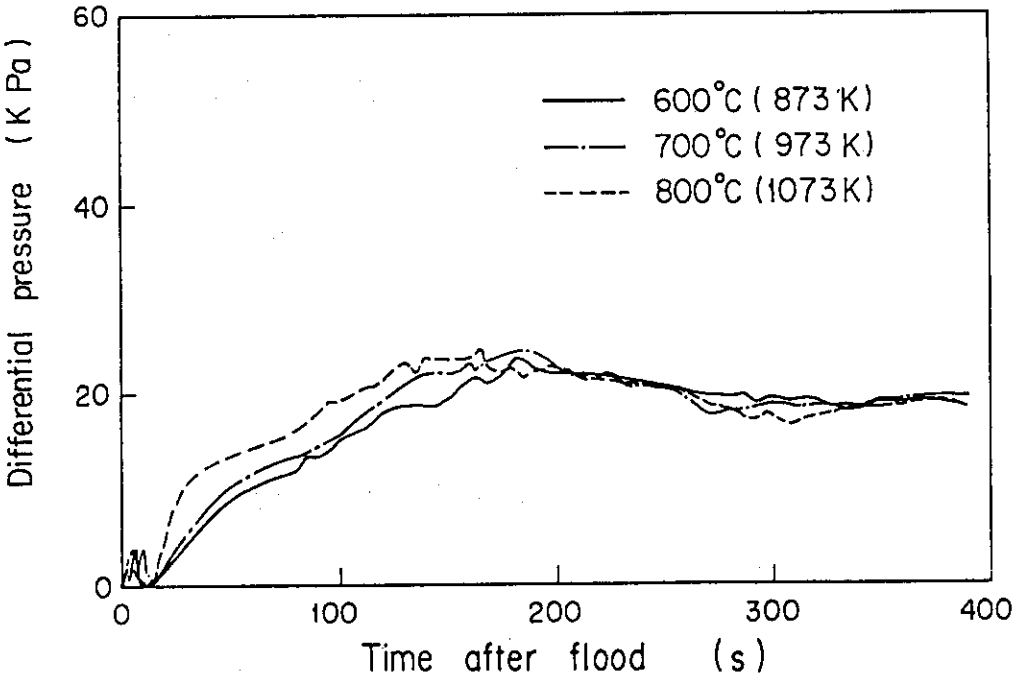

Fig. 3.4 Effect of initial clad temperature on pressure drop at broken cold leg nozzle

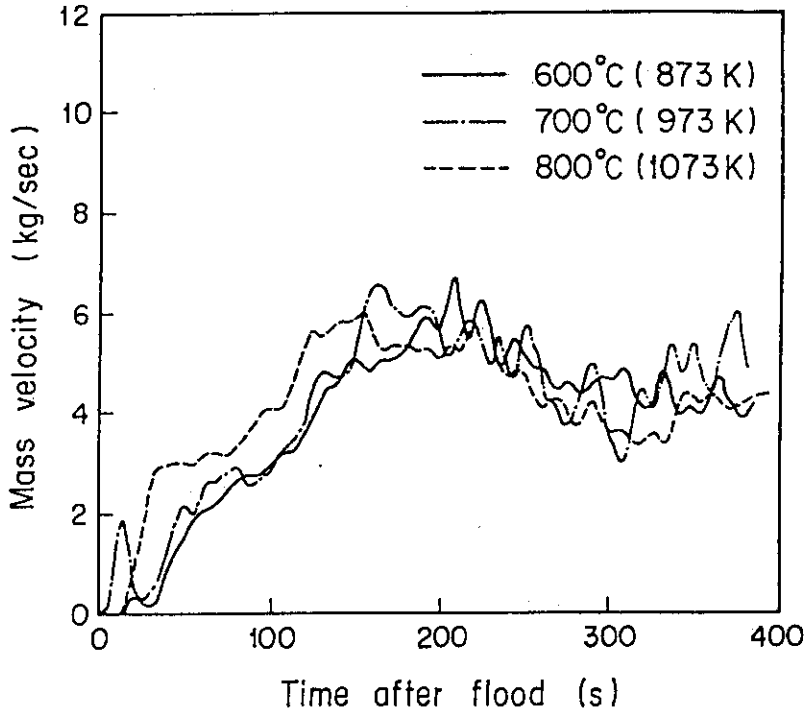

Fig. 3.5 Effect of initial clad temperature on water mass flow rate through broken cold leg

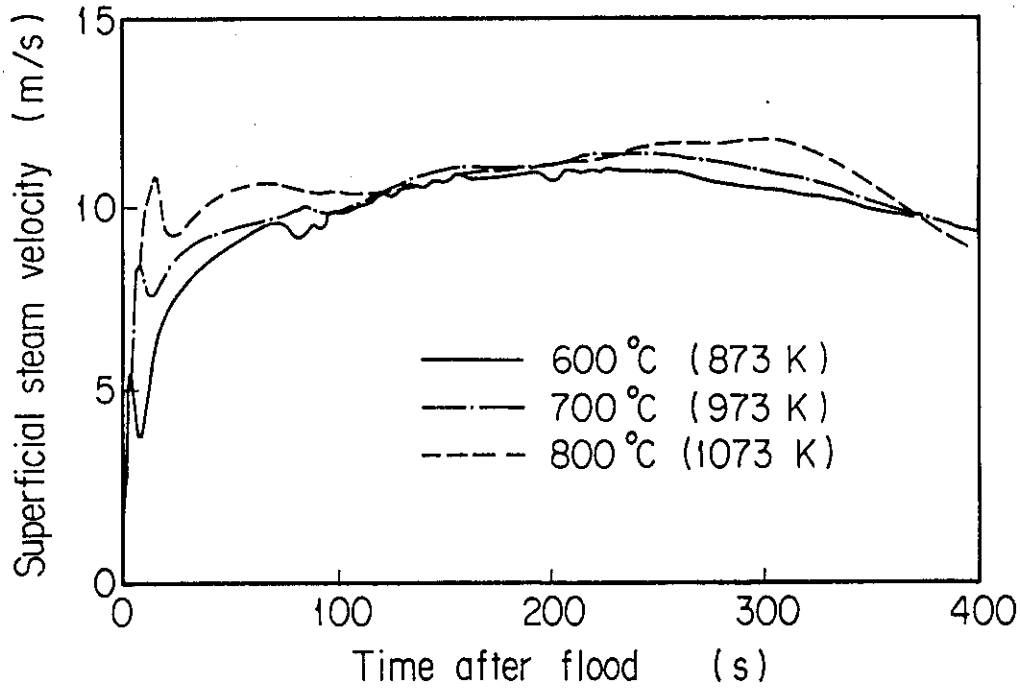

Fig. 3.6 Effect of initial clad temperature on core exit steam mass flow rate

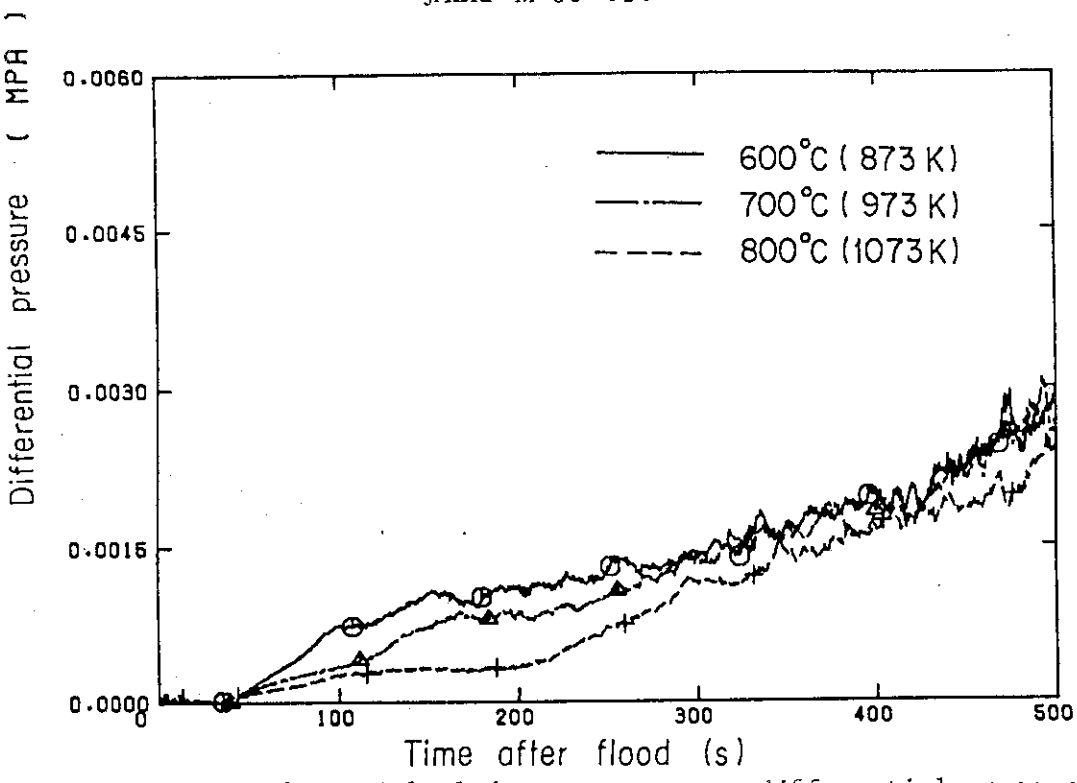

Fig. 3.7 Effect of initial clad temperature on differential pressure in upper plenum

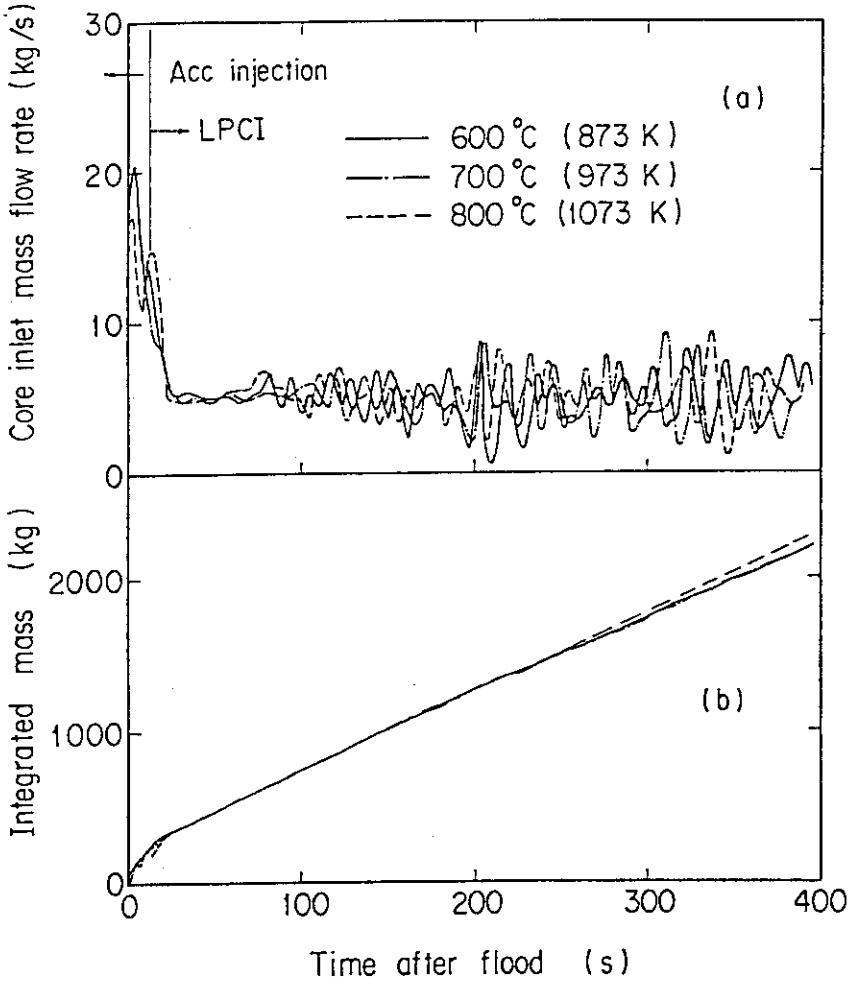

Fig. 3.8 Effect of initial clad temperature on core inlet mass flow rate

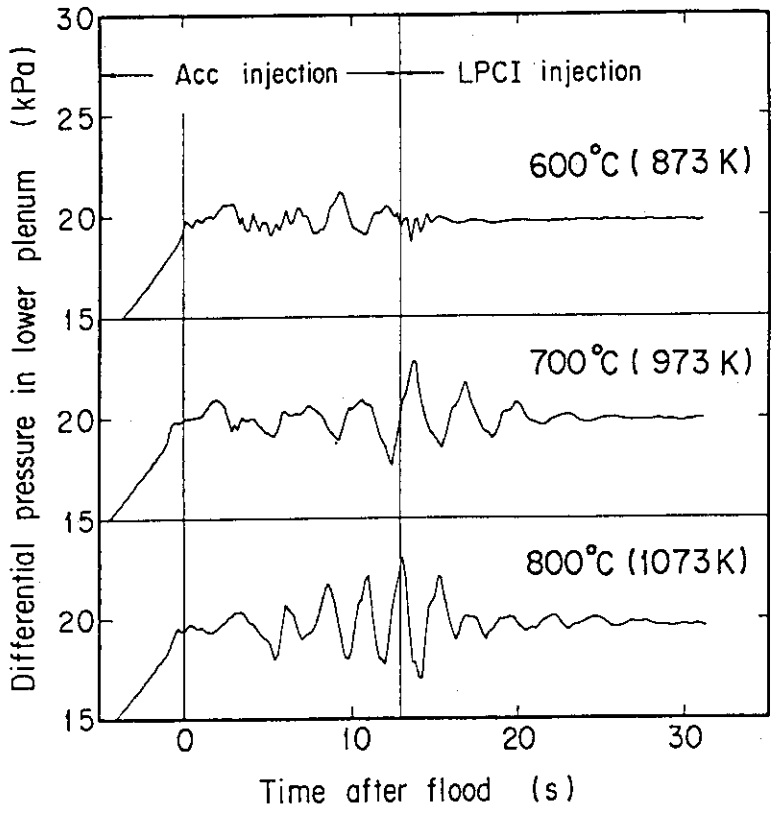

Fig. 3.9 Effect of initial clad temperature on dynamic behavior of differential pressure in lower plenum

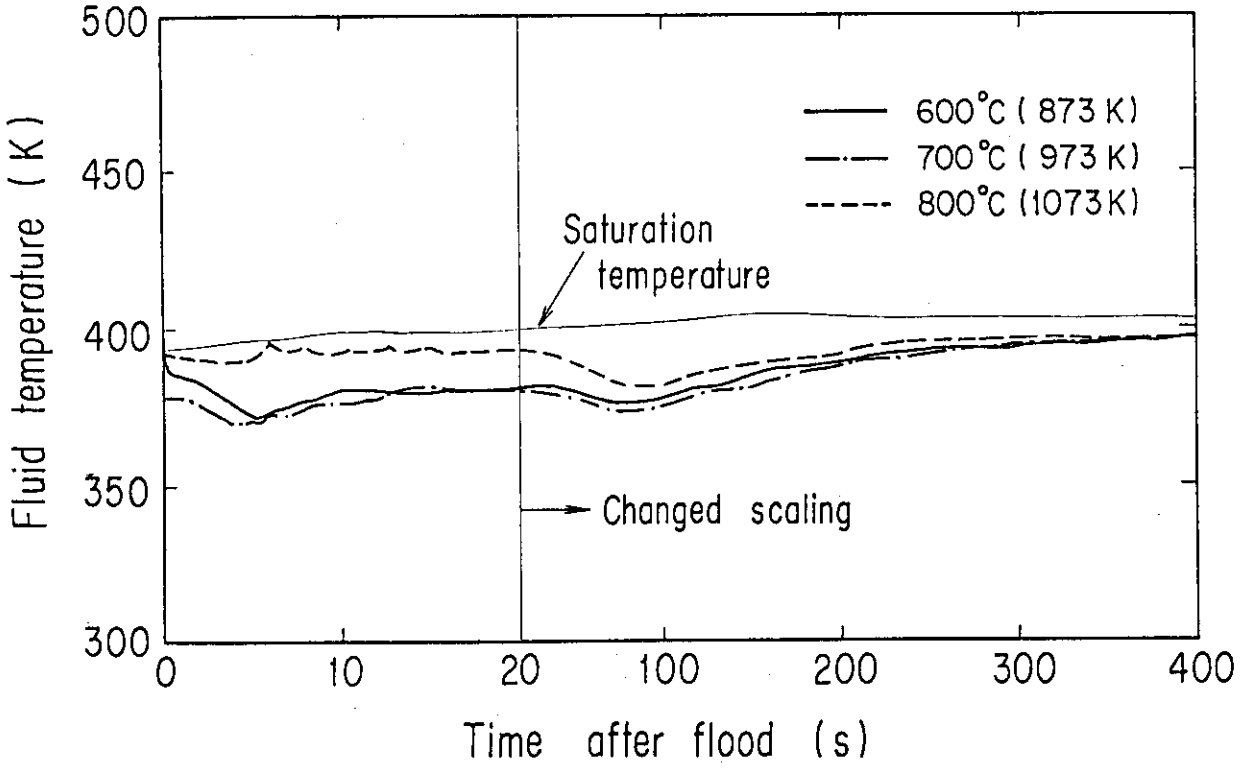

Fig. 3.10 Effect of initial clad temperature on fluid temperature at core inlet

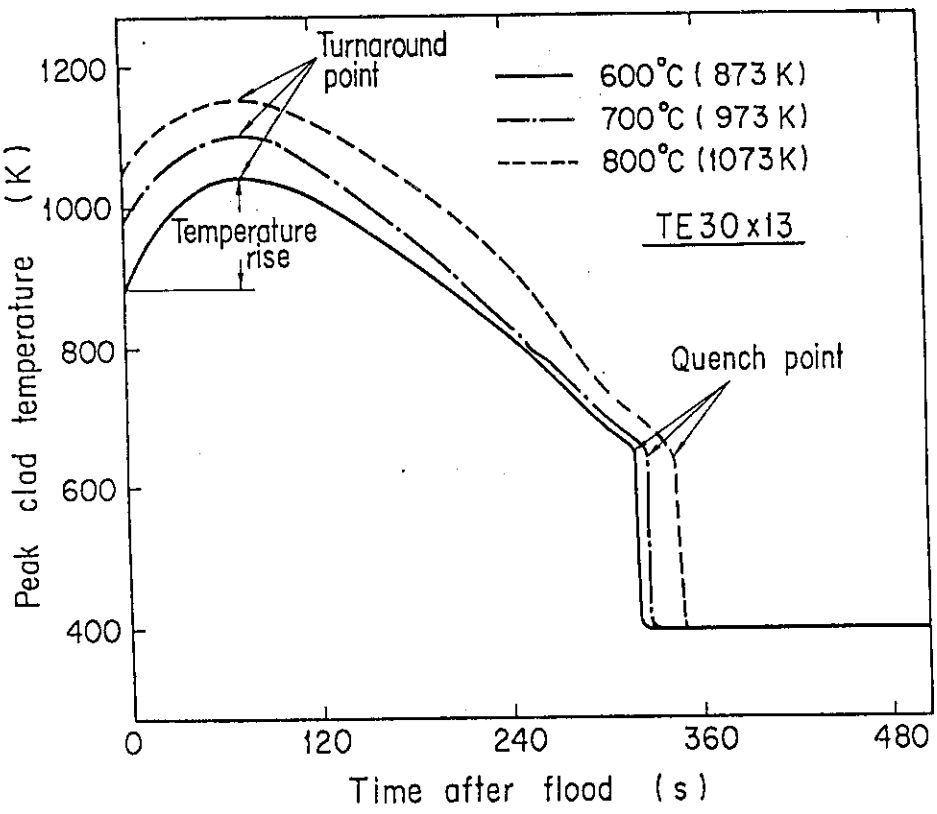

Fig. 3.11 Effect of initial clad temperature on midplane peak clad temperature

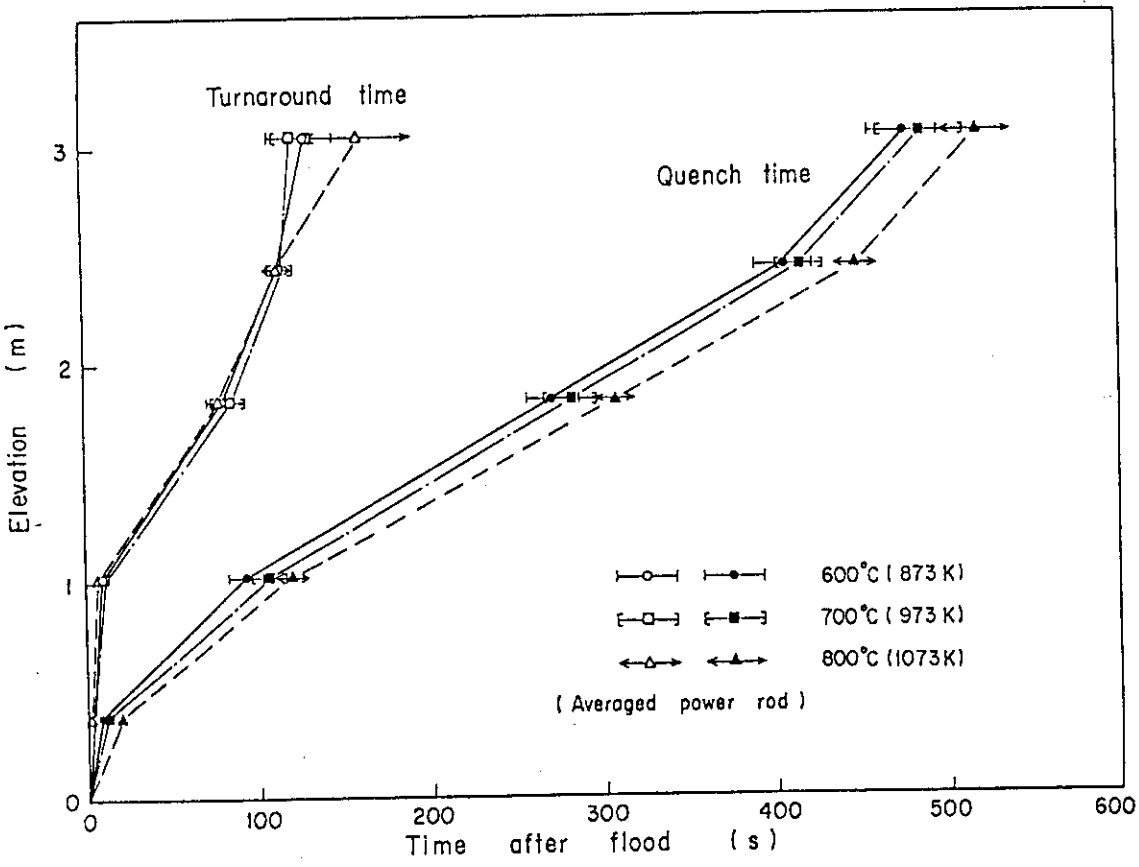

Fig. 3.12 Effect of initial clad temperature on turnaround and quench times

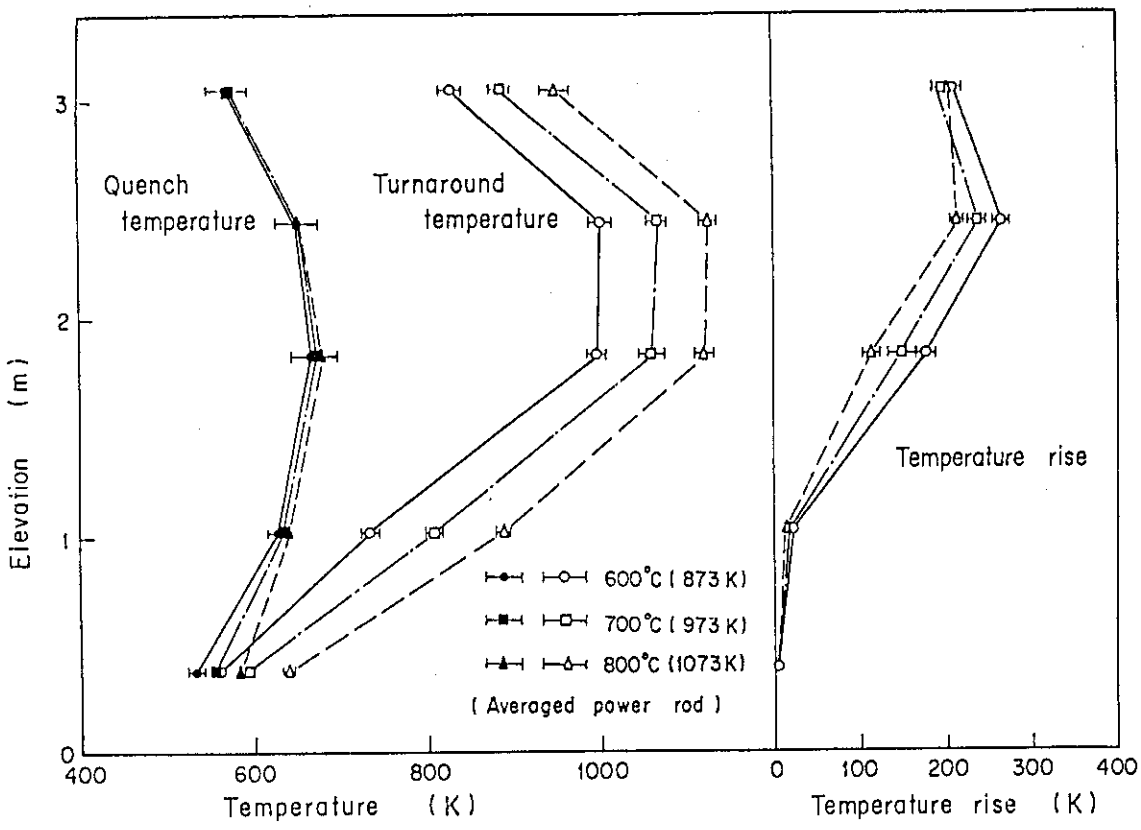

Fig. 3.13 Effect of initial clad temperature on turnaround and quench temperatures, and temperature rise

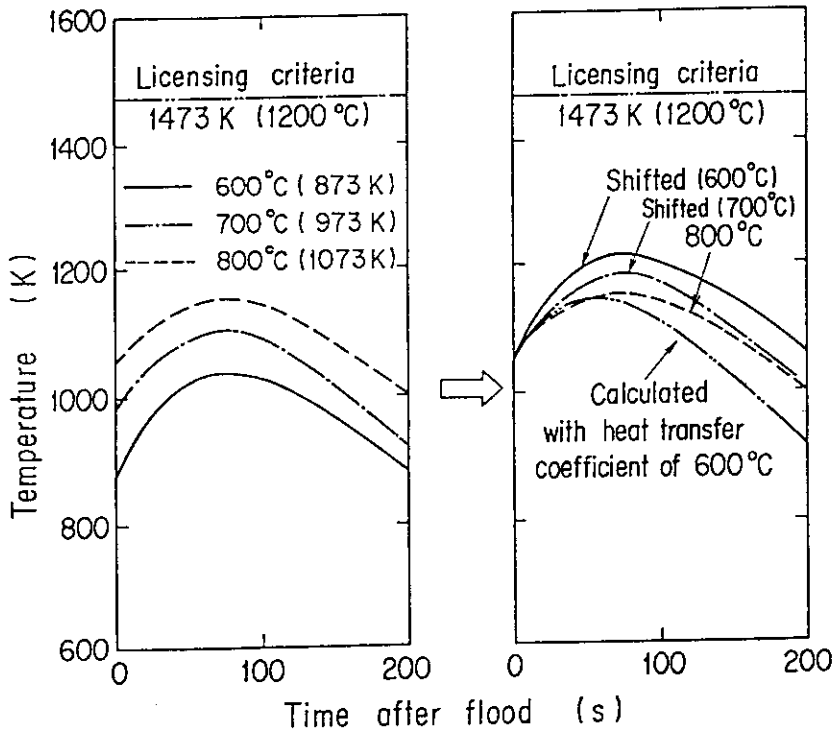

Fig. 3.14 Extrapolation methods of clad temperature obtained with lower initial clad temperature to higher temperature case

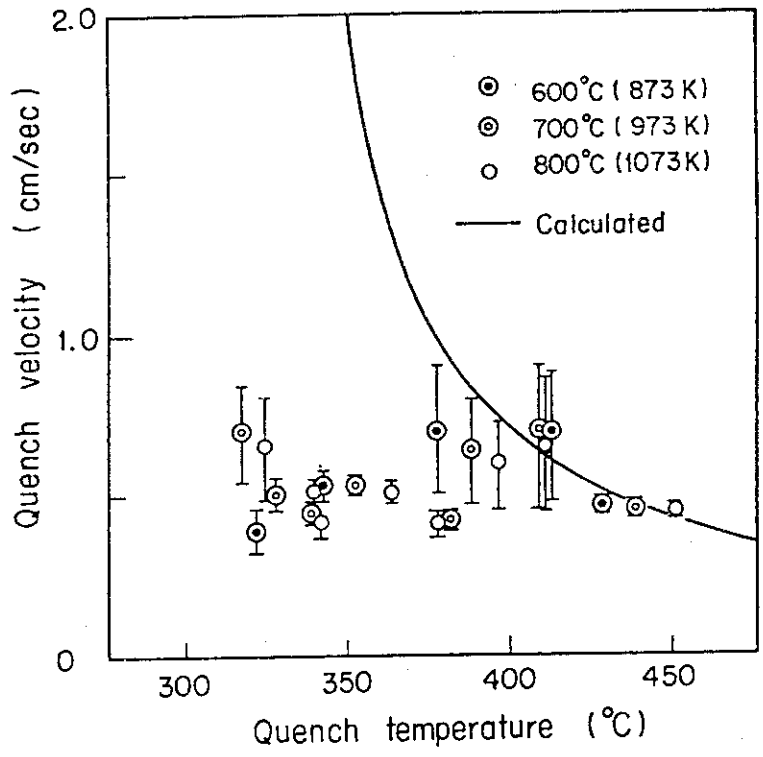

Fig. 3.15 Measured and calculated quench front velocity

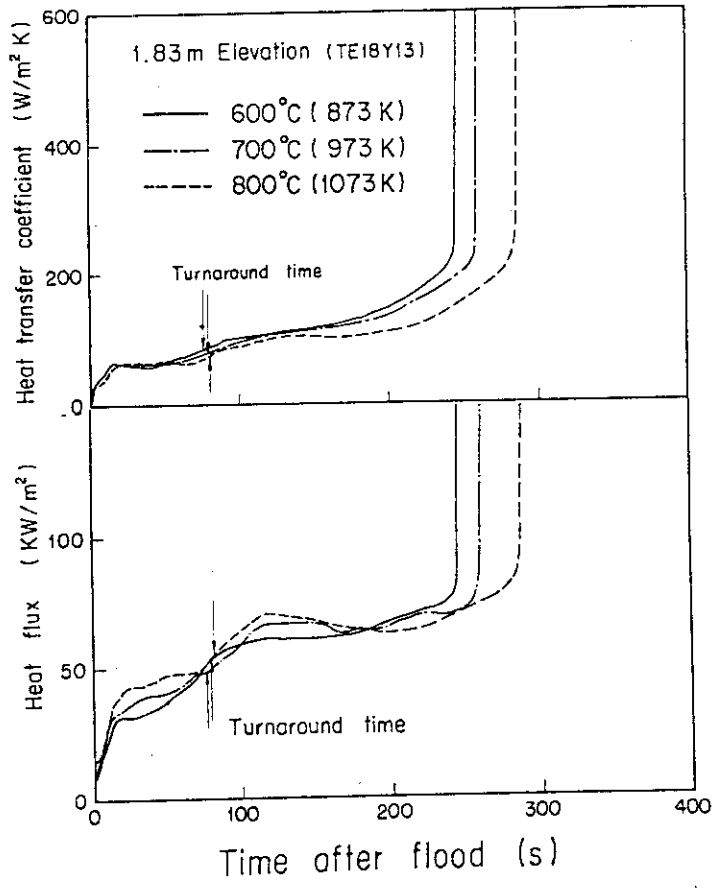

Fig. 3.16 Effect of initial clad temperature on heat transfer coefficient and heat flux at midplane

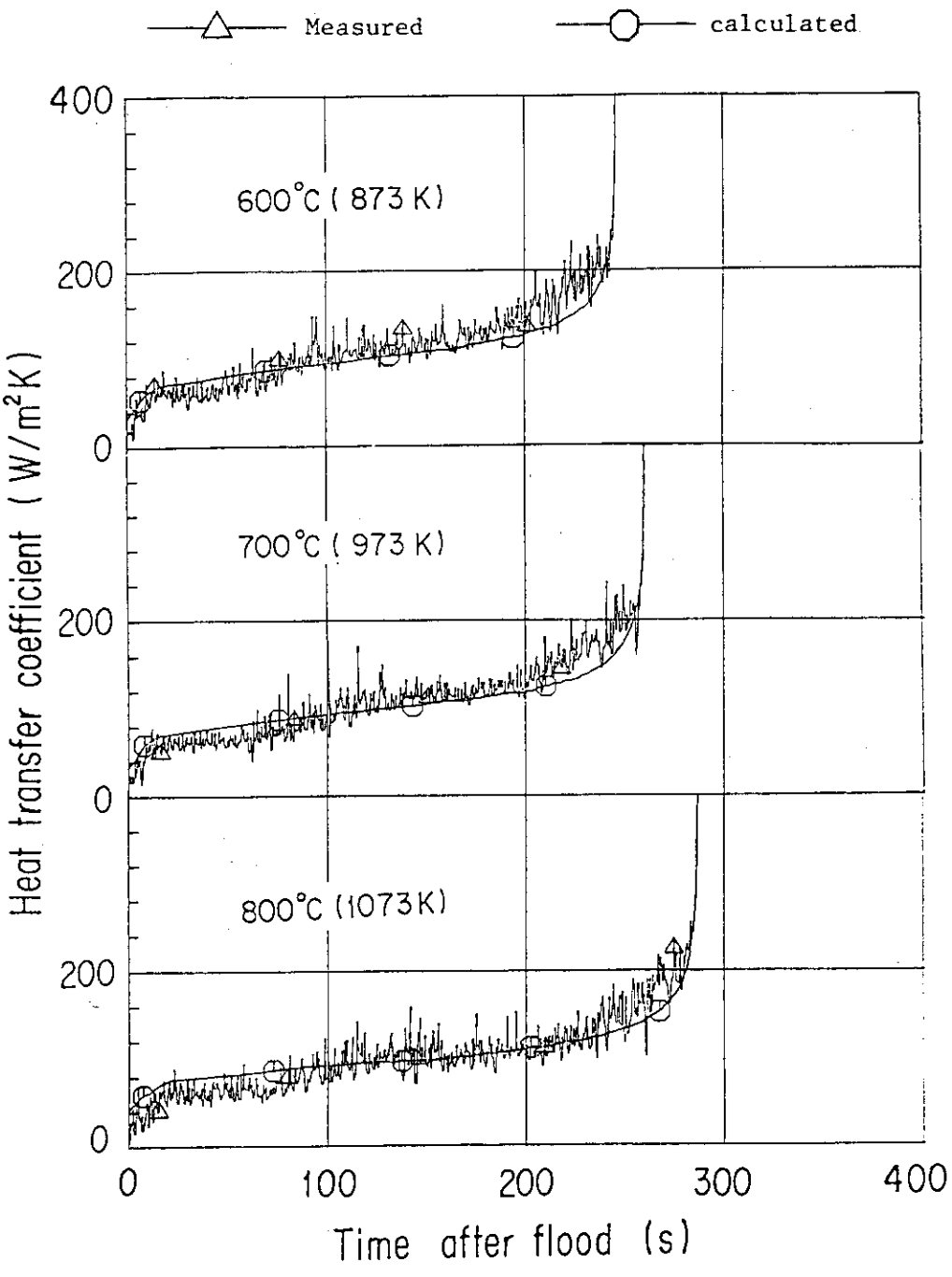

Fig. 3.17 Measured and calculated heat transfer coefficient at midplane

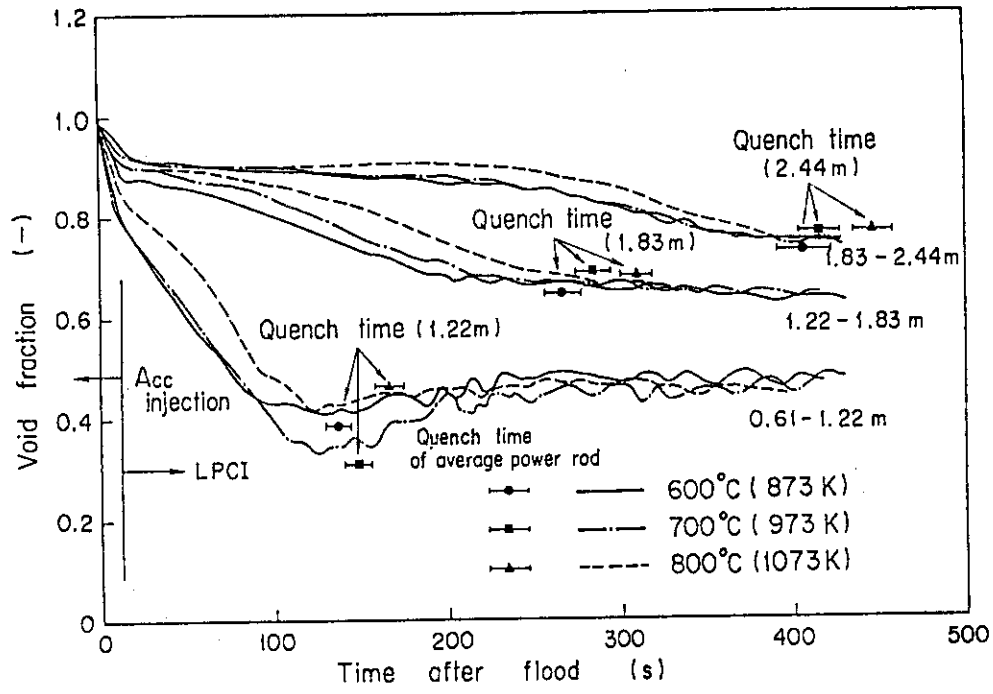

Fig. 3.18 Effect of initial clad temperature on void fractions in core

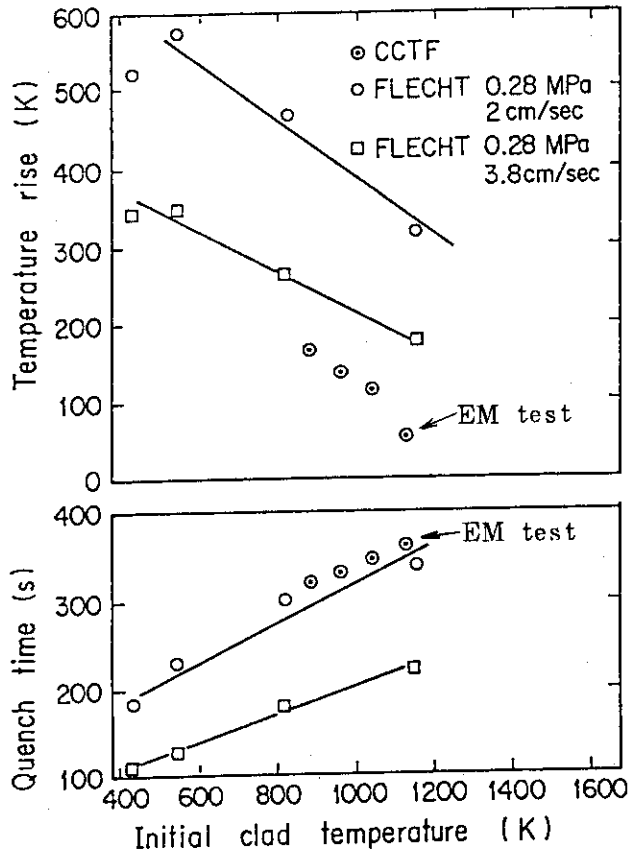

Fig. 3.19 Comparison of temperature rises and quench times versus initial clad temperature in CCTF tests and FLECHT

4. Conclusions

The effects of the initial clad temperaure on the reflood phenomena in the CCTF tests were investigated. The following conclusions were obtained:

(1) With the higher initial clad temperature, the higher water accumulation in the downcomer, the higher loop mass flow rate and the lower water accumulation in the core and the upper plenum were observed during the first stage of the reflood transient due to the larger heat release of the stored energy. The effect of the initial clad temperature on these system behaviors was almost negligible after about 200 s.

(2) The core inlet flow was suppressed by the higher initial clad temperature just after the reflood initiation due to the more rapid vapor generation, however, nearly the same core inlet mass flow rates were obtained for the rest of the transient.

(3) The flow oscillation was observed in the lower plenum just after the reflood initiation. The oscillation was larger with the higher initial clad temperature, probably due to the more rapid vapor generation in the core. The oscillation lasted for less than 20 s causing little effect on the overall system behavior.

(4) In the core, with the higher initial clad temperature, the higher turnaround temperaure and the later quench time were observed. There was little effect on the turnaround time and the quench temperature. The void fraction in the core was higher with the higher initial clad temperature. The heat transfer coefficient was not much affected by the higher initial clad temperature until the turnaround time, which resulted in the lower temperature rise with the higher initial clad temperature.

(5) The heat transfer coefficient and the quench front velocity were compared with the correlations developed with the small scale reflood experiment. The calculated results were in reasonable agreement with the data on the effect of the initial clad temperature.

(6) Both CCTF and FLECHT data showed a similar core thermal behaviors concerning the effect of the initial clad temperature. The general trend of the lower temperature rise with the higher initial clad temperature was confirmed.

Acknowledgements

The authors are very grateful to Dr. M. Nozawa, director of Nuclear Safety Research Center, JAERI, Dr. S. Katsuragi, head of Div. of Nuclear Safety Research, Dr. M. Ishikawa, deputy head of Div. of Nuclear Safety Research, and Dr. K. Hirano, chief of Reactor Safety Laboratory II for their hearty suggestion and encouragement.

They are deeply indebted to Mr. T. Iguchi, Mr. T. Sudoh, Dr. H. Akimoto, and Mr. T. Okubo for their analytical support. They would like to express their appreciation to Mr. H. Adachi, Dr. Y. Sudo, Mr. M. Sobajima, Mr. T. Iwamura, Mr. M. Osakabe, and Mr. A. Ohnuki for their useful discussions, Messrs. K. Sekiguchi, Y. Fukaya, N. Suzuki, T. Oyama, T. Wakabayashi, Y. Niitsuma, J. Matsumoto, T. Nishikizawa, and H. Sonobe for their contribution to the facility operation, to Messrs. R.K. Fujita and D.H. Miyasaki, resident engineers from USNRC, and to Mr. H.G. Herdtle, resident engineer from BMFT, for their devoted help.

References

(1) Lilly, G.P., et al.: "PWR-FLECHT Cosine Low Flooding Rate Test Series Evaluation Report", WCAP-8838, March (1977)

(2) Murao, Y., et al., JAERI-M, to be published

(3) Murao, Y., J. Nucl. Sci. Technol., 15, 12, 875-885 (1978)

(4) Murao, Y. and J. Sugimoto, J. Nucl. Sci. Technol., 18, 4, 275-284 (1981)

(5) Murao, Y., et al., JAERI-M, to be published

Appendix A

Definition of Tag. IDs in Appendix B through Appendix D

Figure list

1. Definition of Tag.ID for clad surface temperatures

Notation : TENNWAM

NN : Bundle number

WA : Power zone

WA = X1, X2 : High power (Local power factor 1.1)

WA = Y1, Y2 : Medium power (Local power factor 1.0)

WA = Z1, Z2 : Low power (Local power factor 0.95)

M : Elevation

	Elevation (m)	Axial power factor
1	0.38	0.568
2	1.015	1.176
3	1.83	1.492
4	2.44	1.312
5	3.05	0.815

2. Definition of power zone and bundle number

See Fig. A-1

3. Definition of Tag.ID for void fraction

See Fig. A-2

4. Definition of Tag.ID for average linear power of heater rod in each power unit zone

See Fig. A-3

5. Definition of carry-over rate fraction (C.R.F)

$$CRF = \frac{\dot{m}_{UP} + \dot{m}_{L}}{\dot{m}_{CR} + \dot{m}_{UP} + \dot{m}_{L}}$$

The calculated data within ±25 s are averaged:

$$(CRF)_i = \frac{1}{101} \sum_{k=i-50}^{i+50} (CRF)_k$$

where

ΔP_{UP} : Average of measured data at four orientations

ΔP_{CR} : Same as above

$$\dot{m}_{UP} = A_{up} \frac{d}{dt} (\Delta P_{UP})$$

$$\dot{m}_{CR} = A_{CR} \frac{d}{dt} (\Delta P_{CR})$$

$$\dot{m}_L = \sum_{k=1}^{4} \dot{m}_{pk}$$

$\dot{m}$: mass flow rate or mass accumulation rate

ΔP: differential pressure

suffix

UP: upper plenum

CR: core

L : loop

p : primary pump

6. Definition of Tag.ID for differential pressure through downcomer, upper plenum, core and lower plenum

See Fig. A-4

7. Definition of Tag.ID for differential pressure through intact and broken loop and broken cold leg nozzle

See Fig. A-5

8. Definition of Tag.ID for fluid temperature in inlet and outlet plenum and secondary of steam generator

See Fig. A-6

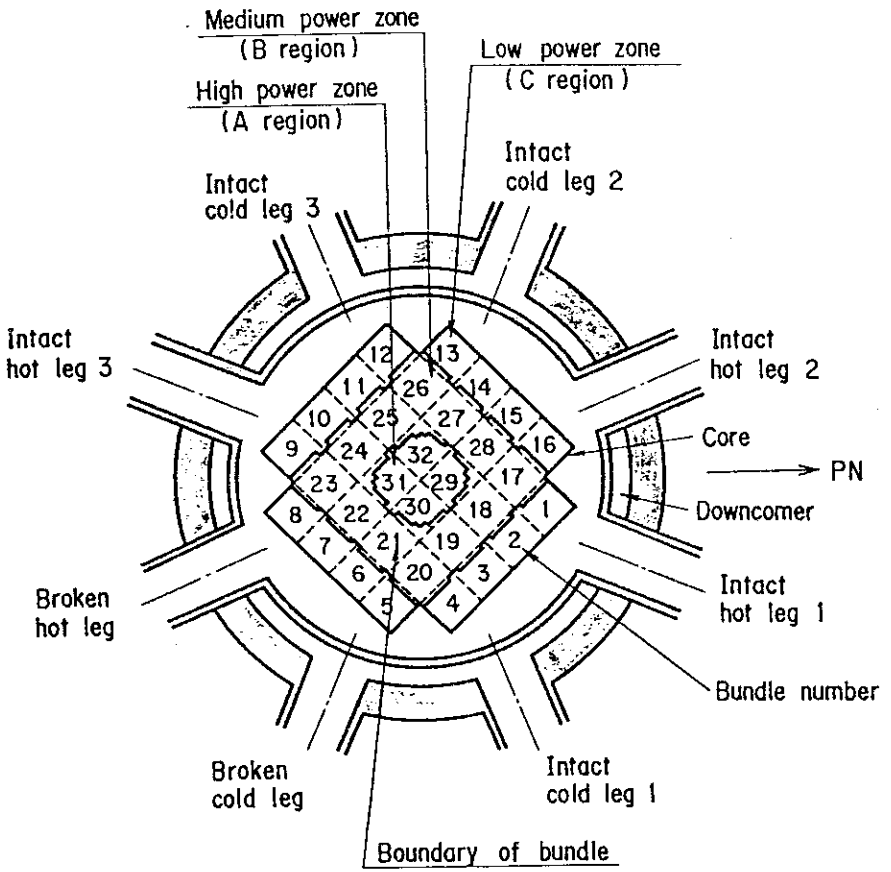

Fig.A-1 Definition of power zones and bundle numbers

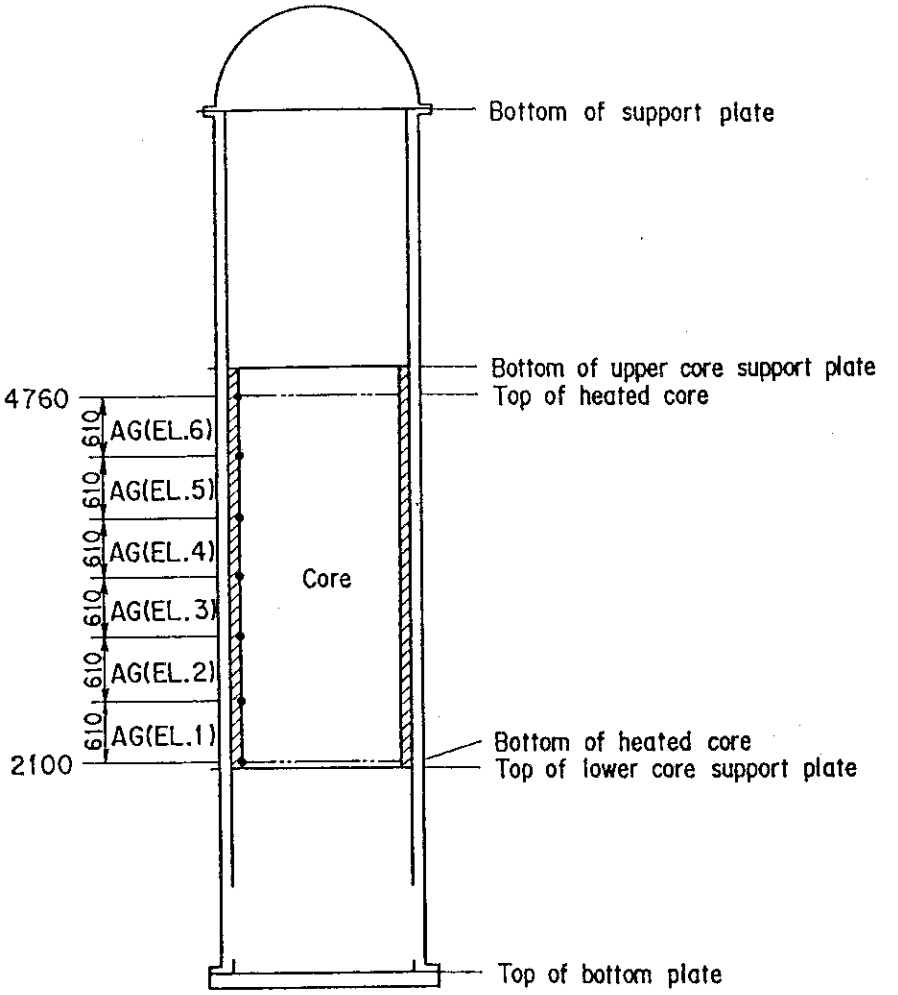

Fig.A-2 Definition of Tag.ID for void fraction (AG(EL.1)～AG(EL.6))

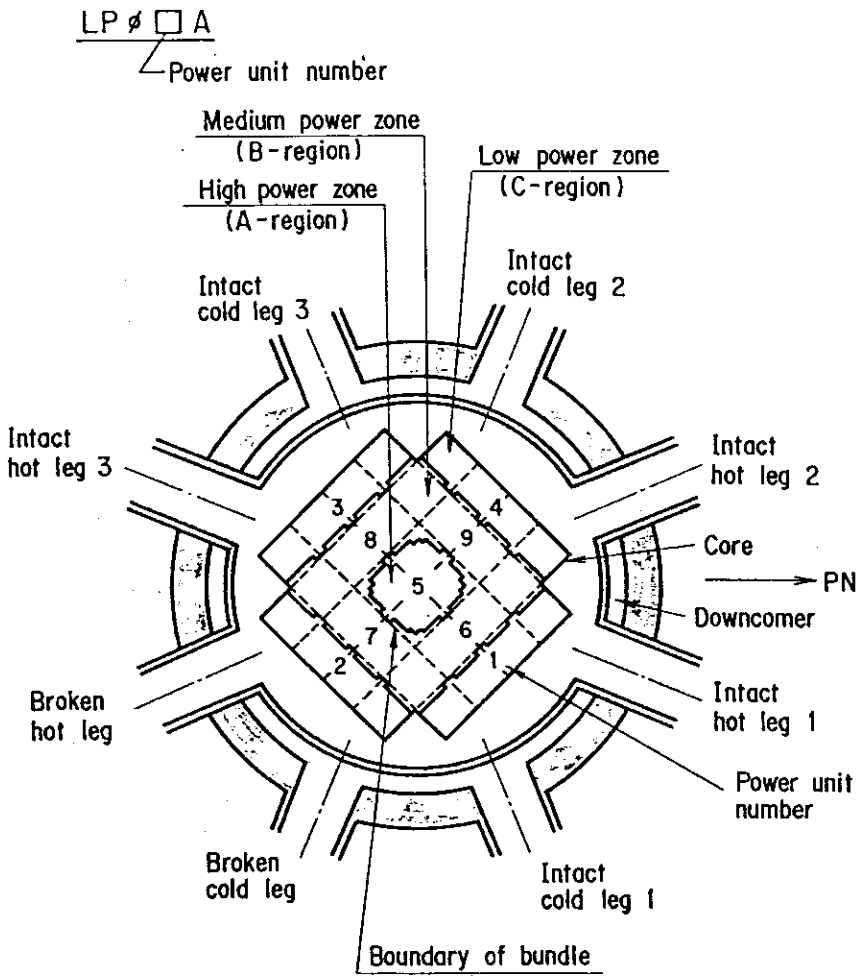

Fig. A-3 Definition of Tag. ID for average linear power of heater rod in each power unit zone (LP01A ~ LP09A)

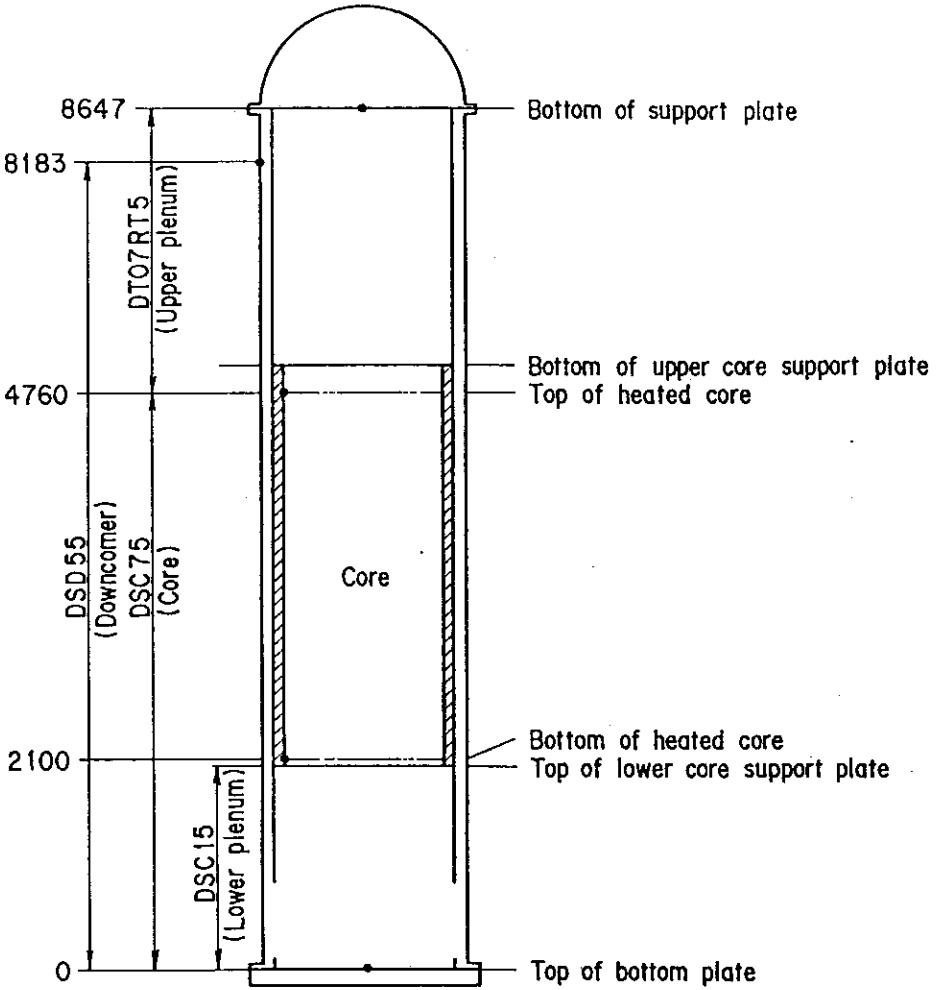

Fig. A-4 Definition of Tag. ID for differential pressure through downcomer, upper plenum, core, and lower plenum (DSD55, DT07RT5, DSC75, DSC15)

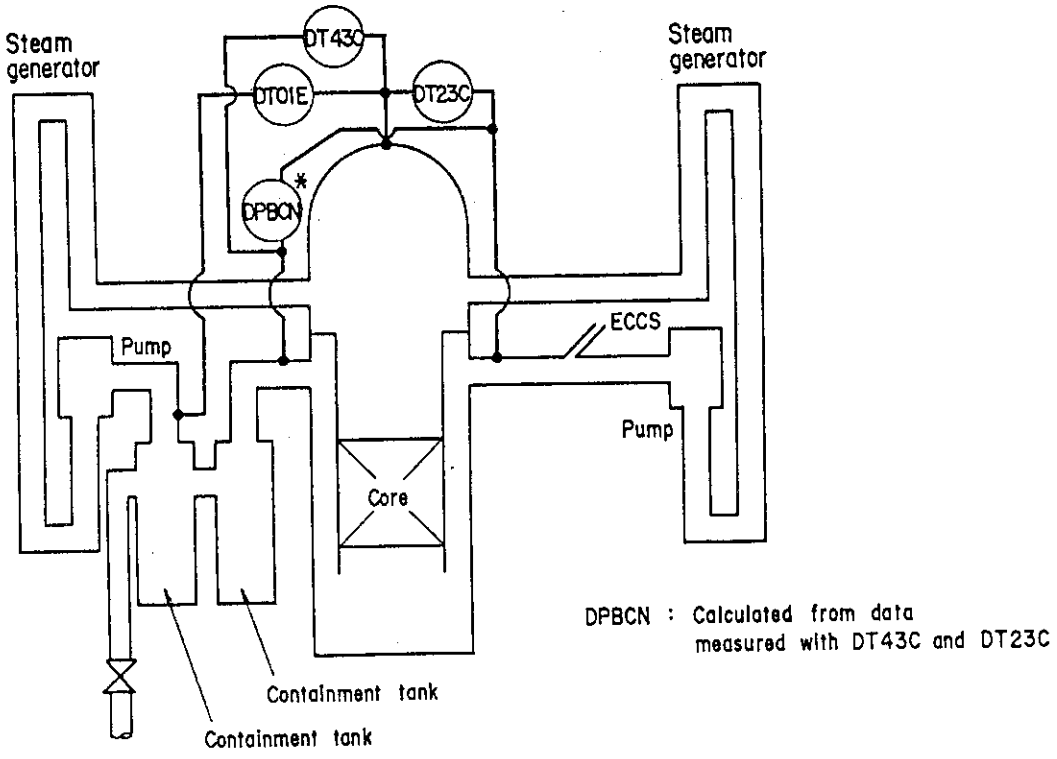

Fig. A-5 Definition of Tag. ID for differential pressure through intact and broken loop and broken cold leg nozzle (DT23C, DT01B, DPBCN)

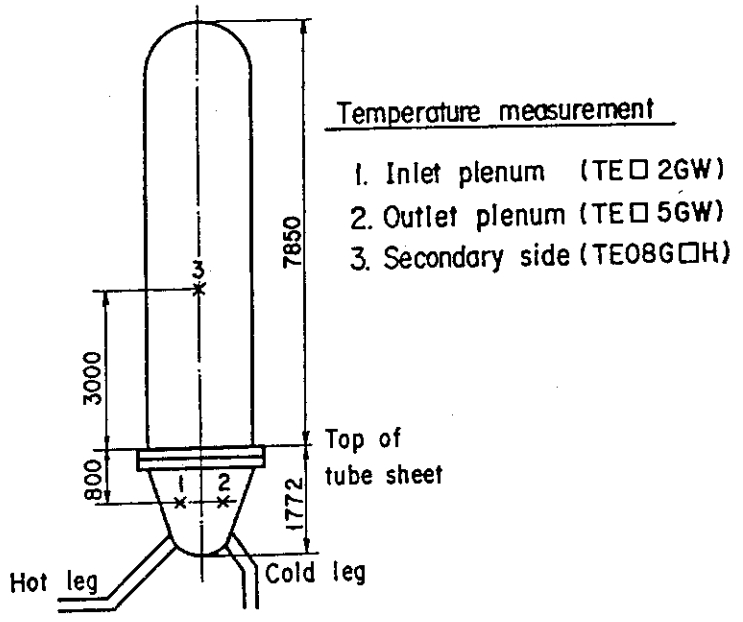

Fig. A-6 Definition of Tag. ID for fluid temperature in inlet and outlet plenum and secondary of steam generator (TE□2GW, TE□5GW, TE08G□H)

Appendix B

Main results of Test C1-5 (Run 14)

Table and Figure List

Table B-1 Summary of test conditions

1. TEST TYPE : Low System Pressure Test
2. TEST NUMBER : RUN 019 3. DATE : Dec.20, 1979
4. POWER : A: TOTAL: 9.39 MW; B:LINEAR: 1.4 KW/M
5. RELATIVE RADIAL POWER SHAPE :

   A: ZONE: A B C

   B: RATIO: 1.07 : 1.0 : 0.82
6. AXIAL POWER SHAPE : CHOPPED COSINE
7. PRESSURE (KG/CM^2A) :

   A: SYSTEM: 1.57, B: CONTAINMENT 1.55,

   C: STEAM GENERATOR SECONDARY: 54
8. TEMPERATURE (DEG.C) :

   A: DOWNCOMER WALL 172, B: VESSEL INTERNALS 108,

   C: PRIMARY PIPING WALL 115, D: LOWER PELNUM LIQUID 106,

   E: ECC LIQUID 39, F: STEAM GENERATOR SECONDARY 267,

   G: CORE TEMPERATURE AT ECC INITIATION 529
9. ECC INJECTION TYPE: C

   A: COLD LEG, B: LOWER PLENUM, C: LOWER PLENUM + COLD LEG
10. PUMP K-FACTOR : ~ 15
11. ECC FLOW RATES AND DURATION :

    A: ACCUMULATOR 269 M^3/HR FROM 0 TO 23 SECONDS

    B: LPCI 30.4 M^3/HR FROM 23 TO 858 SECONDS

    C: ECC INJECTION TO LOWER PLENUM : FROM 0 TO 17.5 SECONDS

    (VALVE OPENING AND CLOSING TIMES ARE INCLUDED IN THE INJECTION DURATION)
12. INITIAL WATER LEVEL IN LOWER PLENUM : 0.89 M.
13. POWER CONTROL : ANS x 1.2 + ACTINIDE (30 SEC AFTER SCRAM)
14. EXPECTED BOCREC TIME FROM ECC INITIATION 12 , SEC
15. EXPECTED PEAK TEMPERATURE AT BOCREC 600 C

Table B-2 Chronology of events

EVENT	TIME (sec)
Test Initiated (Heater Rods Power on) (Data Recording Initiated)	0.0
Accumulator Injection Initiated	55
Power Decay Initiated (Bottom of Core Recovery)	66.5
Accumulator Injection Switched from Lower Plenum to Cold Leg	72.5
Accumulator Injection Ended and LPCI Injection Initiated	78
All Heater Rods Quenched	695
Power Off	770
LPCI Injection Ended	858
Test Ended (Data Recording Ended)	1071

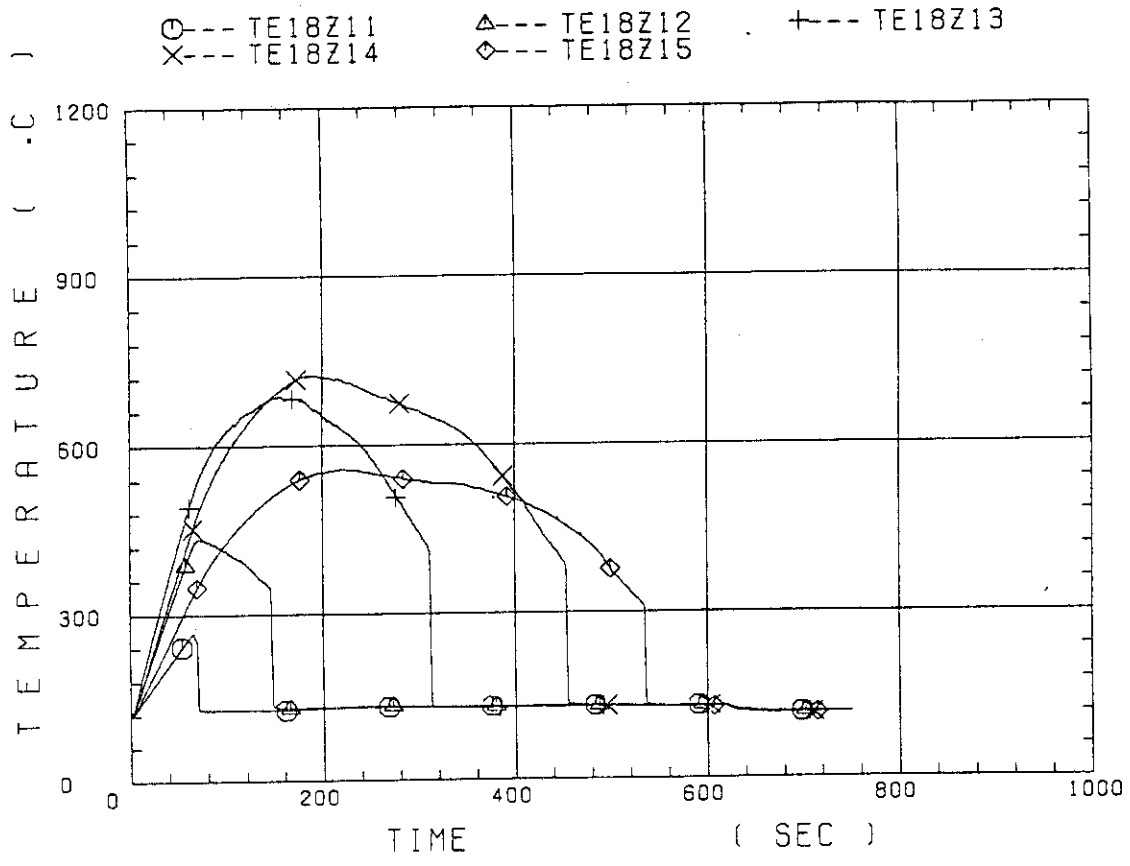

Fig. B-1 Surface temperature on low power rod (Z-rod) in medium power region (B region) (average power rod)

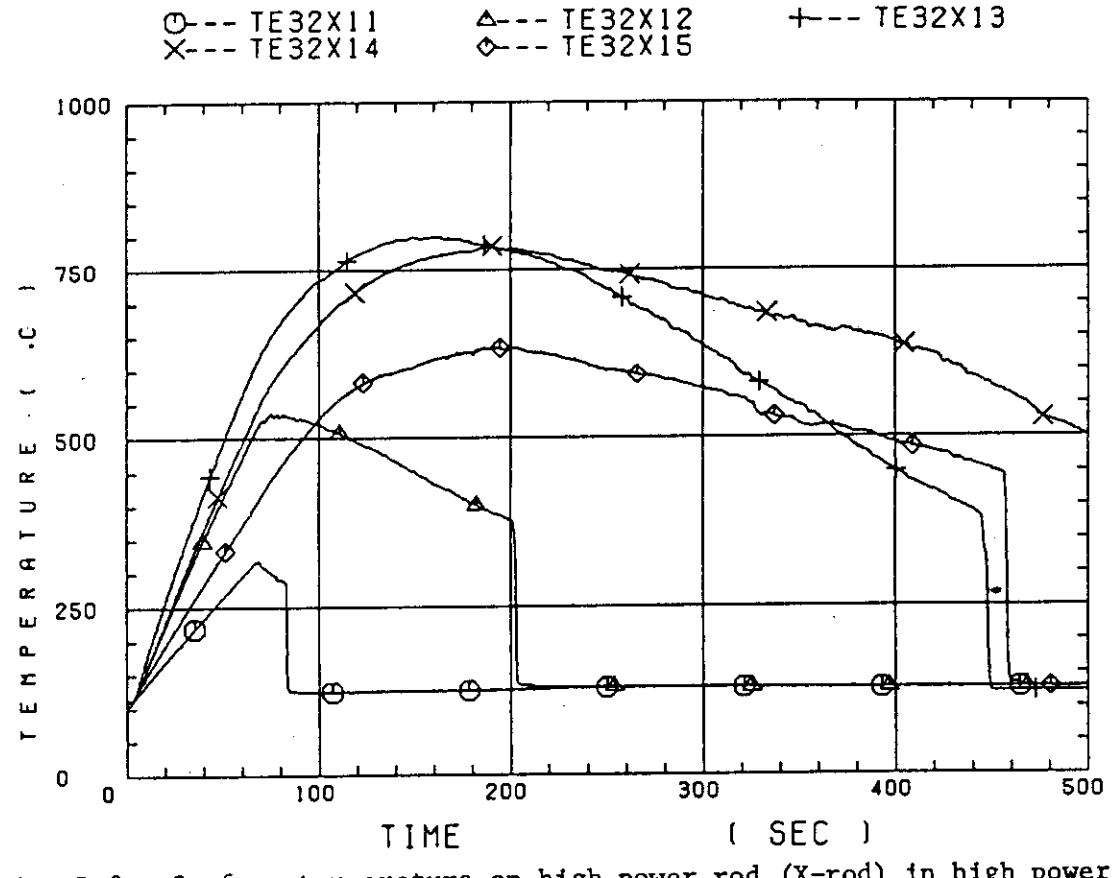

Fig. B-2 Surface temperature on high power rod (X-rod) in high power region (A region) (peak power rod)

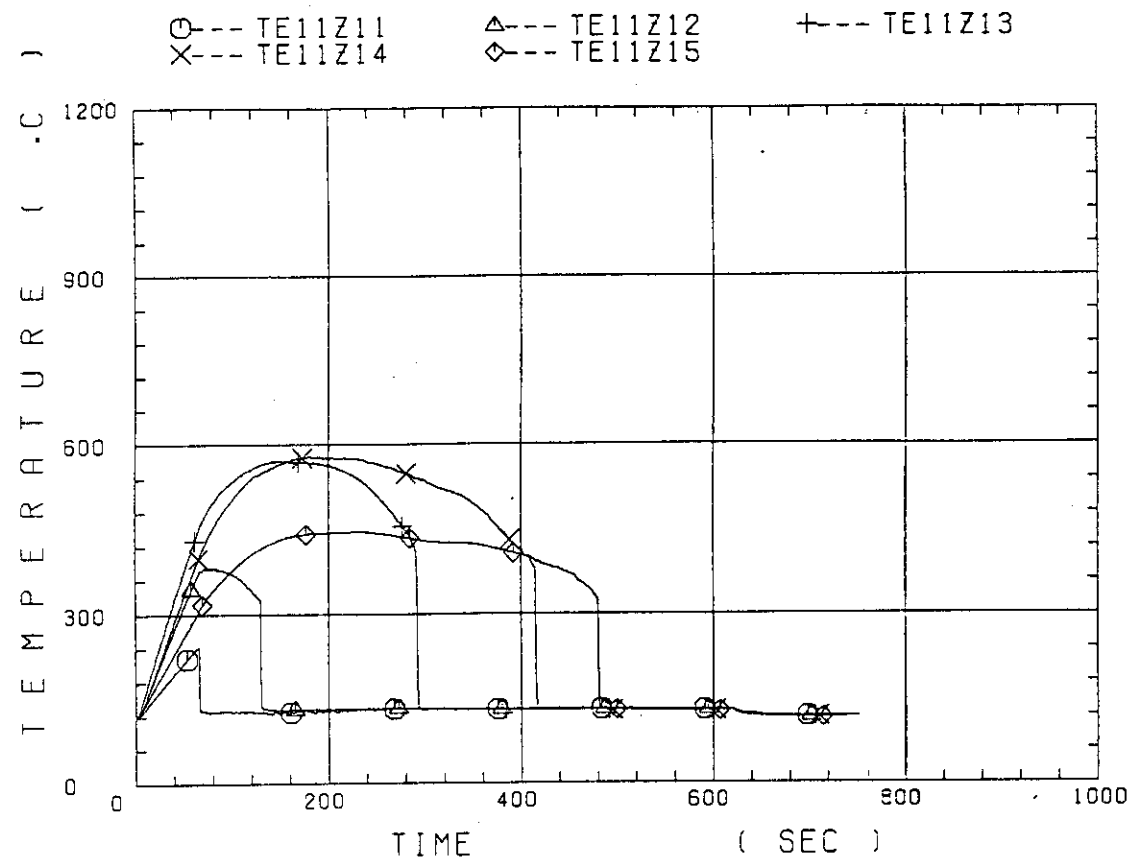

Fig. B-3 Surface temperature on low power rod (Z-rod) in low power region (C region) (lowest power rod)

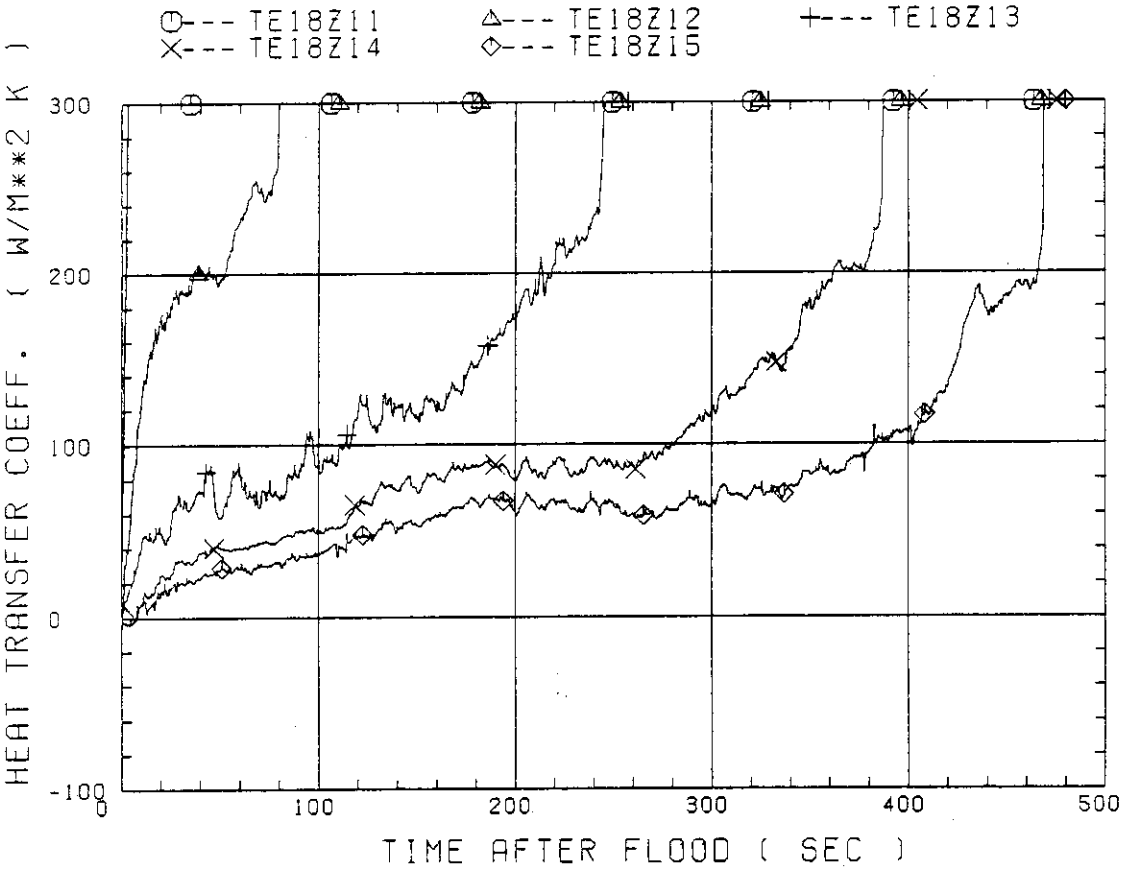

Fig. B-4 Heat transfer coefficient at midplane of low power rod (Z-rod) in medium power region (B region) (average power rod)

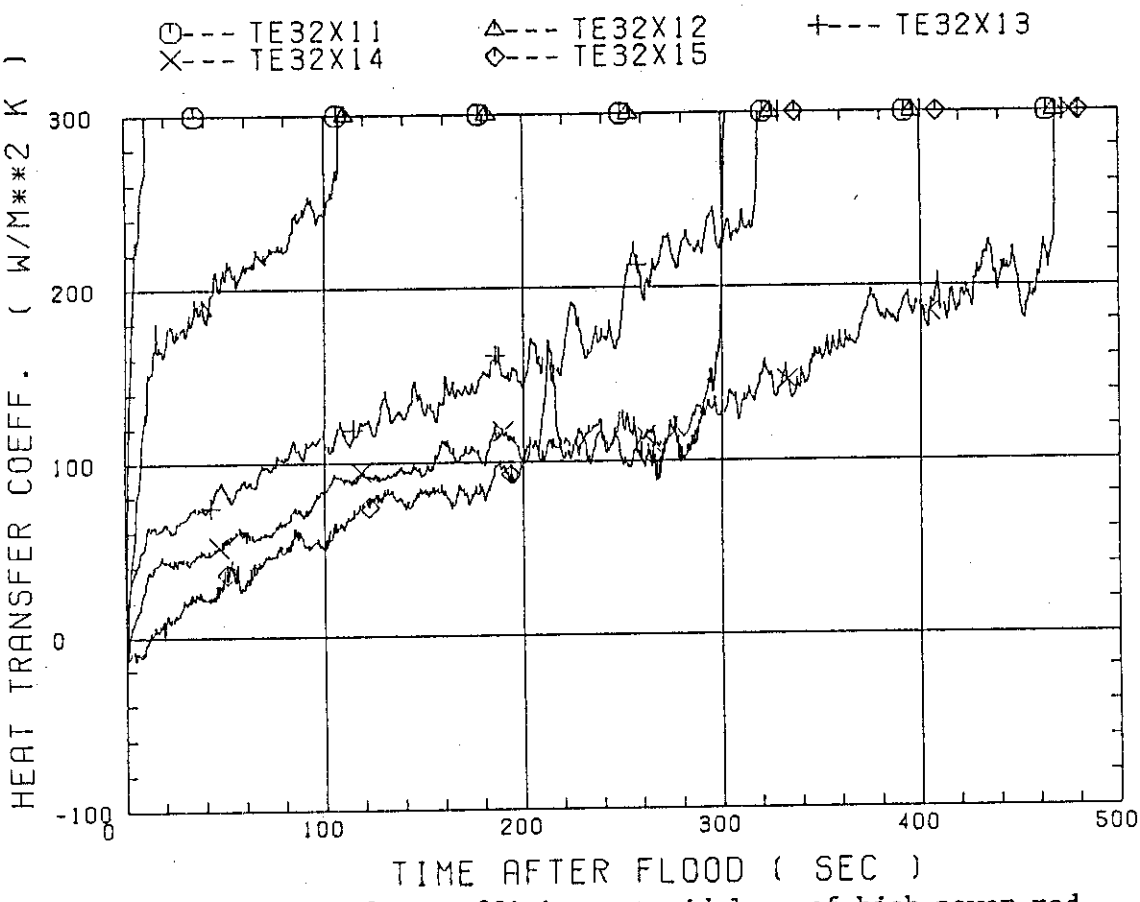

Fig. B-5 Heat transfer coefficient at midplane of high power rod (X-rod) in high power region (A region) (peak power rod)

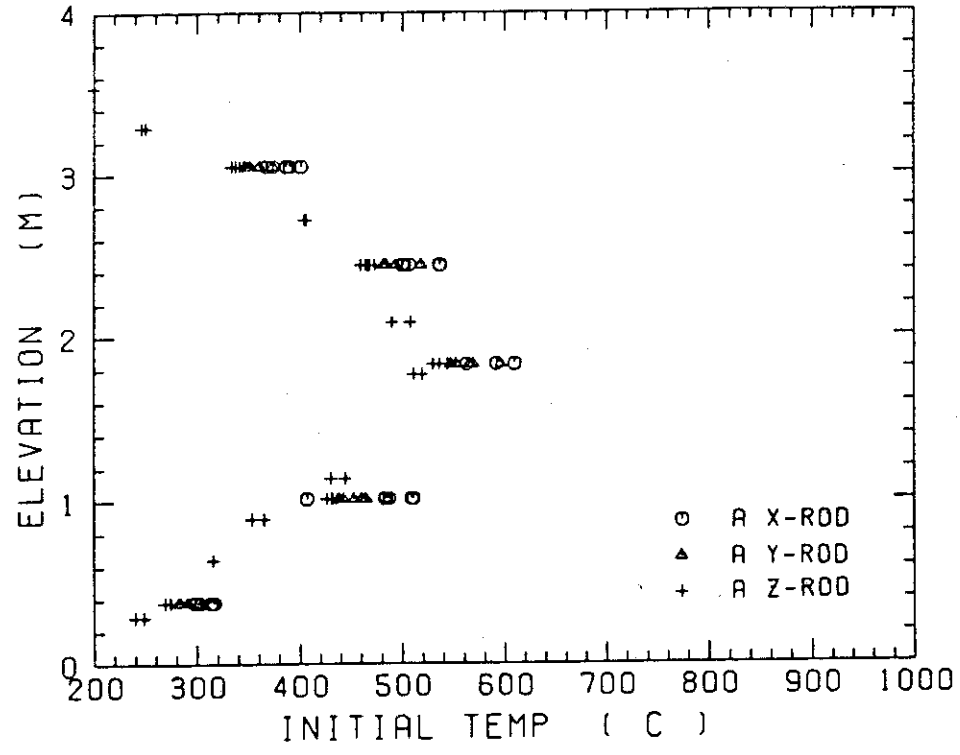

Fig. B-6 Initial rod surface temperature in high power region (A region)

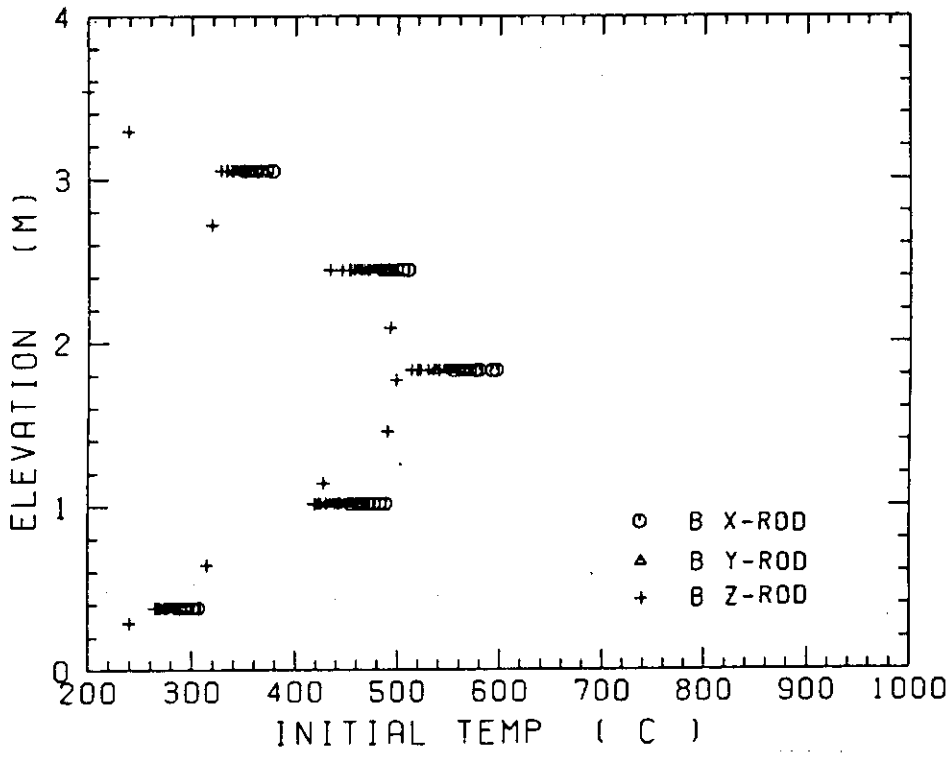

Fig. B-7 Initial rod surface temperature in medium power region (B region)

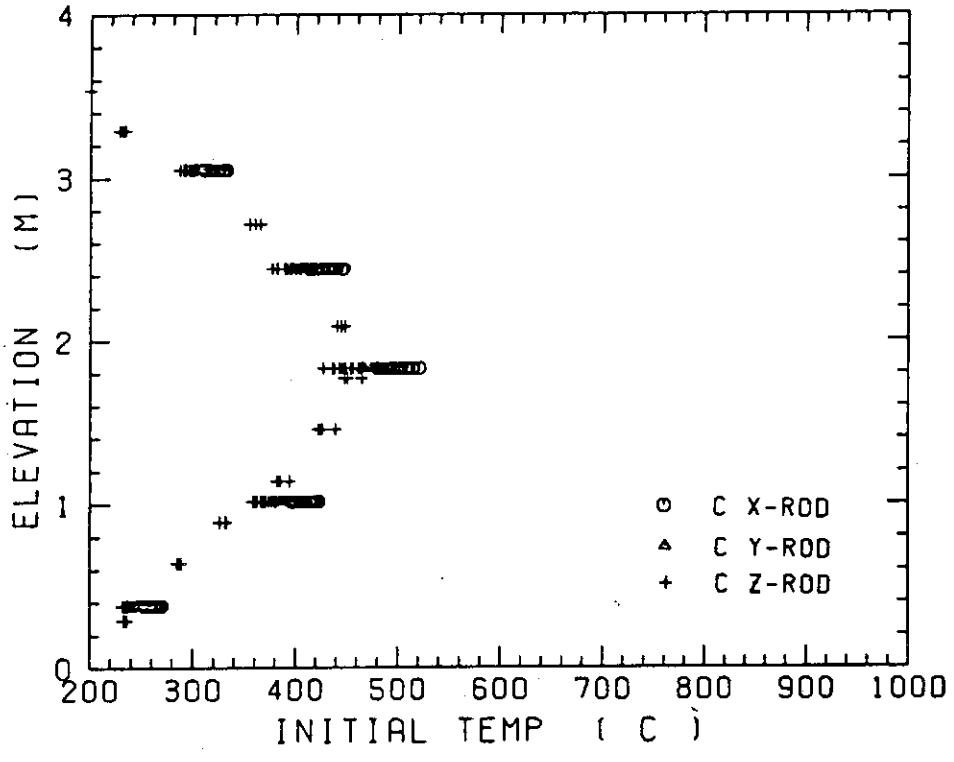

Fig. B-8 Inital rod surface temperature in low power region (C region)

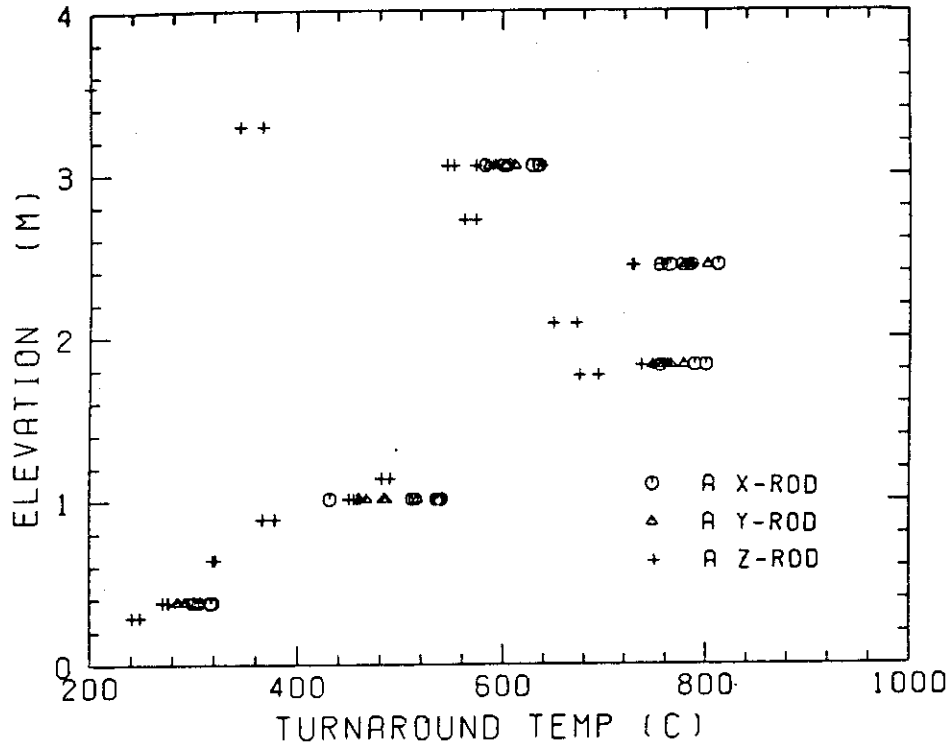

Fig. B-9 Turnaround temperature in high power region (A region)

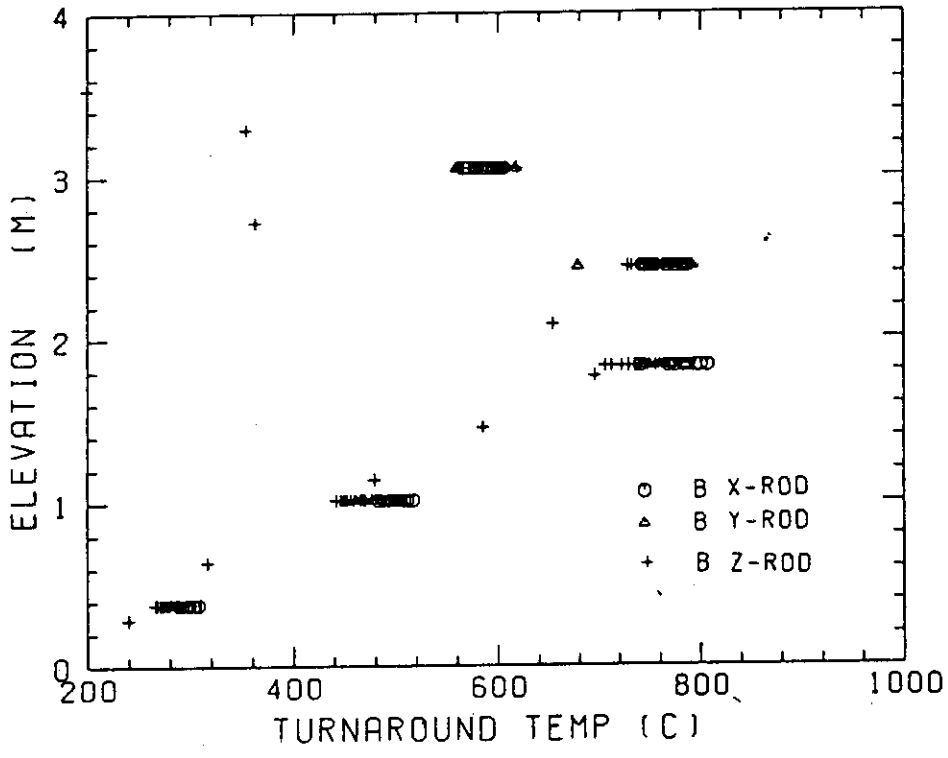

Fig. B-10 Turnaround temperature in medium power region (B region)

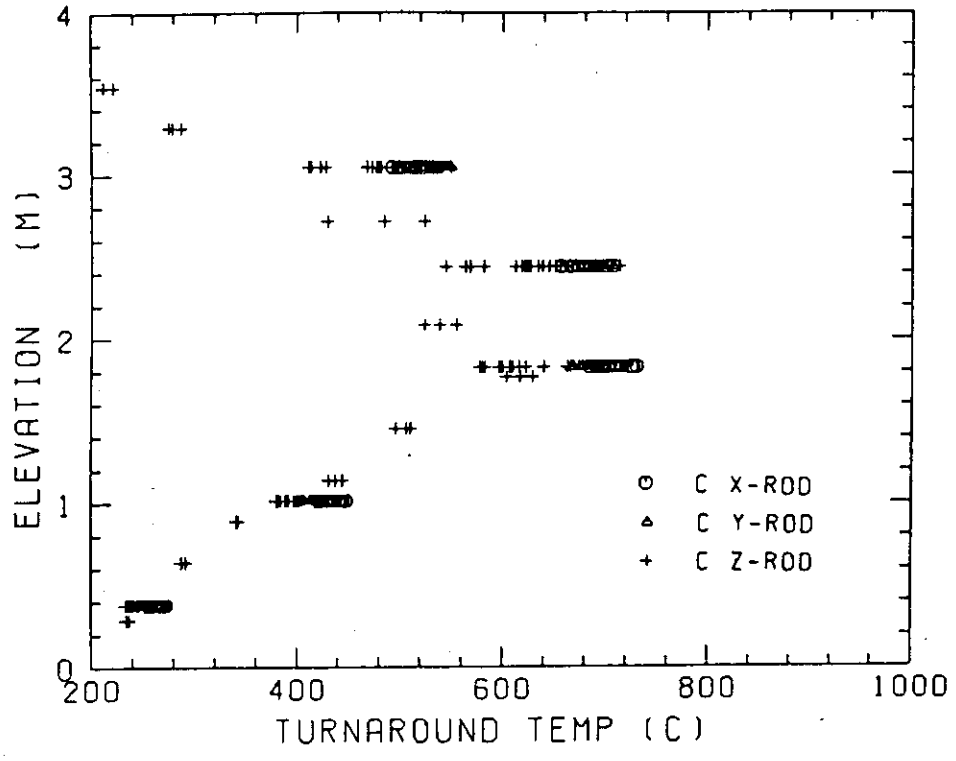

Fig. B-11 Turnaround temperature in low power region (C region)

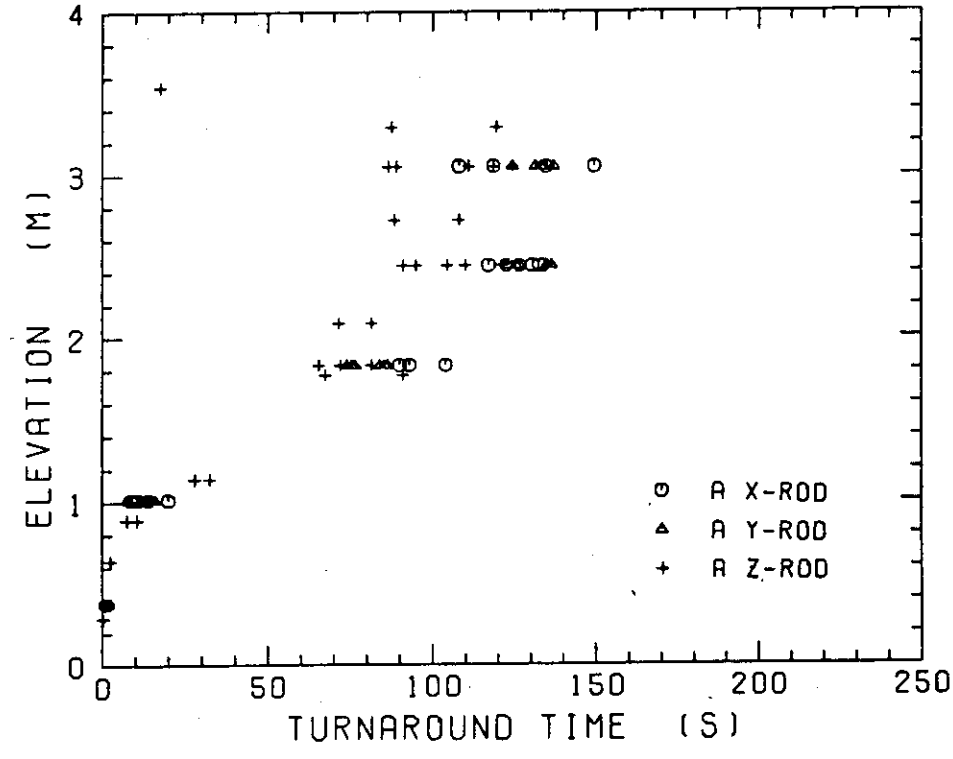

Fig. B-12 Turnaround time in high power region (A region)

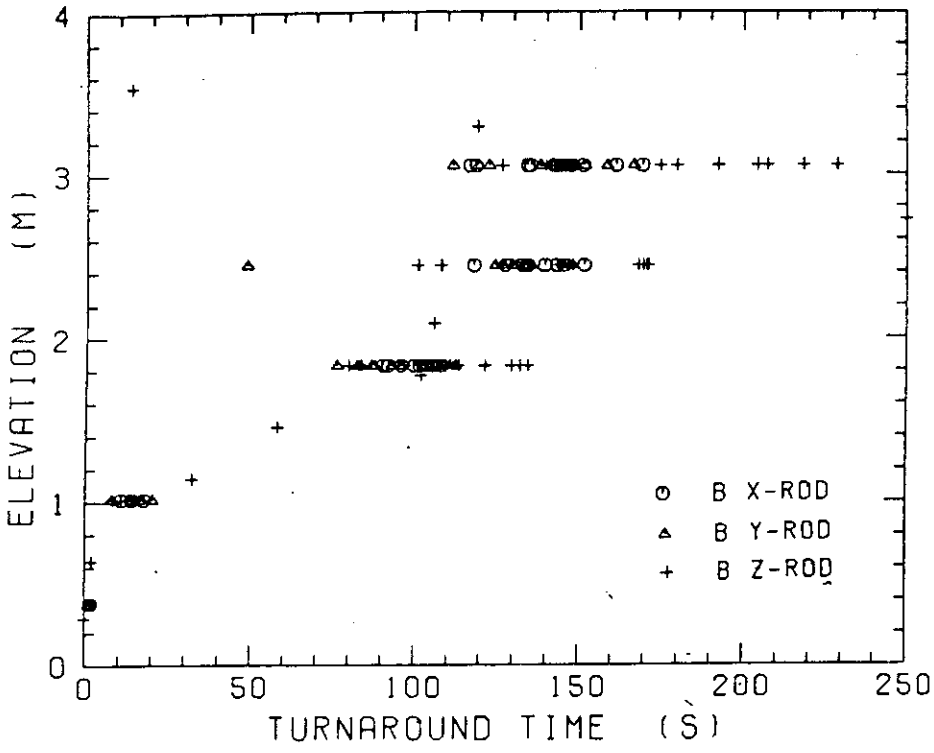

Fig. B-13 Turnaround time in medium power region (B region)

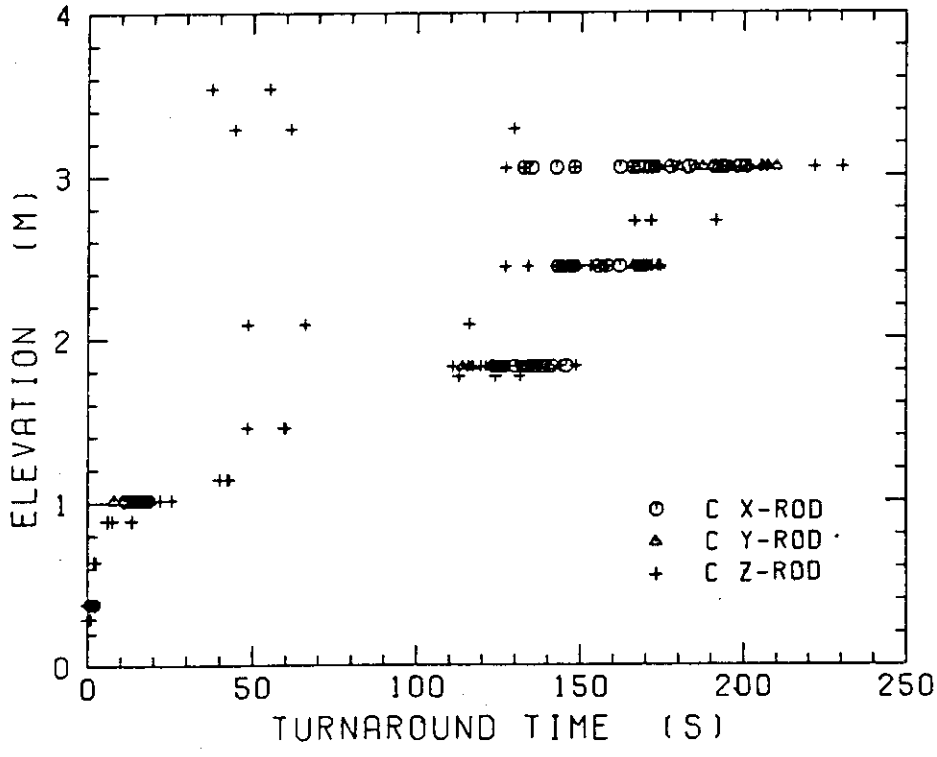

Fig. B-14 Turnaround time in low power region (C region)

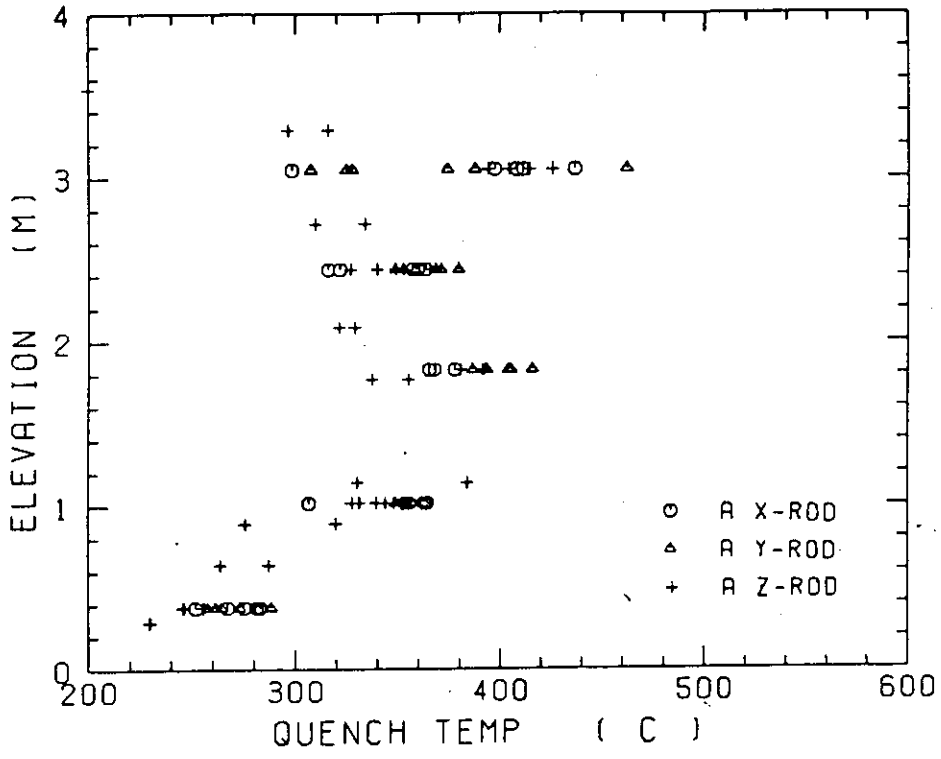

Fig. B-15 Quench temperature in high power region (A region)

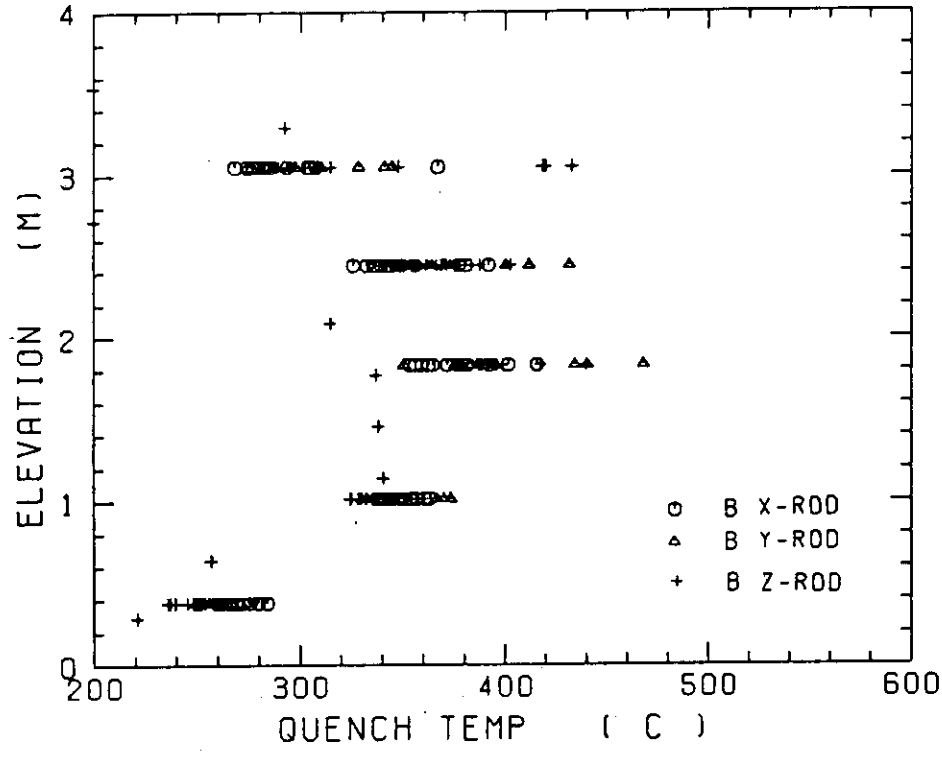

Fig. B-16 Quench temperature in medium power region (B region)

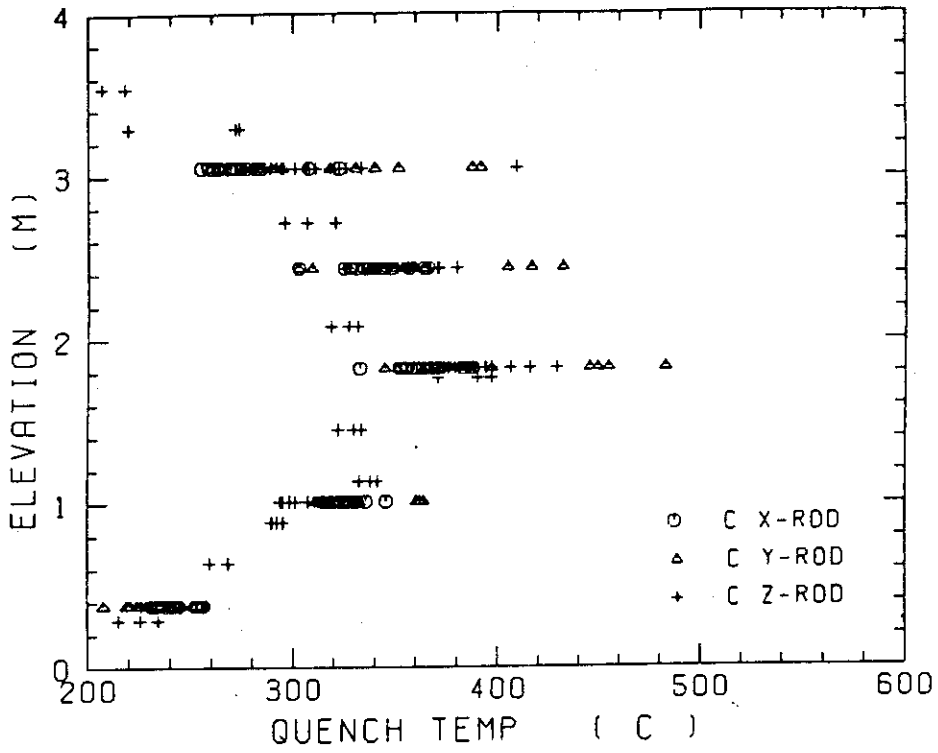

Fig. B-17 Quench temperature in low power region (C region)

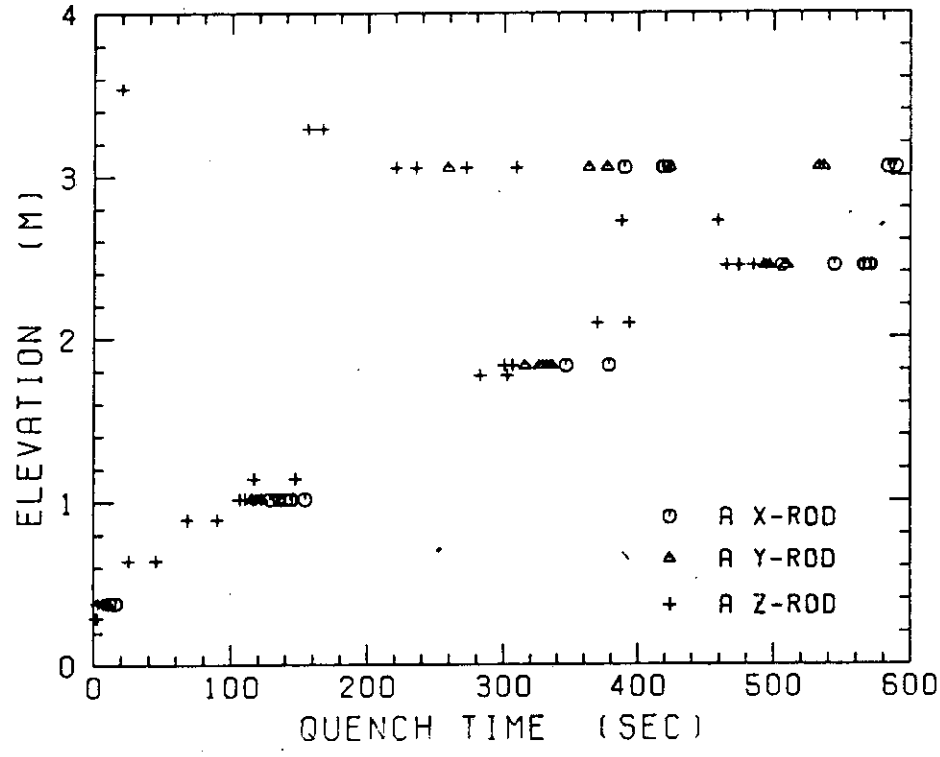

Fig. B-18 Quench time in high power region (A region)

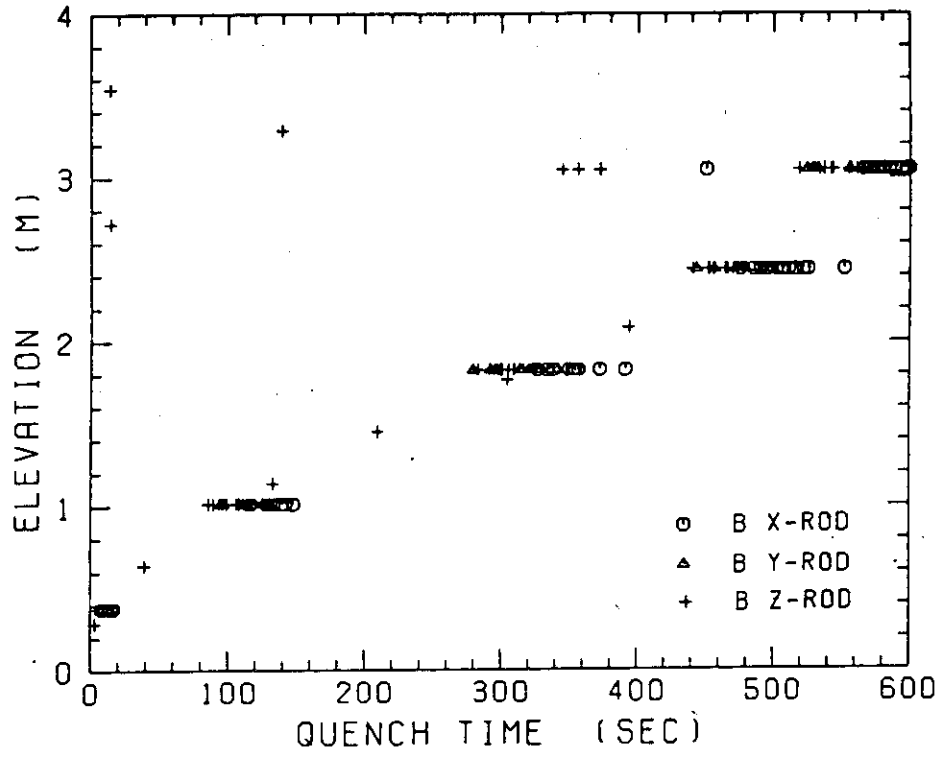

Fig. B-19 Quench time in medium power region (B region)

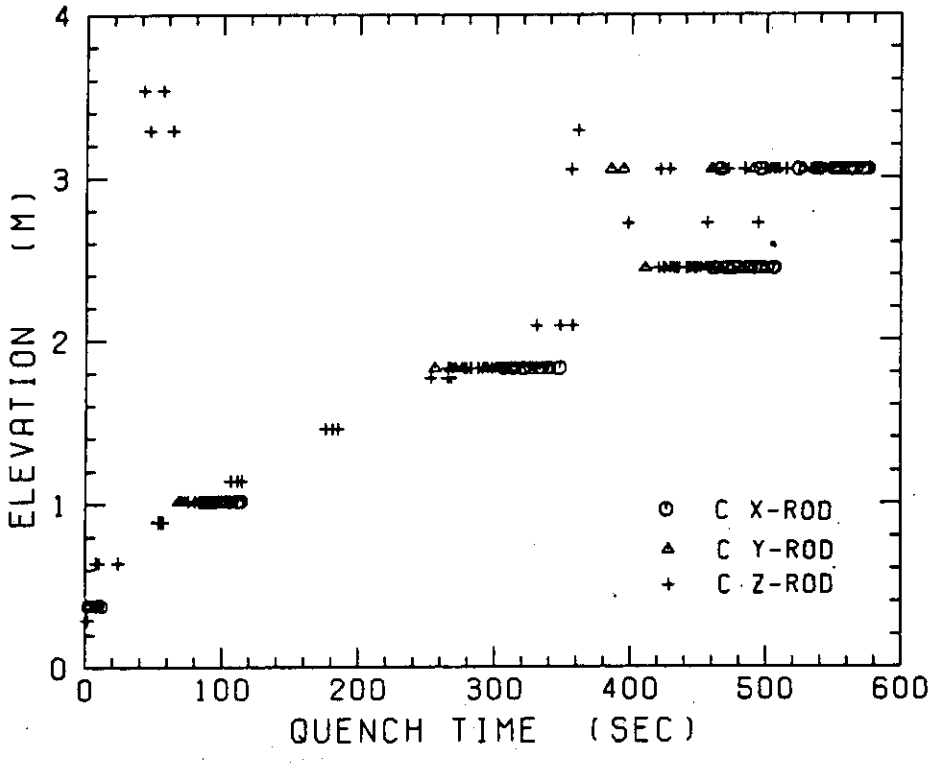

Fig. B-20 Quench time in low power region (C region)

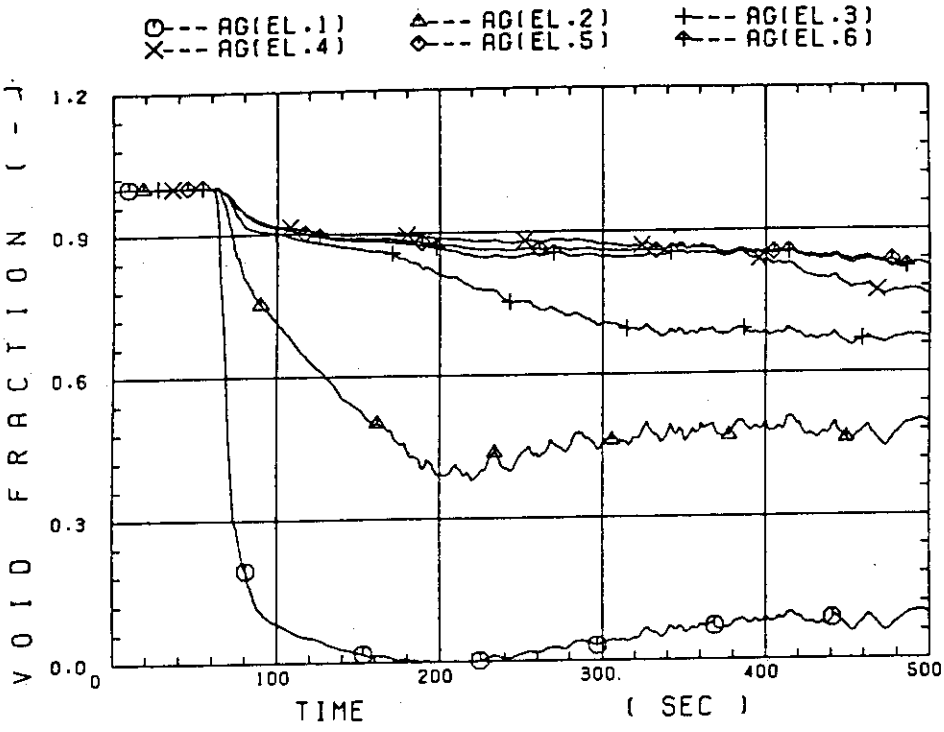

Fig. B-21 Void fraction in core

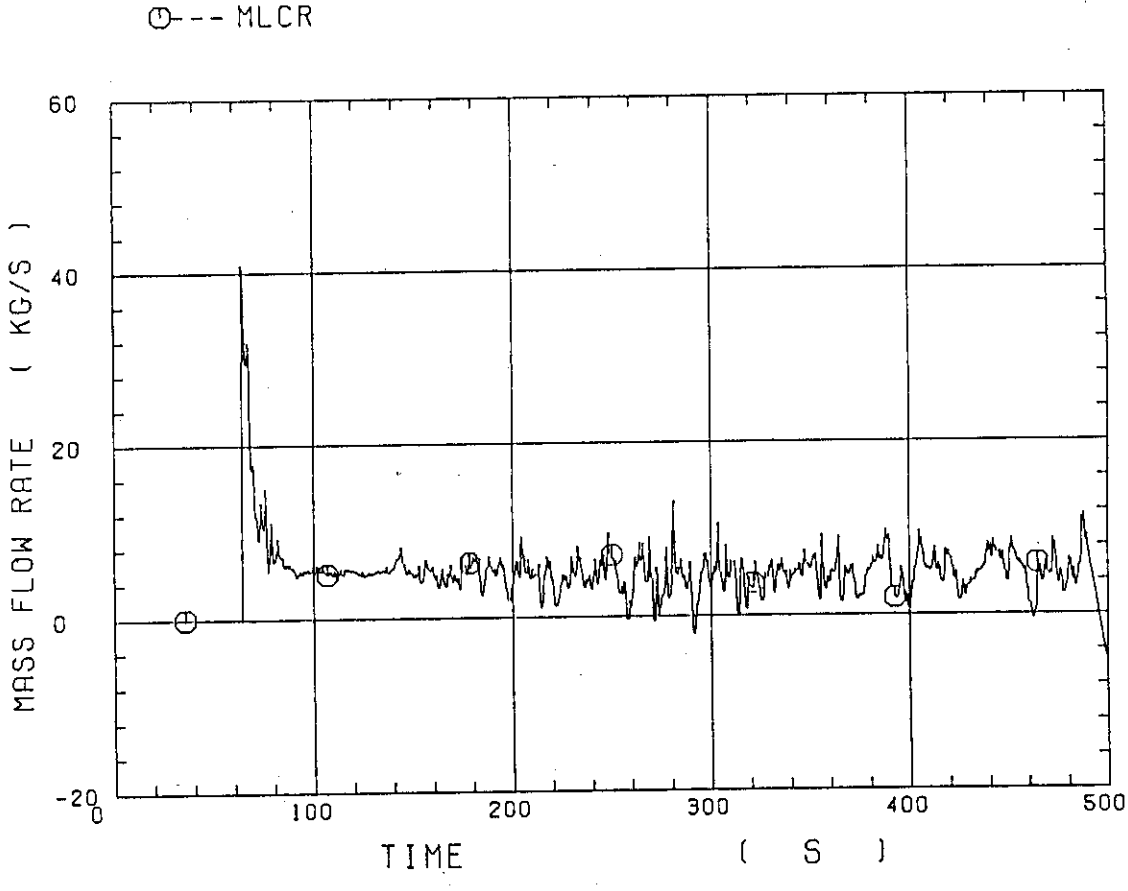

Fig. B-22 Evaluated core inlet mass flow rate

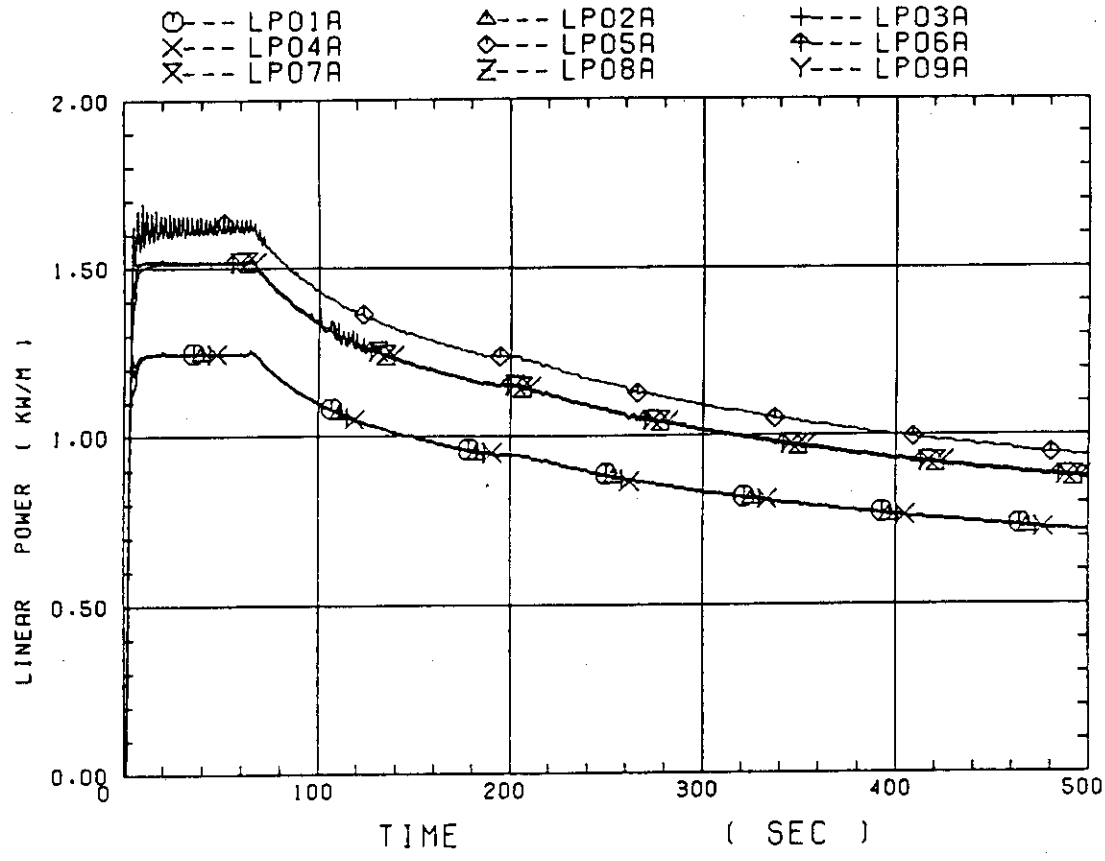

Fig. B-23 Average linear power of heater rod in each power unit zone

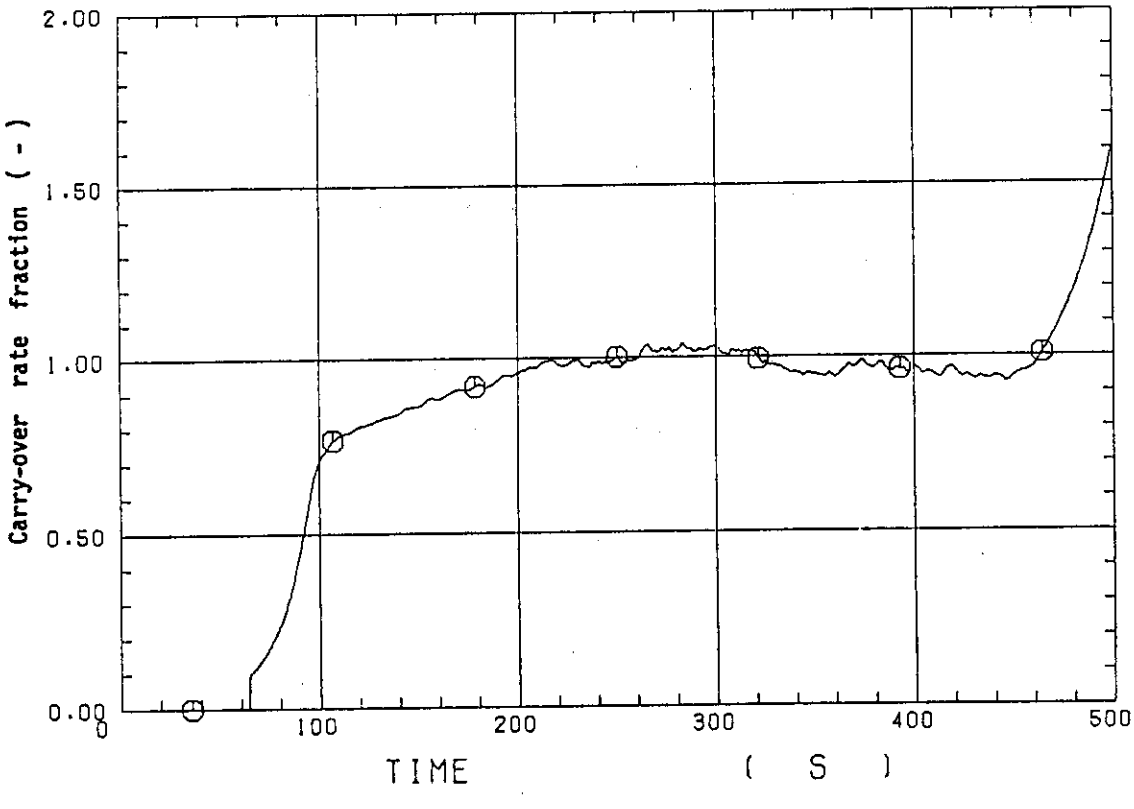

Fig. B-24 Carry-over rate fraction

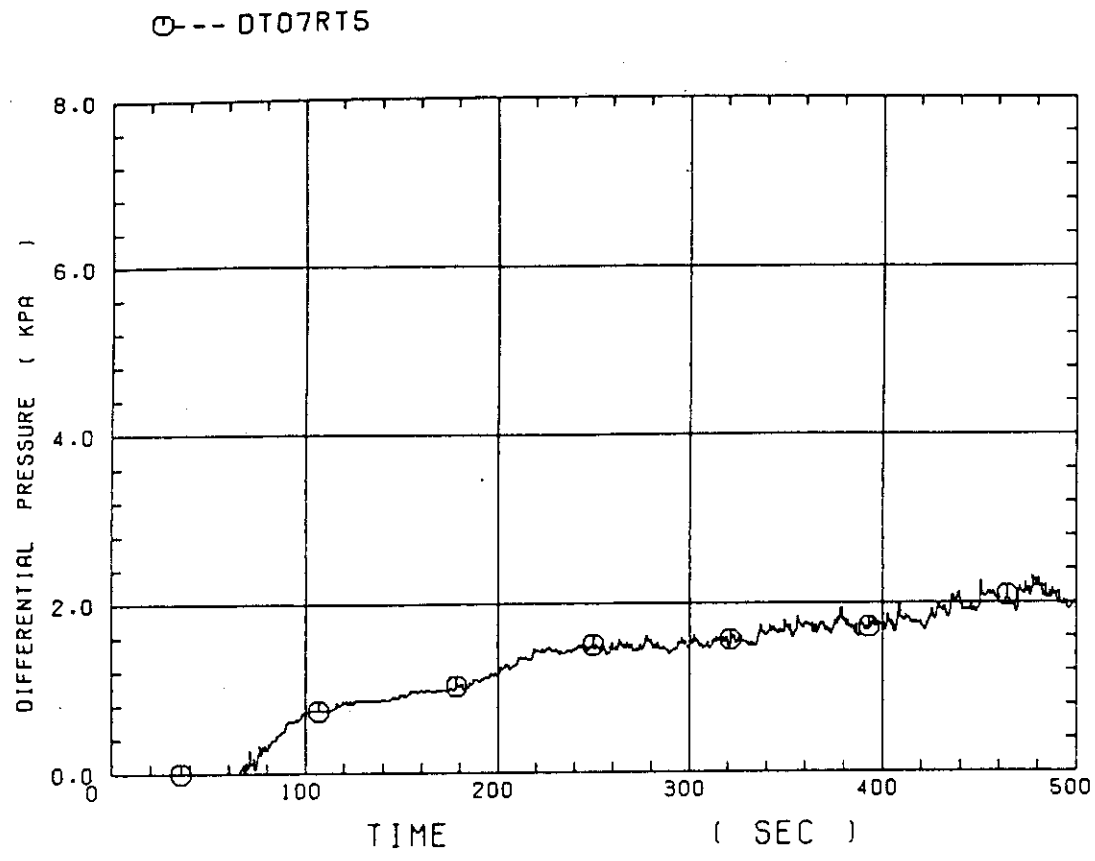

Fig. B-25 Differential pressure through upper plenum

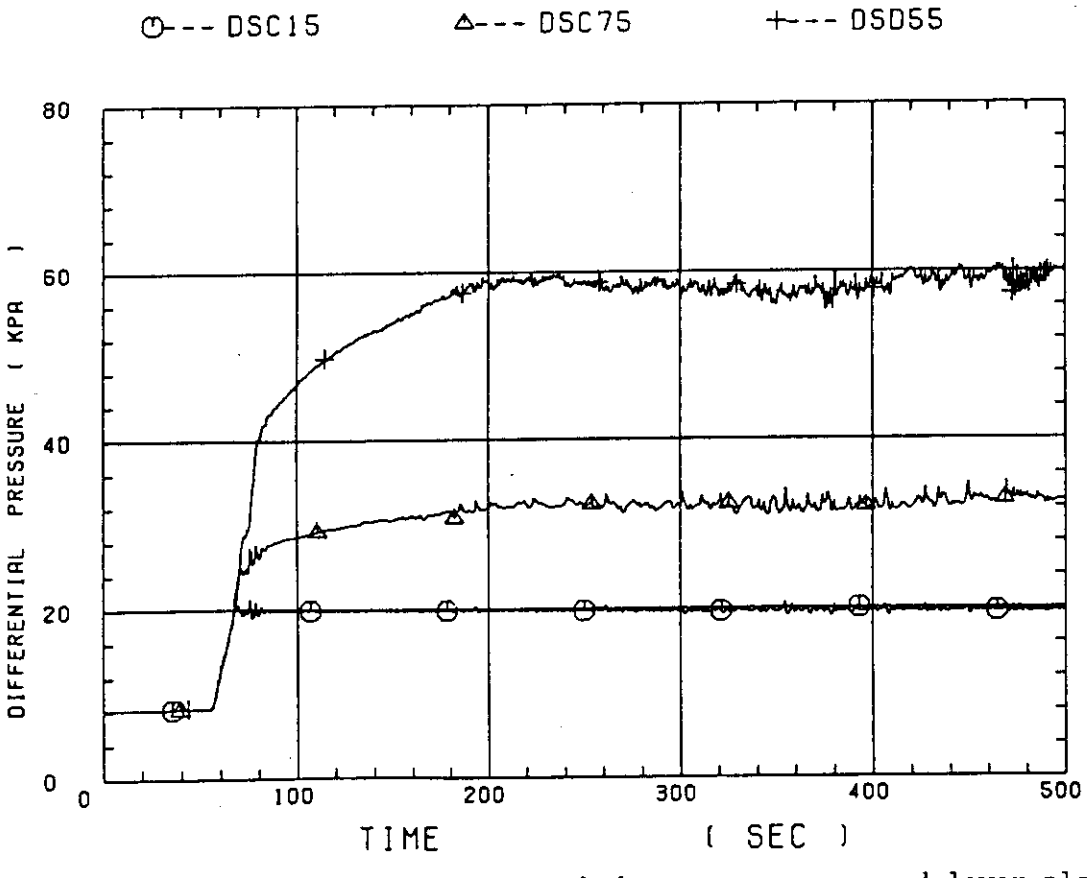

Fig. B-26 Differential pressure through downcomer, core, and lower plenum

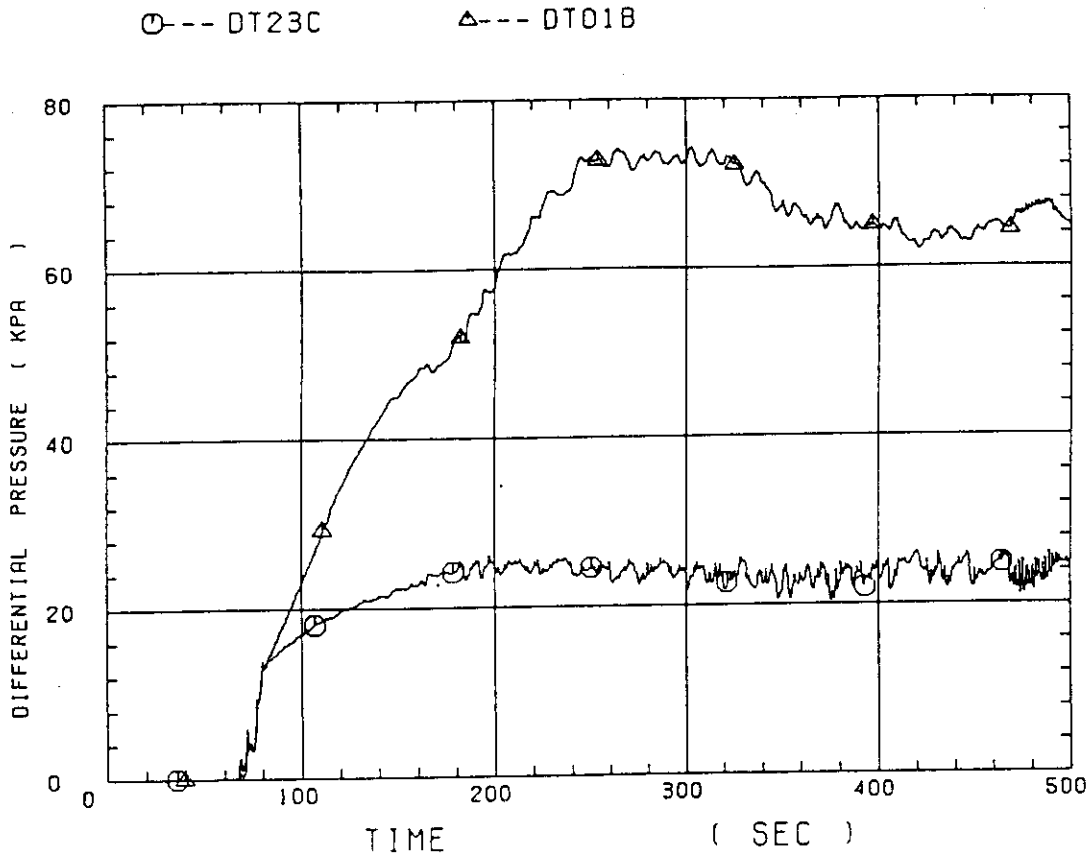

Fig. B-27 Differential pressure through intact and broken loops

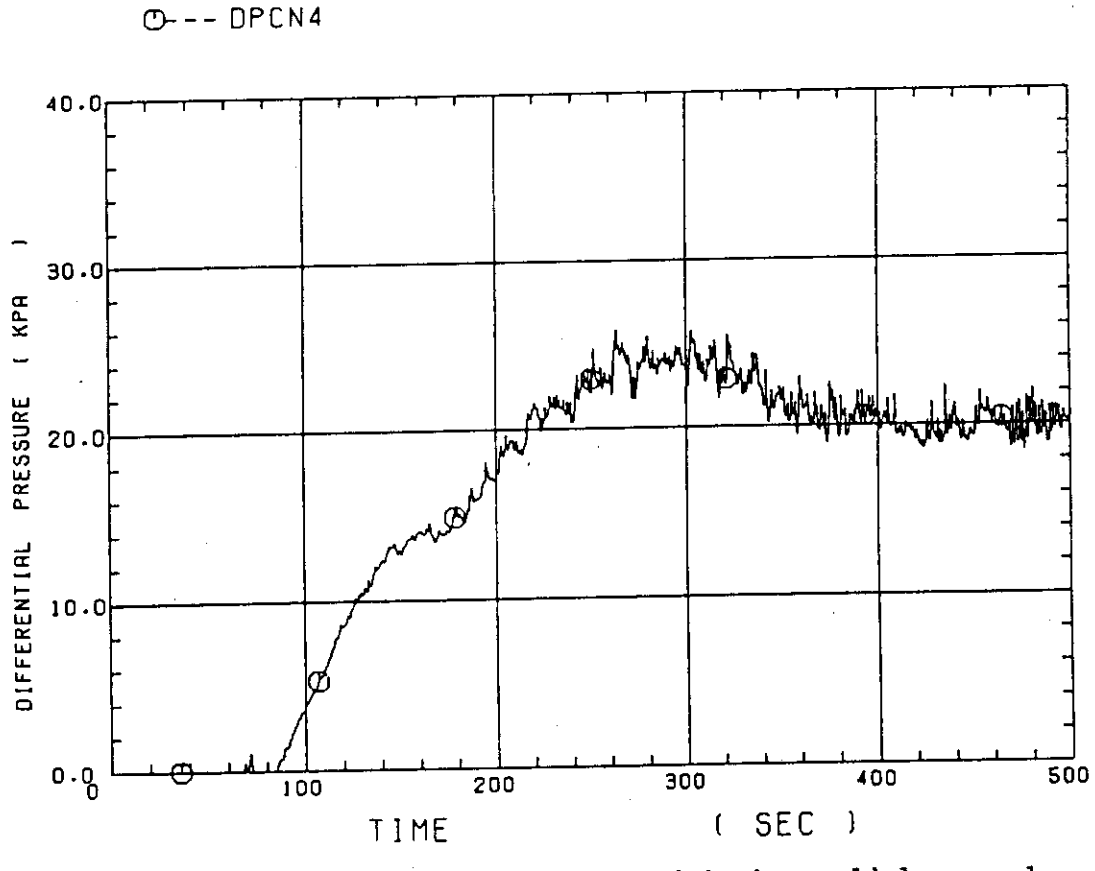

Fig. B-28 Differential pressure through broken cold leg nozzle

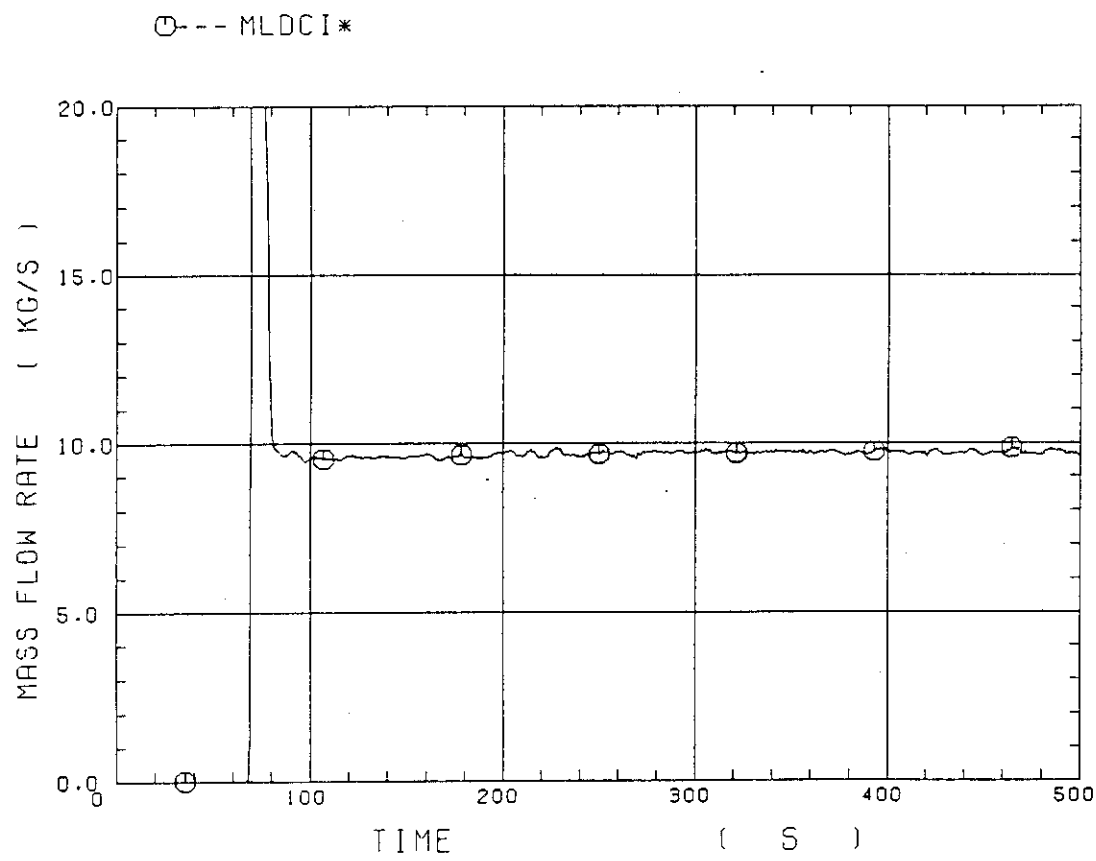

Fig. B-29 Total water mass flow rate from intact loops to downcomer

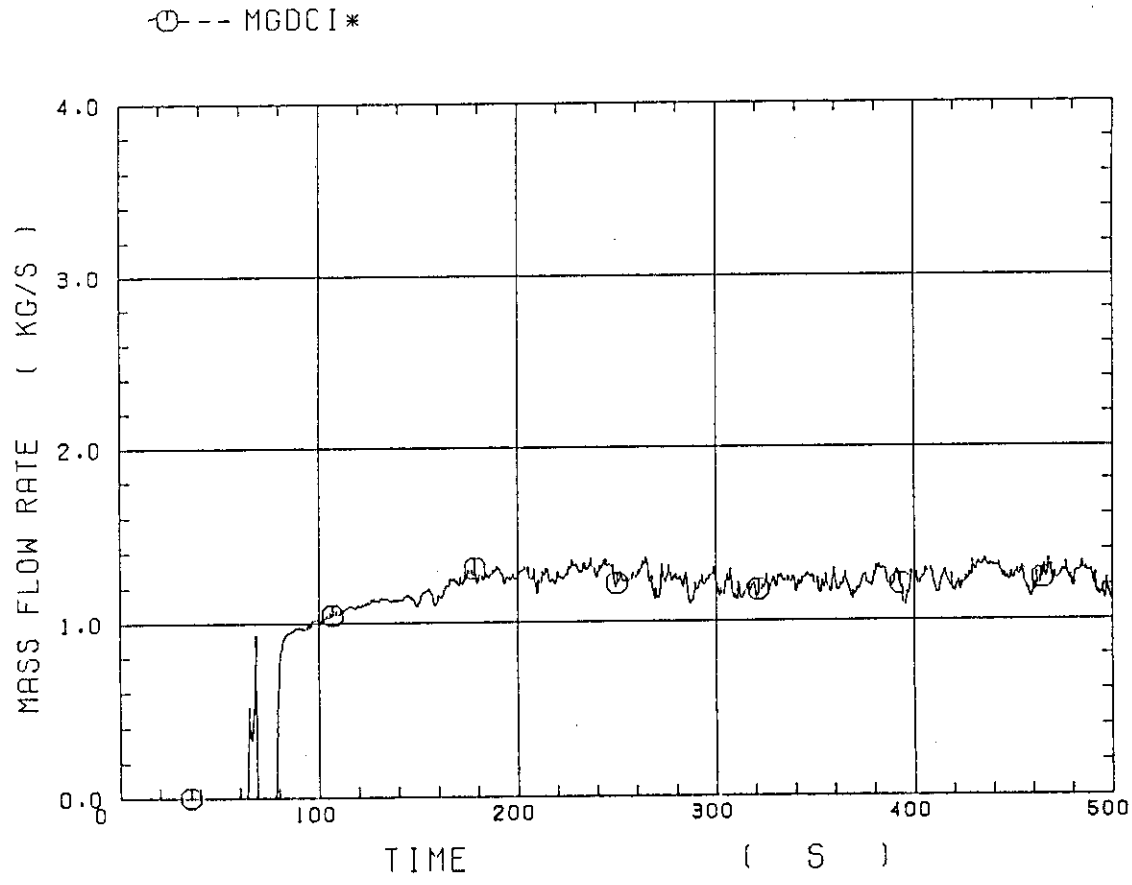

Fig. B-30 Total steam mass flow rate from intact loops to downcomer

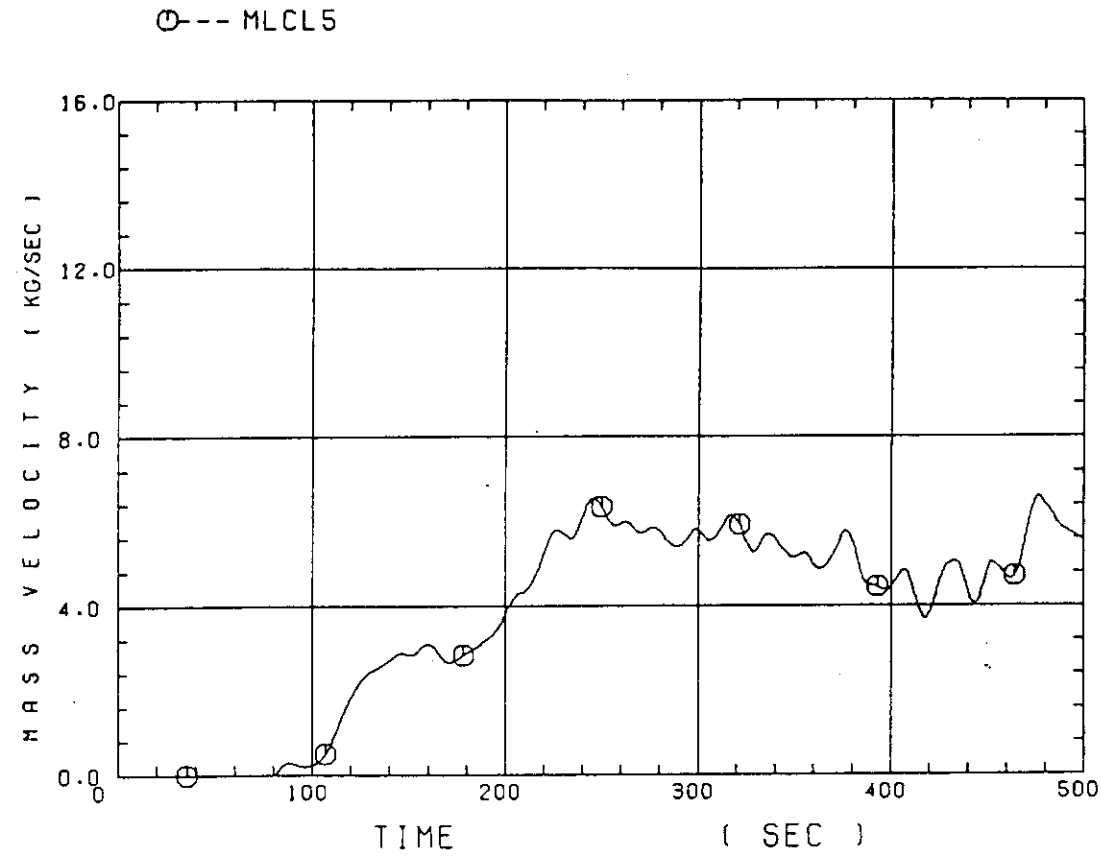

Fig. B-31 Water mass flow rate through broken cold leg nozzle

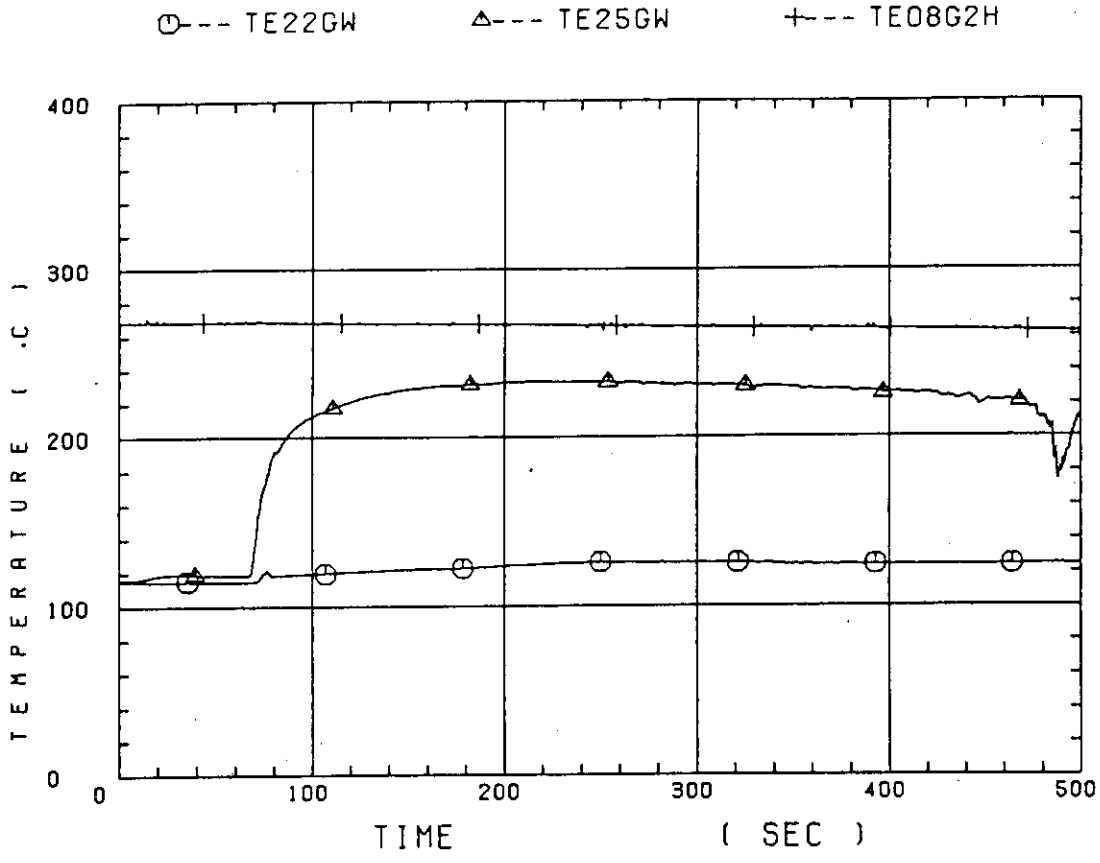

Fig. B-32 Fluid temperature in inlet plenum, outlet plenum, and secondary of steam generator 1

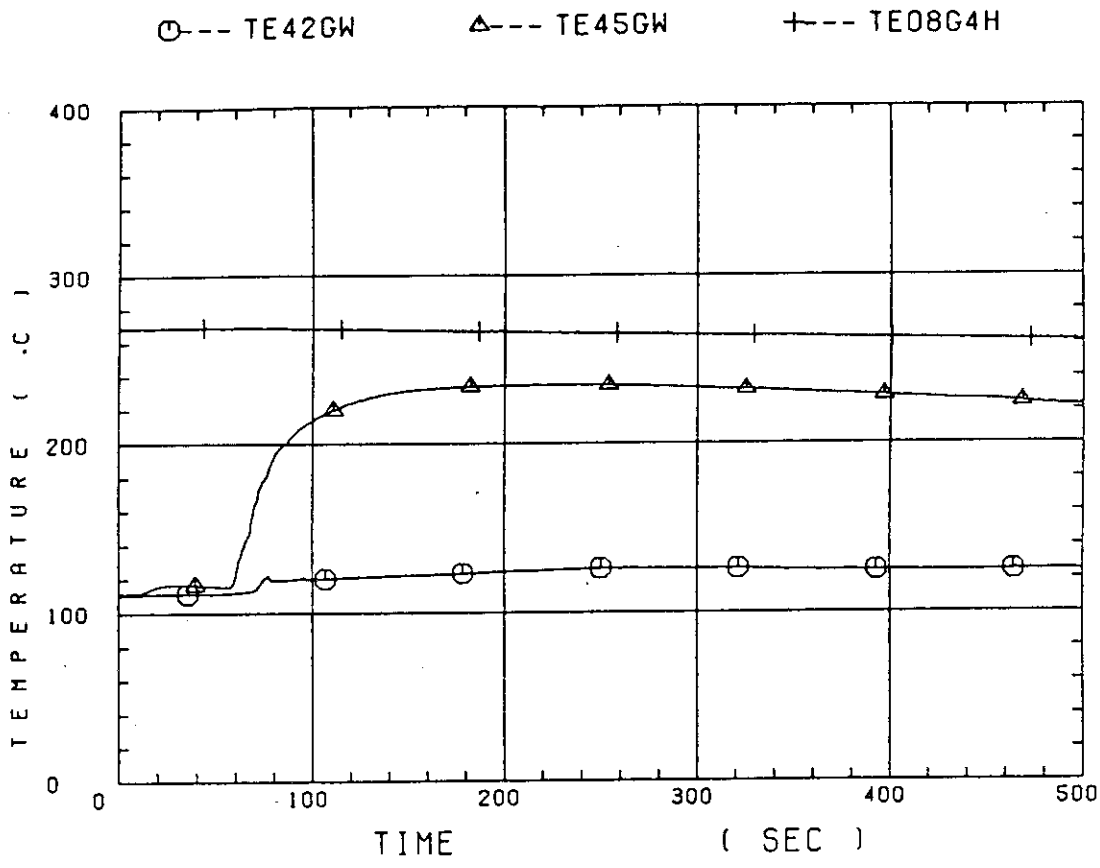

Fig. B-33 Fluid temperature in inlet plenum, outlet plenum, and secondary of steam generator 2

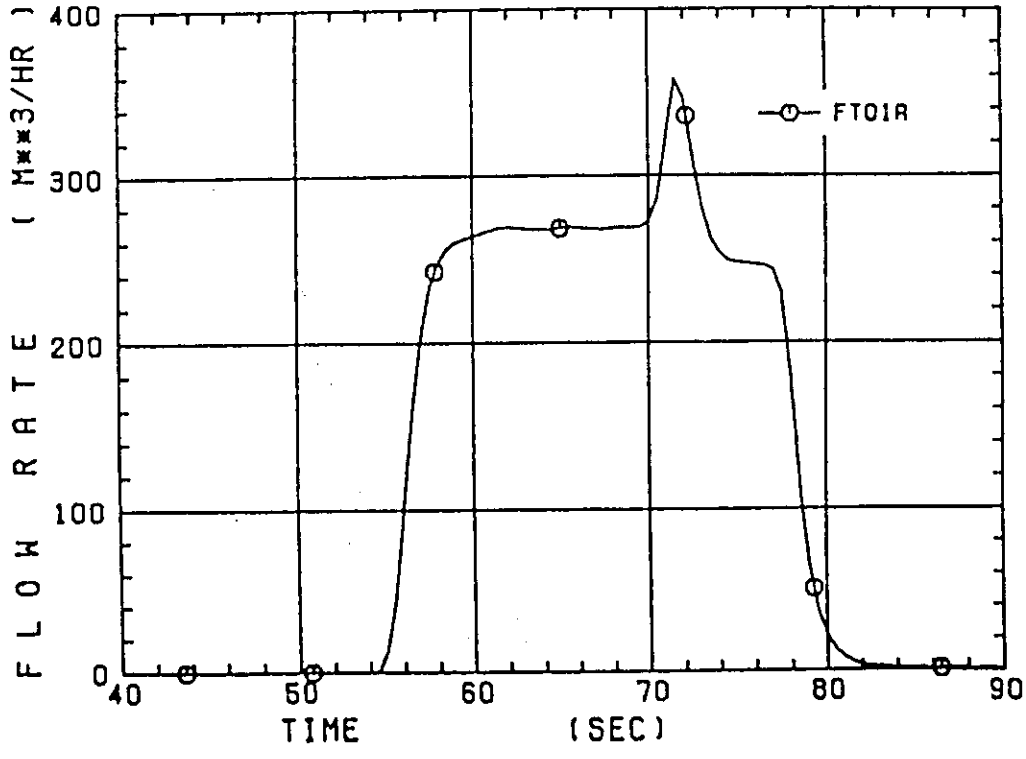

Fig. B-34 Total accumulator injection rate

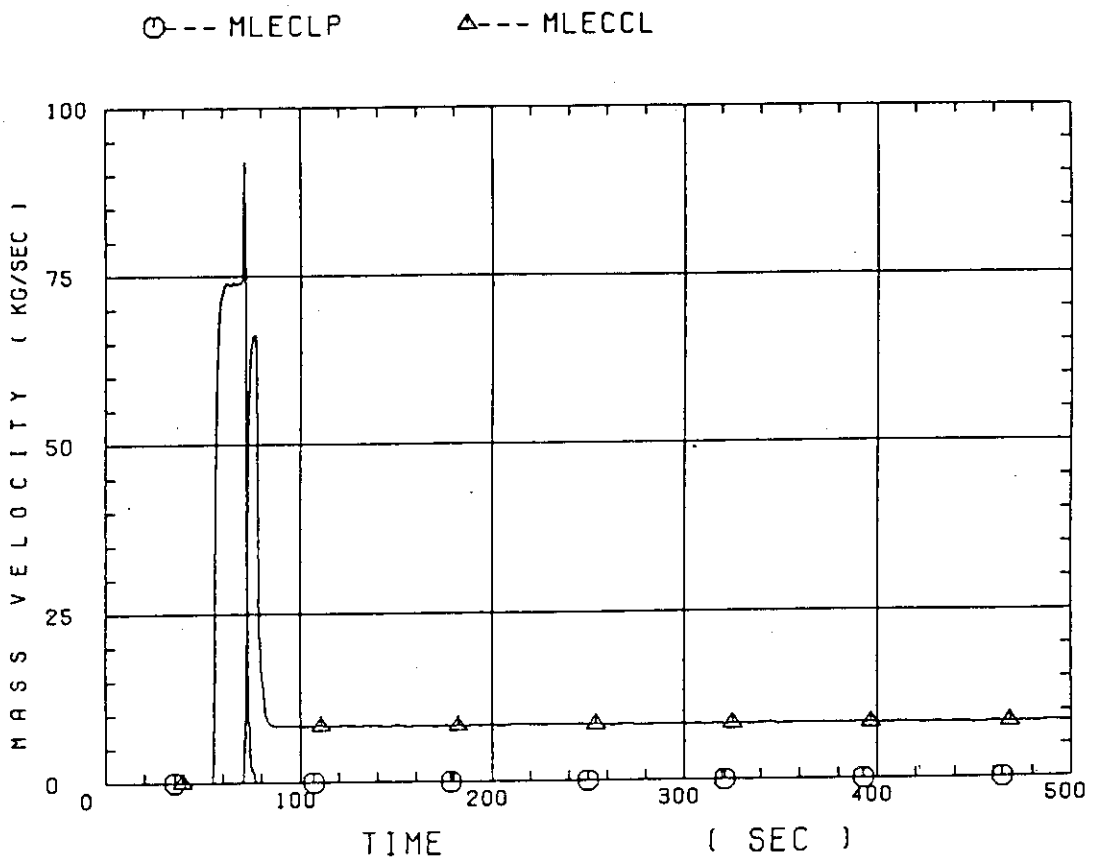

Fig. B-35 ECC water injection rates to lower plenum and to cold legs

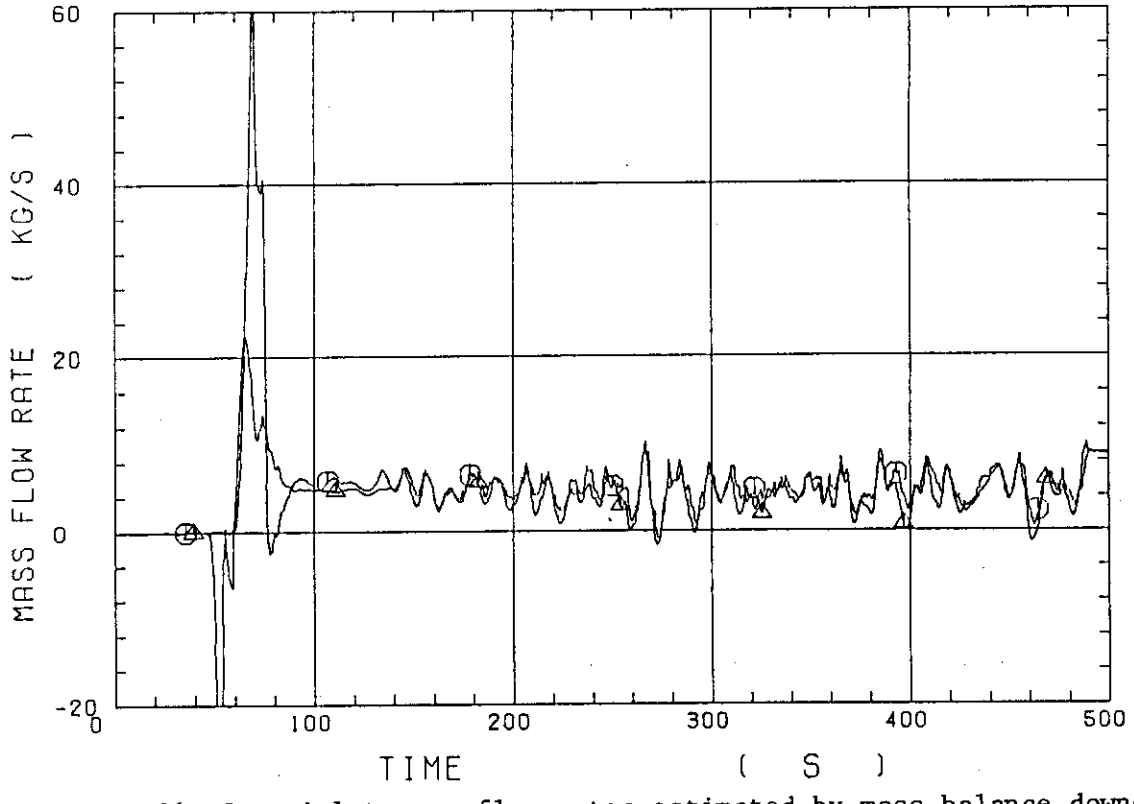

Fig. B-36 Core inlet mass flow rates estimated by mass balance downstream and upstread of core inlet

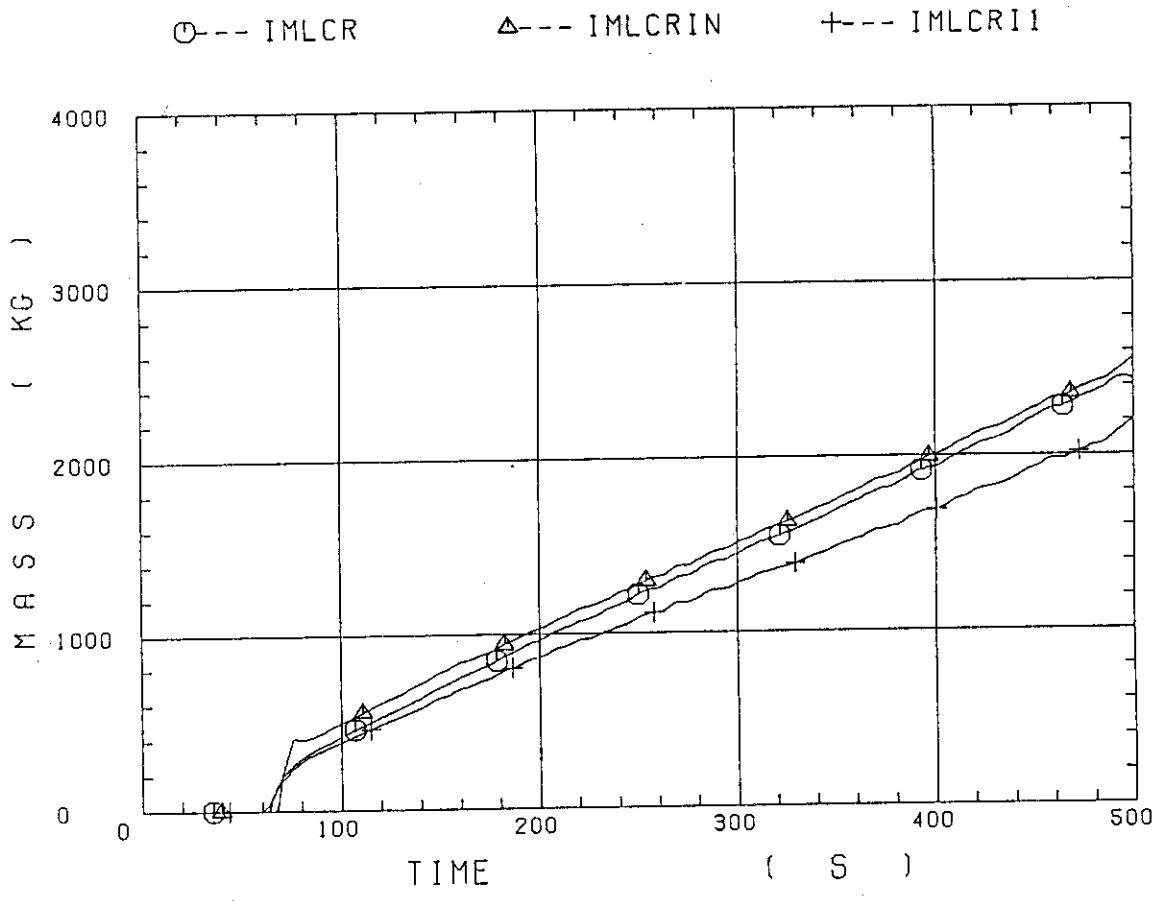

Fig. B-37 Comparison of injected mass into core among two estimation methods and evaluated mass

Appendix C

Main results of Test C1-7 (Run 16)

Table and Figure List

Table C-1 Summary of test conditions

1. TEST TYPE : High Intial Clad Temperature Test
2. TEST NUMBER : C1-7 (RUN o16) 3. DATE : Nov.15, 1979
4. POWER : A: TOTAL: 9.38 MW; B:LINEAR: 1.4 KW/M
5. RELATIVE RADIAL POWER SHAPE :

   A: ZONE: A B C

   B: RATIO: 1.07 : 1.0 : 0.82
6. AXIAL POWER SHAPE : CHOPPED COSINE
7. PRESSURE (KG/CM^2A) :

   A: SYSTEM: 2.00, B: CONTAINMENT 1.98,

   C: STEAM GENERATOR SECONDARY: 51
8. TEMPERATURE (DEG.C) :

   A: DOWNCOMER WALL 180, B: VESSEL INTERNALS 108,

   C: PRIMARY PIPING WALL 120, D: LOWER PELNUM LIQUID 112,

   E: ECC LIQUID 39, F: STEAM GENERATOR SECONDARY 264,

   G: CORE TEMPERATURE AT ECC INITIATION 626
9. ECC INJECTION TYPE: C

   A: COLD LEG, B: LOWER PLENUM, C: LOWER PLENUM + COLD LEG
10. PUMP K-FACTOR : ∿ 15
11. ECC FLOW RATES AND DURATION :

    A: ACCUMULATOR 279 M^3/HR FROM 0 TO 23.5 SECONDS

    B: LPCI 30.4 M^3/HR FROM 23.5 TO 820 SECONDS

    C: ECC INJECTION TO LOWER PLENUM : FROM 0 TO 17 SECONDS

    (VALVE OPENING AND CLOSING TIMES ARE INCLUDED IN THE INJECTION DURATION)
12. INITIAL WATER LEVEL IN LOWER PLENUM : 0.86 M.
13. POWER CONTROL : ANS x 1.2 + ACTINIDE (30 SEC AFTER SCRAM)
14. EXPECTED BOCREC TIME FROM ECC INITIATION 12 SEC
15. EXPECTED PEAK TEMPERATURE AT BOCREC 693 C

Table C-2 Chronology of events

EVENT	TIME (sec)
Test Initiated (Heater Rods Power on) (Data Recording Initiated)	0.0
Accumulator Injection Initiated	68.0
Power Decay Initiated (Bottom of Core Recovery)	79.5
Accumulator Injection Switched from Lower Plenum to Cold Leg	85
Accumulator Injection Ended and LPCI Injection Initiated	91.5
All Heater Rods Quenched	611
Power Off	678
LPCI Injection Ended	888
Test Ended (Data Recording Ended)	1086

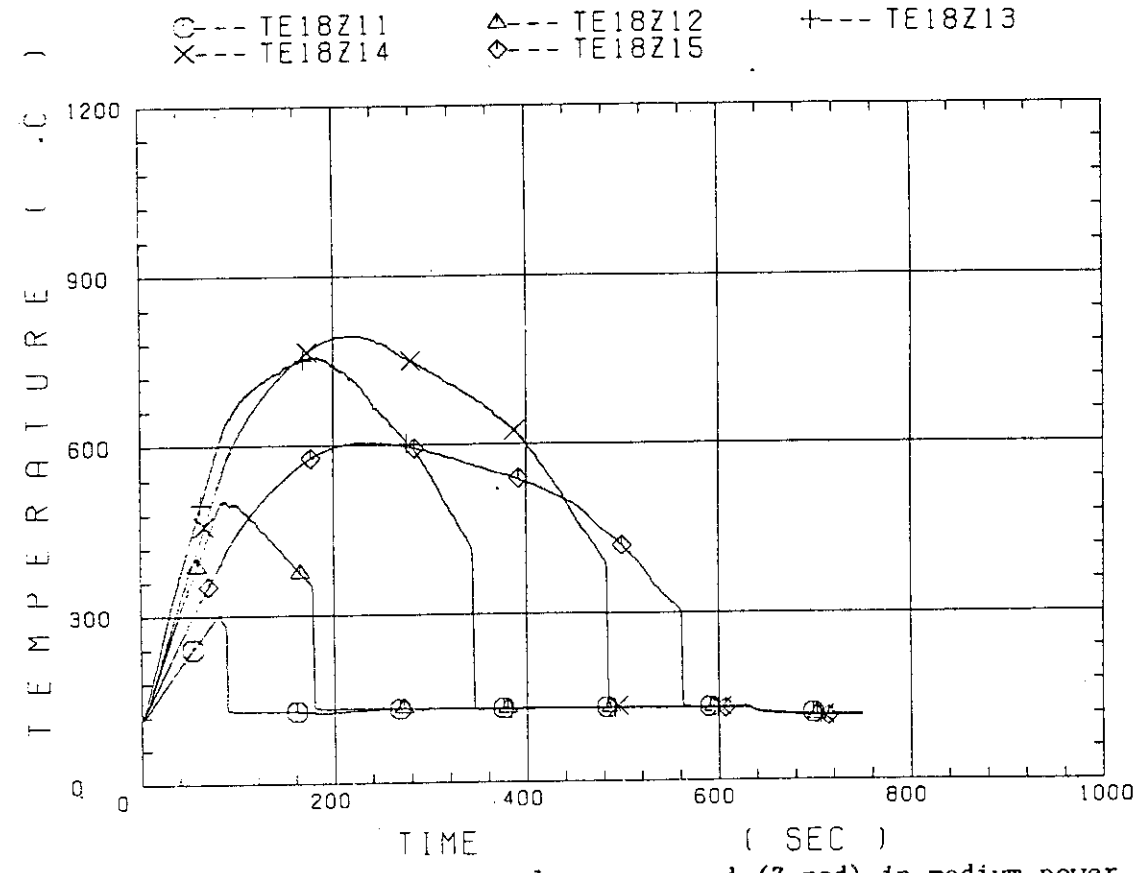

Fig. C-1 Surface temperature on low power rod (Z-rod) in medium power region (B region) (average power rod)

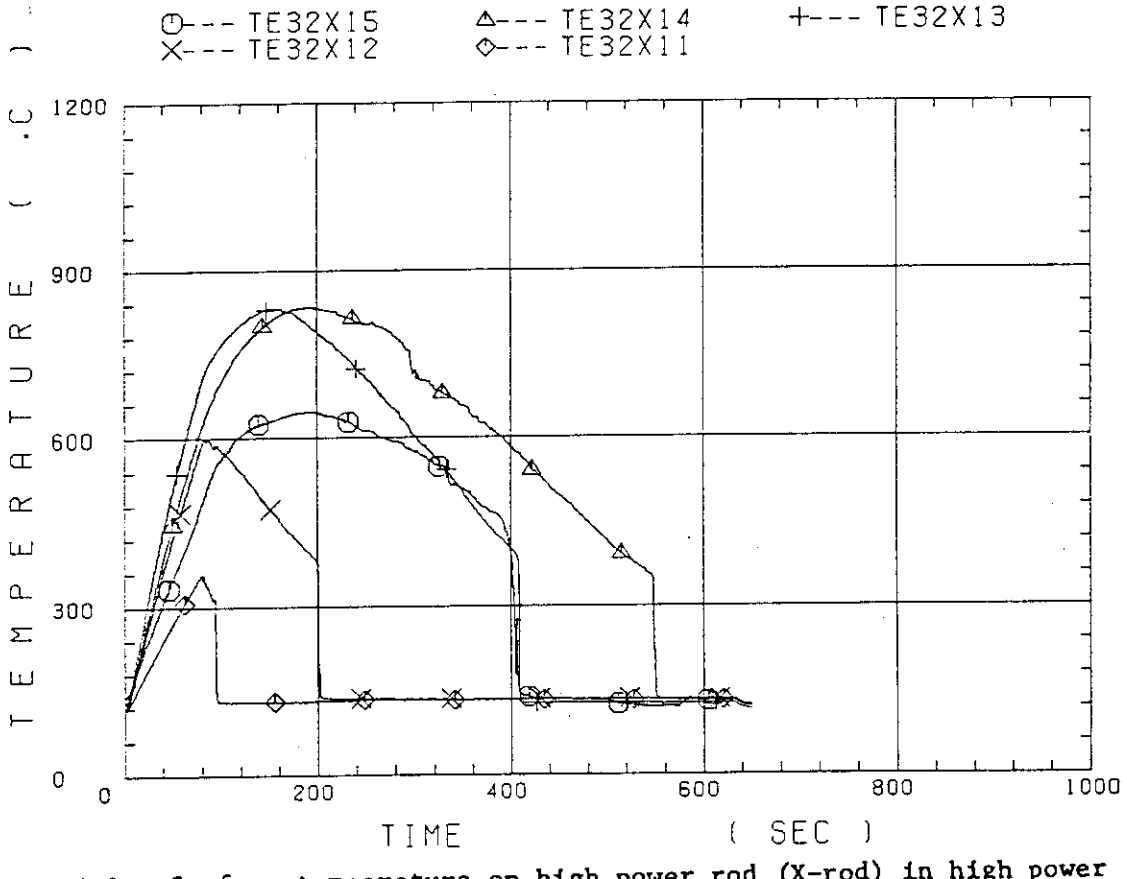

Fig. C-2 Surface temperature on high power rod (X-rod) in high power region (A region) (peak power rod)

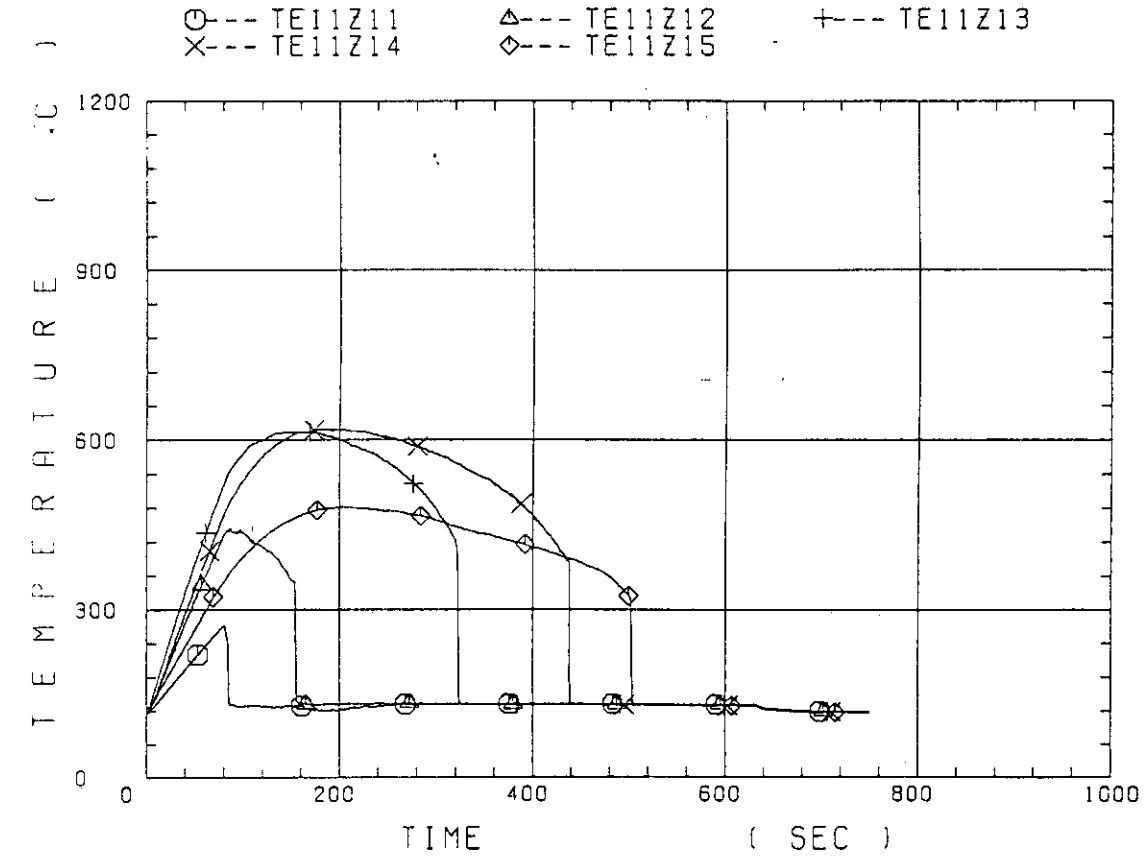

Fig. C-3 Surface temperature on low power rod (Z-rod) in low power region (C region) (lowest power rod)

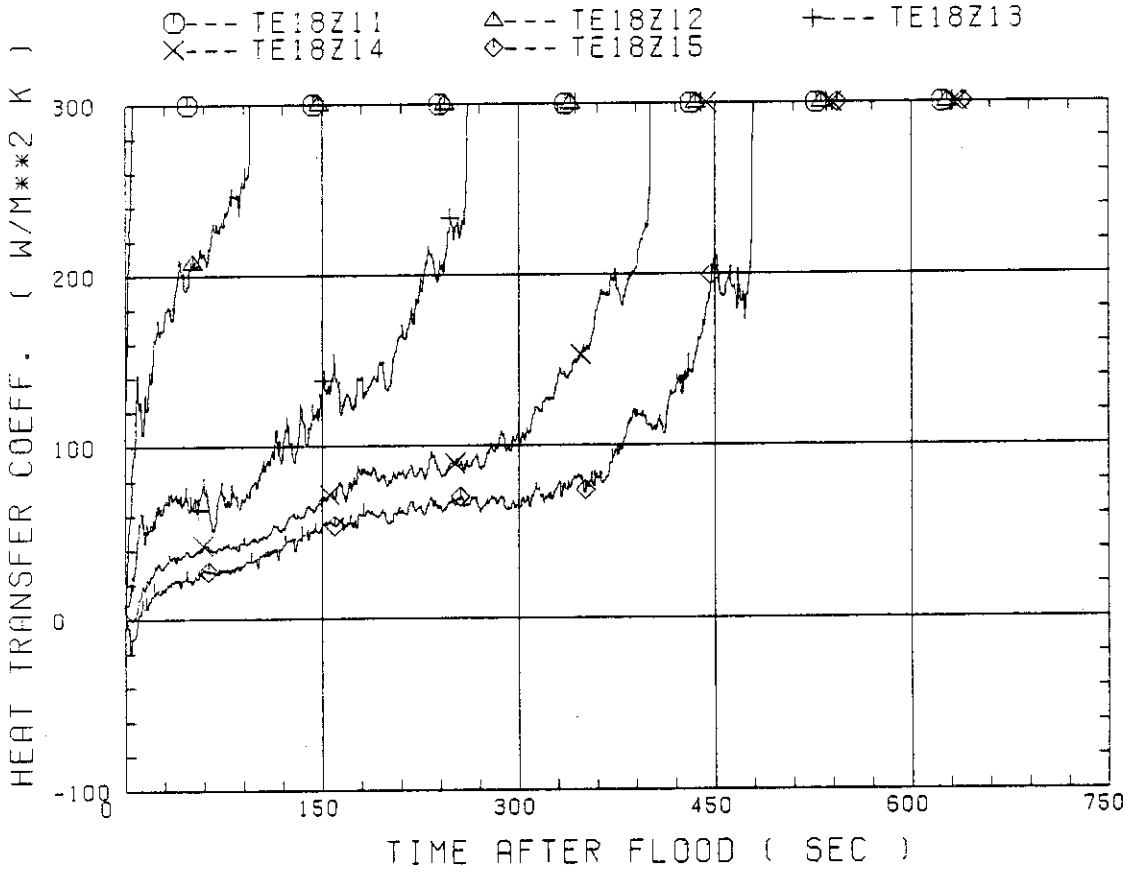

Fig. C-4 Heat transfer coefficient at midplane of low power rod (Z-rod) in medium power region (B region) (average power rod)

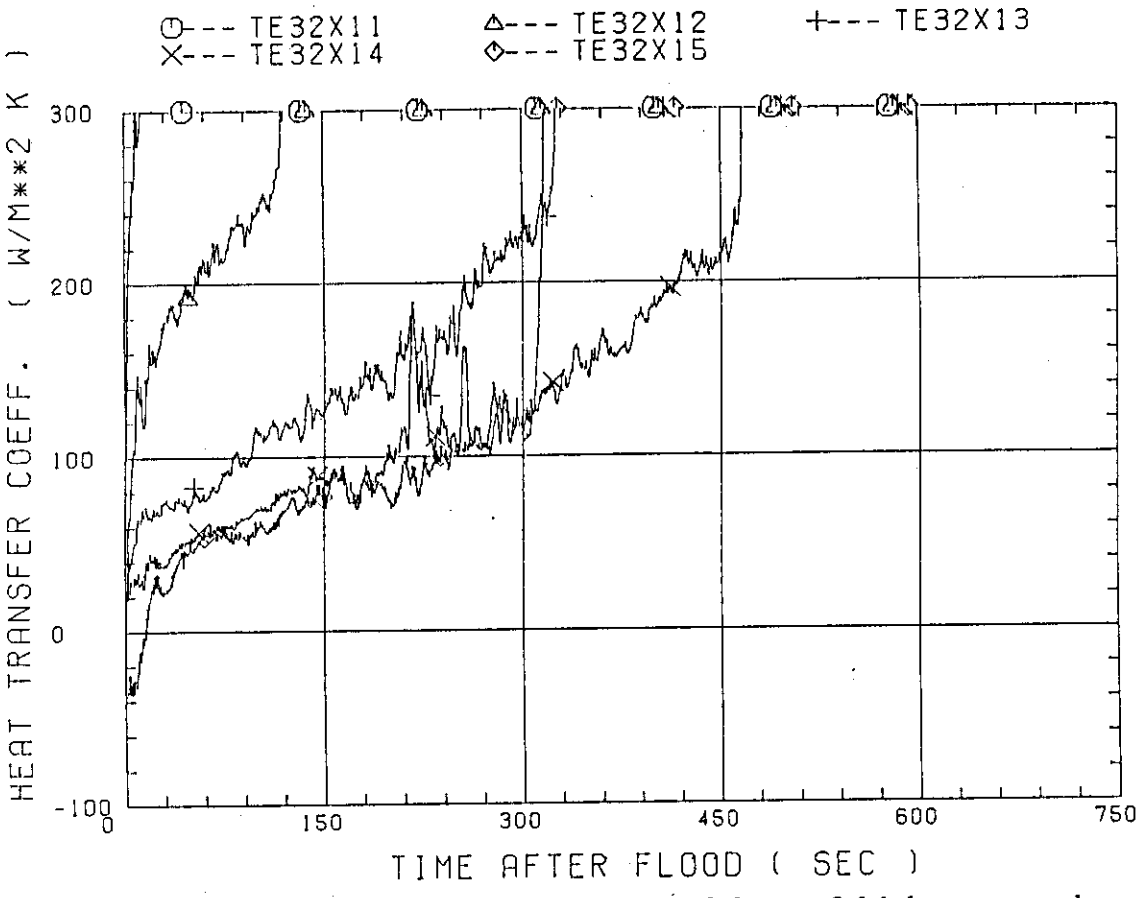

Fig. C-5 Heat transfer coefficient at midplane of high power rod (X-rod) in high power region (A region) (peak power rod)

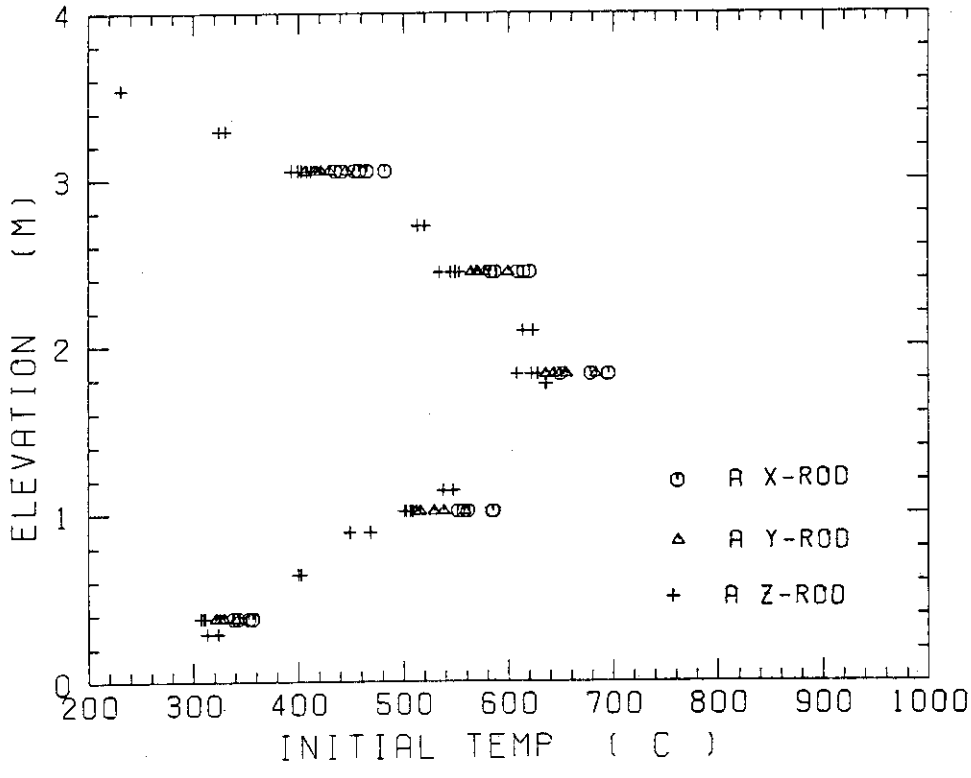

Fig. C-6 Initial rod surface temperature in high power region (A region)

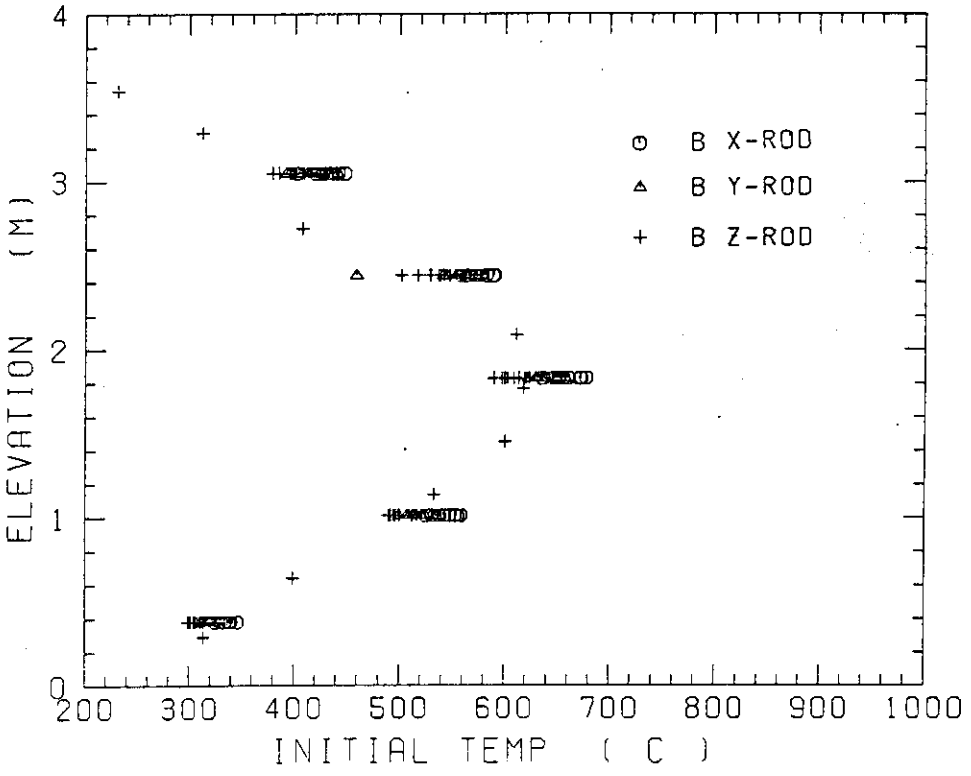

Fig. C-7 Initial rod surface temperature in medium power region (B region)

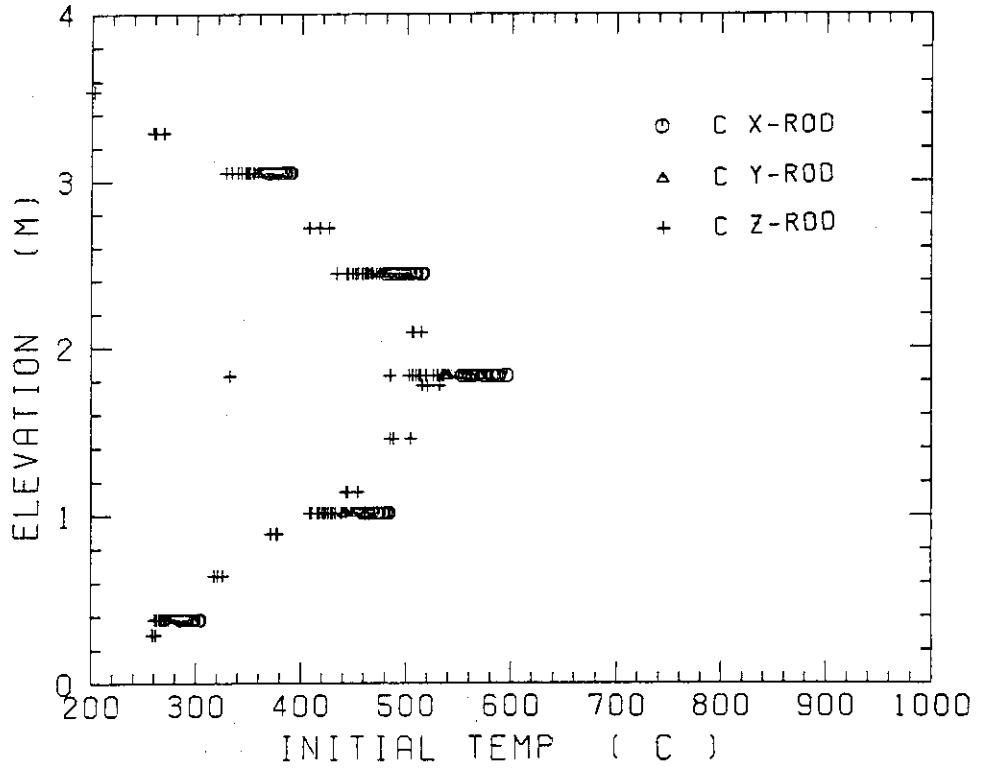

Fig. C-8 Inital rod surface temperature in low power region (C region)

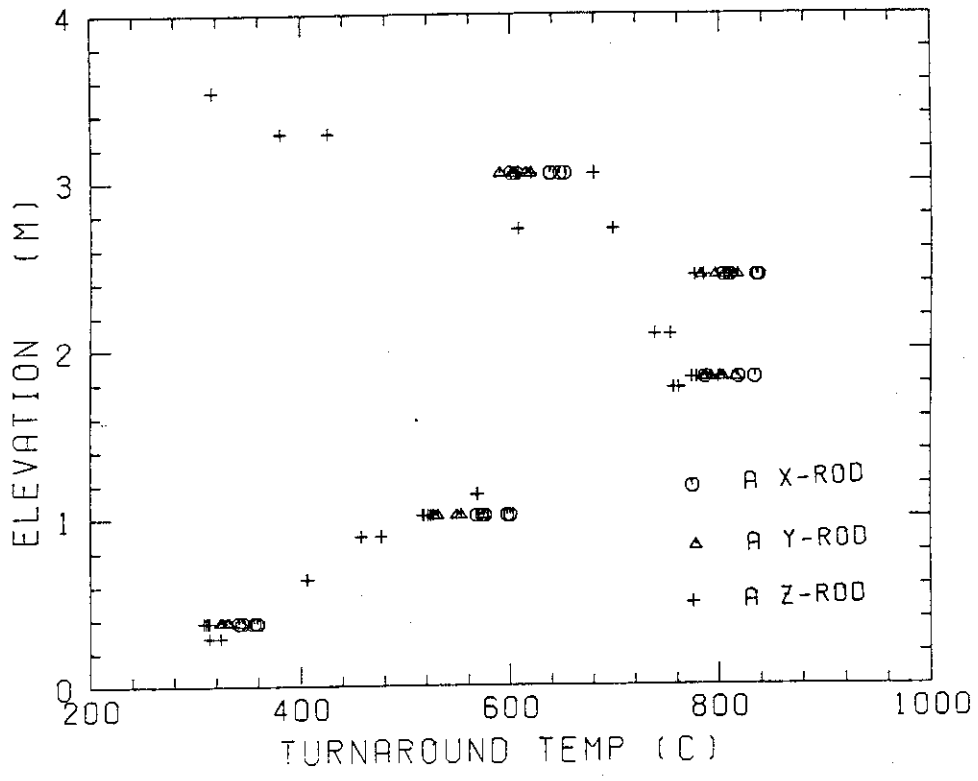

Fig. C-9 Turnaround temperature in high power region (A region)

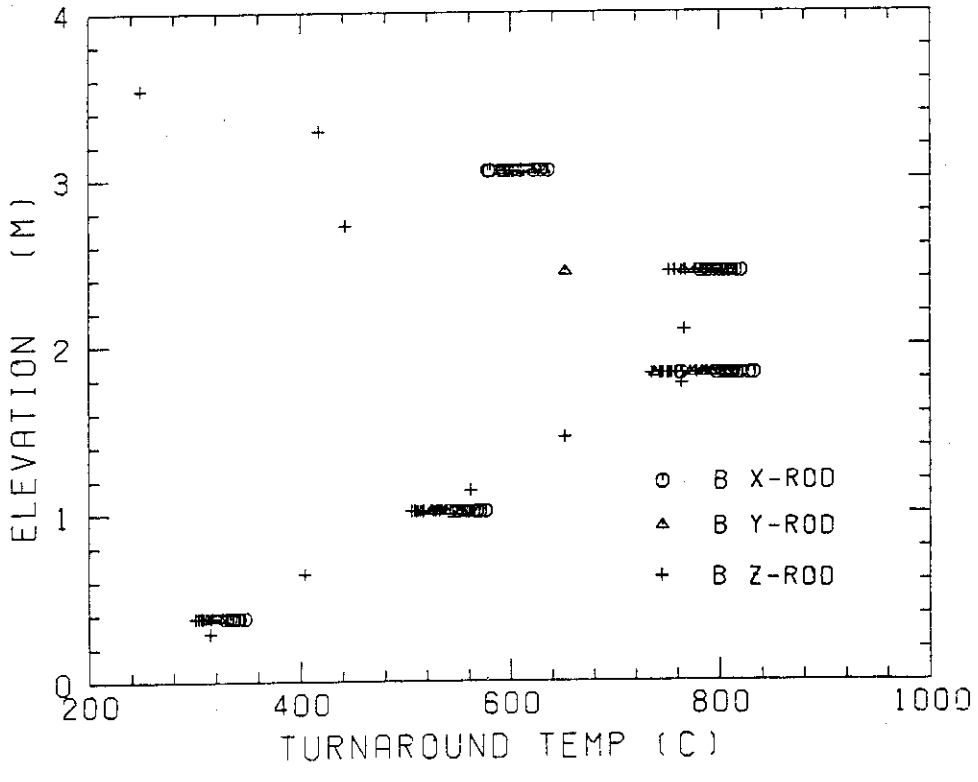

Fig. C-10 Turnaround temperature in medium power region (B region)

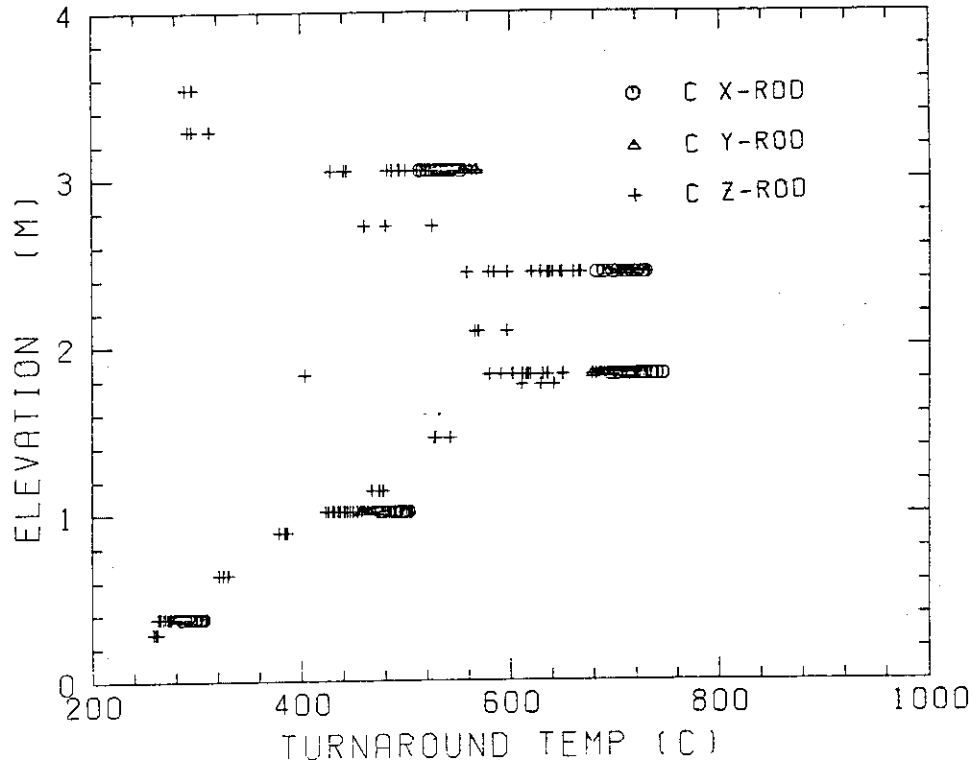

Fig. C-11 Turnaround temperature in low power region (C region)

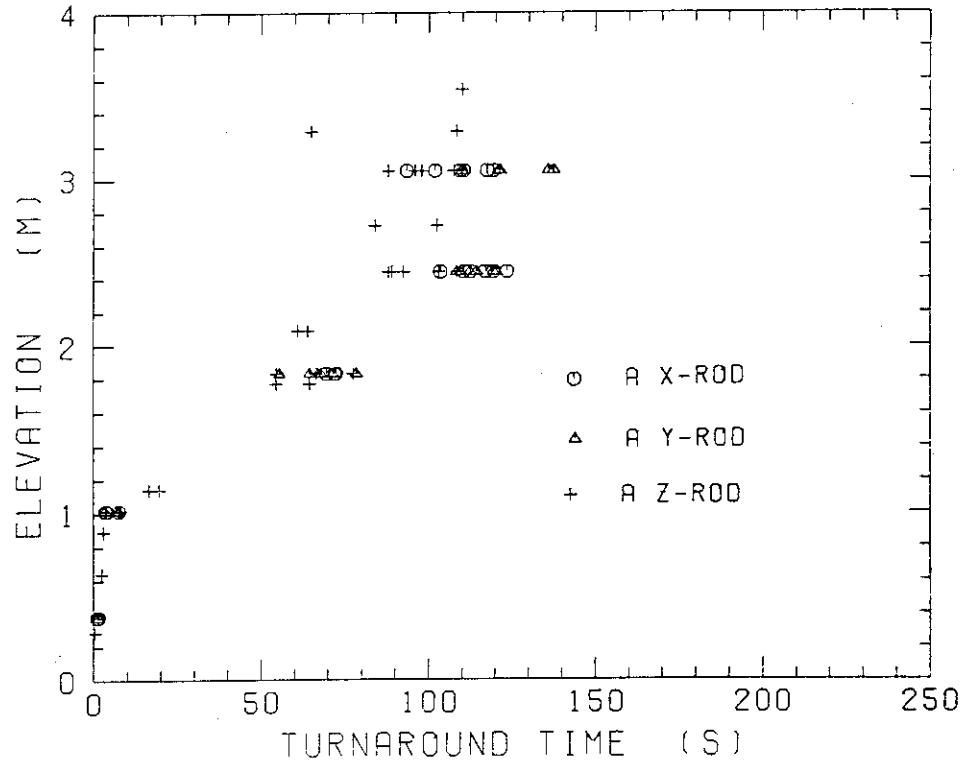

Fig. C-12 Turnaround time in high power region (A region)

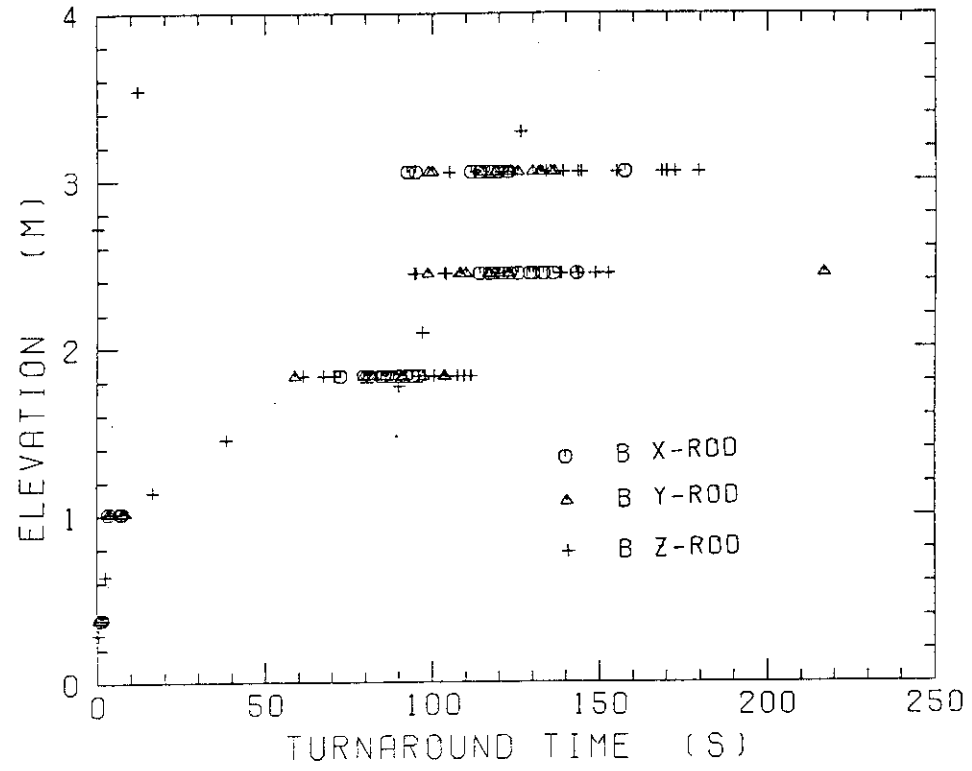

Fig. C-13 Turnaround time in medium power region (B region)

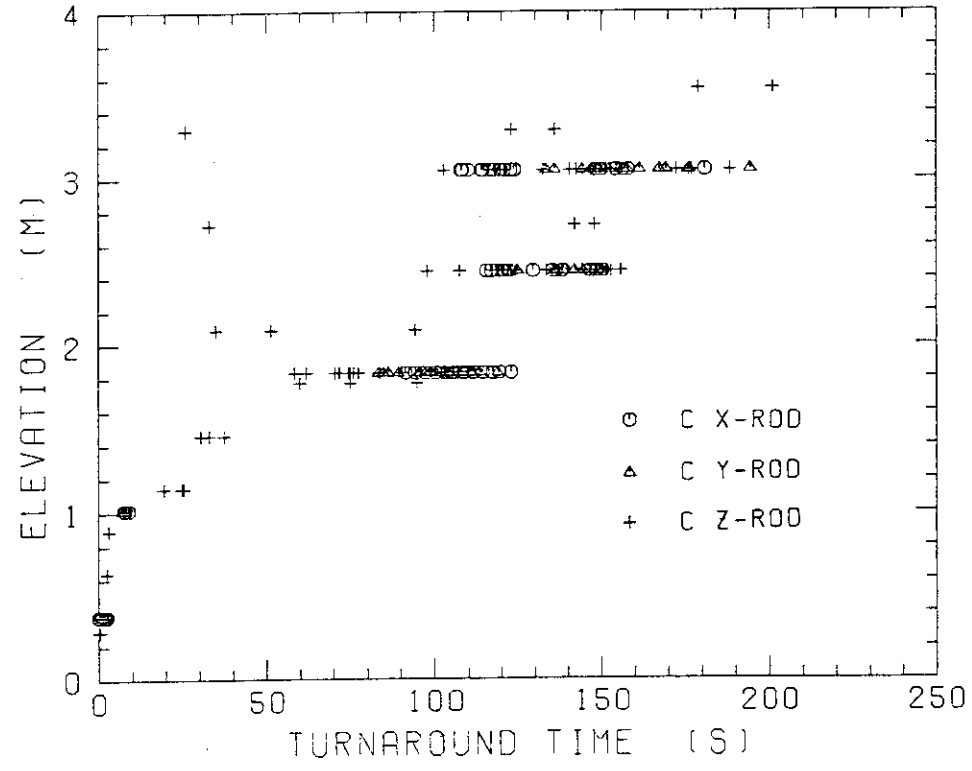

Fig. C-14 Turnaround time in low power region (C region)

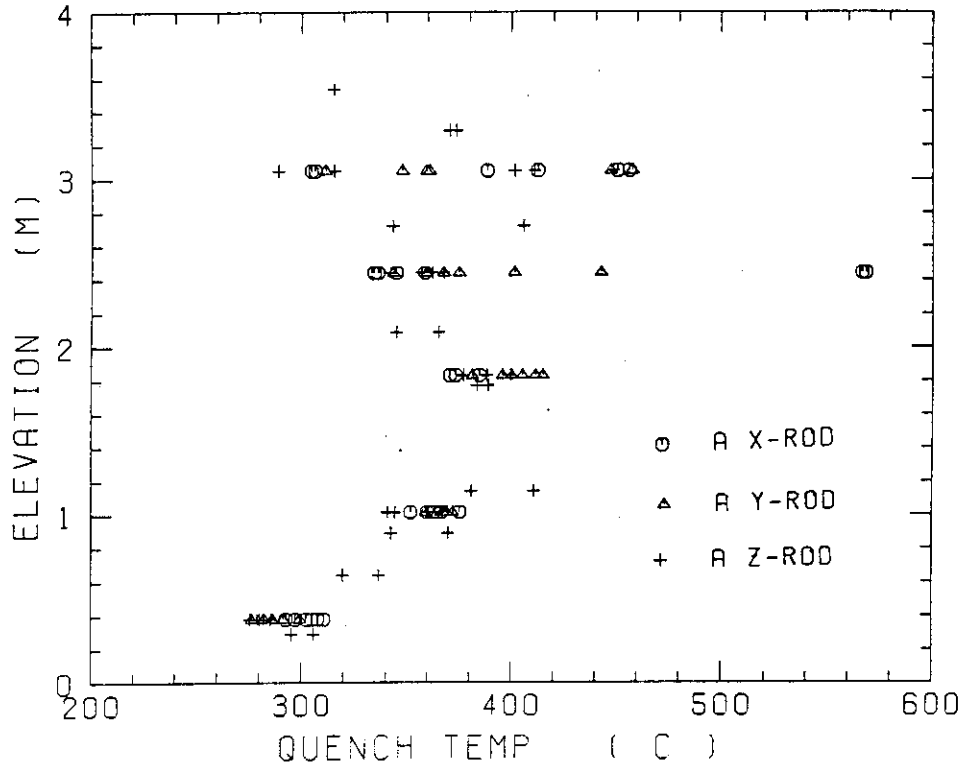

Fig. C-15 Quench temperature in high power region (A region)

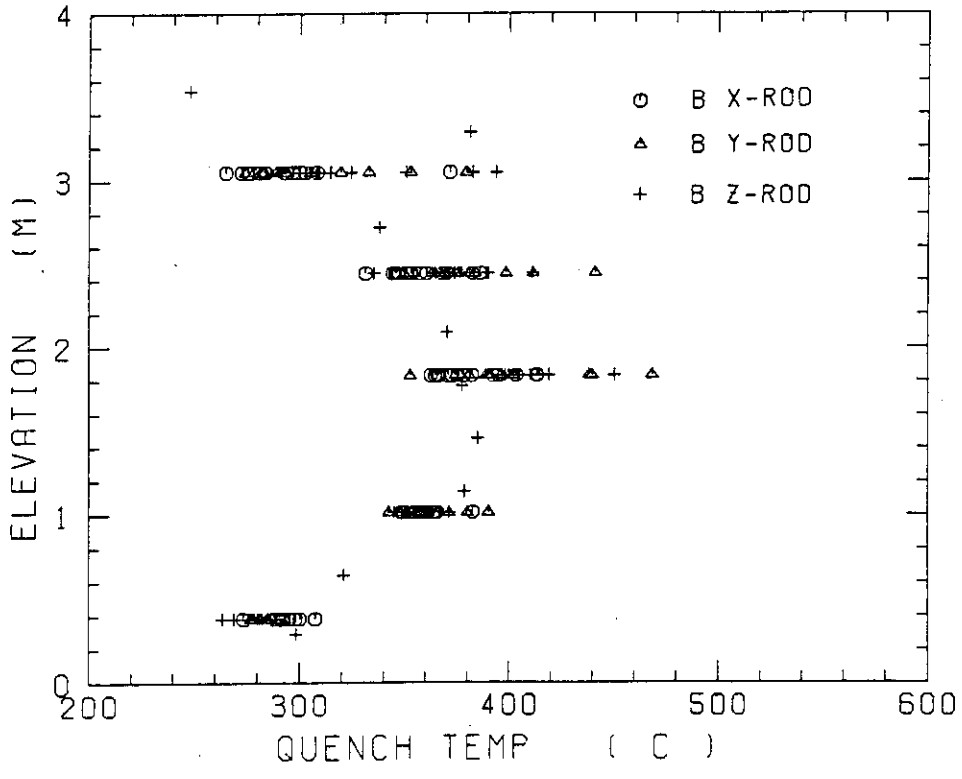

Fig. C-16 Quench temperature in medium power region (B region)

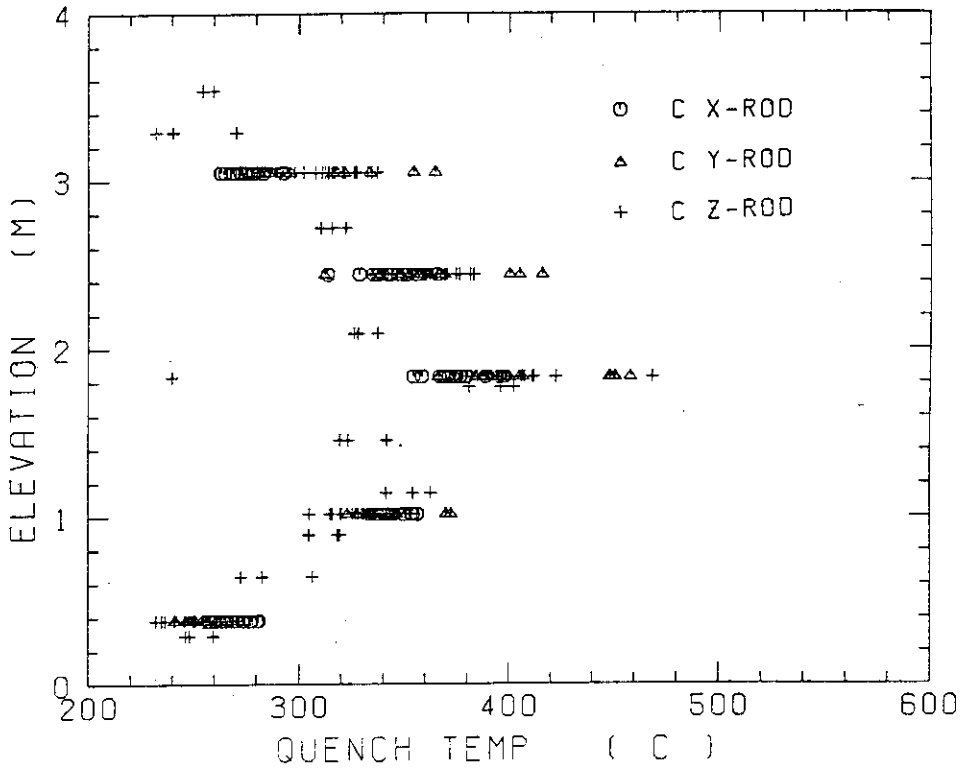

Fig. C-17 Quench temperature in low power region (C region)

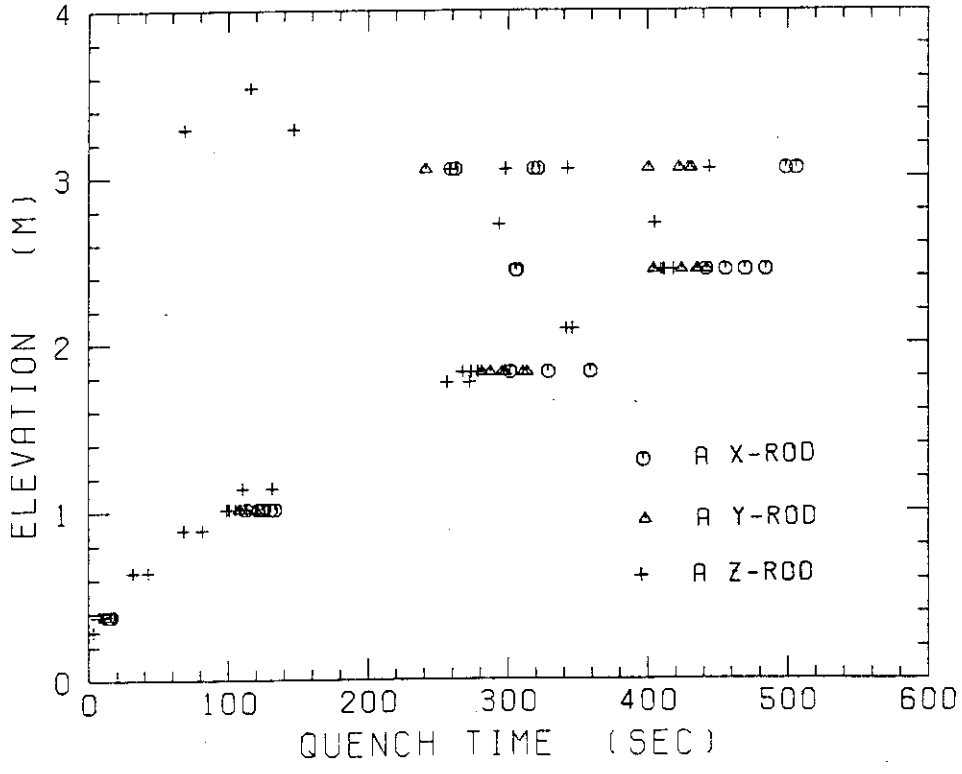

Fig. C-18 Quench time in high power region (A region)

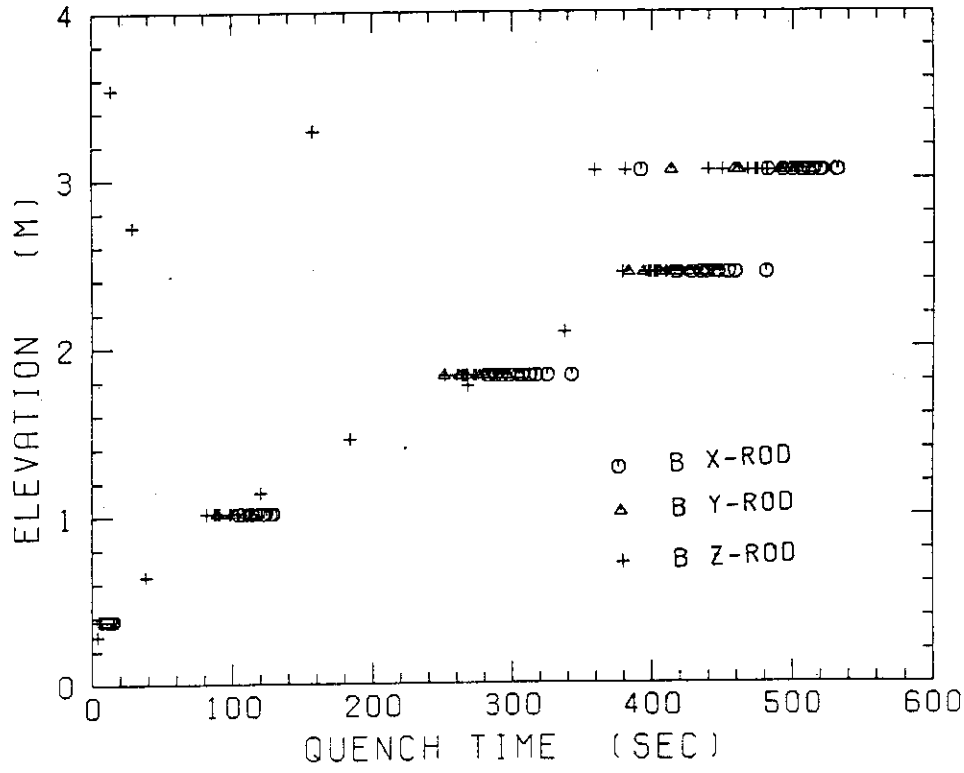

Fig. C-19 Quench time in medium power region (B region)

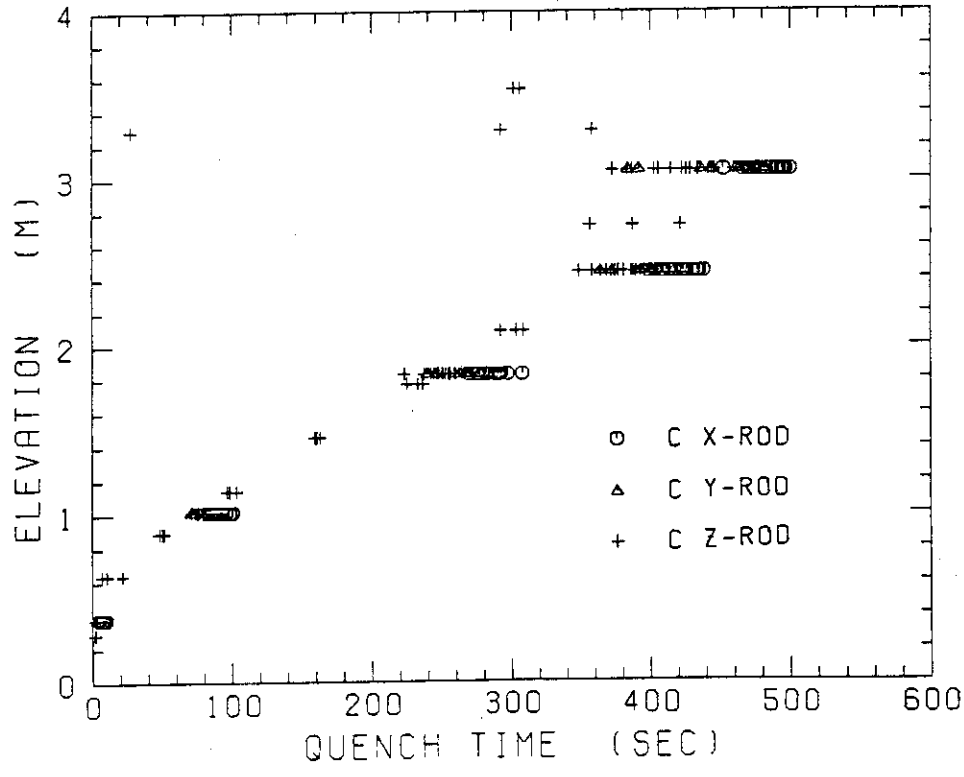

Fig. C-20 Quench time in low power region (C region)

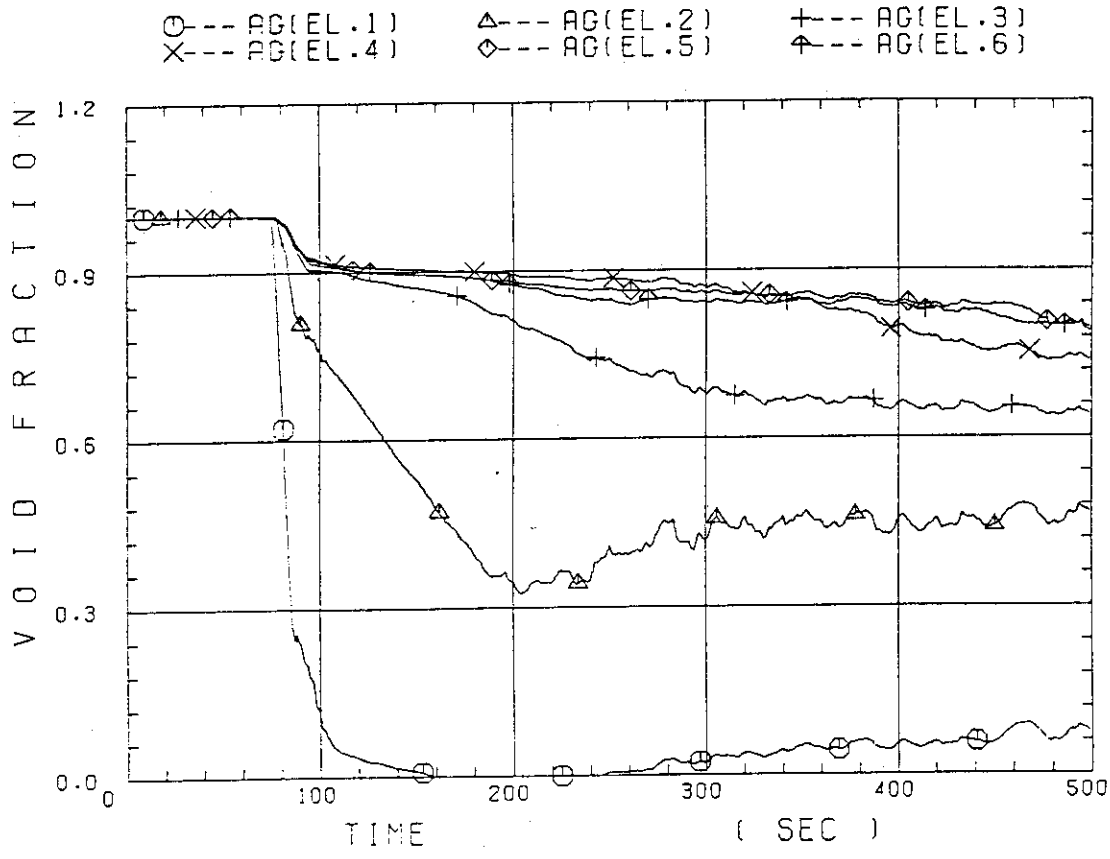

Fig. C-21 Void fraction in core

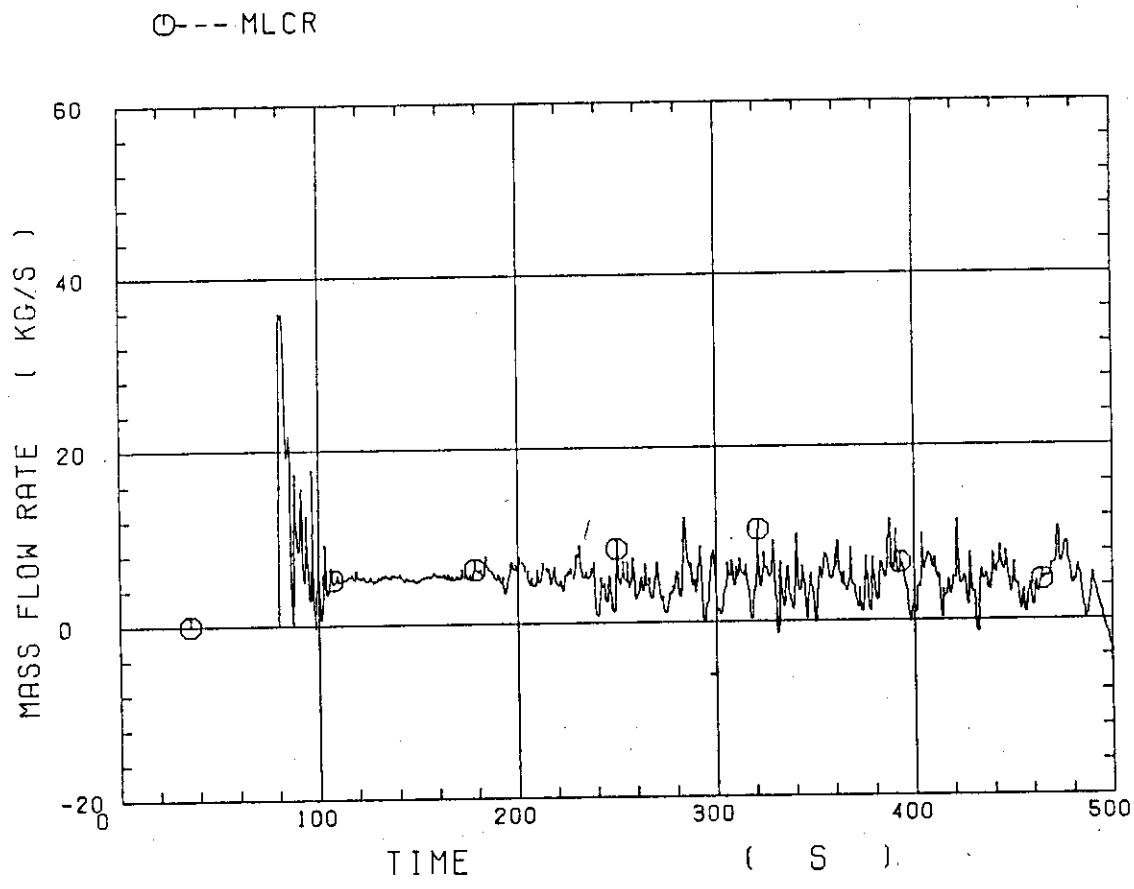

Fig. C-22 Core inlet mass flow rate

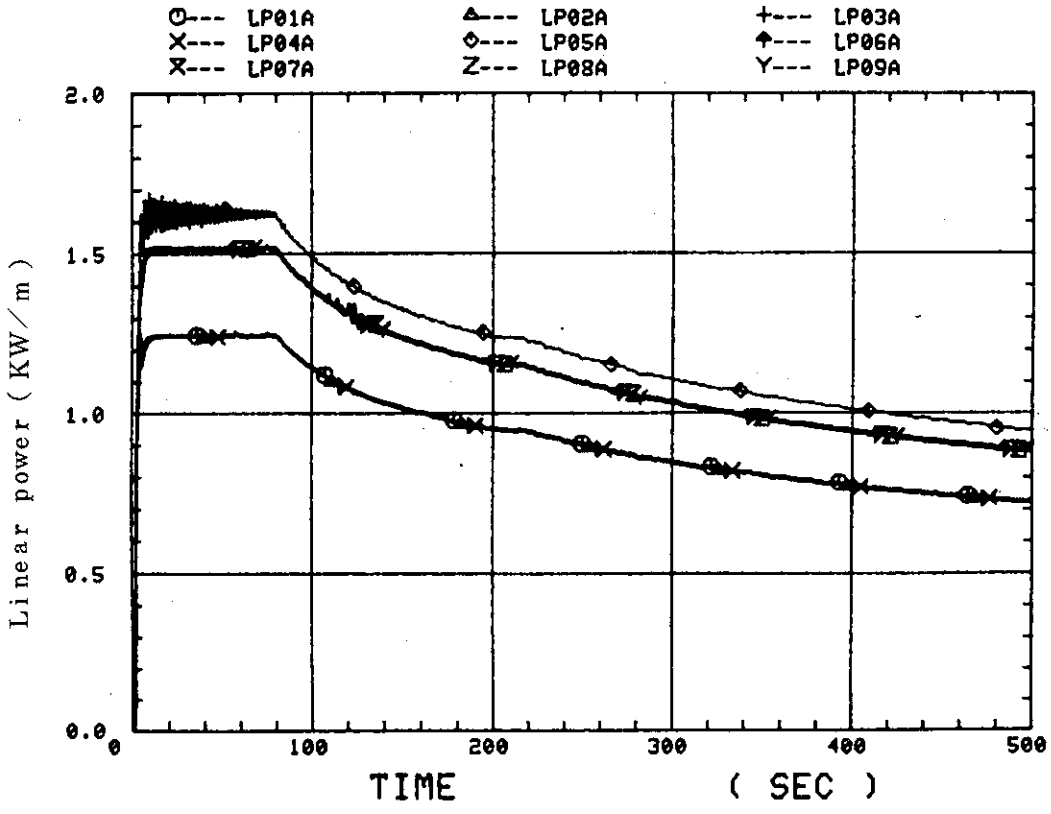

Fig. C-23 Average linear power of heater rod in each power unit zone

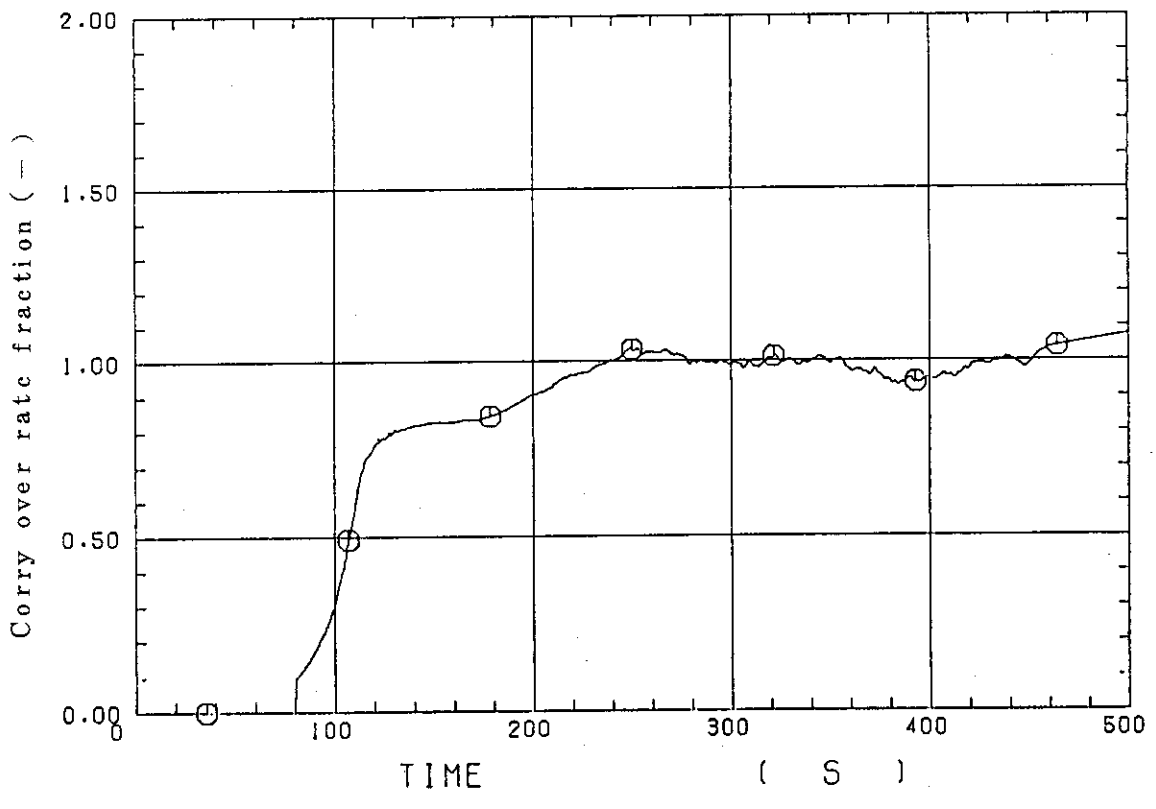

Fig. C-24 Carry-over rate fraction

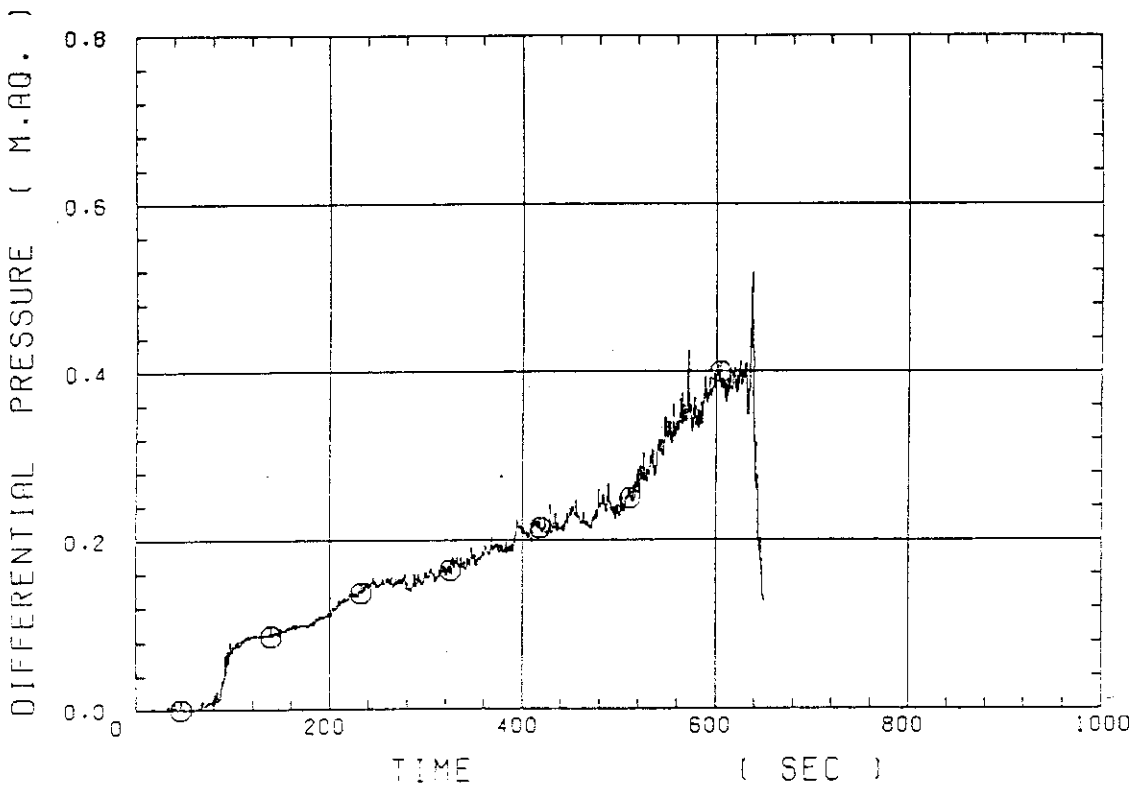

Fig. C-25 Differential pressure through upper plenum

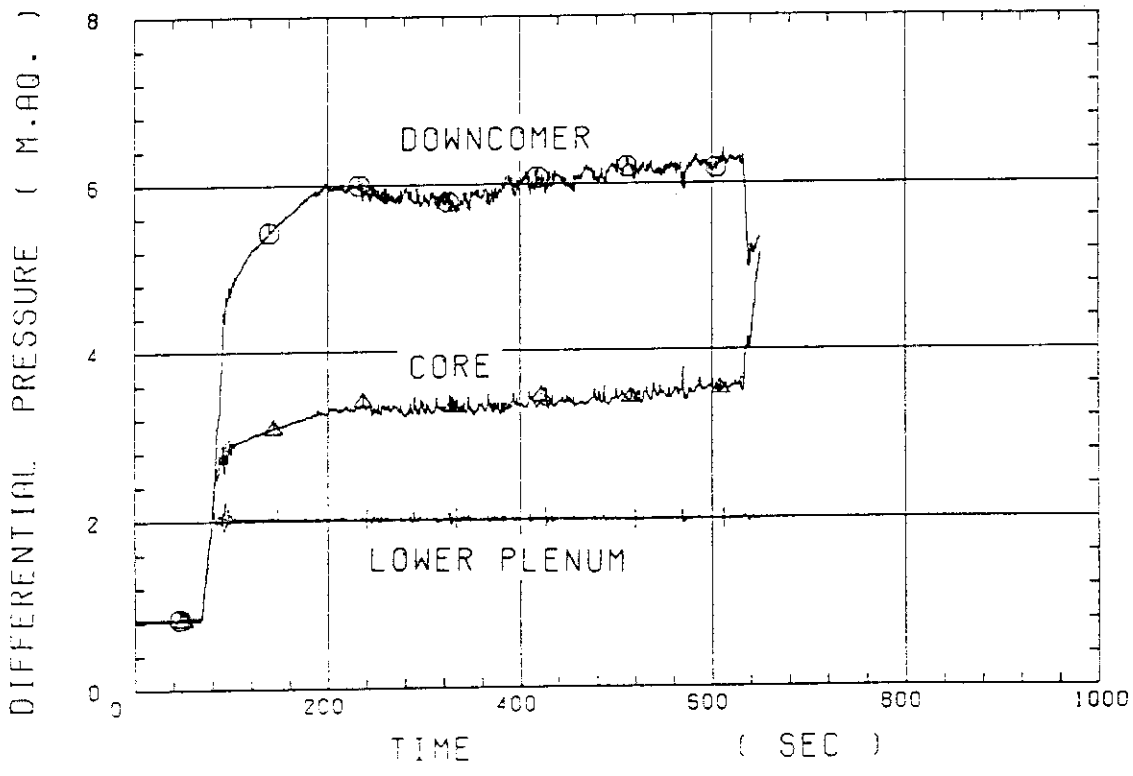

Fig. C-26 Differential pressure through downcomer, core, and lower plenum

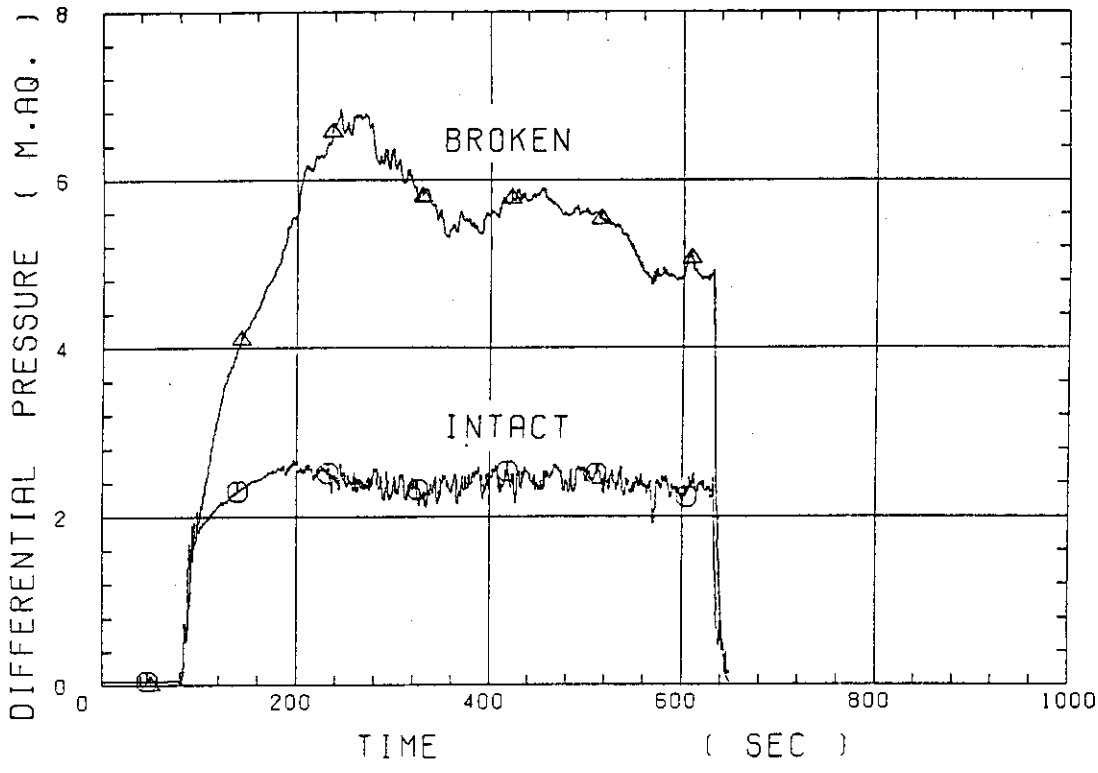

Fig. C-27 Differential pressure through intact and broken loops

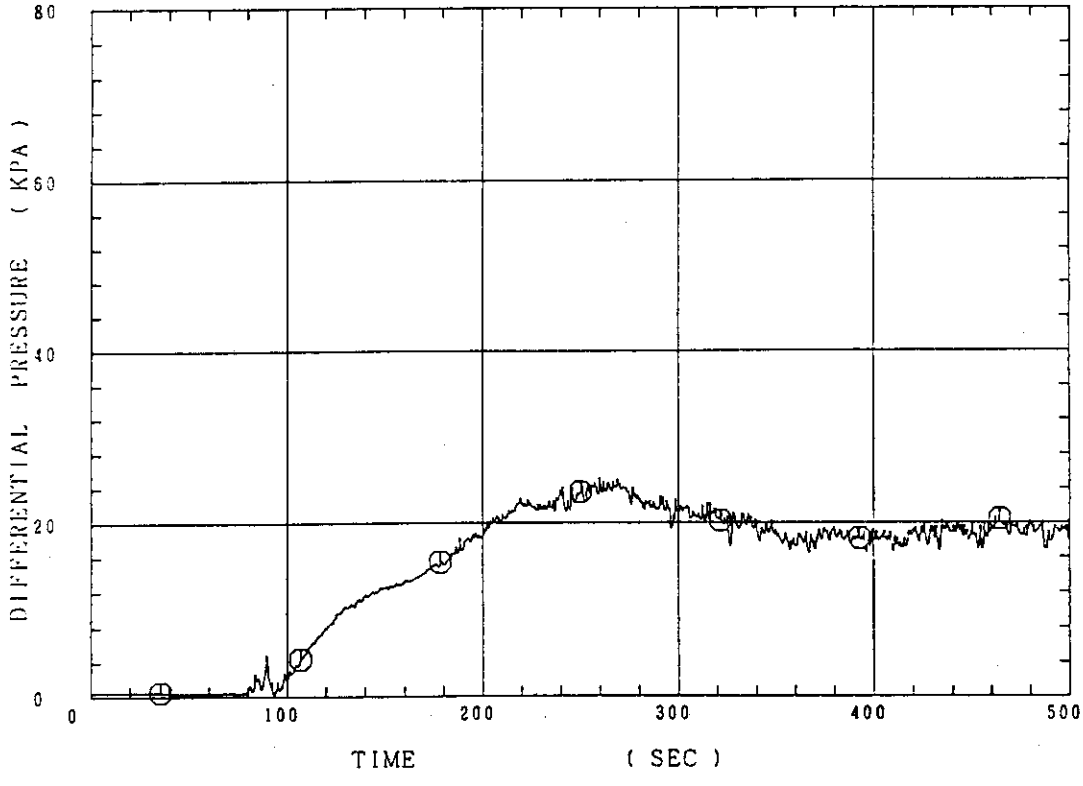

Fig. C-28 Differential pressure through broken cold leg nozzle

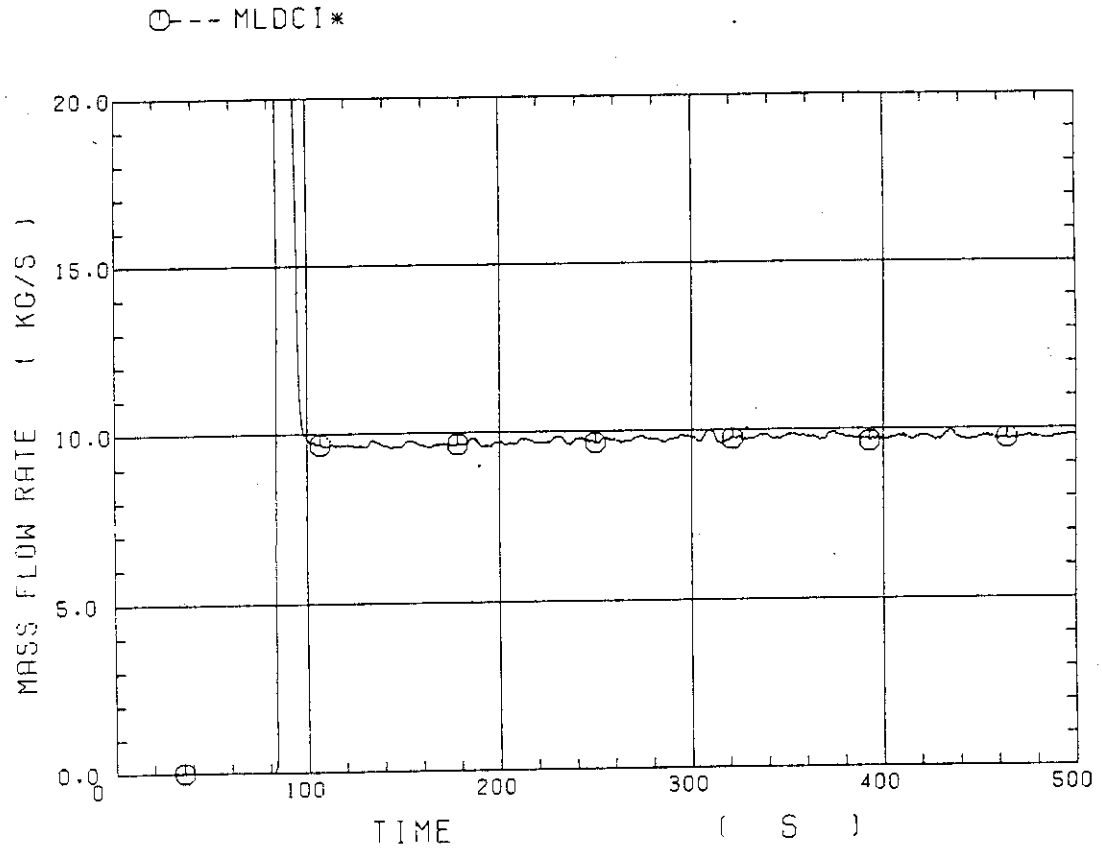

Fig. C-29 Total water mass flow rate from intact loops to downcomer

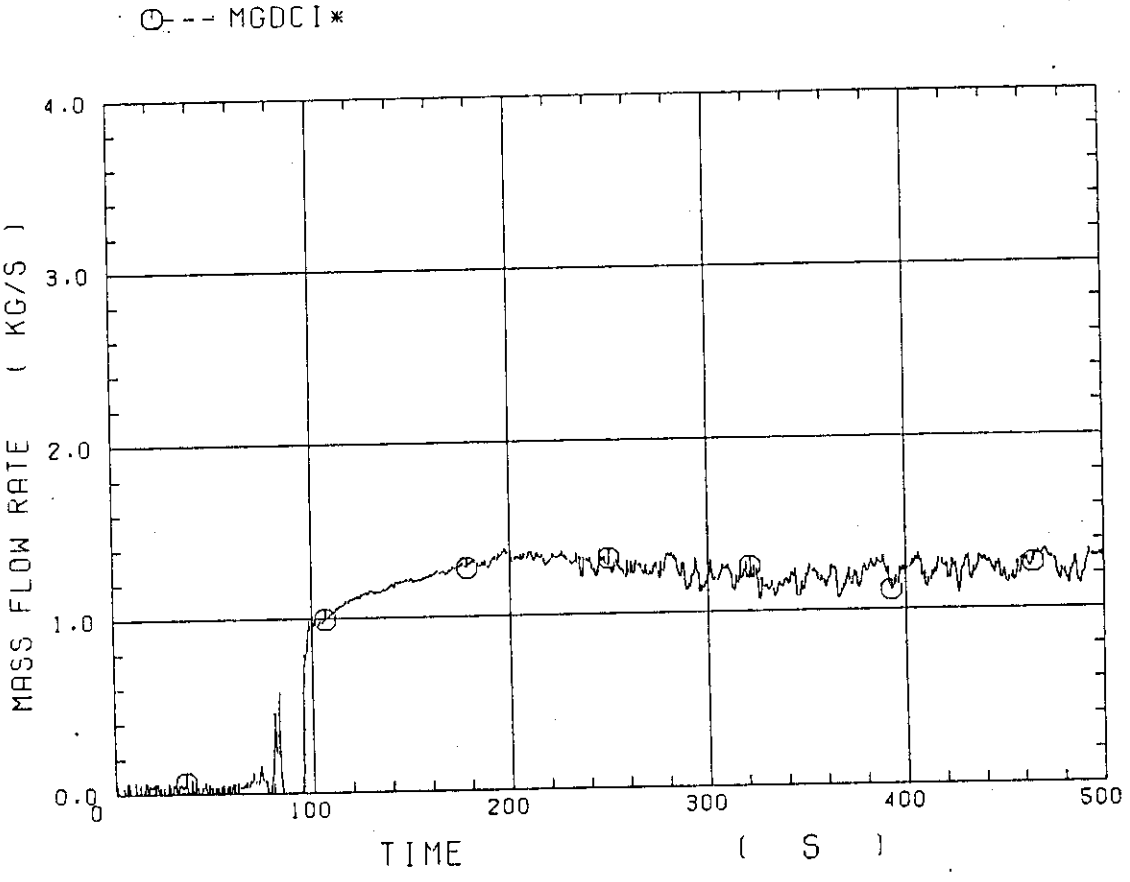

Fig. C-30 Total steam mass flow rate from intact loops to downcomer

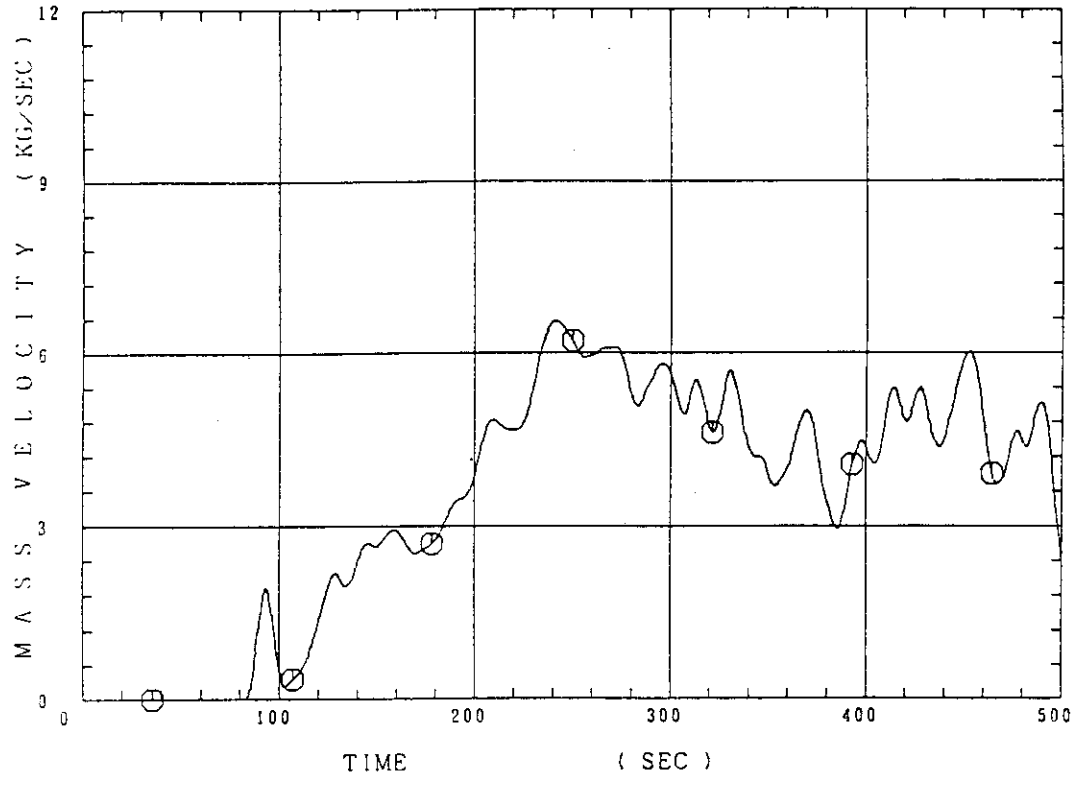

Fig. C-31 Water mass flow rate through broken cold leg nozzle

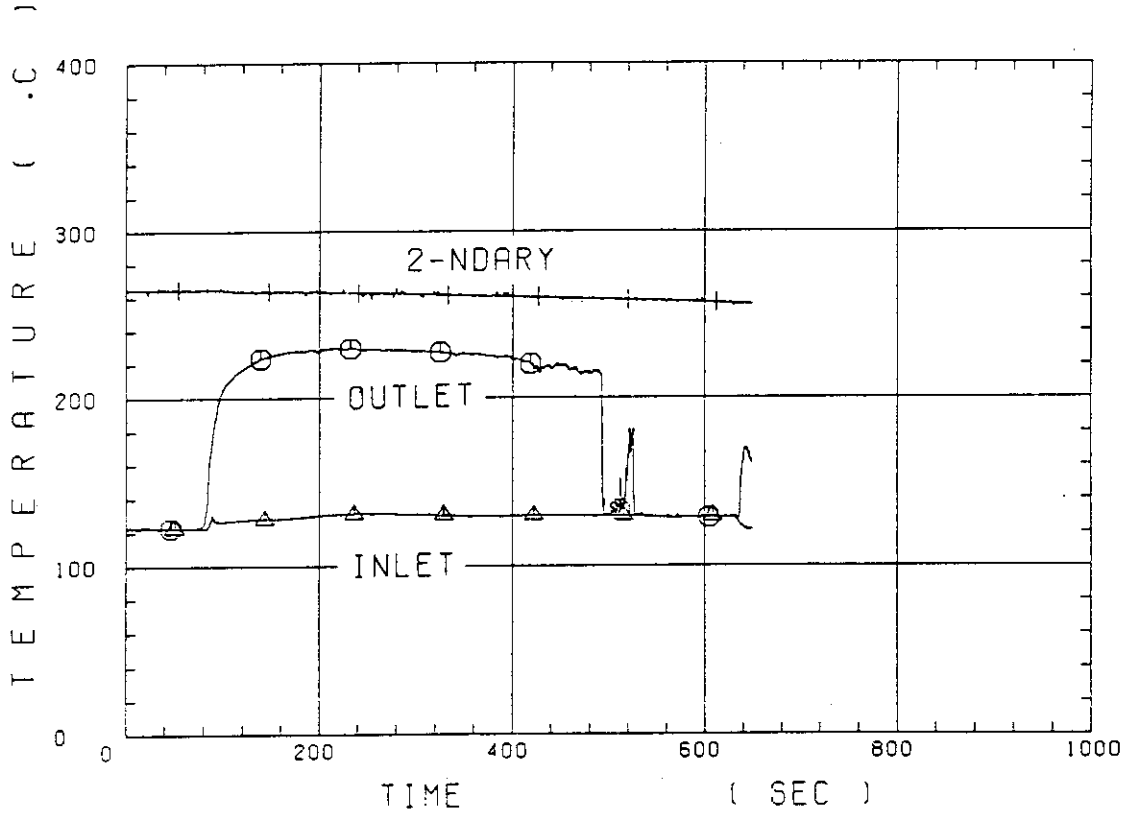

Fig. C-32 Fluid temperature in inlet plenum, outlet plenum, and secondary of steam generator 1

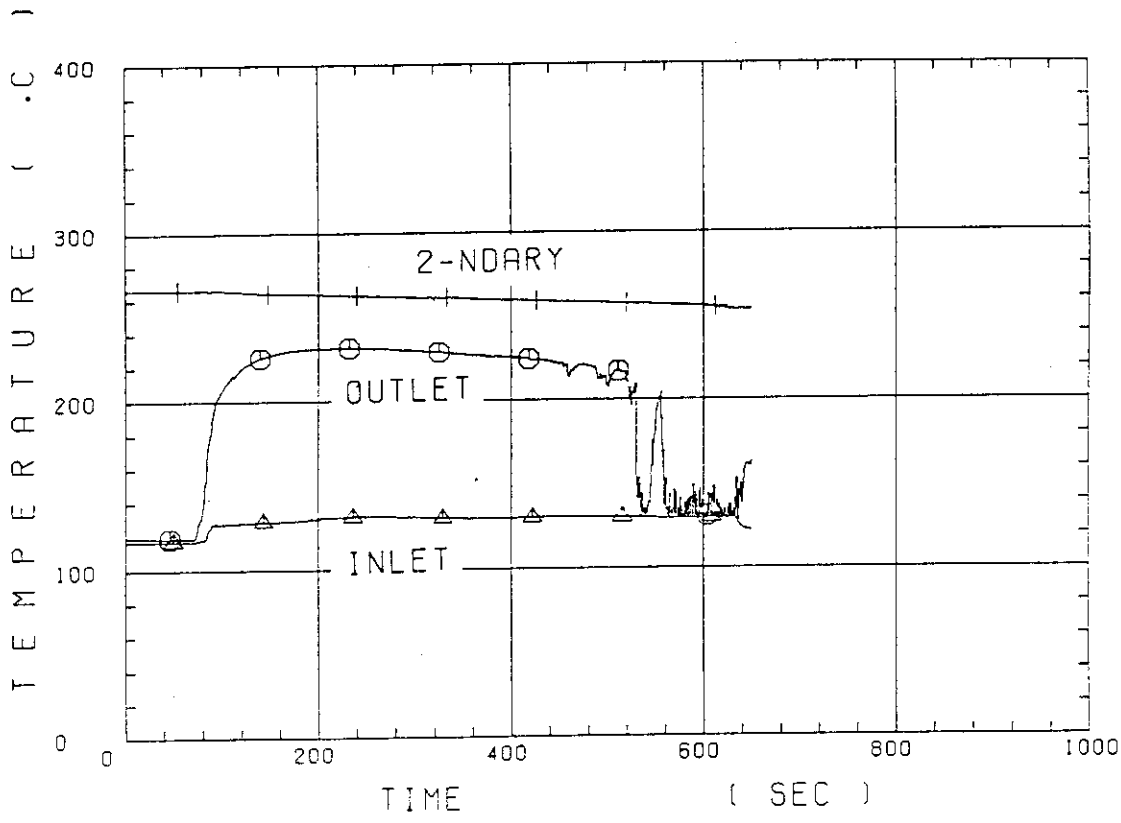

Fig. C-33 Fluid temperature in inlet plenum, outlet plenum, and secondary of steam generator 2

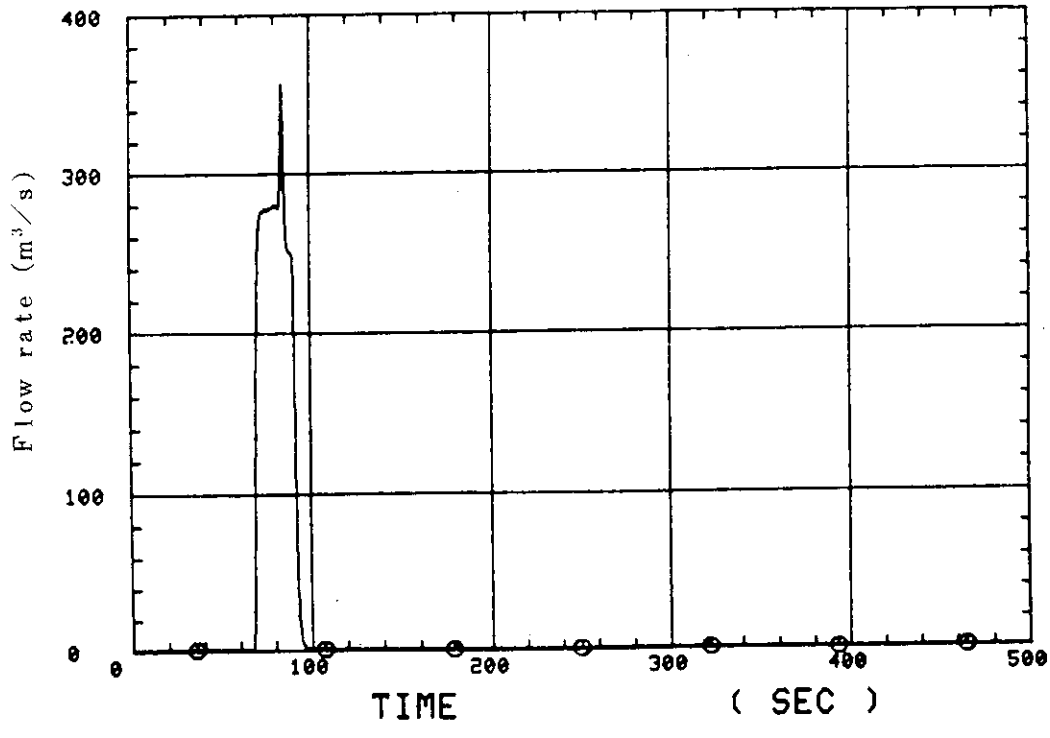

Fig. C-34 Total accumulator injection rate

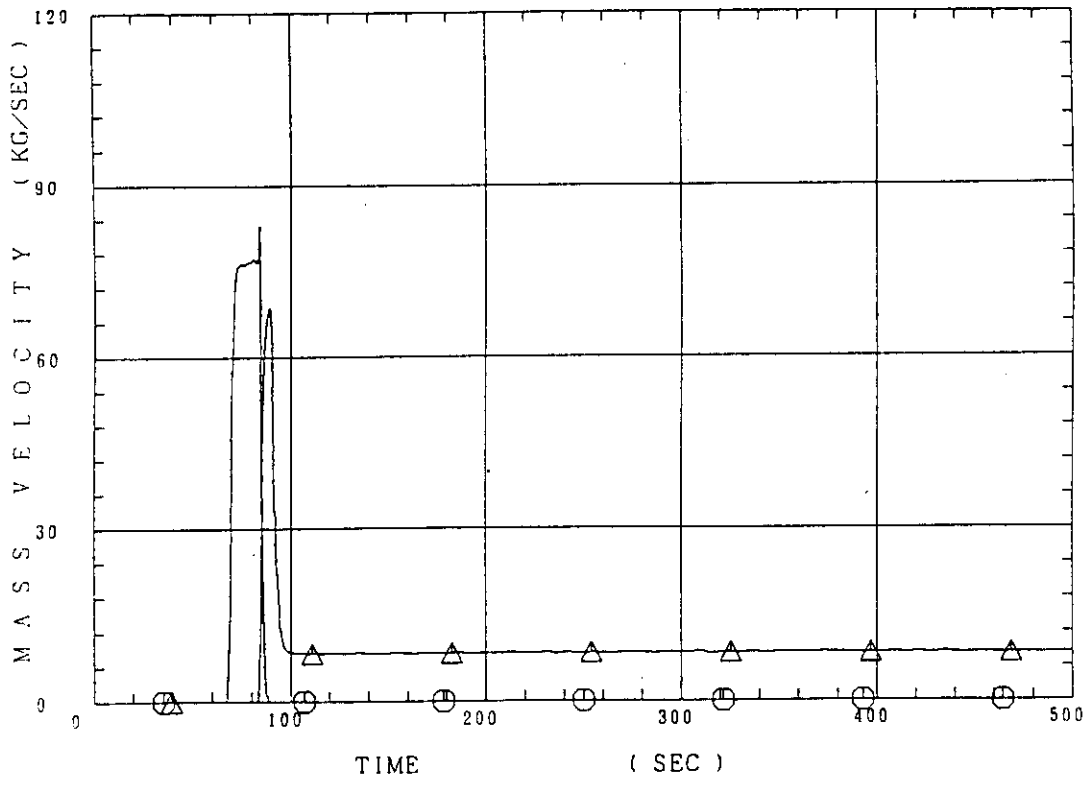

Fig. C-35 ECC water injection rates to lower plenum and to cold legs

○--- MLCRIN △--- MLCRI1

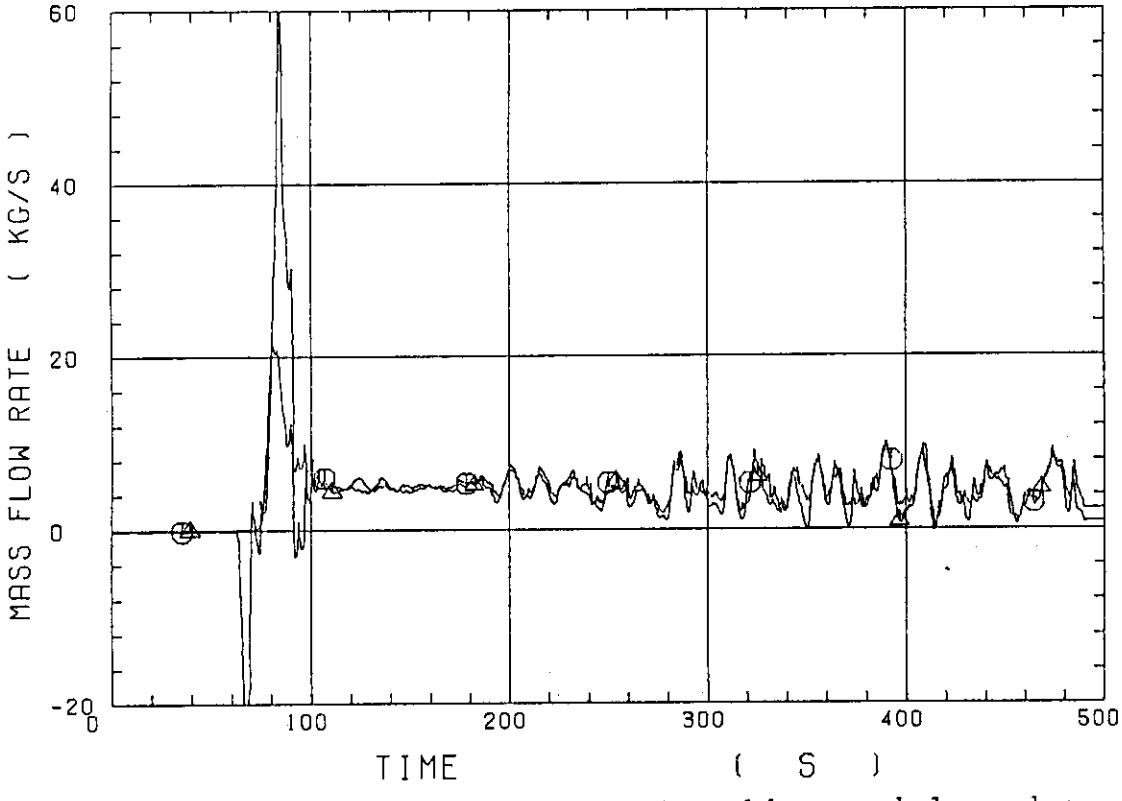

Fig. C-36 Core inlet mass flow rates estimated by mass balance downstream and upstream of core inlet

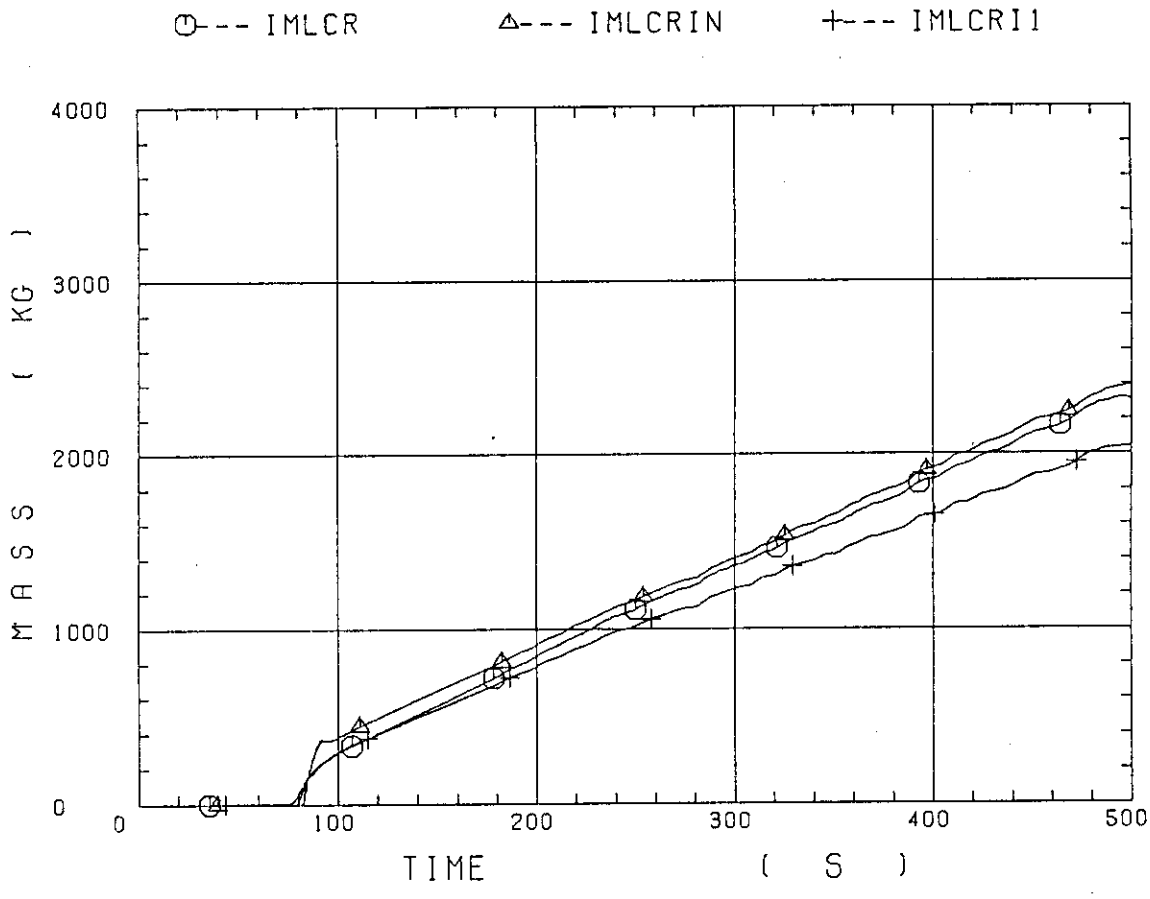

Fig. C-37 Comparison of injected mass into core among two estimation methods and evaluated mass

Appendix D

Main results of Test C1-14 (Run 23)

Table and Figure List

Table D-1 Summary of test conditions

1. TEST TYPE : HIGH INITIAL CLAD TEMPERATURE TEST
2. TEST NUMBER : RUN 023 3. DATE : Feb. 15, 1981
4. POWER : A: TOTAL: 9.40 MW; B:LINEAR: 1.4 KW/M
5. RELATIVE RADIAL POWER SHAPE :

   A: ZONE: A B C

   B: RATIO: 1.07 : 1.0 : 0.82
6. AXIAL POWER SHAPE : CHOPPED COSINE
7. PRESSURE (KG/CM^2A) :

   A: SYSTEM: 2.06, B: CONTAINMENT 2.04,

   C: STEAM GENERATOR SECONDARY: 52
8. TEMPERATURE (DEG.C) :

   A: DOWNCOMER WALL 176, B: VESSEL INTERNALS 122,

   C: PRIMARY PIPING WALL 118, D: LOWER PELNUM LIQUID 121,

   E: ECC LIQUID 40, F: STEAM GENERATOR SECONDARY 264,

   G: CORE TEMPERATURE AT ECC INITIATION 772
9. ECC INJECTION TYPE: C

   A: COLD LEG, B: LOWER PLENUM, C: LOWER PLENUM + COLD LEG
10. PUMP K-FACTOR : ~ 15
11. ECC FLOW RATES AND DURATION :

    A: ACCUMULATOR 277 M^3/HR FROM 0 TO 24 SECONDS

    B: LPCI 30.4 M^3/HR FROM 24 TO 863 SECONDS

    C: ECC INJECTION TO LOWER PLENUM : FROM 0 TO 17 SECONDS

    (VALVE OPENING AND CLOSING TIMES ARE INCLUDED IN THE INJECTION DURATION)
12. INITIAL WATER LEVEL IN LOWER PLENUM : 0.86 M.
13. POWER CONTROL : ANS x 1.2 + ACTINIDE (30 SEC AFTER SCRAM)
14. EXPECTED BOCREC TIME FROM ECC INITIATION 12 SEC
15. EXPECTED PEAK TEMPERATURE AT BOCREC 800 C

Table D-2 Chronology of events

EVENT	TIME (sec)
Test Initiated (Heater Rods Power on) (Data Recording Initiated)	0.0
Accumulator Injection Initiated	85.5
Power Decay Initiated (Bottom of Core Recovery)	96.5
Accumulator Injection Switched from Lower Plenum to Cold Leg	102.5
Accumulator Injection Ended and LPCI Injection Initiated	109.5
All Heater Rods Quenched	660
Power Off	738
LPCI Injection Ended	948
Test Ended (Data Recording Ended)	1104

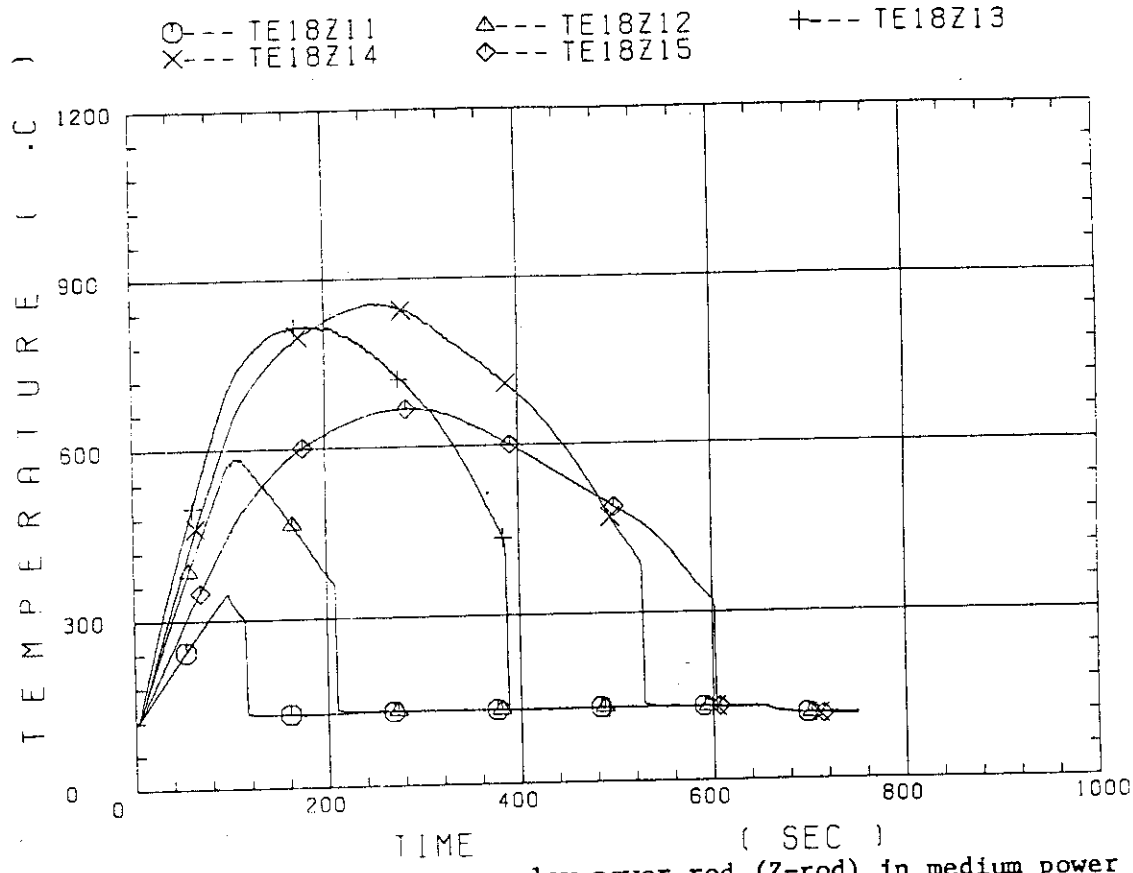

Fig. D-1 Surface temperature on low power rod (Z-rod) in medium power region (B region) (average power rod)

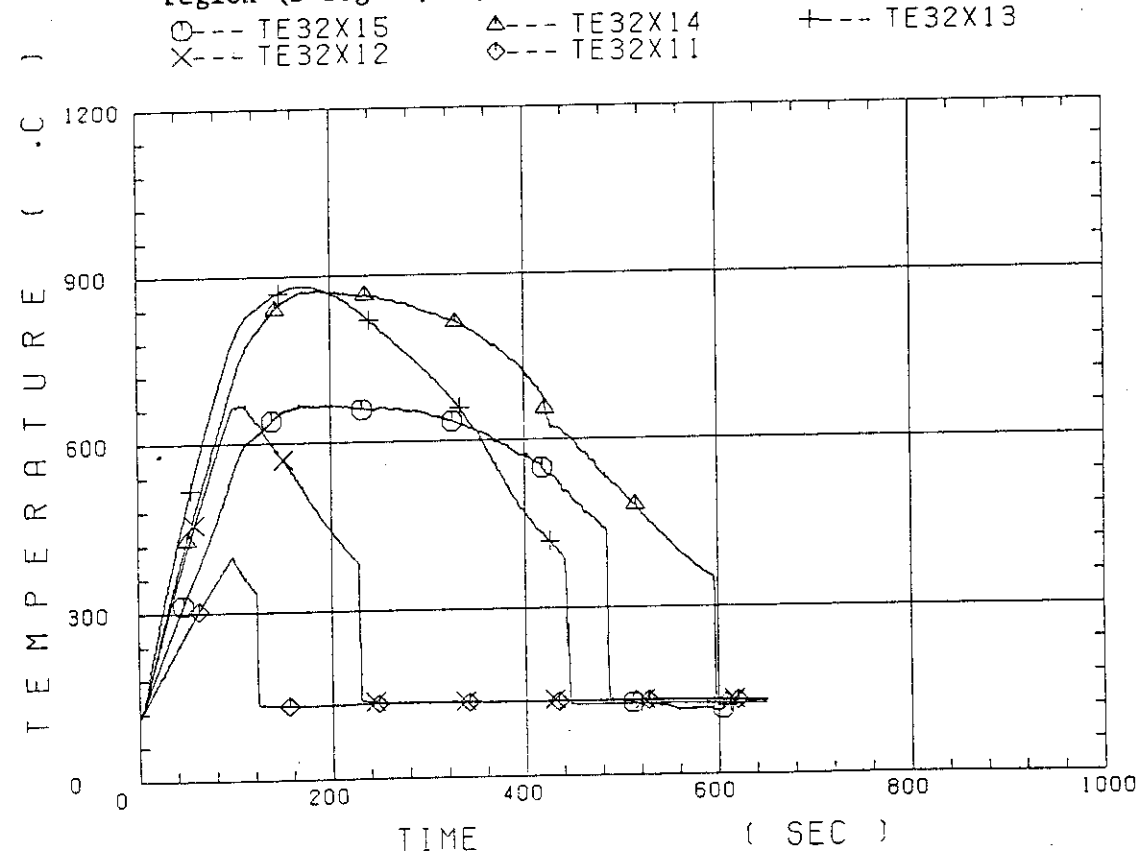

Fig. D-2 Surface temperature on high power rod (X-rod) in high power region (A region) (peak power rod)

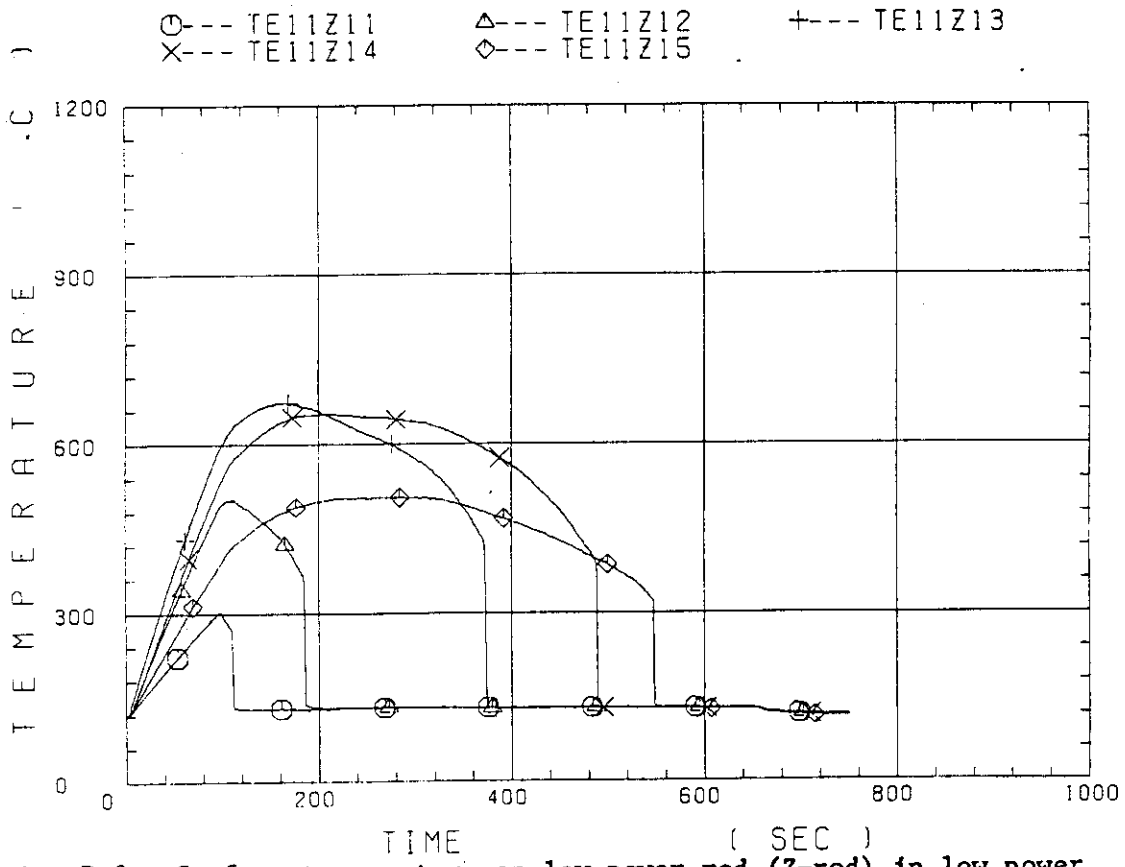

Fig. D-3 Surface temperature on low power rod (Z-rod) in low power region (C region) (lowest power rod)

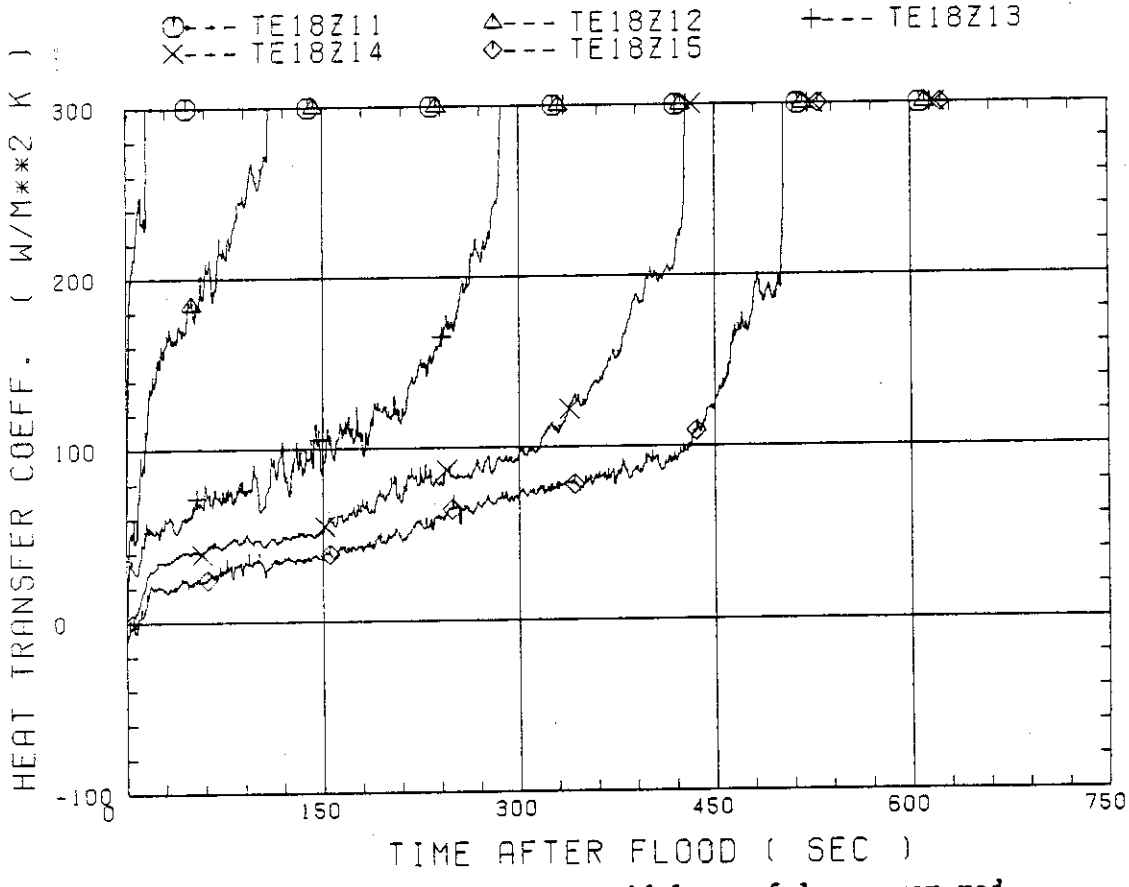

Fig. D-4 Heat transfer coefficient at midplane of low power rod (Z-rod) in medium power region (B region) (average power rod)

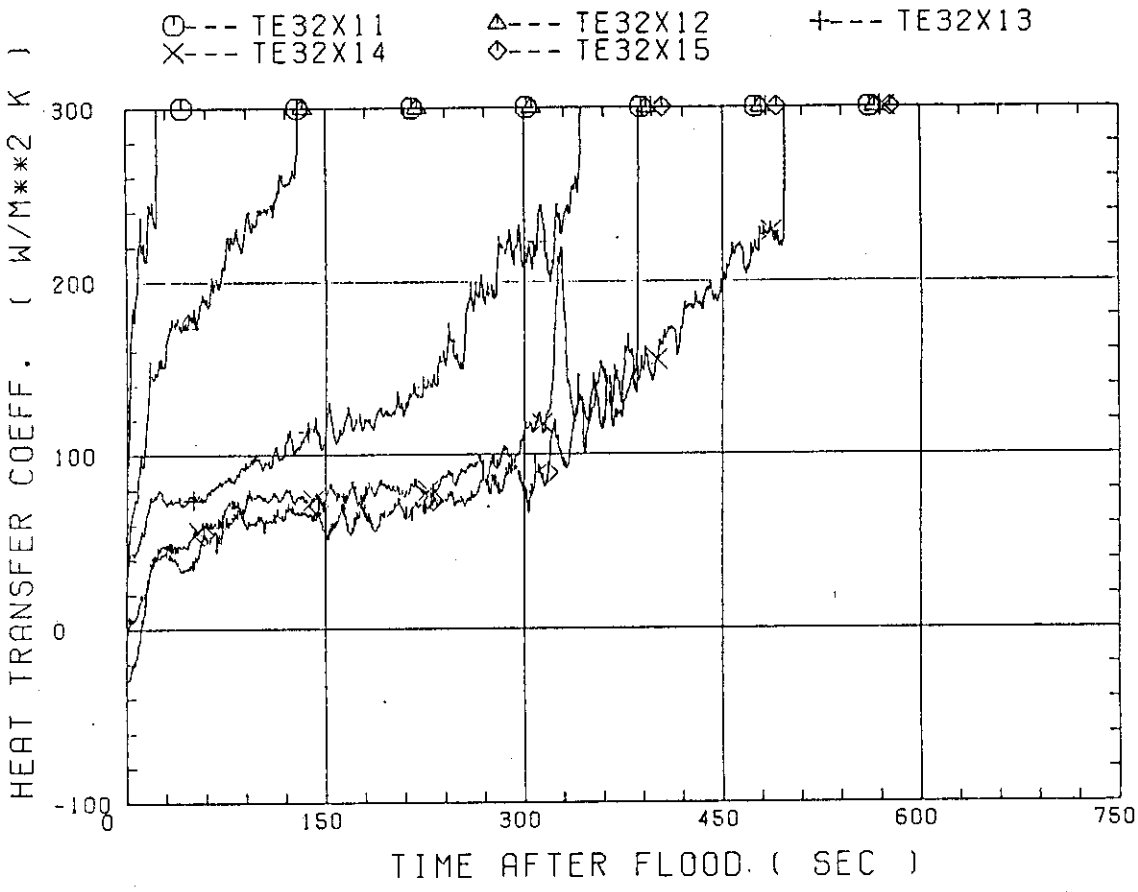

Fig. D-5 Heat transfer coefficient at midplane of high power rod (X-rod) in high power region (A region) (peak power rod)

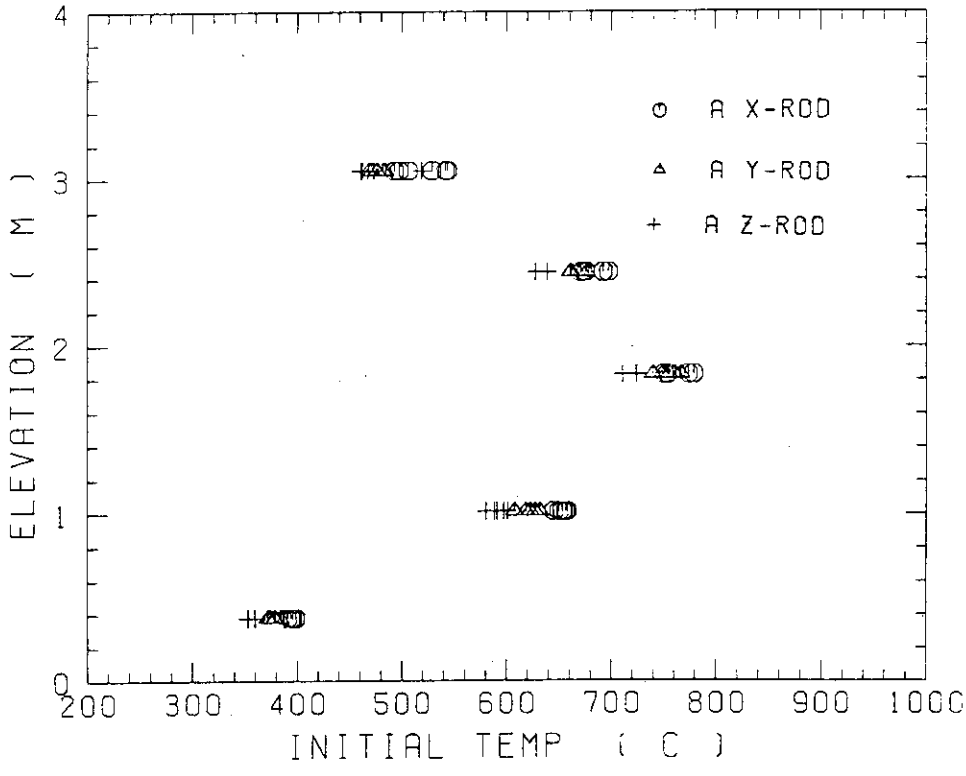

Fig. D-6 Initial rod surface temperature in high power region (A region)

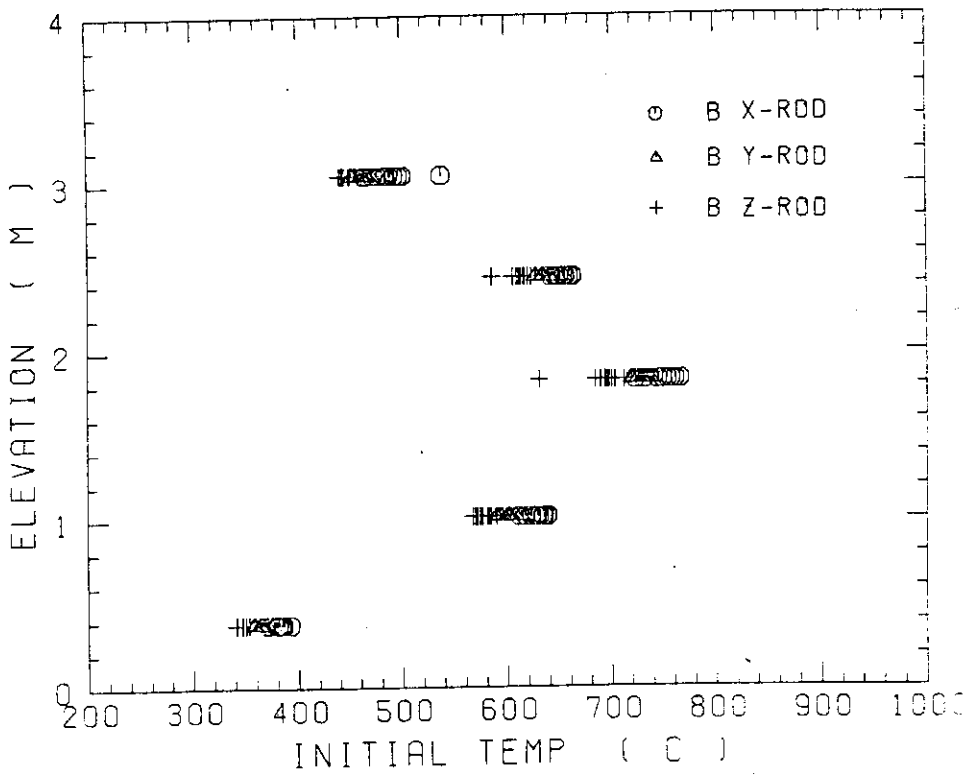

Fig. D-7 Initial rod surface temperature in medium power region (B region)

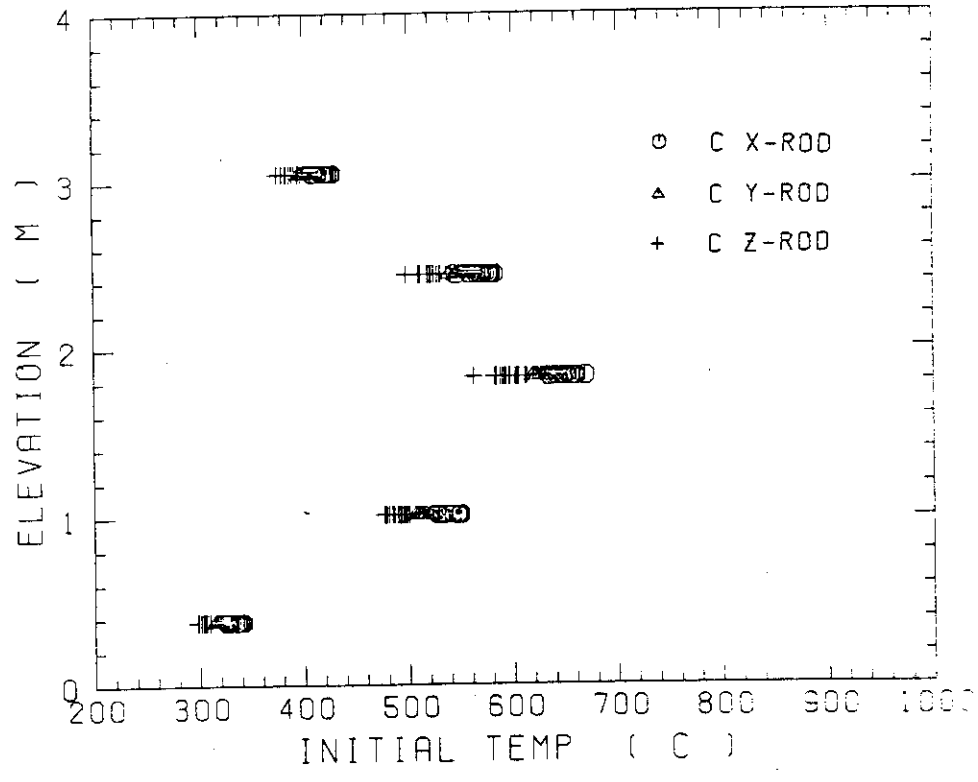

Fig. D-8 Inital rod surface temperature in low power region (C region)

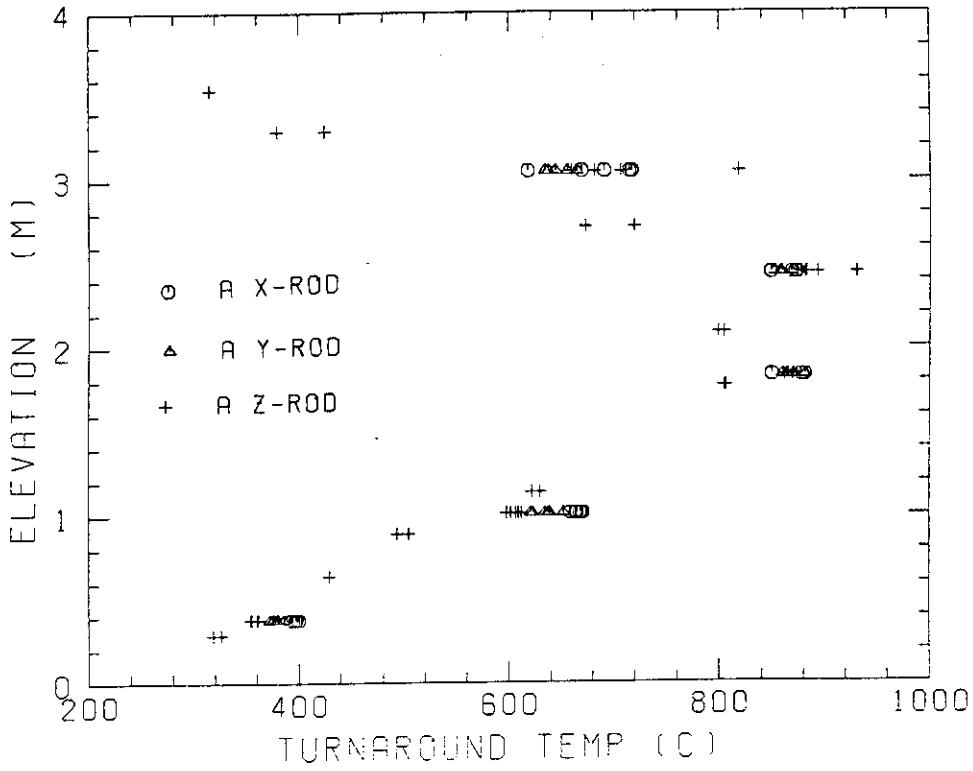

Fig. D-9 Turnaround temperature in high power region (A region)

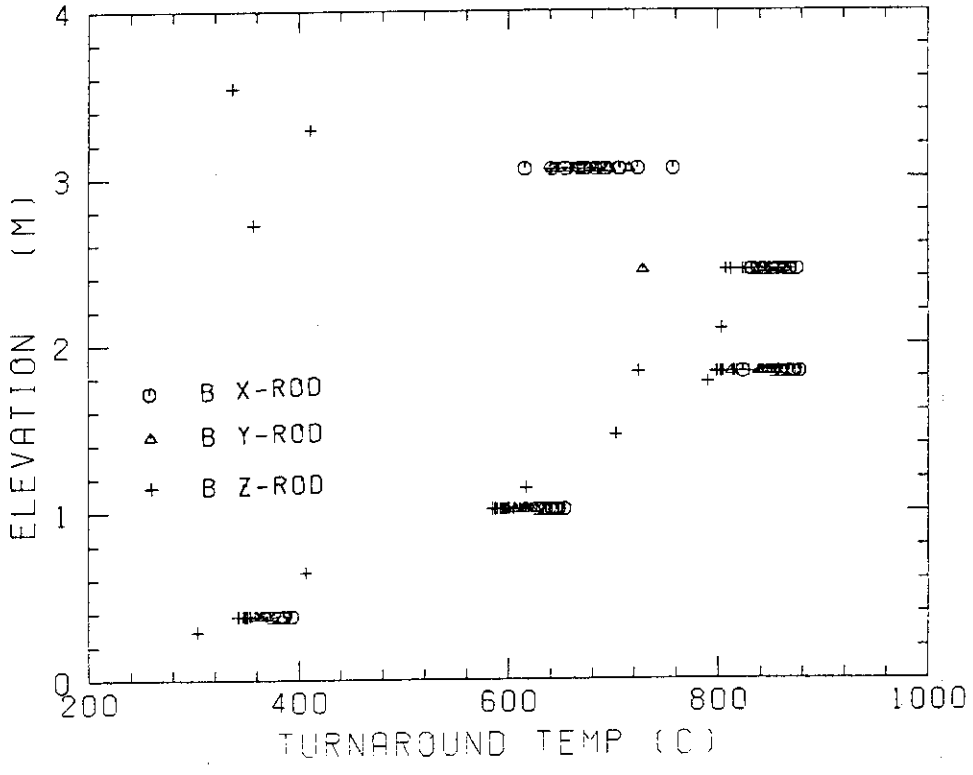

Fig. D-10 Turnaround temperature in medium power region (B region)

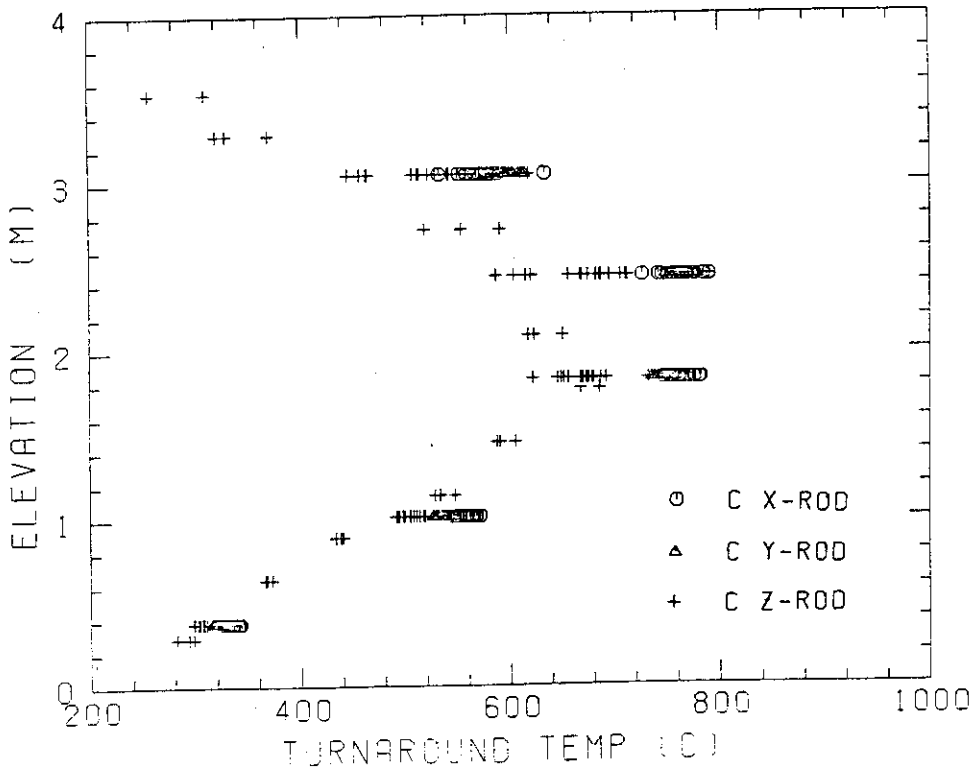

Fig. D-11 Turnaround temperature in low power region (C region)

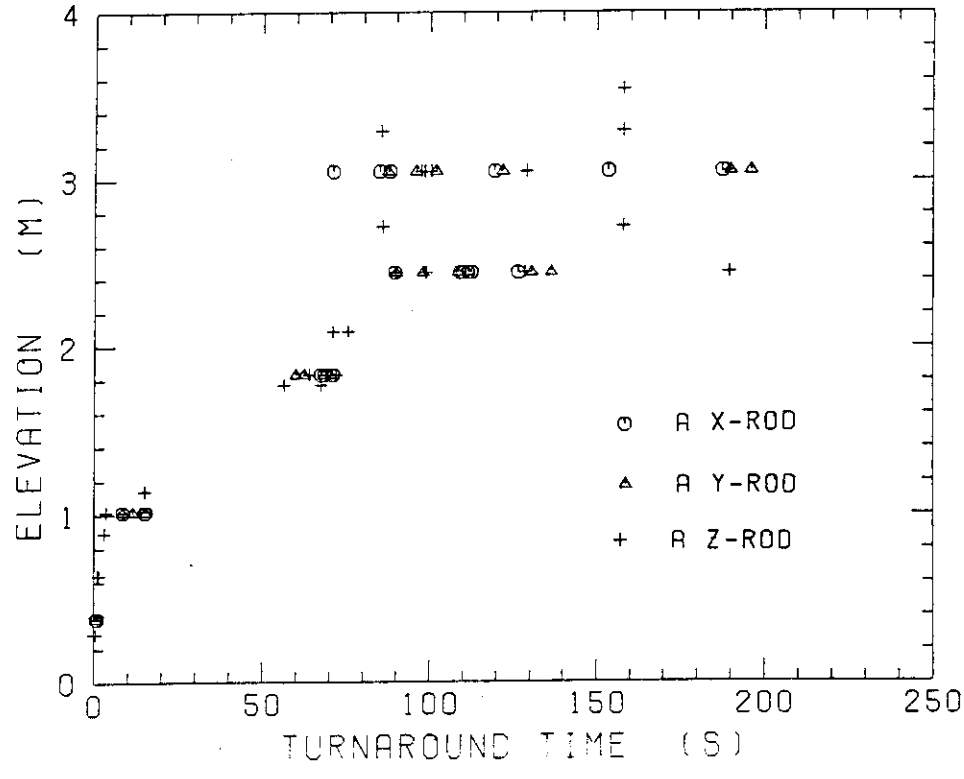

Fig. D-12 Turnaround time in high power region (A region)

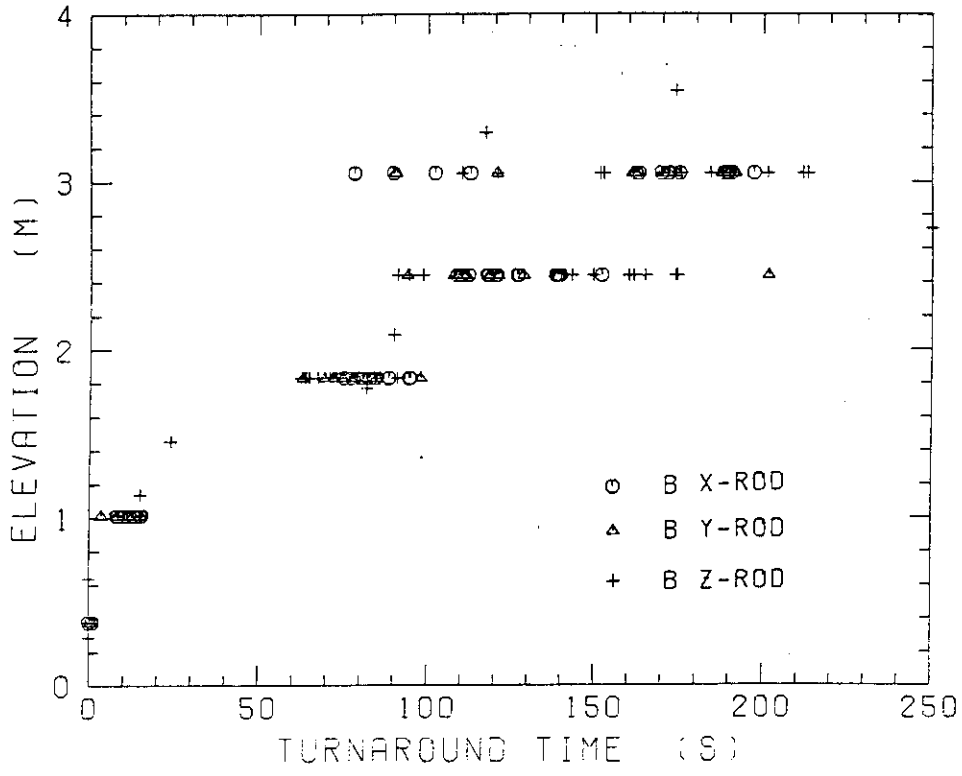

Fig. D-13 Turnaround time in medium power region (B region)

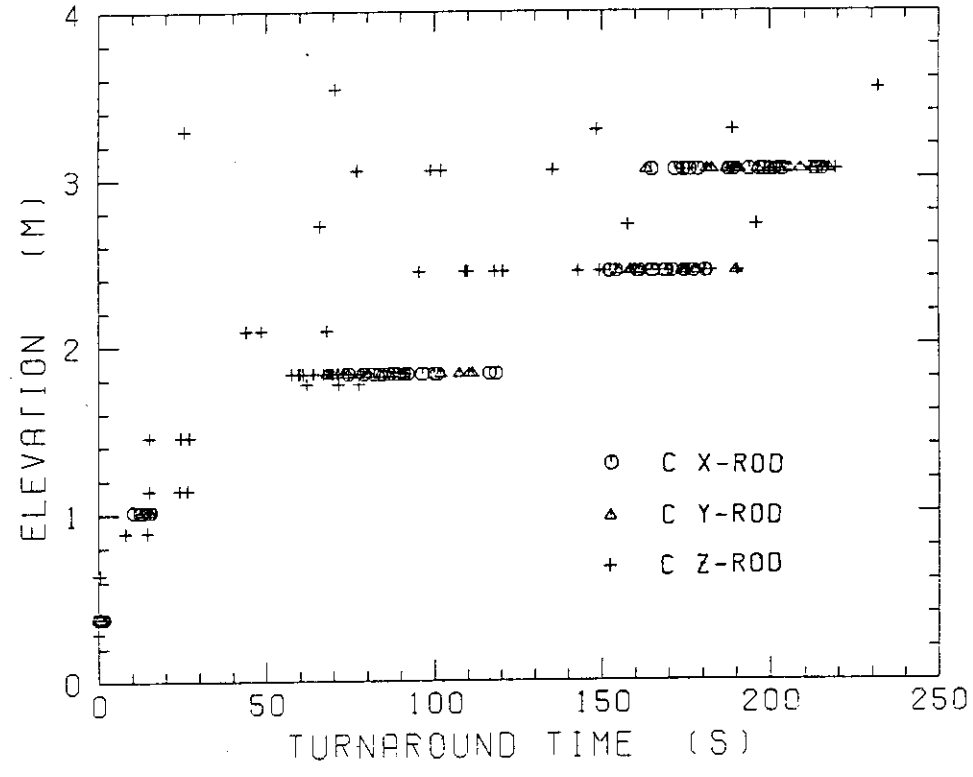

Fig. D-14 Turnaround time in low power region (C region)

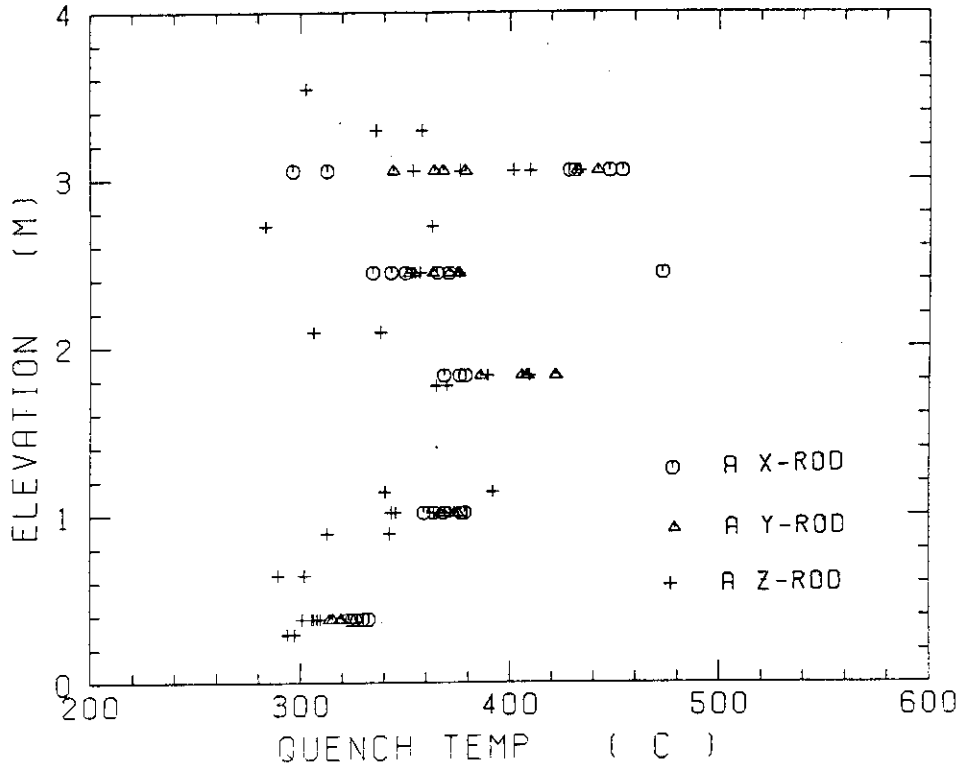

Fig. D-15 Quench temperature in high power region (A region)

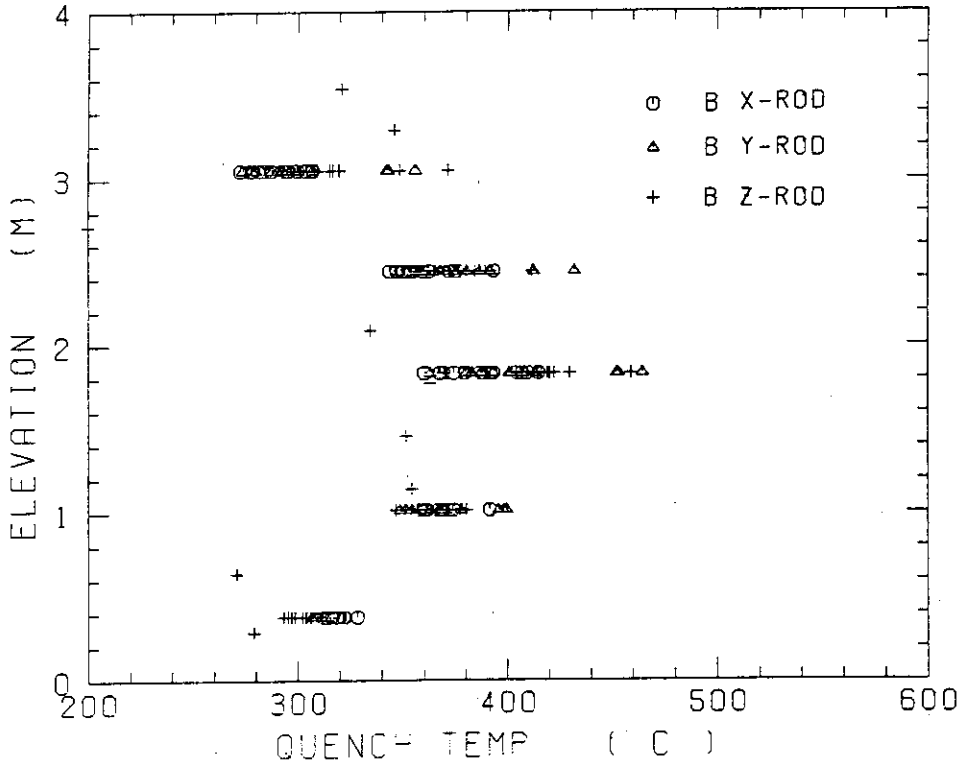

Fig. D-16 Quench temperature in medium power region (B region)

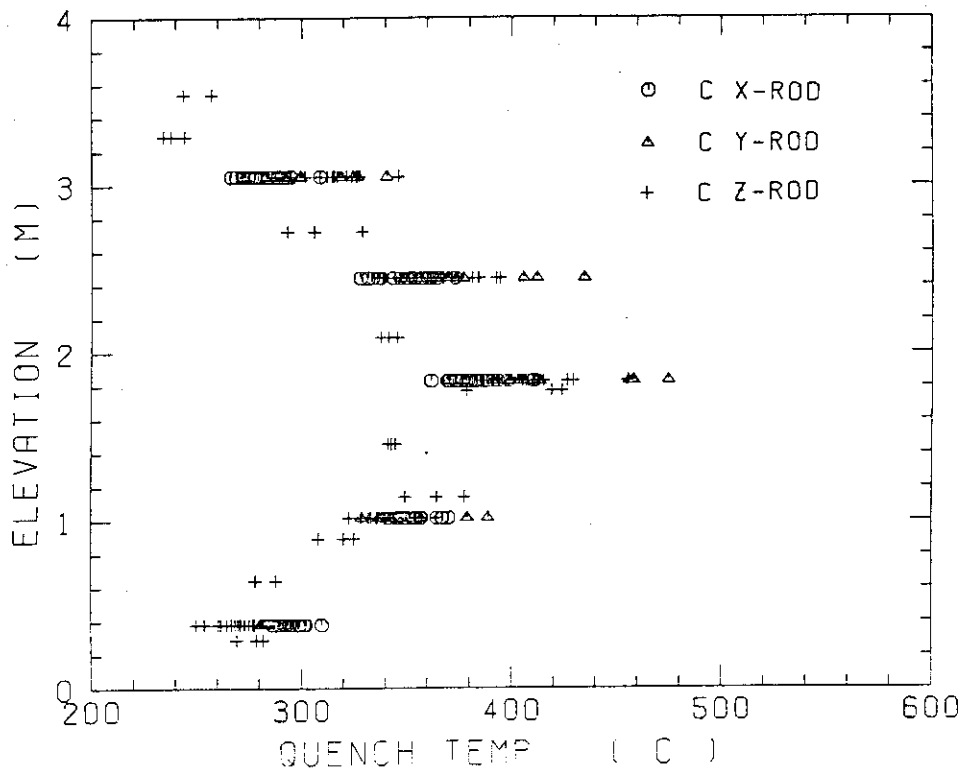

Fig. D-17 Quench temperature in low power region (C region)

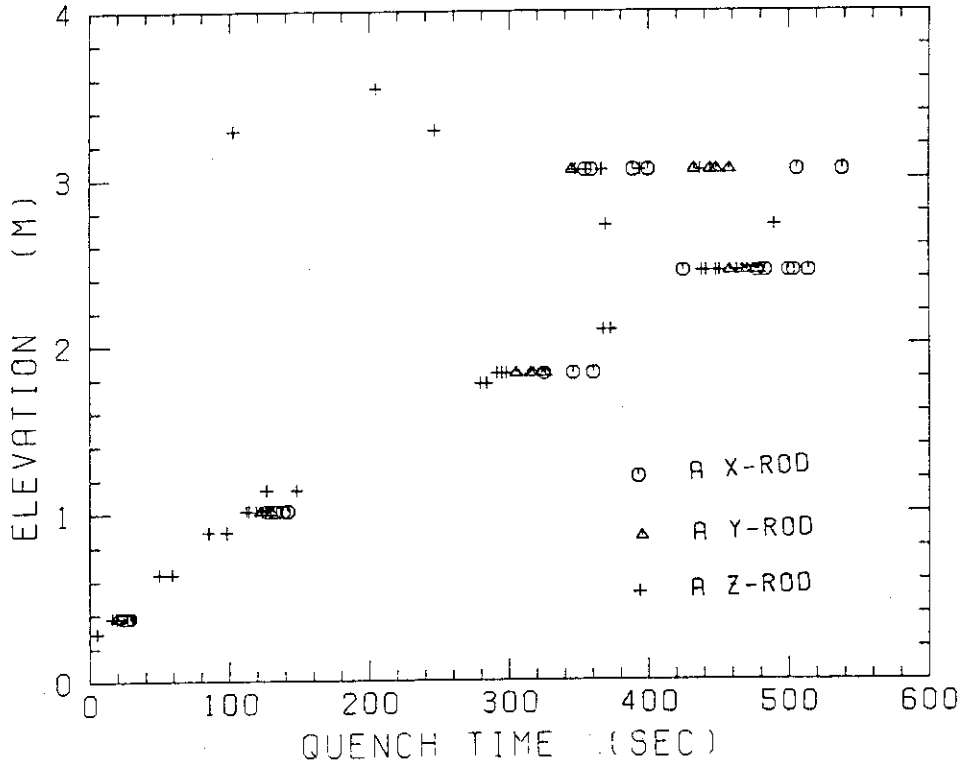

Fig. D-18 Quench time in high power region (A region)

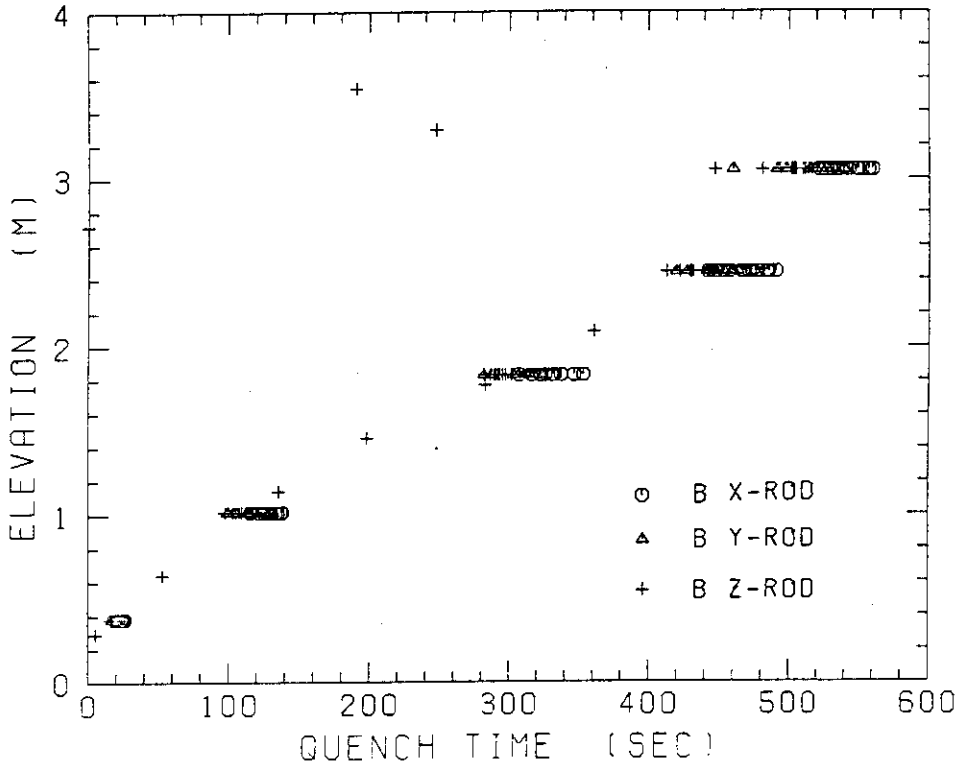

Fig. D-19 Quench time in medium power region (B region)

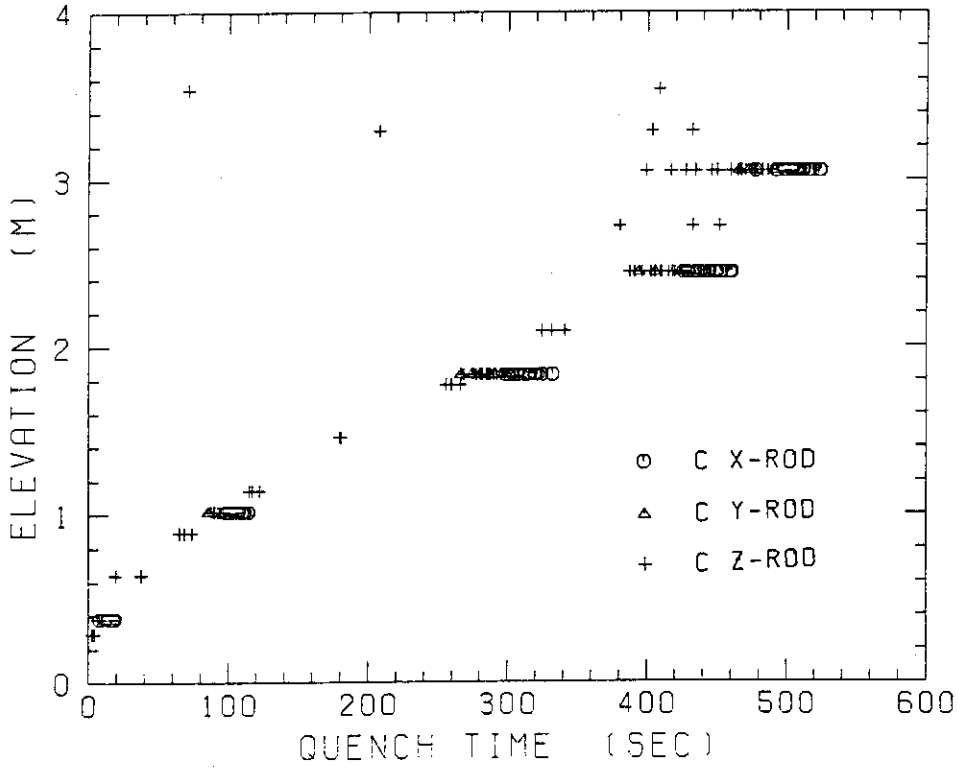

Fig. D-20 Quench time in low power region (C region)

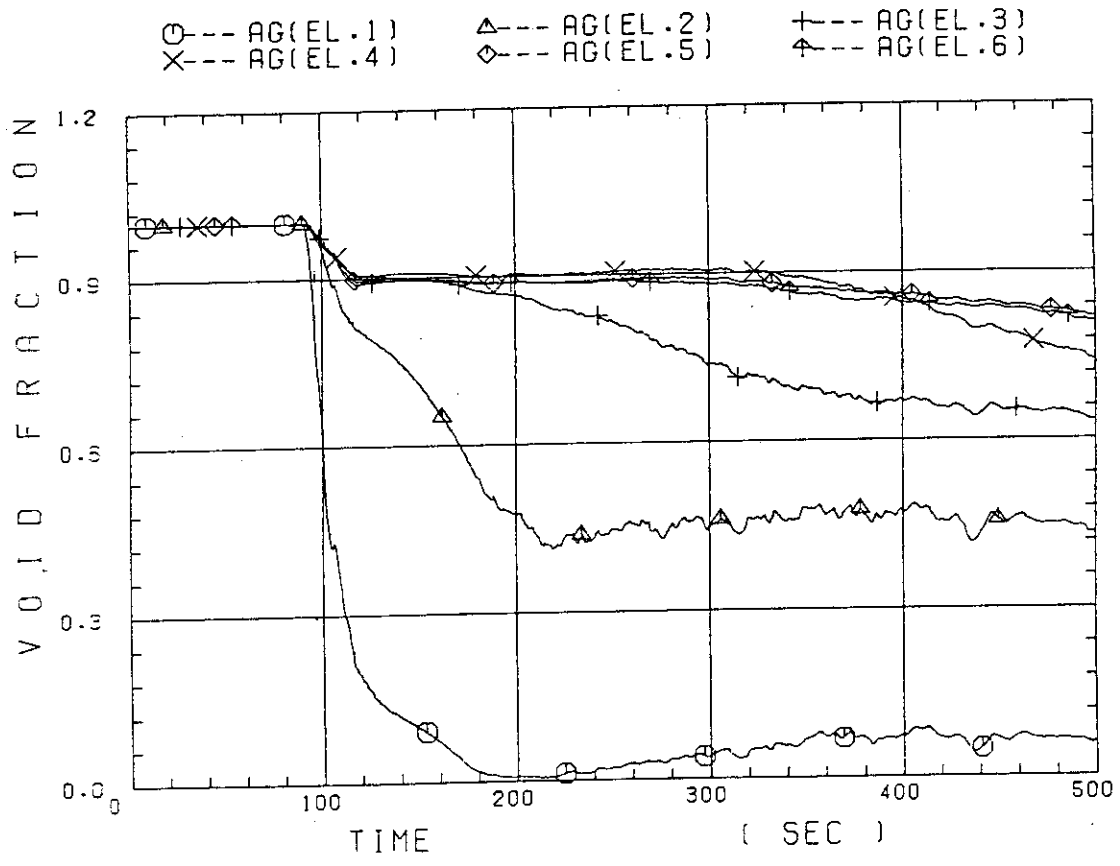

Fig. D-21 Void fraction in core

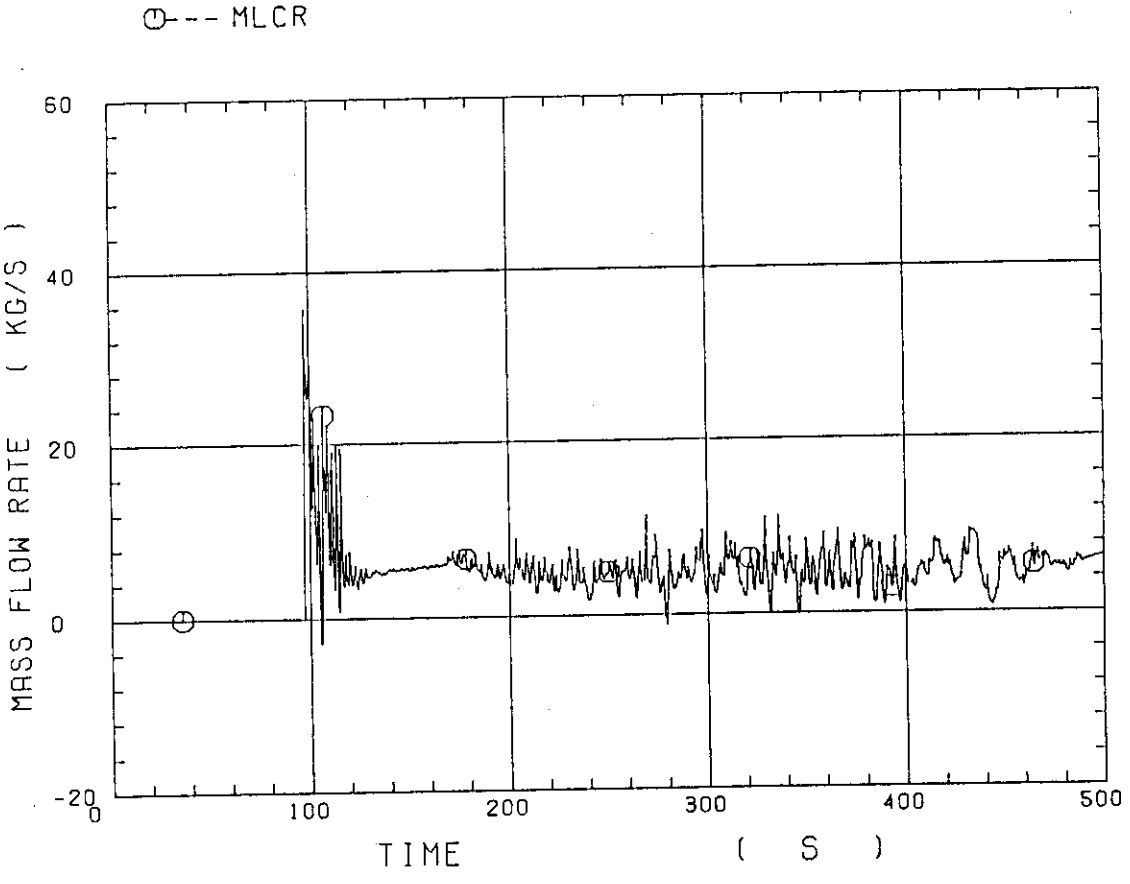

Fig. D-22 Core inlet mass flow rate

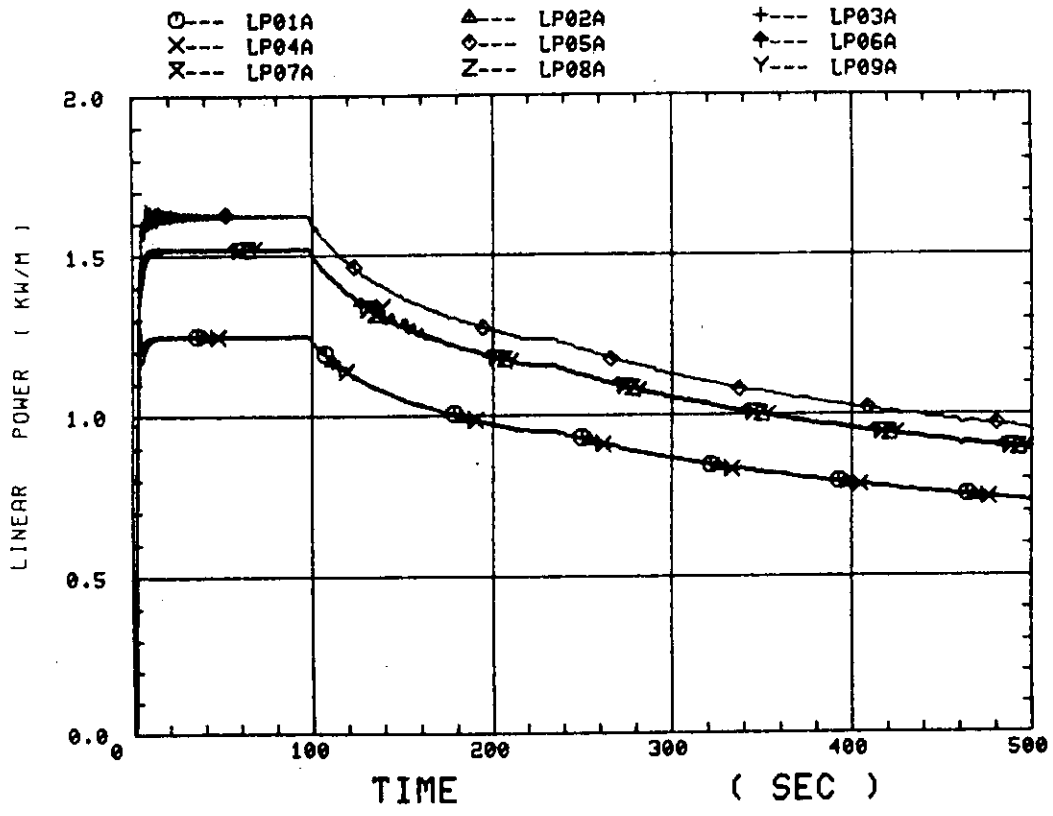

Fig. D-23 Average linear power of heater rod in each power unit zone

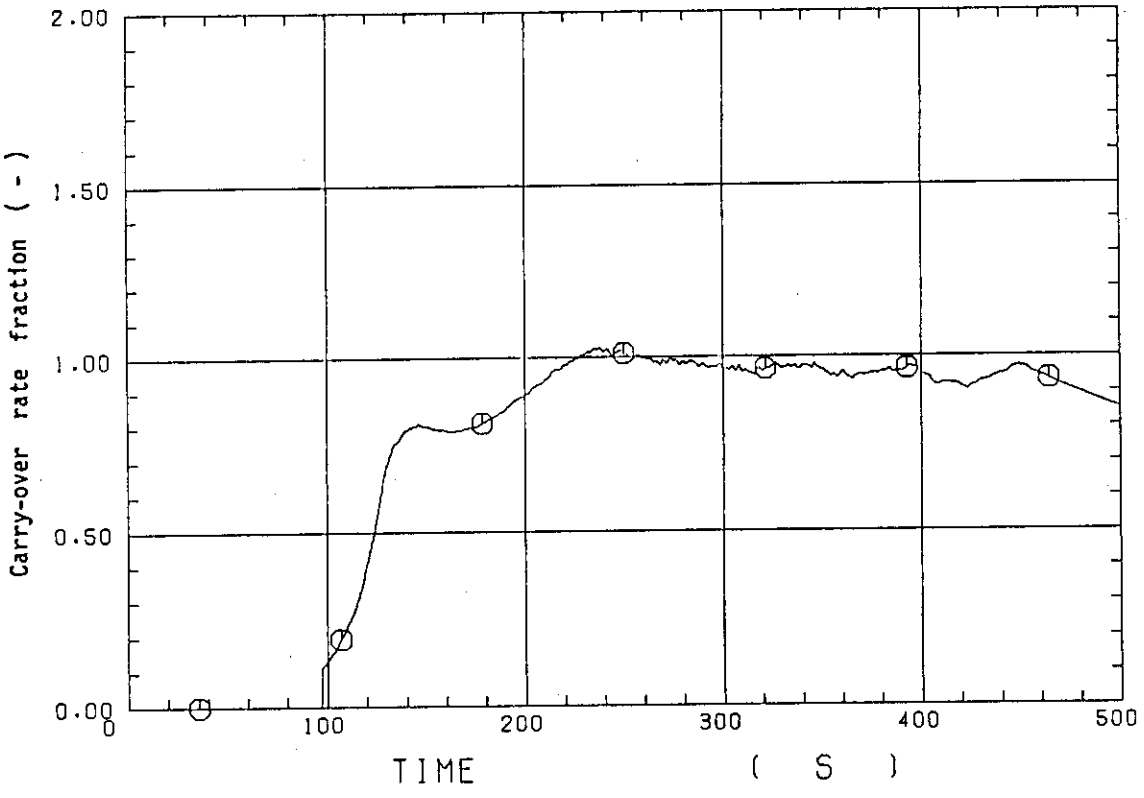

Fig. D-24 Carry-over rate fraction

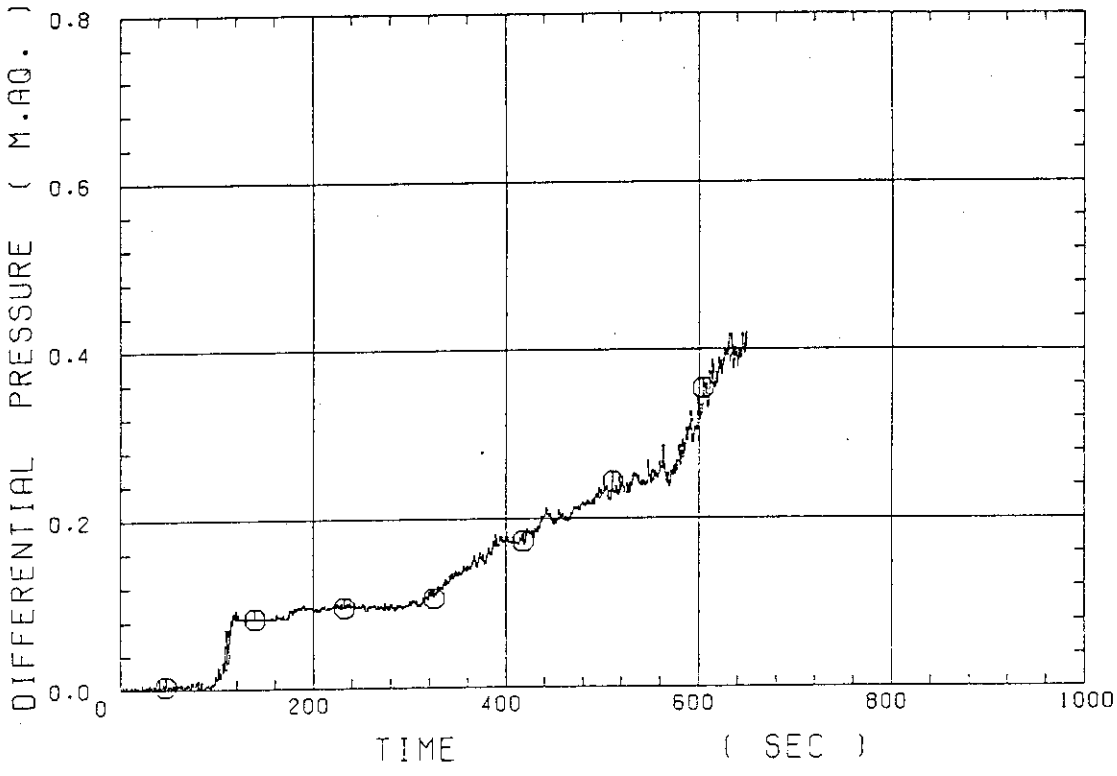

Fig. D-25 Differential pressure through upper plenum

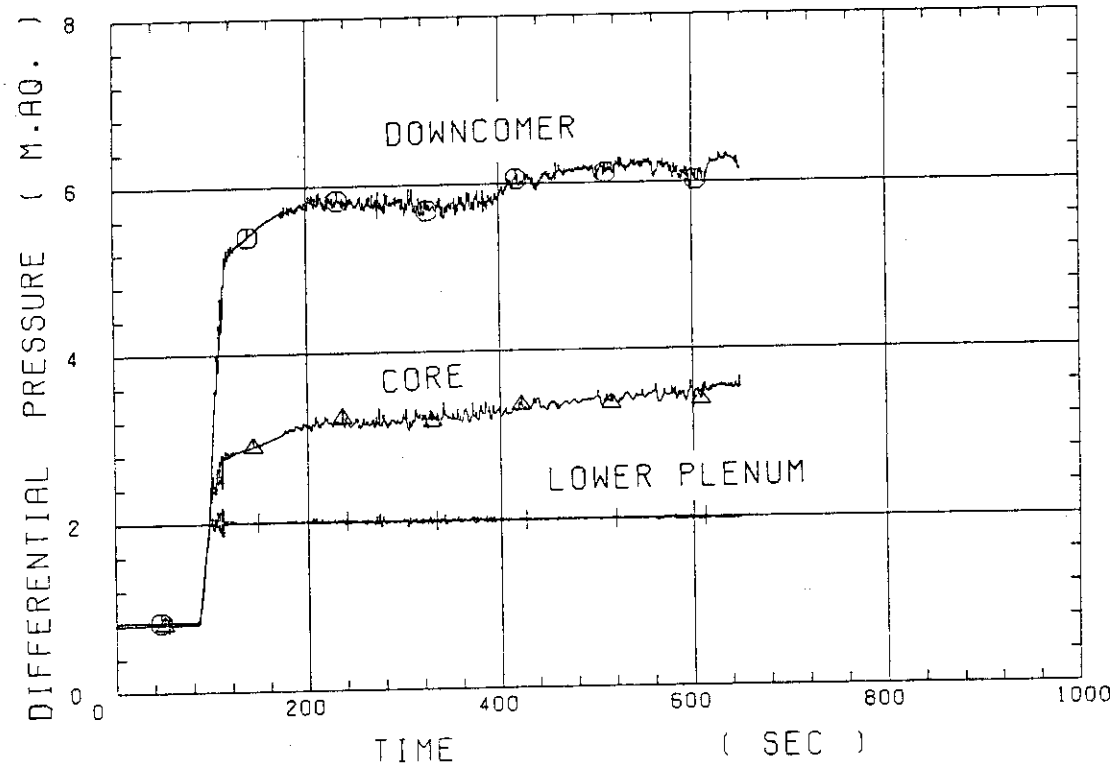

Fig. D-26 Differential pressure through downcomer, core, and lower plenum

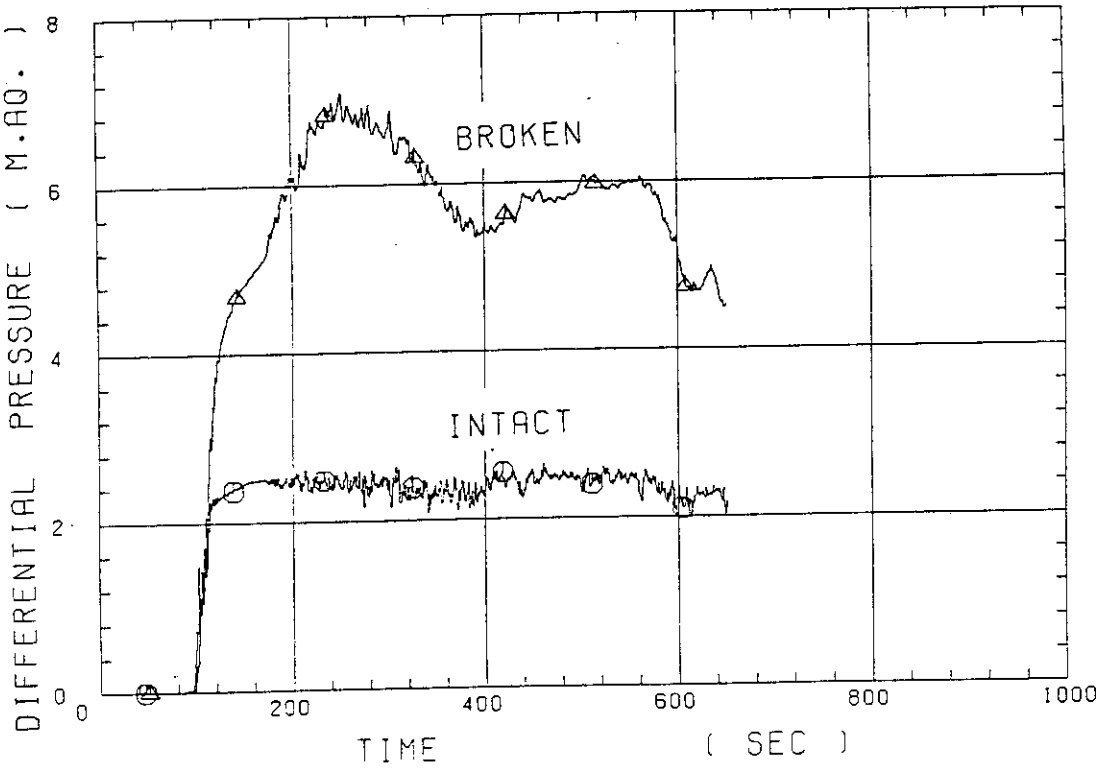

Fig. D-27 Differential pressure through intact and broken loops

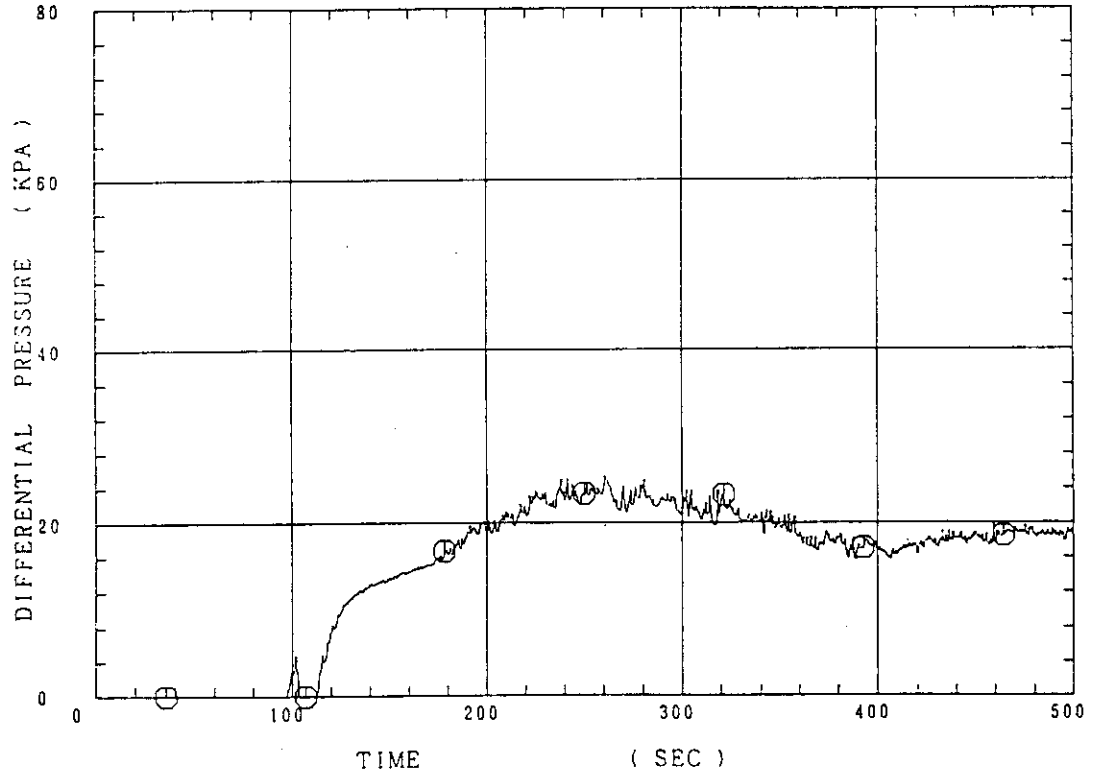

Fig. D-28 Differential pressure through broken cold leg nozzle

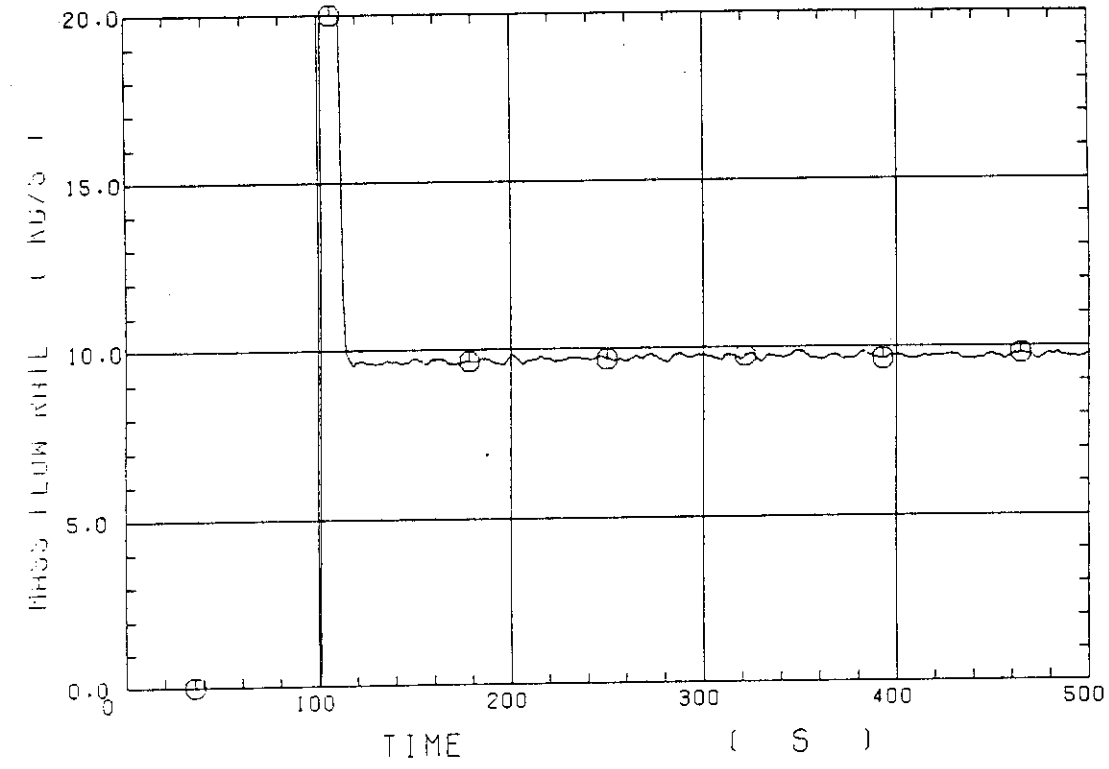

Fig. D-29 Total water mass flow rate from intact loops to downcomer

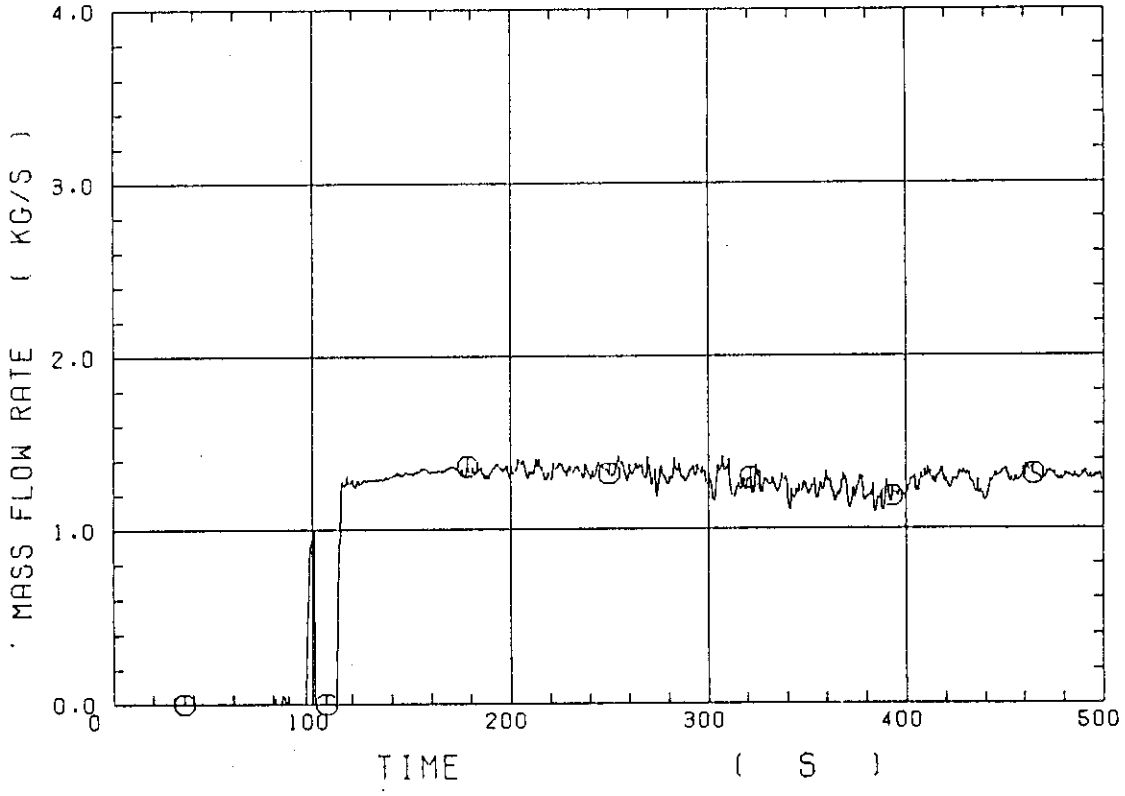

Fig. D-30 Total steam mass flow rate from intact loops to downcomer

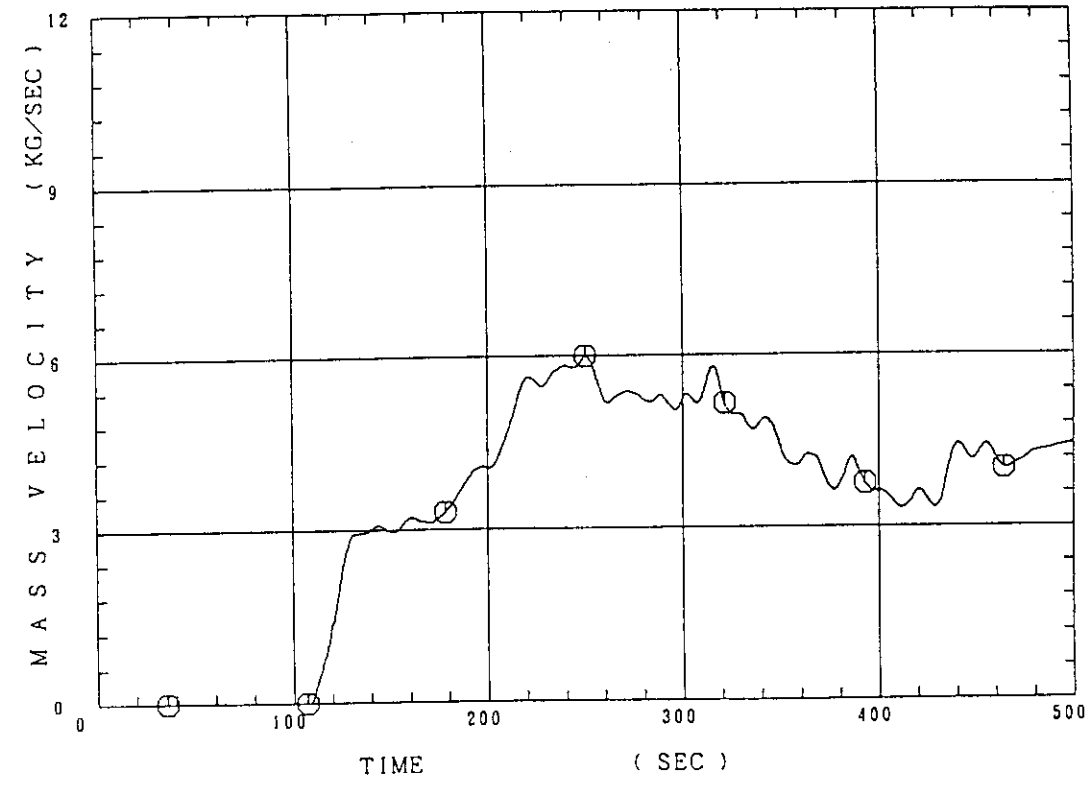

Fig. D-31 Water mass flow rate through broken cold leg nozzle

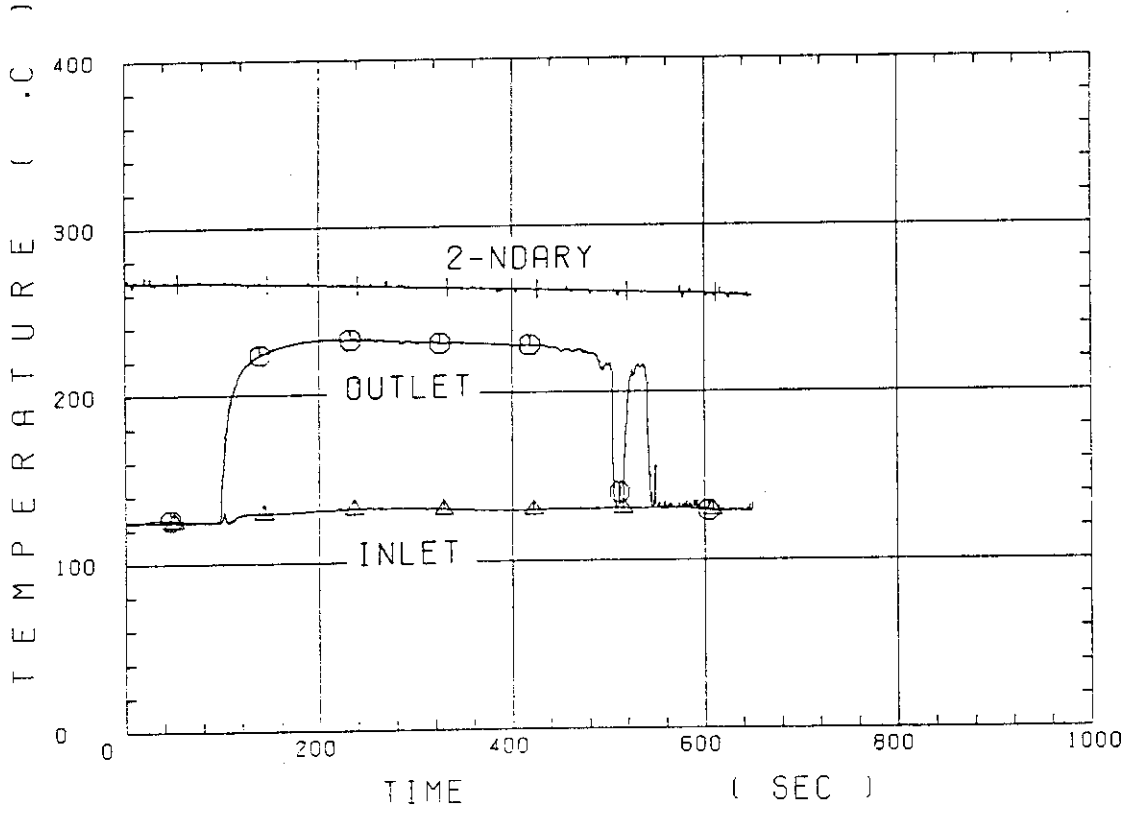

Fig. D-32 Fluid temperature in inlet plenum, outlet plenum, and secondary of steam generator 1

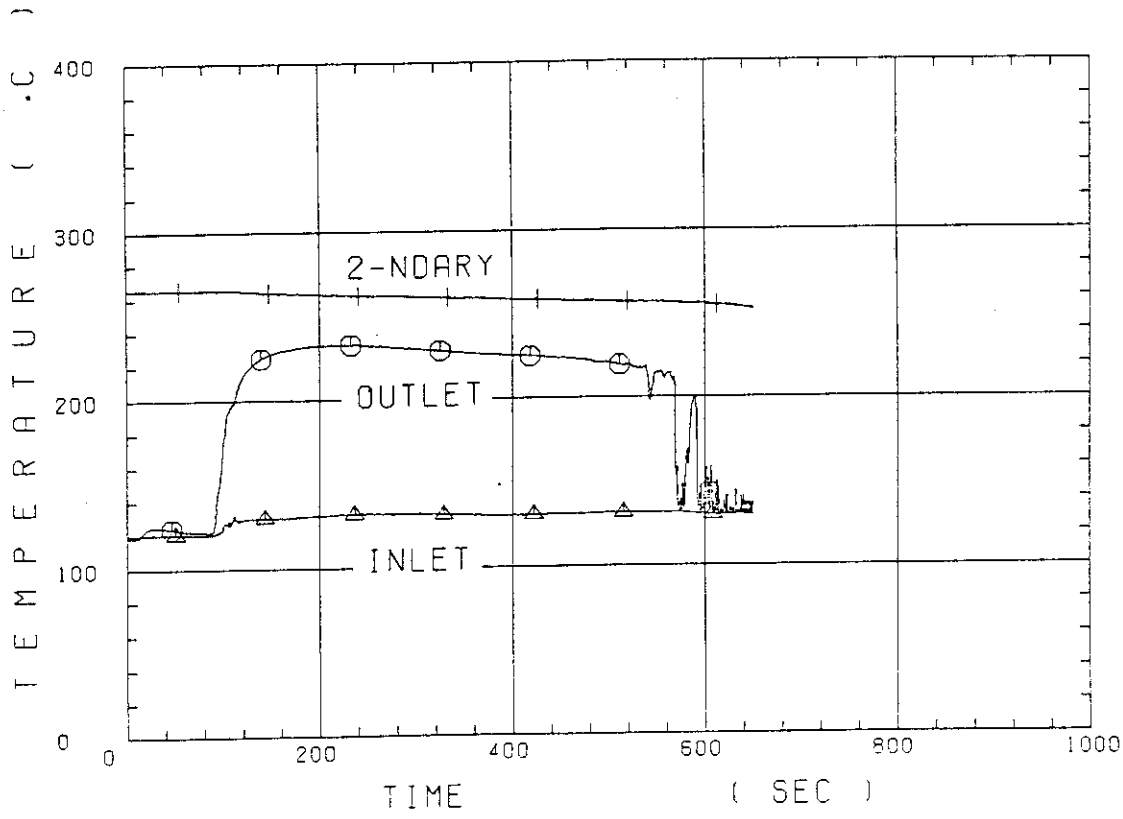

Fig. D-33 Fluid temperature in inlet plenum, outlet plenum, and secondary of steam generator 2

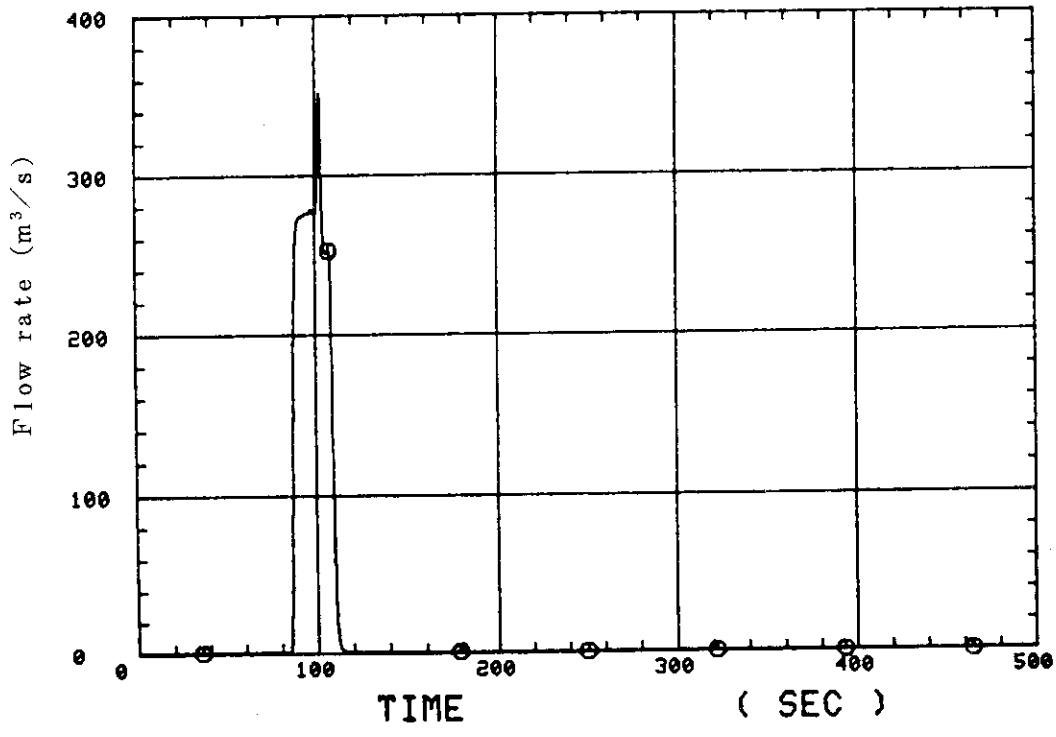

Fig. D-34 Total accumulator injection rate

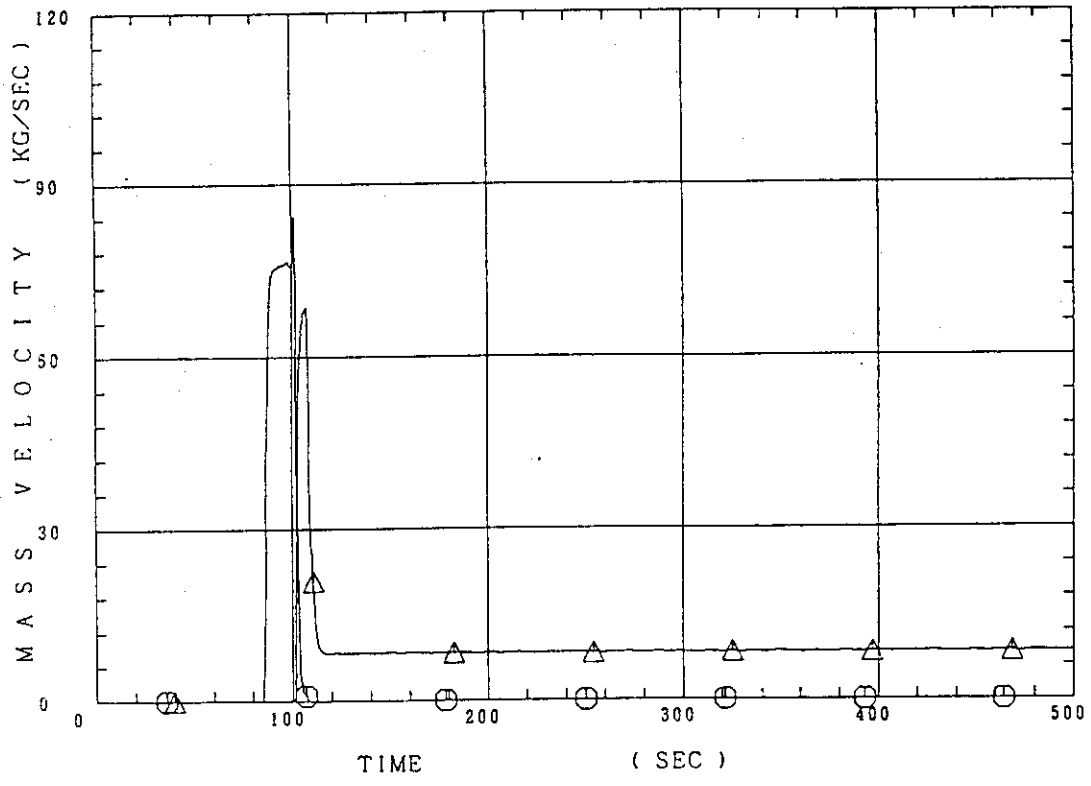

Fig. D-35 ECC water injection rates to lower plenum and to cold legs

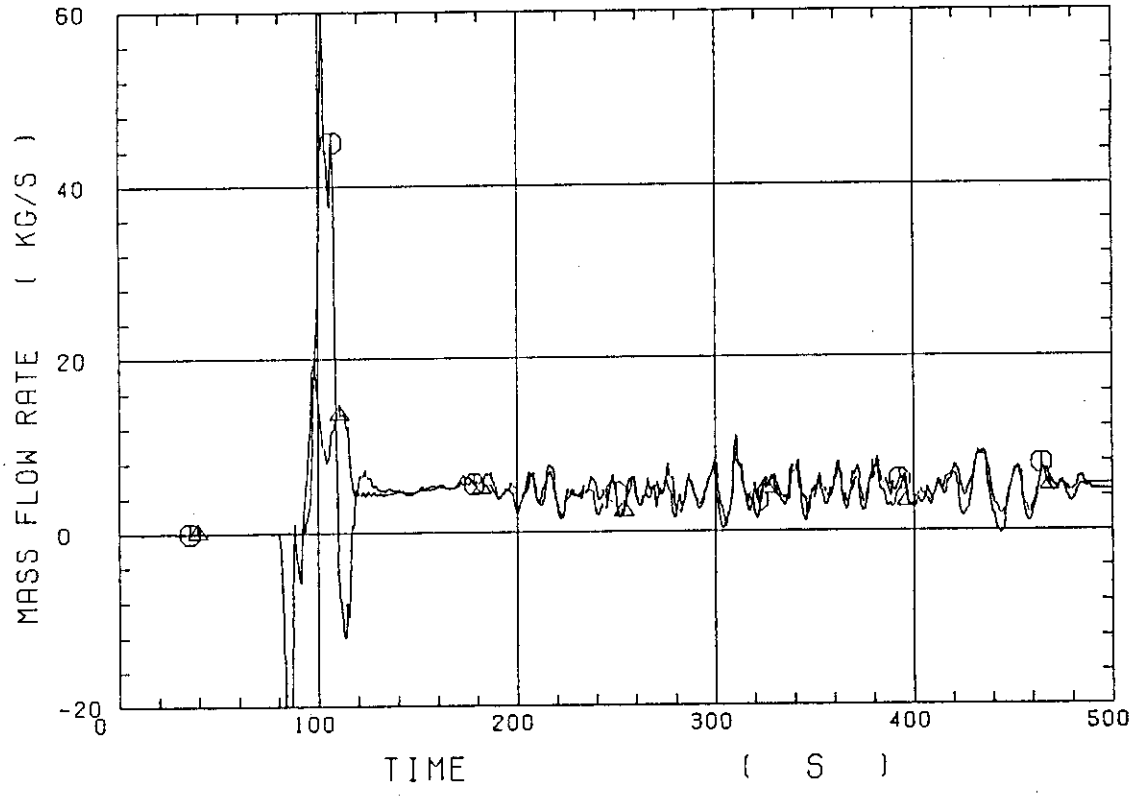

Fig. D-36 Core inlet mass flow rates estimated by mass balance downstream and upstream of core inlet

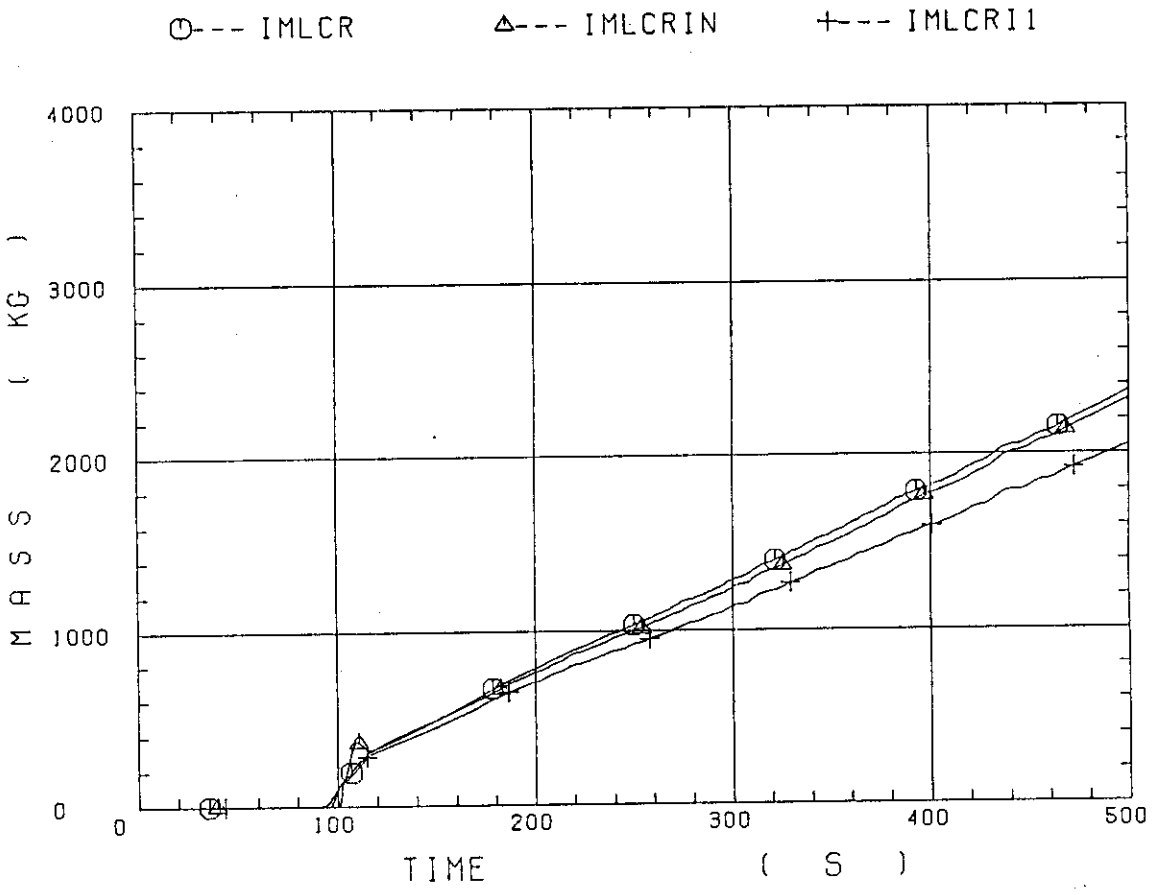

Fig. D-37 Comparison of injected mass into core among two estimation methods and evaluated mass